University of Dundee

DOCTOR OF PHILOSOPHY

Assessment of N-myristoyltransferase and the N-myristoylomeas a potential chemotherapeutic target inTrypanosoma cruzi

Roberts, Adam

Award date:
2014

Link to publication

University of Dundee

College of Life sciences

Assessment of *N*-myristoyltransferase and the *N*-myristoylome as a potential chemotherapeutic target in *Trypanosoma cruzi*

Adam J. Roberts

PhD Thesis

December 2014

Supervisor: Professor Alan H. Fairlamb

Contents

List of figures

Chapter 1   Facing page

Chapter 3   Facing page

Chapter 4   **Facing page**

List of tables

List of abbreviations

AzMyr	Azidomyristate
BLAST	Basic local alignment search tool
CAP5.5	Cytoskeleton associated protein 5.5
DDU	Drug Discovery Unit
DIG	Digoxigenin
DKO	Double knockout
DMEM	Dulbecco's modified eagles medium
DTT	Dithiothreitol
EC$_{50}$	Effective concentration of inhibitor to reduce by 50%
EDTA	2-([2-[Bis(carboxymethyl)amino]ethyl](carboxymethyl)amino) acetic acid
FBS	Foetal bovine serum
FCaBP	Flagellar calcium binding protein
FDKO	Failed double knockout
FRQ1	Frequinin
gDNA	Genomic DNA
HAT	Human African Trypanosomiasis
His$_6$	Hexahistidine tag
HRP	Horseradish peroxidase
HYG	Hygromycin phosphotransferase
K_i	Inhibition constant
K_i^{app}	Apparent inhibition constant
K_m	Michaelis-Menten constant
K_m^{app}	Apparent Michaelis-Menten constant

ix

LB medium	Luria Bertiani medium
LC-MS/MS	Liquid chromatography tandem mass spectrometry
LFQ	Label-free quantitation
MOI	Multiplicity of infection
Myr	Myristic acid
Myr-CoA	Myristoyl-Coenzyme A
NMT	N-myristoyltransferase
ORF	Open reading frame
PAC	Puromycin *N*-acetyltransferase
PBS	Phosphate buffered saline
Pik1	phosphatidylinositol-4-OH kinase
RPT2	Proteasome regulatory subunit 2
RT	Room temperature
RTH	RPMI-1640 supplemented with trypticase and haemin
S.D.	Standard deviation
SDS	Sodium dodecyl sulphate
SDS-PAGE	Sodium dodecyl sulphate polyacrylamide gel electrophoresis
SILAC	Stable isotope labelling of amino acids in cell culture
SKO	Single knockout
SPA	Scintillation proximity assay
TCEP	Tris(2-carboxyethyl)phosphine
TryR	Trypanothione reductase
UTR	Untranslated region
WHO	World Health Organisation

Acknowledgments

Firstly, I would like to thank Professor Alan Fairlamb for providing me with both an interesting and challenging project to form the focus of my thesis. I am extremely grateful for the supervision, guidance and encouragement that he has provided throughout my studies in the lab.

I would also like to thank Dr Susan Wyllie who from the start of my PhD has spent countless hours on training and mentoring me through my studies, for which I am eternally indebted.
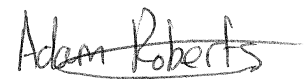
I would like to express my gratitude to all members of the AHF lab and members of the Horn group that I have shared an office with for both their support and friendship over the years. Additionally I would like to thank Anna and Anders for putting up with me for the past 4 years.

Finally, I would like to thank my family and friends who have supported me throughout my studies in Dundee. It has been greatly appreciated.

Declaration

I certify that this thesis is of my own writing and the work reported is based upon the results of my own work carried out under the supervision of Professor Alan H. Fairlamb. Work other than my own has been specifically stated within the text by referencing the relevant researchers and/or their relevant publications. No part of this thesis has previously been submitted for a higher degree.

Adam J. Roberts

I hereby certify that Adam J. Roberts has performed the research described in this thesis, under my supervision and has fulfilled the conditions of the relevant ordinance and regulations of the University of Dundee and that he is qualified to submit the following thesis for the degree of Doctor of Philosophy.

Professor Alan H. Fairlamb

Welcome Trust Principal Research fellow

Abstract

As there is a need for fully validated drug targets in *Trypanosoma cruzi,* the genetic and biochemical essentiality of *N*-myristoyltransferase (NMT) was assessed. The genetic requirement was assessed using a classical gene replacement strategy, attempting to sequentially replace the endogenous alleles with drug resistance genes to generate an *NMT* null parasite. It was only possible to achieve this in the presence of an ectopic copy of *NMT* under constitutive expression, providing the strongest evidence that this gene is essential for the proliferation of the epimastigote. While both NMT and *N*-myristoylation were detected in all lifecycle stages, there were subtle differences in the expression of several myristoylated proteins. However, at least ~10 myristoylated proteins were common throughout the lifecycle. In addition, *N*-myristoylation in this parasite was found to be primarily associated with nascent protein synthesis, as treatment with cycloheximide reduced the number of *N*-myristoylated proteins detected. The sensitivity of epimastigotes to the inhibitor DDD85646 correlated with the expression of NMT, suggesting it to be the target in the parasite. This was confirmed by the dose-dependent depletion of *N*-myristoylated proteins detected in parasites treated with this compound. Mechanism of action studies revealed a cytokinesis defect caused by the inhibition of *N*-myristoylation and NMT. Overexpression of NMT was able to rescue these cells from this phenotype confirming that it is NMT mediated. The *N*-myristoylated proteins comprising the *N*-myristoylome of the epimastigote were identified using the myristic acid analog, azidomyristate and a chemical proteomics approach. Combining label-free and SILAC methodologies, 38 proteins were enriched from azidomyristate labelled cells, 35 of which were predicted to have a glycine after the initial methionine. The findings from these experiments have led to the most comprehensive *N*-myristoylome of *T. cruzi* studied to date and provide several hypotheses, by which the inhibition of NMT leads to the observed cytokinesis defect.

Chapter 1

Introduction

1.1.1 Kinetoplastida

The kinetoplastids are a class of unicellular protozoan organisms belonging to the phylum Euglenozoa. These parasites are named after the unique organelle forming part of their mitochondrion known as the kinetoplast. This consists of a series of interlocking plasmids known as mini or maxi-circles, each ranging from 0.5-40 kbp in length and is found at the base of the flagellum (Westenberger *et al*., 2006). The *Trypanosomatid* parasites belonging to this class are further sub-divided into the sub-genera *Blastocrithidia*, *Crithidia*, *Endotrypanum*, *Herpetomonas*, *Rhynchoidomonas, Leptomonas*, *Phytomonas*, *Leishmania* and *Trypanosoma* (Stevens *et al*., 2001). For the past 100 years, it has been known that parasites of the *Trypanosoma* and *Leishmania* families are the cause of several human diseases, all of which have been classified to be neglected tropical diseases in 2002 (Yamey, 2002). The term, neglected tropical disease was coined due to the low interest of the pharmaceutical industry to start research programs into these organisms, with the aim of finding cures for the diseases that they cause. More than a decade later, these same diseases are still regarded to be neglected by the World Health Organisation (WHO) (Feasey *et al*., 2010).

1.1.2 *Trypanosoma brucei* and Human African Trypanosomiasis

The parasite *Trypanosoma brucei* (*T. brucei*) is the cause of Human African Trypanosomiasis (HAT) and is found in 36 sub-Saharan African countries (WHO Expert Committee, 1998). In 1995 there was an estimated 60 million individuals at risk of infection with >300,000 cases per year, however, in recent times this number has dropped below 10,000[1] (World Health Organization, 2006). It is now estimated that there are ~30,000 individuals infected with *T. brucei*[1]. This parasite is transmitted to humans through the bite of an infected Tsetse fly (Vickerman, 1976). This digenetic

---

[1] http://www.who.int/mediacentre/factsheets/fs259/en/
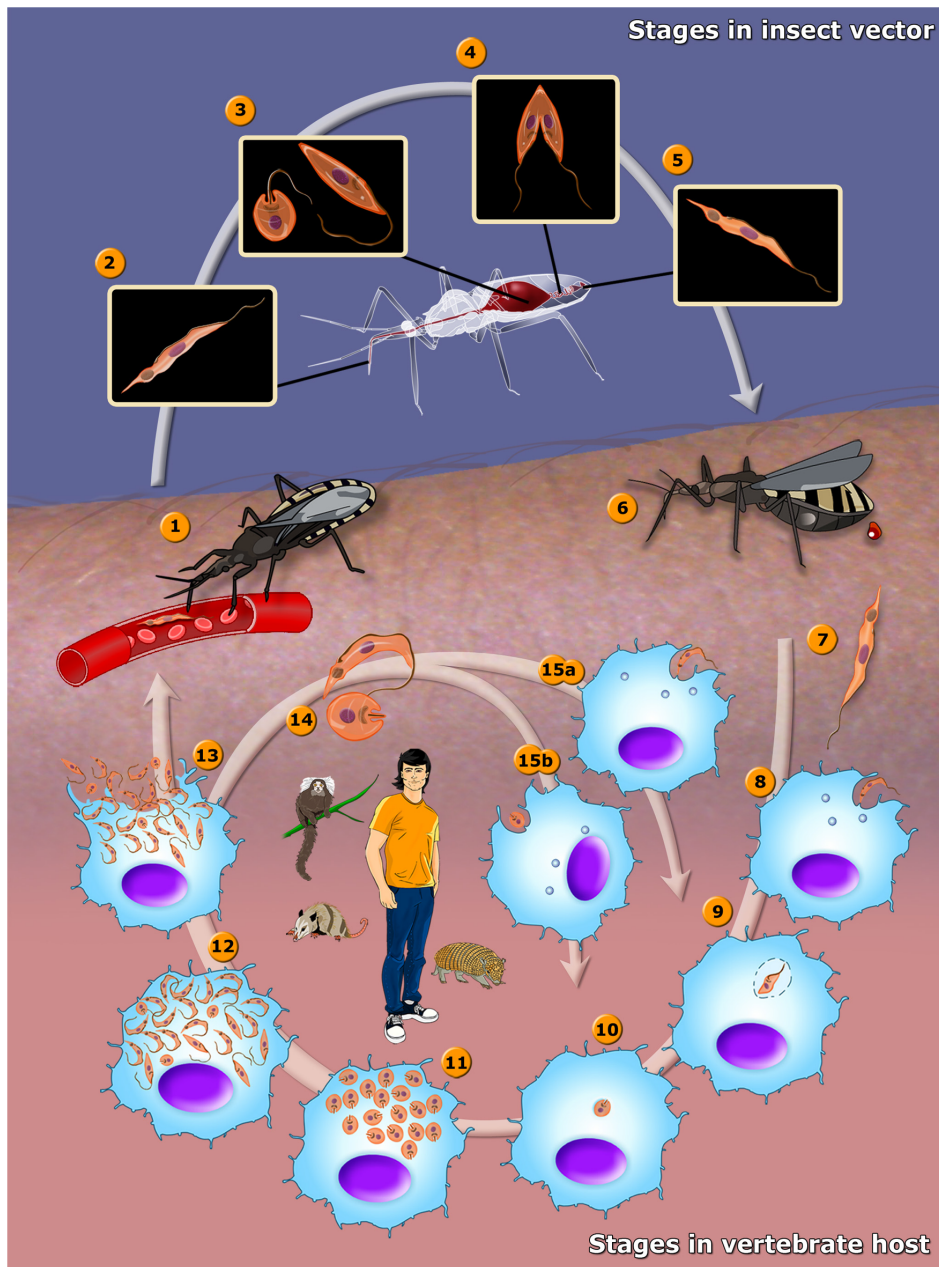
Figure 1.1 Lifecycle of *Trypanosoma cruzi*

1. Triatomine bug ingests trypomastigotes from a blood meal. 2. Trypomastigote. 3. Trypomastigotes transform into the epimastigote in the hindgut. 4 Epimastigotes divide and continue to pass through the digestive tract of the triatomine bug. 5 Epimastigotes transform back into trypomastigotes. 6 Infectious trypomastigotes are passed out in the faeces of the triatomine bug and gain entry to the host cells through a cut in the skin or via a mucosal membrane. 7-10 Parasites gain entry to a host cell and transform into an amastigote. 11 Amastigotes undergo cell division. 12 Most amastigotes transform into trypomastigotes. 13 Mixture of amastigotes and trypomastigotes burst out of a host cell and circulate in the blood. 14 Trypomastigotes and amastigotes are able to infect new host cells or be taken up in a blood meal. Alternatively, trypomastigotes 15a or amastigotes 15b are able to infect host cells and propagate the infection. Figure modified from Texiera *et al*. PLoS Negl Trop Dis. 2012 Aug;6(8):e1749. doi: 10.1371/journal.pntd.00017

organism, possesses two replicative stages, the procyclic forms (PCF), found in the Tsetse fly and the bloodstream form (BSF) found circulating the in the blood of a mammalian host. There are three subspecies of *T. brucei*, the *brucei* subspecies is only infectious to cattle, while *rhodesiense* and *gambiense* strains cause the human disease. The symptoms after the initial infection with this parasite are generally quite mild, with headaches, fevers and stiffness amongst other symptoms being reported (WHO Expert Committee, 1998). However, as the disease progresses, parasites cross the blood brain barrier into the central nervous system leading to lethargy, seizures, comas (from which the disease name is derived) and ultimately death (WHO Expert Committee, 1998).

1.1.3 *Trypanosoma cruzi*

Trypanosoma cruzi (*T. cruzi*), the causative agent of Chagas disease was first identified by the Brazilian physician Dr Carlos Chagas in 1909. This digenetic organism has a complex lifecycle formed of separate, but interlinked mammalian and insect lifecycles (**Figure 1.1**). *T. cruzi* is primarily transmitted through the faeces of the *Triatominae* sub-family of Reduviidae bugs, colloquially referred to as kissing bugs (Dias, 2007). The most important species acting as a vector for the human disease is *Triatoma infestans*. As an infected insect takes a blood meal from a mammalian host, it simultaneously expels its faeces, which contain metacyclic trypomastigote forms of the parasite next to the open wound. The irritation caused by the taking of a blood meal causes the host to scratch the site surrounding the wound, resulting in trypomastigotes gaining access to the blood stream of the host. Alternatively, trypomastigotes can invade via the mucosal membranes of the host such as the eyes, mouth and throat (Hoft *et al*., 1996). Upon entry to the bloodstream, the trypomastigote is able in infect a variety of cell types; however they display a preference for cardiac muscle (Brener,

1973; Buckner *et al*., 1999). This step is essential for the proliferation and propagation of these parasites in the mammalian host, as *T. cruzi* is an obligate intracellular organism. After cell invasion, the trypomastigotes transform into the rounded amastigote stage displaying a greatly shortened flagellum in comparison with the trypomastigote stage (Brener, 1973). The intracellular amastigote undergoes multiple rounds of cell division in the host cell prior to transforming into bloodstream trypomastigotes. A mixture of trypomastigotes and amastigotes burst out of the infected cell and circulate in the blood, thus propagating the infection, as both the trypomastigotes and amastigotes have been reported to be infectious in murine models and *in vitro* (De Carvalho and de, 1986; Fernandes *et al*., 2013; Ley *et al*., 1988). It is at this point, where a triatomine bug may take a blood meal from an infected host and ingest trypomastigotes. As these parasite pass through the digestive tract of the insect, they transform into the insect exclusive, epimastigote stage. Epimastigotes are unable to infect a mammalian host, as they are inactivated by complement-mediated lysis in humans (Norris, 1998). Epimastigotes undergo division by binary fission in the mid-gut of the triatomine, however a study has also shown genetic exchanges may occur in vitro (Gaunt *et al*., 2003). They then transform back into metacyclic trypomastigotes as they continue through the digestive tract before being excreted in the faeces of these insects, thereby completing the full lifecycle of *T. cruzi*.

1.1.4 Sources of human infection

The main route of infection in humans with this parasite is by the direct exposure of the contaminated insect faeces to broken skin, or the mucosal membranes. Another common source of disease outbreaks can be traced back to the oral ingestion of contaminated food or drink (Alarcon de *et al*., 2010; Bastos *et al*., 2010). Although

these make up the vast majority of cases, alternative routes of infection exist. The first is receiving blood or organs from an infected donor. Infection by blood transfusion has been well documented in the literature, with studies estimating that ~20% of patients receiving infected blood later test positive for Chagas (Fearon *et al*., 2013; Young *et al*., 2007). One study has shown these parasites to be extremely resilient, with the recovery of viable parasites from blood stored at 4 °C after 24 h and cultured cells after 28 days at the same temperature (Martin *et al*., 2014). Transplantation of organs from an infected donor also presents a risk of transmission of the parasite and the disease (2002; 2006; Huprikar *et al*., 2013). Screening of donor organs and blood prior to transplantation greatly reduces this risk[2] (Bern *et al*., 2008; Chin-Hong *et al*., 2011). If infected organs are transplanted, the administration of chemotherapeutic treatment and continual monitoring is recommended. With the continued use of this parasite as a model organism and the screening of blood from infected individuals, there is always the possibility of lab-acquired infection (Hofflin *et al*., 1987; Kinoshita-Yanaga *et al*., 2009). Finally, transmission of the parasite from an infected mother across the placenta into an unborn child can lead to congenital transmission. Overall, children born to infected mothers are estimated to acquire the disease in ~5% of cases, with higher rates observed in countries where the disease in endemic (Cevallos and Hernandez, 2014; Howard *et al*., 2014; Moretti *et al*., 2005).

1.2.1 Chagas disease

Globally it is estimated that there are ~8 million infected individuals worldwide, resulting in at least ~10,000 deaths in 2008 alone (Rassi, Jr. *et al*., 2010; World Health Organization, 2012). The disease itself is separated into the acute and the chronic

---

[2]http://www.fda.gov/downloads/BiologicsBloodVaccines/GuidanceComplianceRegulatoryInformation/Guidances/Blood/UCM235960.pdf
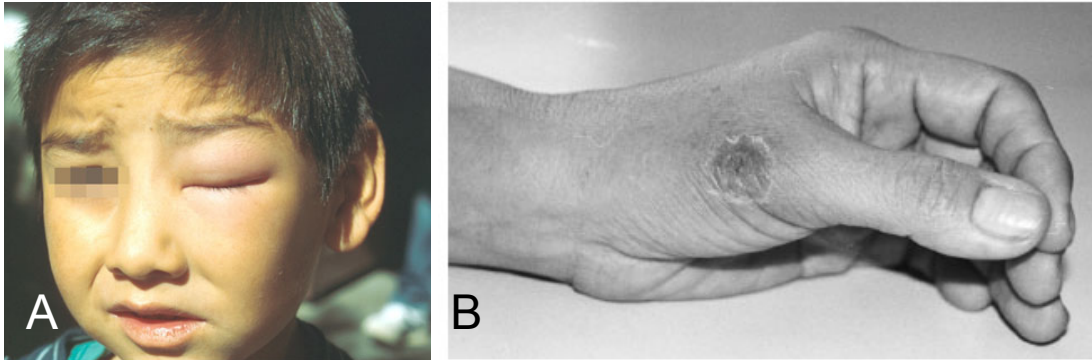
Figure 1.2 Visual symptoms of the acute stage of Chagas disease
(**A**) Romañas sign is a swelling of the tissue surrounding the eye, caused by rubbing parasite-laden faeces into the conjunctival sac. (**B**) A chagoma is an inflamatory lesion found surrounding the point of entry of the parasite. In this case, the cause was a needlestick injury in a lab. Images have been adapted from Muñoz-Saravia, S.G. et al., 2010 and Kinoshita-Yanaga et al., 2009.

stages, separated by an indeterminate phase that can last for many years where patients display no symptoms of the disease.

1.2.1.1 Acute disease

The acute stage of this disease is very short, typically lasting for 4-8 weeks after the initial infection with this parasite (Dias, 1984). This stage of the disease is characterised by high levels of parasitemia in the host, a characteristic that is also observed in animal models of the disease (Brener, 1973). In some cases, patients display one of the two visual signs of infection with this parasite, Romañas sign or a Chagoma (Hemmige *et al*., 2012) (**Figure 1.2**). The first of these is the classic sign associated with this disease and is a swelling around the eyelid caused by rubbing the parasite-containing faeces into the conjunctival tissues. It is important to note that this reaction is not specific and can also be caused by numerous other chemicals and organisms. However, whilst this symptom could be misdiagnosed without a follow-up investigation, two studies have shown Romañas sign to be present in ~50% of acute patients (Anez *et al*., 1999) (Dias, 1984). The second visual symptom, is a skin lesion found around the point of infection that is usually the wound left from where a triatomine bug took a blood meal, however it can also occur at the site of an accidental inoculation (Hofflin *et al*., 1987). While these symptoms can be indicators of infection with this parasite, they are not always present, in as many as 50% of patients (Anez *et al*., 1999) (Dias, 1984). The following non-cutaneous symptoms have also been associated with the acute stage of Chagas disease, fever, nausea, vomiting, muscle pain, headaches, heart failure, hepatomegaly and oedema and diarrhoea (Anez *et al*., 1999; Bastos *et al*., 2010). Despite the number of symptoms caused by the disease, many are mild and non-specific to Chagas disease and ~15% of patients will not display any symptoms of infection (Anez *et al*., 1999).

Whilst the acute disease can occur in adults, there is a higher prevalence of children diagnosed during this stage of the disease with over 60% of cases being reported in 1-5 year olds (Dias *et al*., 1956). A review of acute cases by Dias found an increased severity associated with younger age groups. They observed a 20% mortality rate during the acute stage of patients aged 0-2 years old, decreasing to 0% observed for those older than 11 years (Dias, 1984). Overall, the acute mortality rate reported was 8.3% and 8.6% in a study carried out in the state of Barinas in Venezuela (Parada *et al*., 1997). With the short acute phase and the large range of mild and non-specific symptoms, it is estimated that only ~1% of infected individuals will be diagnosed during this stage (WHO Expert Committee, 2002).

1.2.1.2 Chronic disease

The chronic form of this disease follows the acute stage, but does not appear immediately after the subsidence of the acute symptoms. Instead, there is a latent period ranging from 10-30 years, before an estimated 30% of individuals develop the chronic disease. The remaining 70% of people will remain in the asymptomatic, indeterminate phase for the remainder of their lives. During this phase, the numbers of circulating parasites in the blood significantly decreases (with the exception of HIV positive patients), but those with the indeterminate form will continue to be natural reservoirs of the disease for the rest of their lives (Sartori *et al*., 2002). The symptomatic chronic form is divided into the cardiac or "mega organ" forms; however, they are not mutually exclusive and a small proportion of patients display both forms of the disease. The cardiac form of the disease is the most common symptomatic stage with an estimated 85-90% of patients displaying this pathology (Rassi *et al*., 2010). There are several clinical outcomes for the cardiac disease, ranging from
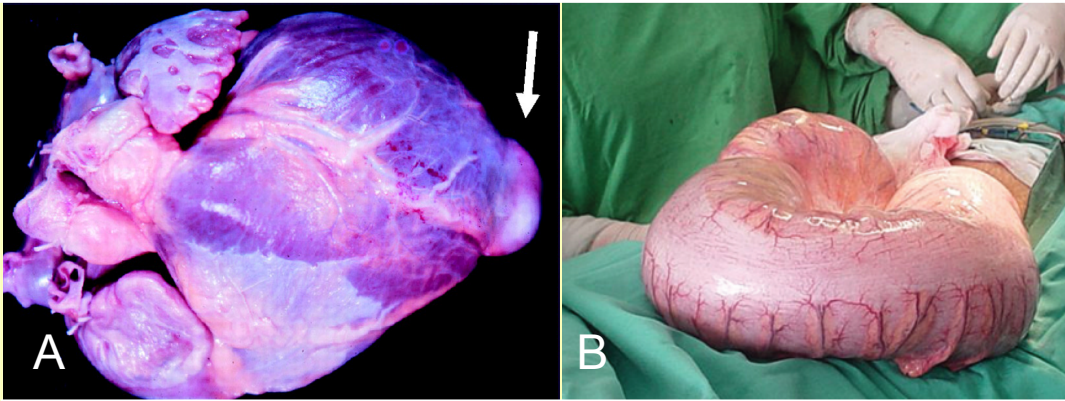
Figure 1.3 Symptoms of the chronic stage of Chagas disease
(**A**) Cardiac failure in a patient that had chronic Chagas disease. Arrow shows cardiac aneurysm (**B**) The megacolon form of chronic chagas disease. Images have been adapted from Muñoz-Saravia, S.G. et al., 2010 and Marin-Neto *et al*,. Heart Disease in Latin America, Circulation. 2007; 115: 1109-1123.

cardiomyopathies (**Figure 1.3A**) to cardiac arrhythmias, leading to cardiac failure and death (Rassi, Jr. *et al*., 2010).

Unlike the cardiac form, the mega organ disease does not affect only one organ, but can affect several points within the digestive system, starting with the oesophagus and ending with the colon (Pinazo *et al*., 2014; Rassi, Jr. *et al*., 2010). Similar to the cardiac disease, parasites or parasite DNA has been detected in diseased organs (Brandariz *et al*., 1995; Marcon *et al*., 2011). Organs with mega disease are found to be massively dilated, in comparison with un-infected organs and experience neuronal loss (**Figure 1.3B**) (da Silveira *et al*., 2007; Figueiredo *et al*., 2000). This enlargement impairs the peristaltic function of these organs leading to dysphagia (difficulty in swallowing) or constipation for the mega oesophagus and mega colon diseases, respectively.

A third form of the disease that is far less common involves the central nervous system, but it does not present on its own, and typically accompanies the cardiac disease. In a handful of cases, reports of *T. cruzi* induced meningoencephalitis has been documented. The majority of cases are in patients with reactivation of Chagas disease or, are infected with the HIV virus leading them to develop acquired immunodeficiency deficiency syndrome (AIDS) (Sartori *et al*., 1998; Sartori *et al*., 2002) (Almeida *et al*., 2010). A review of disease reactivation in AIDS patients has found an involvement with the CNS in 75% of all patients. Studies of patients that have acute forms of meningoencephalitis also found the presence of trypomastigotes in the cerebral spinal fluid (Sartori *et al*., 2002).

For many years, there has been a disagreement about the underlying cause of chronic Chagas disease, with two hypotheses based upon the persistence of the parasite within the host, or the autoimmune theory. It has only been within the past decade that

Estimated global population infected by *Trypanosoma cruzi*, 2009

Legend:
- No estimated cases
- Less than 1,000
- 1,001 - 10,000
- 10,001 - 100,000
- 100,001 - 1,000,000
- 1,000,000 and above
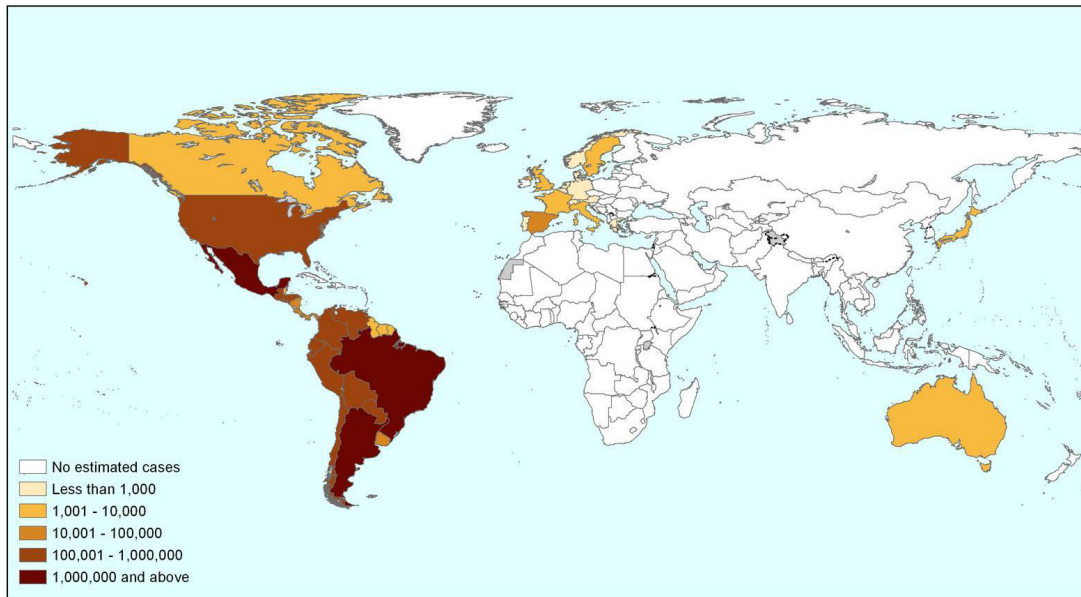
Sources:
1. OPS/HDM/CD/425-06 Estimación cuantitativa de la enfermedad de Chagas en las Américas.
2. Guerri-Guttenberg RA, Grana D.R., Giuseppe Ambrosio, Milei J. Chagasic cardiomyopathy: Europe is not spared! European Heart Journal (2008); 29: 2587-2591.
3. Schmunis. G. A. Epidemiology of Chagas Disease in non-endemic countries: the role of international migration. Mem Inst Oswaldo Cruz, Rio de Janeiro, Vol. 102(Suppl. I): 75-85, 2007.
4. De Ayala A.P. Pérez-Molina J.A., Norman F., and López-Vélez R.Chagasic cardiomyopathy in inmigrants from Latin America to Spain. Emerging Infectious Disease Volume 15, Number 4–April 2009.
5. According to the numbers of inmigrants registered for 2007in the website of the Japanese Ministry of Justice and estimated seroprevalence for non endemic countries according to
Paricio-Talayero J.M. Vigilancia epidemiológica de la transmisión vertical de la enfermedad de Chagas en tres maternidades de la Comunidad Valenciana. Enferm Infecc Microbiol Clin 2008;26(10):609-13.

Figure 1.4 Worldwide distribution of Chagas disease
A map showing the estimated, worldwide distribution of infected individuals. This figure has been adapted from
http://thehealthcoach1.com/wp-content/uploads/2012/06/MapChagasJun09_large.jpg.

the organ damage caused has become increasingly understood to involve both mechanisms (Girones and Fresno, 2003; Gutierrez *et al*., 2009). It has been demonstrated in both murine models and in humans that parasites persist during the chronic infection, despite the lack of circulating parasites, see reviews (Marcon *et al*., 2011; Tarleton, 2003). The majority of studies have detected parasite DNA in the cardiac, skeletal and smooth muscle cells, although, on the basis of murine models, amastigotes have also been found to reside in adipocytes both in culture and in adipose tissue (Combs *et al*., 2005; Ferreira *et al*., 2011). The latter authors noted that the pathogenic organisms *Rickettsia prowazekii* and *Mycobacterium tuberculosis* are also able to persist in adipose tissue, which has been suggested as a potential reservoir for the former species. The identification of parasites in human adipose tissue raises the possibility that adipocytes may play an important role in the pathology and persistence of these parasites in the chronic disease.

1.2.2 **Worldwide distribution of the disease and association with poverty**

Due to the primary nature of transmission, Chagas disease is mainly localised to the Latin American countries where the triatomine bugs are present (**Figure 1.4**). However, due to the increased economic and social mobility of individuals, the disease has been identified in countries that have no sylvatic cycle, or insect vectors to transmit the disease (Gascon *et al*., 2010; Schmunis, 2007). There have been multiple studies carried out over the years to estimate the prevalence of Chagas disease in the migrant populations, in non-endemic populations. In Spain, the Latin American migrant population is estimated to account for 3.85% of the total population of the country[3]. A study carried out at a treatment centre in Barcelona identified that 2.87% of Latin

---

[3] http://www.ine.es/en/prensa/np854_en.pdf

American individuals had a chronic form of Chagas disease with 19% of those patients displaying cardiac or cardiodigestive forms of the disease (Roca *et al*., 2011).

1.2.3 Economic burden of the disease

The chronic stage of this disease does not have the same high levels of morbidity and mortality associated with other neglected diseases such as malaria. Nonetheless, the global burden of this disease has been calculated to be in the region of 7.2 billion dollars per annum, which is higher than the similar costs of other disease such as cervical cancer and Lyme disease (Lee *et al*., 2013). As expected, the highest cost of this disease was predicted to be in Latin American countries even when taking into account the lower treatment costs compared with North America and Europe. Despite this massive economic burden, there has been little progress in developing new, safer and more effective drugs to treat this disease.

1.2.4 Vector control to combat Chagas disease

Since vector-born transmission accounts for the majority of cases, there have been several attempts to interrupt the transmission of this parasite by eliminating the insects that transmit the disease. The governments of six countries (Argentina, Bolivia, Brazil, Chile, Paraguay and Uruguay) formed a coalition called the southern cone initiative (SCI) with the aim of eradicating the main vector of the disease, *Triatoma infestans* (Schofield and Dias, 1999). The Andean initiative and central American initiatives were also set up to combat the transmission of the disease by similar methods (1998; Guhl, 2007). The success of the SCI has been demonstrated on multiple levels, with the interruption of transmission in multiple countries (World Health Organization, 1998; World Health Organization, 2000a; World Health Organization, 2000b). This resulted

in a decreased number of infected individuals (~70% reduction) identified across the countries monitored by the randomised screening (Dias, 2007; Moncayo, 2003). In particular, Brazil has reported savings of $17 for every $1 spent on their vector elimination program (Moncayo, 2003). Despite having interrupted transmission in multiple countries, this approach requires continued treatment and monitoring by the countries involved due to the presence of a sylvatic lifecycle (Apt *et al*., 1987; Navin *et al*., 1985). Even if the insect vectors could be completely eradicated, it is likely that this disease will continue to be a major health problem in Latin America for many decades to come due to the long incubation period before the appearance of the chronic disease (*Section 1.2.1.2*)

1.2.5 Immune response to infection with *T. cruzi*

Studies have shown that both innate and adaptive immune responses play a role in the control of *T. cruzi* infection. It is the later that scientists hope to exploit to produce a successful vaccine capable of providing protective immunity (*Section 1.2.6*). It has been shown experimentally that parasite antigens are able to elicit the activation of natural killer cells which produce interferon (IFN)γ after stimulation by interleukin 2 (Basso, 2013). The subsequent increase in nitric oxide production has been shown to be important in the control of parasitemia. A study has found in increase in parasitemia and mortality of infected mice when the production of nitric oxide is inhibited (Vespa *et al*., 1994). Treatment of parasites with a S-nitroso-acetyl-penicillamine, which is a nitric oxide donor was found to directly kill parasites *in vitro* suggesting that nitric oxide is an important component of the innate immune response for controlling parasitemia.

1.2.6 Vaccination as a strategy against Chagas disease

In addition, to vector control and the chemotherapeutic treatment (***Section 1.3.2***) programs that currently are in operation, there have been multiple labs looking into the development of a vaccine. The underlying hypothesis behind this approach is that by controlling the parasite load it may subsequently lead to a reduction in, or control of the tissue damage caused by the parasite (Quijano-Hernandez and Dumonteil, 2011; Vazquez-Chagoyan *et al*., 2011). One study has shown a protective effect against the cardiac damage caused by infection with the parasite in a murine model when the mice were pre-immunised with a DNA-prime/MVA-boost vaccine (Gupta and Garg, 2013). However, despite a considerable amount of work that has been reported over the years, there has yet to be a vaccine to make it into clinical trials in humans. There are several challenges that need to be addressed in order to produce a successful treatment. Firstly, it would need to target the extracellular trypomastigote and intracellular stages in order to be fully effective. Secondly, there is a large diversity in the different strains of this parasite (Zingales *et al*., 2009), so a vaccine would need to be effective across multiple strains from the different DTU's.

1.3 Diagnosis and treatment of Chagas disease

1.3.1 Diagnosis

One of the major challenges facing the development of new drugs and the eradication of this disease is a lack of knowledge of suitable diagnostic markers for the eradication of the parasite (Andrade *et al*., 2011). Over the years, many different methods have been developed for assessing infection, by observing the parasite directly, indirectly or the causative effects of the parasites presence. Xenodiagnosis and haemoculture both observe the parasite by microscopy, but they have drawback that they are not very

sensitive, becoming less effective at monitoring the chronic disease where the numbers of circulating parasites decreases. PCR and serological diagnosis methodologies offer greater sensitivities, at the cost of providing conflicting results. It has been well documented in the literature that patients can remain seropositive, but are negative by PCR (Pinazo *et al*., 2010). It is recommended that diagnosis is confirmed using two serological tests, with a mixture of PCR and serology being used in clinical assessment of treatments (Chin-Hong *et al*., 2011; deAndrade *et al*., 1996; Kinoshita-Yanaga *et al*., 2009).

1.3.2 Current drugs

Currently, nifurtimox (Lampit, Bayer) and benznidazole (Roche, LAFEPE) are the only two approved drugs available for the treatment of Chagas disease. These nitro-aromatic compounds were identified in the 1960's and 70's by a phenotypic approach and are derivatives of 5-nitrofuran and 2-nitroimidazole scaffolds. Early mechanism of action studies of these compounds found that treated parasites generated reactive oxygen species. Further studies identified that the functional nitro-groups of these drugs undergo a one or two electron reduction (Docampo *et al*., 1981; Docampo and Moreno, 1984; Docampo and Moreno, 1986; Docampo and Stoppani, 1979; Koder *et al*., 2002; Roldan *et al*., 2008; Wilkinson *et al*., 2008). It was initially thought that these drugs exerted their anti-parasitic effects by causing oxidative stress, however more recent studies suggested that the mechanism may involve the modification of DNA, lipids and proteins by drug metabolites (Diaz-de-Toranzo *et al*., 1988; Maya *et al*., 2007). A recent metabolomics study carried out by Trochine has identified a variety of benznidazole metabolites formed by treatment of *T. cruzi* with this drug (Trochine *et*

Table 1.1 Summary of the current clinical drugs available for the treatment of both acute and chronic Chagas disease.

Drugs	Benznidazole and Nifurtimox
Acute stage efficacy	~70% cure
Chronic stage efficacy	~8% when treated with benznidazole (Cancado, 2002)
Side effects	Skin irritation
	Headaches
	Nausea
	Vomiting
Cessation of treatment	In as many as 30% of patients treated with either drug

al., 2014). Several of these metabolites were identified as adducts of major low molecular weight thiols from the parasite, namely, trypanothione and glutathione.

Although approved for the treatment of Chagas disease, both drugs have a range of attributes that make them far from ideal treatments for this disease (Table 1.1). If diagnosed during the acute stage of infection the cure rates for both drugs are in the region of 60-80% in children and adults depending on study and location (Cancado, 2002; Urbina and Docampo, 2003). The efficacy of treatment significantly decreases throughout the progression of the disease, producing parasitological cures in 8-30% of treated, chronic stage individuals (Cancado, 2002; WHO Expert Committee, 2002). The treatment regimens for both drugs are long, lasting 30-60 or 60-90 days for benznidazole and nifurtimox respectively. However, aside from this and poor efficacy against the chronic stage, both drugs have been reported to have a high incidence of toxic side effects that are associated with their use. Symptoms can include nausea, vomiting, skin irritations, central nervous system depression and fever (Hasslocher-Moreno *et al*., 2012; Jackson *et al*., 2010). These side effects can ultimately lead to the interruption or discontinuation of treatment in up to 30% of patients (Hasslocher-Moreno *et al*., 2012; Jackson *et al*., 2010). A lower occurrence of adverse reactions has been observed when treating infants and children, where these drugs are better tolerated (Altcheh *et al*., 2011). Current guidelines suggest that the drugs are prescribed for patients in the acute phase or the early chronic stage, which as the majority of individuals are diagnosed in the chronic stages makes these both poor but the only options for treatment of their disease.

As is the case with all drugs used in the clinic, there is always the danger of resistance to the drug generated with its use in the field. Studies of these drugs found naturally occurring resistance to both nifurtimox and benznidazole in some strains but

not others (Filardi and Brener, 1987; Neal and van Bueren, 1988). The extent of this natural resistance to these drugs also varied strain by strain, however, almost all strains were found to be cross-resistant to both drugs demonstrating their similar mode of action (Filardi and Brener, 1987). In *T. cruzi*, two genes in particular have been associated with resistance to these nitro drugs, a type I nitroreductase and prostaglandin F2α synthase also known as old yellow enzyme (Mejia-Jaramillo *et al*., 2011; Murta *et al*., 2006). Loss of a single allele of NTR in *T. cruzi*, confers resistance to both drugs (Wilkinson *et al*., 2008). This observed cross-resistance highlights the problem with multiple clinical candidates that have the same mode of action, as resistance to the first drug can render the second drug completely inactive.

1.3.3 An overview of the current clinical pipeline for Chagas disease

Although the curative rate of benznidazole against the chronic stage is far from desirable, a large clinical trial has been underway since 2009 (Set to conclude in 2014) to investigate the potential benefits of the continued treatment with this drug (Marin-Neto *et al*., 2009). The logic underpinning this study is that in chronically infected animal models, the continued treatment with either of the current drugs reduces the cardiac damage in these mice and simultaneously reduces both the number of circulating parasites and serological titres (Garcia *et al*., 2005; Molina-Berrios *et al*., 2013). If proved a success, the results of this trial may shape the future way that the chronic disease is treated, as this drug is not consistently prescribed during the chronic stage of infection. However, this would be more of a life prolonging or improving treatment rather than a cure for the chronic disease, similar to the treatment of HIV[+] individuals.

The lanosterol 14α-demethylase inhibitors Posaconazole (Schering-plough) and E1224 (ESAI) are both in phase II assessment for the treatment of the asymptomatic disease[4]. A recent report had described the successful use of posaconazole, after treatment with benznidazole failed to cure a woman of the chronic disease (Pinazo *et al.*, 2010). Despite the co-administration with immunosuppressive therapies to treat her systemic Lupus, follow up examinations by diagnostic PCR revealed no parasite DNA detectable in the circulating blood, despite antibody titres remaining high throughout the follow up period. This continued pattern of positive serological tests has been seen elsewhere where a patient is deemed to be cured, so the patient in the study was considered to have been cured using the PCR results alone. Despite the apparent success of treatment in this case, the result of which has underpinned its clinical assessment. The cost of treatment was reported to be ~£8000 making it highly unsuitable for the mass treatment of patients in endemic areas due to the high costs (Clayton, 2010; Pinazo *et al.*, 2010). A recent clinical trial of posaconazole found the treatment failure of benznidazole to be ~6%, whereas failure rates of 90% and 80% were observed in those treated with the low and highest possible doses of this drug, respectively (Molina *et al.*, 2014). The authors of this study note that whilst negative PCR tests observed for all patients in the trial after 14 days of treatment with either drug, two patients receiving the low dose of posaconazole had reverted to positive PCR results by the 60th day of treatment. Follow up studies found patients treated with the low dose, to revert to seropositive significantly earlier than those receiving the high-dose, however benznidazole was clearly the more effective drug in the study.

Ravuconazole, a pro-drug also known as E1224 has also been assessed for use in the treatment of Chagas disease. This drug has the benefit of being cheaper to produce than posaconazole whilst maintaining anti-parasitic activity in animal models (Diniz *et*

---

[4] **http://clinicaltrials.gov NCT01162967 and NCT01489228**

al., 2010; Urbina *et al*., 2003). However, it was recently announced that E1224 had failed its clinical assessment as a monotherapy. Despite its potency in suppressing the parasitic loads in patients, the suppression was not permanent[5]. As a result, E1224 is going to be re-assessed as a dual therapy treatment for this disease with an as yet, unnamed partner drug[5]. Despite both posaconazole and E1224 producing extremely promising results in the murine models of the disease, these CYP51 inhibitors have failed be curative in human disease, the underlying cause of which remains unknown (Molina *et al*., 2014; Urbina *et al*., 2003) .

The Drugs for Neglected Diseases initiative (DNDi) reports two molecules in pre-clinical development, K-777 a cruzipain inhibitor and Fenarimol the mechanism of which is currently unknown[6]. The nitro-drugs fexinidazole and VL-2098 are currently being studied for Chagas disease with the aim of progressing them as clinical candidates[7] (Bahia *et al*., 2012). Perhaps the major concern with pursuing another nitro drug for the clinical portfolio is naturally occurring resistance to the current drugs, in particular fexinidazole whose mechanism of action has been demonstrated to be nitro-reductase dependent in *L. donovani* (Wyllie *et al*., 2012).

Since the introduction of benznidazole and nifurtimox into the clinic for the treatment of Chagas disease, the therapeutic pipeline has remained virtually unchanged until very recently. There are clear advantages with to a drug-repurposing strategy, such as greatly reduced costs, known pharmacokinetic profiles of the compound and safety profiles established in Phase I trials (Sardana *et al*., 2011). This strategy is becoming more commonplace in the pharmaceutical industry, with 30% of drugs registered with the FDA in 2009 having been repositioned (Sardana *et al*., 2011).

---

[5] http://www.dndi.org/media-centre/press-releases/1700-e1224.html
[6] http://www.dndi.org/diseases-projects/portfolio.html
[7] http://www.dndi.org/diseases-projects/portfolio/nitroimidazole-chagas.html

Whilst this tactic has successfully been used to produce drugs for the clinical treatment of various parasitic diseases, there has yet to be a successful anti-*T. cruzi* drug produced by this strategy.

1.3.4 Pathways known to be essential in *T. cruzi*

With high cost and project attrition rates reported by the pharmaceutical industry, the validation of potential drug targets is considered vital before embarking on any drug discovery project (Frearson *et al*., 2007). In recent years, multiple studies have identified key biological pathways in *T. cruzi*. For instance, the type I nitroreductase that is involved with the activation of the current clinical drugs has been demonstrated to be essential for virulence in *Trypanosoma cruzi*, as the loss of both functional copies of *Tc*NTR produced a severe virulence defect (Mejia *et al*., 2012; Wilkinson *et al*., 2008).

Ergosterol is a derivative of the classic steroid ring first and is notably absent from humans. In fungi, it plays in important role and is found in the membranes of these organisms (Iwaki *et al*., 2008; Zhang *et al*., 2010). Treatment of *T. cruzi* with inhibitors of lanosterol 14a demethylase (CYP51) led to an increase in the cellular levels of C-14-methyl sterols (Doyle *et al*., 2010; Urbina *et al*., 1998). The biological effect of one inhibitor reduced or abolished the ability of *T. cruzi* epimastigote and amastigotes to proliferate *in vitro* (Goad *et al*., 1989). In a murine model of Chagas disease, treatment with the CYP51 inhibitor posaconazole was able to cure between 60-75% of chronic stage model mice 177 days after infection (Urbina *et al*., 1998). In the acute model, the parasitological cure rates were between 90-100%. The reduced effectiveness of this drug against the chronic disease is similar to what is observed with the current drugs. Posaconazole and a related inhibitor E1224 have been clinically

assessed for the treatment of chronic Chagas disease (***Section 1.3.3***). It is also of note itraconazole, another CYP51 inhibitor, has been used in experimental models of Chagas disease and in patients with varying success (Apt *et al*., 2013; Apt *et al*., 2005; Moreira *et al*., 1992). However, 20 years after itraconazole treatment, only 32% of individuals were deemed to be cured, based on ECG examination (Apt *et al*., 2013).

Squalene synthase (SQS) catalyses the first committed step of the biosynthesis of ergosterol in *T. cruzi* thus making this enzyme a potential drug target in this parasite. Several studies have assessed this enzyme for the potential treatment of Chagas disease and inhibitors capable of the *in vitro* eradication of intracellular parasites developed (Lorente *et al*., 2005; Urbina *et al*., 2002). Two of these inhibitors that target *Tc*SQS, E5700 and ER-119884, although found to be potent against the parasites in culture, only E5700 maintained a protective effect against the acute stage model of the murine disease (Urbina *et al*., 2004). The other inhibitor was only able to provide partial protection against the disease.

The majority of studies focusing on essential processes in *T. cruzi* are assessed in the insect stage of the parasite. However, this overlooks fact that this in an obligate intracellular organism in the mammalian stage. An alternative approach to assessing important pathways for the growth of these parasites in infected cells, is by the genome-wide RNAi knockdown of host cell genes that has been reported by the Burleigh lab. These studies have identified a number of cellular process that are required for the invasion and replication of these parasites within mammalian cells (Caradonna *et al*., 2013). Specifically the host Akt kinase was found to play an essential role in the proliferation of intracellular amastigotes. An earlier study has found the expression of Akt to be up regulated in Vero cells when treated with membranes prepared from trypomastigotes (Wilkowsky *et al*., 2001). It is also known that this enzyme is a

downstream target of phosphatydilinositol 3-kinase (PI3K) and treating mammalian cells with PI3K inhibitors reduces the ability of trypomastigotes to invade these cells, however does not completely abolish infection. Interestingly, this increased expression of Akt due to parasite infection leads to the inhibition of pro-apoptocic genes at the transcriptional level (Chuenkova and PereiraPerrin, 2009). The results of this study suggest that Akt may play an important role in the survival of the host cell during high parasite burden. Clearly, further work is required to determine if Akt is a valid and druggable target as a cure for this disease, which may be further complicated by the variety of cellular types that these parasites can invade.

The major cysteine protease in *T. cruzi*, known as cruzain has been shown to be a druggable target in this parasite (Engel *et al*., 1998b). The inhibitor K777 has is currently being progressed through the clinical pipeline for assessment against Chagas disease (***Section 1.3.3***). Several studies of various inhibitors against murine models of this disease have shown these inhibitors to be highly effective at prolonging life and in one case show better protection than benznidazole (Doyle *et al*., 2007; Engel *et al*., 1998a; Ndao *et al*., 2014).

1.4 Fatty acylation

The fatty acylation of proteins represents one of the most diverse groups of protein modifications known to occur. Acylated proteins have been identified in eukaryotes bacteria and archaea (Pugh and Kates, 1994; Thao *et al*., 2010). These co- and post-translational modifications include the addition of fatty acids of various chain lengths, ranging from 2-20 carbons onto specific amino acids of proteins (Ali *et al*., 1990; Herriott, 1935) (Mattoo *et al*., 1989).

1.4.1 *N*-myristoylation

Originally, several groups identified myristoylation to occur in eukaryotic cells and was found to specifically modify multiple proteins (Schlesinger *et al*., 1980). Studies by Magee et al identified that in cultured eukaryotic cell lines, these modifications appeared to fall into one of two categories (Magee and Courtneidge, 1985). In the first type, all proteins labelled with palmitic acid were found to be sensitive to treatment with hydroxylamine, indicating their attachment via the side chain of a cysteine residue originally postulated (Magee *et al*., 1984). The second type of labelling was found in [^{3}H]-myristic acid labelled cells where several proteins were found to be resistant to hydroxylamine and alkali treatment suggesting that myristic acid was attached by an amide bond. These studies also suggested the existence of dually acylated proteins, a hypothesis that has since been confirmed by multiple labs for numerous different proteins (Denny *et al*., 2000; Galbiati *et al*., 1999; Godsel and Engman, 1999; Hertz-Fowler *et al*., 2001a; Mills *et al*., 2007). An original study demonstrated that *N*-myristoylation in eukaryotes was tightly coupled to protein synthesis (Buss *et al*., 1984). However, it has only been in recent years that post-translational *N*-myristoylation has been identified. The first to be discovered was the pro-apoptotic protein BID, which was found to undergo caspase 8-mediated cleavage exposing an internal glycine for *N*-myristoylation (Zha *et al*., 2000). Subsequent studies have found many more proteins that undergo post-translational modification after proteolytic processing by a caspase (Martin *et al*., 2012; Martin *et al*., 2008; Perinpanayagam *et al*., 2013; Sakurai and Utsumi, 2006; Vilas *et al*., 2006). It would appear that the post-translational modification is involved in the apoptotic pathway, a pathway that that trypanosomes most notably lack, however, there have been several reports of an apoptosis-like process in these parasites (Ameisen *et al*., 1995; Irigoin *et al*., 2009; Jimenez *et al*., 2008; Piacenza *et al*., 2007).

However, the hypothesised function of this lipid modification has been reported to vary depending upon protein. The increased hydrophobicity of modified proteins is known to help promote membrane association and plays a role in the correct subcellular localisation of multiple proteins that have been studied to date (Lee and Shaw, 2008; Lu and Hrabak, 2013; Maric *et al*., 2011; Martins *et al*., 2010; Robbins *et al*., 1995; Sahin *et al*., 2008; Wingard *et al*., 2008). Another aspect of myristoylation identified that for some proteins the presence of myristate is found to enhance their binding to membranes, particularly in Ca^{2+} binding proteins such as recoverin (Desmeules *et al*., 2002). Nuclear magnetic resonance studies of recoverin have identified that in the absence of calcium, the myristoyl group is sequestered into a hydrophobic pocket and is solvent accessible in the calcium bound form (Ames *et al*., 2000). This activation has also been described as a myristoyl-switch, in that an external factor affects the affinity of the protein for a membrane such as calcium, leading to a conformation change in the protein. However, this is not simply limited to calcium binding proteins, as glucose levels have been reported to affect the myristoyl mediated membrane localisation of the ß-subunit of AMP activated protein kinase (Oakhill *et al*., 2010). These studies have shown that the *N*-myristoylation of proteins does not automatically lead to an increased membrane association on its own, but can be dependent upon the metabolic state of the cell. Interestingly, localisation studies of fusion proteins has revealed that there are other factors of the protein that play a role in the correct localisation of these proteins, such as palmitoylation (Godsel and Engman, 1999; Oakhill *et al*., 2010). There have also been several reports of cancerous cells having higher levels of NMT expression than their non-cancerous counterparts do (Selvakumar and Sharma, 2007; Shrivastav *et al*., 2007).
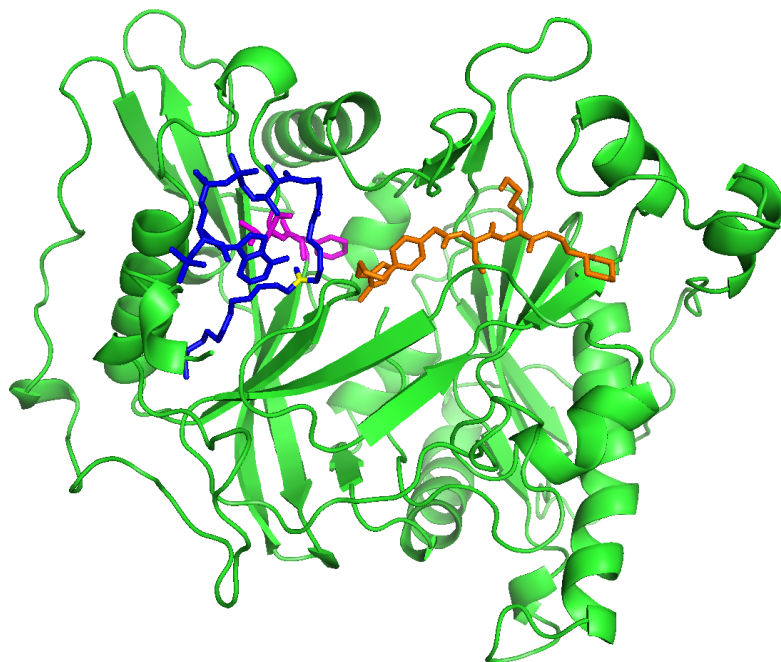
Figure 1.5 Structure of NMT with bound analogs of substrates

The structure of NMT from *S. cerevisiae* (PDB accession: 2NMT) with the Myr-CoA analog, *S*-(2-oxo)pentadecyl-CoA bound to the active site (blue). The residues that form the oxyanion hole have been highlighted in magenta, with the carbonyl bond that would be depolarised marked in yellow. A peptide analog is shown in orange.

1.4.2 *N*-myristoyltransferase

The enzyme that catalyses the addition of myristic acid onto the *N*-terminal glycine, *N*-myristoyltransferase (EC 2.3.1.97) was first purified to homogeneity from *Saccharomyces cerevisiae* (Towler *et al*., 1987). Kinetic characterisation of this enzyme has found it to have an ordered bi-bi mechanism, in which myristoyl-CoA binds before the peptide substrate (**Figure 1.5A**). After catalysis, CoA is released prior to the *N*-myristoylated peptide (Rocque *et al*., 1993; Rudnick *et al*., 1991). The structures of NMT from multiple species have been solved by X-ray crystallography (Bhatnagar *et al*., 1998; Brannigan *et al*., 2010; Farazi *et al*., 2001; Goncalves *et al*., 2012b; Sogabe *et al*., 2002). The *S. cerevisiae* enzyme structure has been solved in complex with a non-hydrolysable myristic acid analog known as S-(2-oxo)pentadecylCoA, with the region corresponding to the thioester bond of Myr-CoA positioned within the oxyanion hole formed by phenylalanine and leucine (Figure 1.5) (Bhatnagar *et al*., 1998). This was confirmed with Myr-CoA NMT binary complex solved 3 years later (Farazi *et al*., 2001). The transfer of the acyl group onto the N-terminal glycine of the peptide occurs via a nucleophilic addition elimination reaction (Bhatnagar *et al*., 1998; Farazi *et al*., 2001). The oxyanion hole partially polarises the c1 carbonyl group of myristate making it susceptible to nucleophilic attack with the oxygen hydrogen bonding with the oxyanion hole residues. The N-terminal ammonium group of the peptide substrate is de-protonated to an amine by a basic residue in the active site. This amine attacks the carbonyl of Myr-CoA (nucleophilic attack) forming a stabilised reaction intermediate, followed by the release of CoA and the myristoylated peptide (Bhatnagar 1998).

The homologs from *Plasmodium sp*., *Leishania major*, *Homo sapiens* and *T. brucei* have since been expressed and purified as recombinant fusion proteins from *E.*

coli (Brannigan *et al*., 2010; Frearson *et al*., 2010; Panethymitaki *et al*., 2006). The mass of all NMTs characterised to date range between 46-60 kDa, and with the exception of bovine brain NMT, are monomeric (Bhatnagar *et al*., 1997; Glover and Felsted, 1995; Sogabe *et al*., 2002; Towler *et al*., 1987). All of these enzymes preferentially utilise myristoyl-CoA (Myr-CoA) as the acyl-donor for the reaction. Several studies have probed the lipid specificity of NMT, by altering the chain, by substituting atoms and by testing the effects of unsaturated fatty acids (Devadas *et al*., 1992; Heuckeroth *et al*., 1988; Heuckeroth *et al*., 1990; Kishore *et al*., 1993). A number of studies have shown a level of divergence in the peptide substrates recognised by the different homologs, with much larger difference observed between higher and lower eukaryotes (Towler *et al*., 1988; Traverso *et al*., 2013). However, the majority of substrates of each enzyme conform to the consensus *N*-myristoylation motif below.

M-G-X-X-X-S-K-X

The majority of studies to date have reported *N*-myristoylation to be a uniquely eukaryotic process; however, several pathogenic bacteria have been found to have *N*-myristoylated proteins reviewed (Maurer-Stroh and Eisenhaber, 2004). The proteins identified are secreted into a host plant cell undergoing *N*-myristoylation by the host's NMT (Nimchuk *et al*., 2000). More recently an enzyme with *N*-myristoyltransferase activity has been identified from *Pseudomonas aeruginosa* (Jyomoto *et al*., 2006). This bacterial enzyme is unrelated to eukaryotic NMTs and is unusual in that it does not require CoA for the transfer of myristic acid onto an octapeptide (Islam *et al*., 2008). In addition the enzyme could catalyse the transfer of myristic acid onto the alanine of a G2A mutant peptide, an activity not yet reported for the eukaryotic enzyme.

The genetic requirement for this enzyme has been assessed in multiple eukaryotic organisms studied to date.

1.4.3 NMT as a potential chemotherapeutic target

Despite these enzymes catalysing the same biochemical reaction, the diverse peptide substrate specificities of different NMT homologs have made them promising targets for rational drug design. The first selective inhibitors generated were peptide mimics of known substrates for the enzyme and designed to target NMT from the pathogenic fungi *Candida albicans* (Devadas *et al*., 1997; Devadas *et al*., 1995). Using this approach of targeting the peptide binding pocket has allowed the generation of highly specific NMT inhibitors with selectivity over the human isoforms of greater than 560-fold. In recent years there have been several high-throughput inhibitor screening programs undertaken against the NMT homologs from *Plasmodium spp.*, *Trypanosoma brucei* and *Leismania major* (Bell *et al*., 2012; Frearson *et al*., 2010; Goncalves *et al*., 2012b). As a result, there have been many highly selective and species-specific inhibitors of recombinant NMT's developed from a large range of chemical scaffolds (Zhao and Ma, 2014). A screen of compounds at the University of Dundee Drug Discovery Unit (DDU) against *T. brucei* NMT identified a hit that was further optimised, leading to the development of the inhibitor DDD85646 (Frearson *et al*., 2010). This compound was identified to be a competitive inhibitor of the peptide binding site of *Tb*NMT, with the presence of Myr-CoA increasing the affinity of the inhibitor for the enzyme by 33-fold to a k_d of 1 nM. This site of binding was confirmed by the co-crystalisation of DDD85646 and Myr-CoA into the *L. major* NMT protein crystal. This pyrazole sulfonamide inhibitor was found to be highly potent against parasites in axenic culture, with an EC_{50} value of 2.1 nM, increasing to 16.6 nM with the overxpression of NMT in the parasites

demonstrating that the inhibitor was targeting the enzyme in the parasite. Despite the high potency of DDD85646 against the parasite, at the enzyme level, the inhibitor was only 2-fold more potent against *Tb*NMT than *Hs*NMT. However, at the cellular level DDD85646 did not maintain its potency against the human derrived MRC5 cell line, finding the inhibitor to be 200-fold less potent than agaist the parasite. This compound was found to be highly efficacious in the murine model of the disease, curing all mice infected with the non clininically relevant strain *T. brucei brucei* with as little as 12.5 mg kg^{-1} over 4 days of treatment. The clinically relevant *rhodeinse* strain was more resiliant, requiring 50 mg kg^{-1} over a period of 4 days, which the authors note is not due to a reduced potency of the inhibitor against the parasite, but is more likeley due to the distribution of the parasite in the host.. Whilst this inhibitor is successful against the acute stage of the disease, the chances of the current series of compounds to treat the second stage after the parasite has crossed the blood-brain barrier is markedly lower. This is due to the compounds being unable to cross this barrier into the brain with to any great level in addition to poor selectivity between the human and parasite enzymes (Brand *et al*., 2012). In summary, these works have demonstrated that NMT is a druggable target in the African trypansome, despite requiring further optimisation to develop it as a suitable drug target.

1.5 Aims

As there is a current inequality between the worldwide burden caused by this disease and the current clinical portfolio, the aim of my project is to assess the suitability of potential drug targets in *Trypanozoma cruzi*. The enzyme selected for this study is the enzyme *N*-myristoyltransferase. Specifically, we aim to investigate if NMT is essential for the survival of this parasite. If found to be essential, the full characterisation of the

enzyme will be undertaken to assess its suitability as a potential drug target against *T. cruzi*. This study is carried out with the aim of assessing if *Tc*NMT may be a druggable target in *T. cruzi* to treat Chagas disease.

Chapter 2

Materials and methods

2.1 Materials

All reagents, enzymes and chemicals used in this study were of the highest grade and purity available from commercial companies.

2.2 Parasite culture and genetic manipulation

2.2.1 Epimastigotes

T. cruzi epimastigotes of the strain Silvio X10/7 (MHOM/BR/78/Silvio; clone X10/7) (Silveira *et al*., 1979) were routinely grown at 28 $^\circ$C in sealed flaks with RTH/FBS (RPMI 1640 supplemented with 4.9 g L^{-1} trypticase, 10 mg l^{-1} haemin, 50mM HEPES pH 7.4 and 10% heat inactivated foetal calf serum (FBS, PAA) (Hunter *et al*., 1994) . The clone Silvio X10/7A was isolated by limiting dilution and was used in the subsequent experiments. Epimastigotes were routinely sub-cultured every 3-4 days from a density of ~1 $\times$ 10^7 cells ml^{-1} to ~ 1 $\times$ 10^5 cells ml^{-1} into fresh medium.

For SILAC studies, parasites were first adapted for growth in SDM-79 medium by gradually replacing RTH/FBS with the new medium over 10 sequential subcultures (Brun and Schonenberger, 1979; Greig *et al*., 2009). SDM-79 medium depleted of L-arginine, L-lysine and 10% FBS was first reconstituted with either light (R0K0) or heavy (R6K4) labelled isotopes of these amino acids at the same concentration described in the original formulation (L-arginine.HCl U^{13}-C6, L-lysine.2HCl 4,4,5,5-D4, CK Gas Products). Prior to sterile filtration (0.22 µm), the medium was futher supplimented with 100 µM putrescence in addition to 10% FBS that had been heat inactivated and dialysed (PAA).

2.2.2 Vero cells

Confluent Vero cell (*Cercopithecus aethiops* kidney cells, ATCC® CCL-81™) monolayers were detached from culture flasks by treatment with 1 × trypsin EDTA (GIBCO) for 10 mins at 37 °C (Ammerman *et al*., 2008). The resulting suspension of cells was diluted with an equal volume of Dulbecco's Modified Eagle Medium supplemented with 10% heat inactivated FBS (DMEM/FBS) and the cells harvested by centrifugation (200 × g, 5 min, RT). Harvested cells were then resuspended in the original volume of DMEM/FBS and diluted 1 in 10, into a new flask containing fresh medium and incubated at 37 °C with 5% CO_2 in a humidified incubator. Vero cells were routinely sub-cultured as described every 3-4 days when the monolayer reached 90% confluence.

2.2.3 Trypomastigote infection

The differentiation of *T. cruzi* epimastigotes into the infectious trypomastigote forms has been reported in the literature (Figueiredo *et al*., 2000). A mixed population of epimastigotes and metacyclic trypomastigotes derived from a 7-9 day old culture were washed in twice in PBS before resuspending in DMEM/FBS. Vero cell infections were set up by overlaying a monolayer with parasites at a multiplicity of infection (MOI) of 10:1. The infected monolayer was subsequently washed with PBS to remove free-swimming parasites and overlaid with fresh DMEM/FBS. After 5-7 day incubation, trypomastigotes released from infected cells were recovered and used to infect a fresh Vero monolayer.

2.2.3 Purification of *T. cruzi* amastigotes

Amastigotes were purified from a mixed population of trypomastigotes and amastigotes released from infected Vero cell monolayers (Marques *et al*., 2011). Briefly, parasites were collected by centrifugation (10 min, RT, 4000 × g) and the pellet was overlaid with DMEM/FBS and incubated for 3 h at 37 ^{o}C. Motile trypomastigotes released into the supernatant were removed and the pellet was resuspended in DMEM/FBS. This process was repeated two to three times to produce a homogenous population of amastigotes (~95%).

2.2.4 Quantifying the infectivity of transgenic parasites

Transgenic parasites were left to infect Vero cell monolayers overnight with an MOI of 5:1 (***Section 2.2.3***). Extracellular parasites were removed by extensive washing with PBS. The infected Vero cells were detached by trypsin EDTA treatment and washed in DMEM/FBS several times to remove excess trypsin. Infected cells were counted using a Neubauer haemocytometer and diluted to 5×10^5 cells ml^{-1} in DMEM/FBS before plating 100 µl per well into Corning® 384 well CellBIND® plates. The plate was incubated at 37 °C with 5% CO_2 for 72 hours before fixing with PBS containing 1% formaldehyde overnight at room temperature. To visualise the nuclei of both the parasite and Vero cell, plates were stained with 5 µg ml^{-1} Hoechst 33342 diluted in $1 \times$ PBS containing 0.01% (v/v) Triton X100 for 15 minutes. Images were acquired with an Operetta high content fluorescence microscope (Perkin Elmer) using the 40X objective and capturing 5 fields of view per well. Images were processed using the Columbus image analysis software package, which was trained to distinguish between the nuclei of the parasite and the Vero cell. A threshold of >2 parasite nuclei per Vero cell was counted as an infected cell whilst less than 2 was counted as uninfected. The percentage

of infected Vero cells and the mean number of parasites per infected cell were calculated for each of the parasite cell lines. The results are expressed for 24 separate measurements for each transgenic parasite cell line tested. The significance of the infectivity was determined using an unpaired Students t test.

2.2.5 Transfection

Transfection of overexpression or knockout constructs into *T. cruzi* epimastigotes were carried out using an Amaxa Nucleofector[TM] electroporator, as previously described (Xu *et al*., 2009). A total of 2-10 µg of ethanol precipitated DNA was transfected into early-mid-log epimastigotes (1×10^7), suspended in Human T cell Nucleofector[TM] solution (100 µl, Lonza), using the program U-33. Twenty-four hours following transfection, 10 µg ml^{-1} puromycin dihydrochloride (Sigma), 250 µg ml^{-1} Geneticin® (G418, Gibco®) or 500 µg ml^{-1} hygromycin B (Roche) were added to cultures to select for transgenic parasites.

2.2.6 Generating a clonal population of *Trypanosoma cruzi*

Clonal parasite populations were obtained by plating onto semi-solid RTH/FBS agar plates ($1 \times$ RTH/FBS + 1% Noble agar) and incubating at 28 °C for 3 weeks. Plates for cloning transgenic parasites were supplemented with 20 µg ml^{-1} puromycin dihydrochloride, 500 µg ml^{-1} G418 or 750 µg ml^{-1} hygromycin B, as appropriate. Individual colonies were picked and used to inoculate 1 ml of RTH/FBS plus appropriate drug and examined for motile parasites by light microscopy. After 7 days, the 1 ml cultures were used to inoculate 10 ml cultures.

2.2.7 Cell counting and drug dose response (EC$_{50}$) determination

To determine the density of parasites in culture, they were diluted into $1 \times$ PBS + 1%

paraformaldehyde and counted with a neubauer haemocytometer or a CASY model TT

cell counter (Roche). The concentration at which DDD85646 was able to inhibit the

proliferation of *T. cruzi* epimastigotes by 50% (EC$_{50}$) was determined by seeding

parasites at 1×10^5 cells ml^{-1} and co-incubating with a range of inhibitor concentrations

(0-100 μM) for 5 days at 28 °C. Parasites were counted using a Neubauer

haemocytometer and expressed as 0-100% of the no drug control. Data were processed

using GRAFIT (version 5.0.4; Erithacus software) and fitted to a 2-parameter equation

to obtain EC$_{50}$:

$$y = \frac{100}{1 + \left(\dfrac{[I]}{EC_{50}} \right)^m}$$

In this equation [*I*] represents inhibitor concentration and *m* is the slope factor.

The data are presented as the mean ± standard error.

2.3 General molecular biology

2.3.1 Isolation of genomic DNA

Parasites were washed in PBS and 5×10^8 cells were resuspended in 500 μl of gDNA

lysis buffer (10mM Tris-HCl pH 8, 100 mM NaCl, 25 mM EDTA, 0.1 mg/ml

proteinase K, 0.5% (w/v) SDS) and incubated at 56 °C overnight. One volume of

phenol:chloroform:isoamyl alcohol (PCI, 25:24:1) was added to the lysate and mixed,

the upper phase containing the DNA was removed after centrifugation (13,000 $\times$ g, 1

min), and re-extracted using with another volume of PCI. The upper phase was then

extracted with one volume of chloroform isoamyl alcohol, before precipitating the

Table 2.1 List of primers used in this study to generate recombinant expression, ectopic expression and gene replacement constructs. Sites for restriction endonuclease digestion are underlined, the complimentary sequence *pmel*, used in the knit PCR reaction is in lowercase.

Use	Primer	Sequence

Recombinant

| | NMT F | <u>CATATG</u>GCAGAAGAGGGTTCAGGTTTACATCAG |
| | NMT R | <u>GGATCC</u>CTATAGCATGAACAATCCCACGTCACTTGG |

Ectopic

| | NMT F | <u>GAATTC</u>ATGGCAGAAGAGGGTTCAGGTTTACATCAG |
| | NMT R | <u>CTCGAG</u>CTATAGCATGAACAATCCCACGTCACTTGG |

Knockout construct

	5' NMT F	ataagaat<u>gcggccgc</u>GTGATCTTCTCAACAACAAAAATGGATGA
	5' NMT R	gtttaaacttacggaccgtc<u>aagctt</u>TCCTTCAAAAGGCGATCAAGTCCAAAATTAC
	3'NMT F	gacggtccgtaagtttaaac<u>ggatcc</u>GATGCGGGCGGAATTTAGGAGAGAAGT
	3' NMT R	ataagtaa<u>gcggccgc</u>CCGCATCCAGCAGATGGATTAATCACCGT

Localisation constructs

	FCaBP	<u>GAATTC</u>ATGGGTGCTTGTGGGTCGAAG
	FCaBP G2A	<u>GAATTC</u>ATGGcTGCTTGTGGGTCGAAG
	FCaBP R	<u>CCATGG</u>AGGCGTTCTTGCCGTCCTTATC
	X6 F	<u>GAATTC</u>ATGGGCCAGGATAATTCATTTG
	X6 G2A	<u>GAATTC</u>ATGGcCCAGGATAATTCATTTG
	X6 R	<u>CCATGG</u>AAAGCGCTTCCATTTCAAATAAAC
	ARF1 F	<u>GAATTC</u>ATGGGCCAGTGGTTAGCGTC
	ARF1 G2A	<u>GAATTC</u>ATGGcCCAGTGGTTAGCGTC
	ARF1 R	<u>CCATGG</u>AGCCCACCATCAGAATGCGCAC
	PP2C F	<u>GAATTC</u>ATGGGCAGCATGCTGCCGAA
	PP2C G2A	<u>GAATTC</u>ATGGcCAGCATGCTGCCGAA
	PP2C R	<u>CCATGG</u>AAGCGCCGATGCGGTAATTACC

recovered gDNA by the addition of 2.5 volumes of 100% ethanol. The isolated gDNA was resuspended in TE buffer (10 mM Tris-HCl and 1 mM EDTA, pH8) and purified samples were confirmed to be pure by spectrophotometry (260:280 ratio >1.8).

2.3.2 PCR

Polymerase chain reaction (PCR) was carried out using, Pfu (Promega), GoTaq (Promega) or Platinum Taq polymerases (Invitrogen) as per the manufacturer's standard protocol using the appropriate primers (*Table 2.1*). The template concentrations used ranged from 1-10 ng for gDNA and 10-100 pg for purified plasmid DNA and optimised for each target of interest.

2.3.3 Agarose gel electrophoresis

Agarose gels (0.8% (w/v), VWR) containing 10 µg ethidium bromide per 100 ml, were made in TAE buffer (40 mM Tris, 20 mM acetic acid, and 1 mM EDTA). DNA samples were separated by electrophoresis at 80 V in TAE until the desired separation was achieved. The separation of a DNA marker (1 kbp DNA ladder, Promega) allowed the size of the samples to be estimated by comparing the relative migrations through the gel. Gels were imaged by UV transillumination.

2.3.4 TOPO® cloning

PCR products between 0.5-1.5 kbp (**2.2.3**) were routinely cloned into Zero Blunt® TOPO® or TOPO® TA vectors both of which utilise a *Vaccina* viral DNA topoisomerase I that is covalently attached to the 3´ strand. The bound topoisomerase integrates the PCR product into the linear vector to forming the circular plasmid.

Table 2.2 List of media and antibiotics concentrations used for the selection and culture of transformed *E. coli*.

Plasmid	*E. coli* strain	Selection Media
TOPO Zero® blunt®, TOPO TA®	TOP10	LB-(agar or broth), 50 kanamycin
pGEM5zf, pET15b-TEV	JM-109, XL-10 Gold, XL-1 Blue	LB-(agar or broth), 50 μg ml^{-1} ampicillin
pET15b-TEV	Rosetta 2 (DE3) pLysS	LB-(agar or broth), 50 μg ml^{-1} ampicillin, 12.5 μg ml^{-1} Chloramphenicol,
	ArticExpress (DE3) RP	LB-(agar or broth), 50 μg ml^{-1} ampicillin, X μg ml^{-1} gentamycin,

Plasmids were transformed into chemically competent *E. coli* and cloned as described below (*Section 2.3.5*).

2.3.5 TOPO® XL cloning

Larger PCR products (>3 kbp, *section 2.3.2*) were separated on a 0.8% agarose gel containing 1.5 µg ml^{-1} crystal violet to visualise the DNA. The band of interest was excised from the gel and purified using the S.N.A.P^{TM} purification kit (Invitrogen) as described in the manufacturer's protocol, and eluted with dH$_2$O. Gel purified PCR products were cloned into the TOPO® XL vector using the same principles as for the standard TOPO® reactions. The TOPO® XL reaction was carried out as per the protocol. TOPO® ligations were transformed into TOP10 cells (*section 2.3.5*).

2.3.5 Transformation of competent cells

Plasmid DNA was transformed into a variety of chemically competent *E. coli* cell lines (TOP10, JM109, XL-10 gold, Rosetta 2 (DE3) pLysS and Xl-1 blue) by heat shock. Approximately 5-100 ng of plasmid or ligation reaction was added to 50 µl of cells and incubated on ice for 30 min before the cells were incubated at 42 °C for 30 s. Cells were incubated on ice for a further 2 minutes before adding 250 µl of SOC medium and incubating at 37 °C with agitation at 200 rpm for 1h. The entire transformation was spread onto LB agar plates containing the appropriate antibiotic for the resistance gene encoded on the plasmid (*Table 2.2*) and incubated at 37 °C overnight. JM-109 and Xl-1 blue cells were used for the routine transformation of plasmid DNA whilst Xl-10 gold cells were used for the transformation of ligations (*section 2.3.9*).

2.3.6 Isolation of plasmid DNA

Individual colonies of positive transformants were picked and grown in Luria Broth (LB) plus the appropriate antibiotic (50 μg ml^{-1} ampicillin or 50 μg ml^{-1} kanamycin) overnight in a 10 ml culture at 37 °C with agitation. Cells were pelleted by centrifugation (3000 × g, 10 min at 4 °C) and plasmids purified using the Qiagen Miniprep kit, eluting in 50 μl of elution buffer.

2.3.8 DNA sequencing

All plasmids in this study were sequenced by the DNA sequencing service at the University of Dundee (http://www.dnaseq.co.uk/home.html). Plasmids containing generic priming sequences were sequenced with their respective primers, whilst pTREX and pTEX plasmids were sequenced with gene specific primers (***Table 2.1***).

2.3.9 Construct generation

Sequence verified inserts were excised from their respective plasmids using the appropriate restriction endonucleases. Double digestions were carried out simultaneously in a compatible buffer wherever possible, however; failing that sequential digestions were performed. The linearized target vector was dephosphorylated with Antarctic phosphatase (NEB) as per the manufacturer's protocol to prevent self-ligation of the linearized plasmid by removal of the 5′ phosphate overhangs. Digested DNA was gel purified (QIAquick gel extraction kit, Qiagen) prior to the ligation of the insert into the linearized vector using a molar ratio of 2:1 (insert: vector) with T4 DNA ligase (Roche) overnight at room temperature. Ligations were directly transformed into XL-10 Gold ultracompetent cells using the standard transformation protocol (***Section 2.3.5***)

2.3.10 Synthesis of Southern blot probes

Dig labelled probes for Southern blotting were generated using the PCR DIG synthesis kit (Roche). Primers designed against the 5′ UTR or the ORF (*Table 2.1*) of NMT in addition to the *PAC* and *HYG* ORF's were used to amplify and label the target region of DNA from 10 pg of plasmid DNA, as described in the manufacturers standard protocol. In addition to the DIG labelling reaction, a control reaction was also set up to determine the success of incorporating the DIG labelled UTP into the resulting PCR product. Efficient labelling was confirmed by DIG labelled products displaying a reduced electrophoretic mobility on an agarose gel (*Section 2.3.3*), in comparison with the unlabelled reaction.

2.3.11 Southern blot

A total of 5 µg of genomic DNA (gDNA) was digested with appropriate restriction endonucleases (NdeI, AfeI, AgeI, XhoI, HindIII or NotI) overnight at 37 °C. Digested gDNA was separated on a 0.8% agarose gel (containing 20 µg of ethidium bromide per 200 ml) over 3h at 80V in TAE buffer. The gel was washed in 0.25 M HCl for 10 min to de-purinate the DNA before equilibrating in 0.4 M NaOH. DNA was transferred onto positively charged nylon membrane (Roche) by reverse capillary action for 1 h using 0.4 M NaOH as the transfer buffer. The membrane was pre-incubated in DIG Easy Hyb solution for 1 hour at 42 °C, prior to overlaying the membrane with fresh Easy Hyb solution containing 3 µl at 400 ng µl^{-1} of appropriate DIG labelled probe. After an overnight incubation, the membrane was washed in 5 × SSC supplemented with 0.01% (w/v) Sodium dodecyl sulphate (SDS) at 42 °C for 5 min, to remove any excess probe. A further two stringency washes were carried out using 0.5 × SSC containing 0.01 % (w/v) SDS. The blot was developed using the DIG block and wash

buffer set (Roche) as per the manufacturer's instructions. The DIG labelled probe was detected using an anti-dig HRP conjugated antibody (Roche) and the chemiluminescent substrate, CSPD (Roche). Blots were exposed onto Amersham Hyperfilm™ and developed using a KODAK film developer.

2.4. Protein Biochemistry

2.4.1 Quantification of protein concentrations

The concentration of protein in a sample was determined using a coomassie based protein-binding assay (Bradford, Bio-Rad), using known amounts of bovine serum albumin to produce a standard curve.

2.4.2 Sodium dodecyl sulphate polyacrylamide gel electrophoresis (SDS-PAGE)

Protein samples, or whole cell lysates were prepared in $2 \times$ Laemmli buffer containing either 50 µM DTT or 715 mM 2-mercaptoethanol as a reducing agent. Samples were boiled for 5 min prior to separation on NuPAGE® Bis-Tris 4-12% gradient gels (Invitrogen) at 200 V in NuPAGE MES SDS running buffer (50 mM MES, 50 mM Tris Base, 0.1% SDS, 1 mM EDTA, pH 7.3).

2.4.3 Coomassie blue

Gels were washed briefly with H_2O before staining in Coomassie Brilliant Blue staining solution (2.5 g L^{-1} Coomassie brilliant blue R250, 10% acetic acid and 40% methanol) at room temperature with agitation for 1h. Coomassie stain was then removed and the gel incubated in de-staining solution for several hours (10% acetic acid + 40% methanol). The gels were subsequently imaged with a UGenius gel imager.

2.4.4 In-gel fluorescence

Fluorescently labelled proteins separated on SDS-PAGE gels were imaged using an ODYSSEY® SA near infrared imager (LI-COR Biosciences). Proteins labelled with the IRDye 800CW were imaged on the 800 nm channel whilst the pre-stained protein ladder was visible on the 700 nm channel. Gels were scanned with a resolution of 50 µm using the appropriate sensitivity settings for each channel and a focal path length of 3.5 mm. Coloured images were converted to grayscale and in-gel fluorescence quantified in Image Studio Lite version 3.1 (LI-COR Biosciences).

2.4.5 Western blotting

After separating whole cell lysates by SDS-PAGE, gels were briefly equilibrated in Towbin's buffer. Proteins from the gel were transferred onto Whatman Protran nitrocellulose membrane by semi-dry electro transfer (BioRad Trans-Blot®) for 20 min at 25 V in Towbin's buffer. The membrane was typically blocked in 5% milk (Marvel) made up in PBST ($1 \times$ PBS + 0.05 Tween20 (v/v)) for 1h at RT. Primary rat antisera (either Rat anti-*Tc*NMT or *Tc*TryR) were diluted 1 in 500 into PBST and incubated with the membrane for 1h, before washing with PBST (3×5 min) (Tovar and Fairlamb, 1996). Blots were then probed with a polyclonal HRP-conjugated rabbit anti-rat antiserum (1 in 10,000, DAKO) for 1h followed by 3×5 min washes. The blot was developed with the enhanced chemiluminescence mixture (ECL, Amersham) and several exposures of the membrane to Amersham Hyperfilm™ ECL taken, typically ranging from 30 sec to 5 min. Films were developed using a Kodak film developer.

2.4.6 Densitometry ImageJ

Developed films were scanned as a TIFF image and converted to grayscale. The intensity of each band was quantified using Image J (http://imagej.nih.gov/ij/), before subtracting a background measurement. To compare relative changes in the expression of NMT in different transgenic parasites, the background-subtracted measurements were adjusted by relative changes in the intensity measured for trypanothione reductase in each lysate, compared to the WT.

The mass of NMT per cell was determined in the epimastigote, trypomastigote and amastigote forms by densitometry analysis of a known number of parasites against known quantities of purified recombinant protein. A calibration curve using the measured values from the known amounts of NMT was produced by fitting the data to a non-linear regression (Insert equation). The cellular concentration of NMT could then be calculated using the calibrated values and previously published cell volumes for each stage of the parasite (Rohloff *et al*., 2003).

2.5 Metabolic labelling and click chemistry

2.5.1 L-[^{35}S]-methionine

Parasites grown in RTH/FBS medium (***Section 2.2.1***) were harvested by centrifugation ($1620 \times$ g, 15 min at RT) and resuspended in methionine free RTH/FBS medium. Parasites were incubated with 10 µCi ml^{-1} [^{35}S] L-methionine (Perkin Elmer) for 5.5 hours before washing cells twice (1620 g, 15 min at 4 $^{\circ}$C) in PBS buffer to remove unincorporated label. Parasite lysates were made in Laemmli buffer and separated by SDS-PAGE. The gel was treated with En3hance solution (Perkin Elmer) for 1 hour and the fluors precipitated by incubating in cold water for 30 mins. The gel was dried using a gel drier over 3 hours at 80 $^{\circ}$C under vacuum (BioRad 583), and then exposed to

Kodak BioMax MS film overnight at -80 °C, using a low-energy intensifying screen (Kodak).

2.5.2 [³H] Myristic acid

Myristic acid ([9,10-³H(N)], 185 MBq, Perkin Elmer) stored in ethanol was dried under nitrogen stream and resuspended in PBS containing 10 mg ml⁻¹ fatty acid free bovine serum albumin (Company). Parasites grown in RTH/FBS medium were harvested by centrifugation (1620 × g, 15 min at RT) and resuspended in methionine and FBS free medium, supplemented with 50 mg ml⁻¹ fatty acid free bovine serum albumin. [9,10-³H(N)] Myristic acid was added to a final concentration of 100 µCi ml⁻¹ and incubated for 6 hours at 28 °C. Parasites were washed and treated in an identical manner to that described for [³⁵S] L-methionine samples. Dried gels were exposed to film for 4 weeks.

2.5.3 12-Azidododecanoic acid (azidomyristate)

Parasites were labelled with 50 µM azidomyristate (Molecular Probes or SiChem) over a period of 4-20 h under using standard RTH/FBS or ᔆᴵᴸᴬᶜSDM-79 (*Section 2.2.1*). Parasites were washed twice with PBS to remove excess azidomyristate and lysates of parasites made in either RIPA buffer (50 mM Tris-HCl, pH 7.4,150 mM NaCl, 1% sodium deoxycholate, 0.1% SDS, 1% Triton X-100 and a cOmplete mini EDTA-free protease inhibitor cocktail tablet). Alternatively, cells for enrichment studies were resuspended and lysed in the urea lysis buffer supplied with the protein enrichment kit (Molecular probes).

2.5.4 Detection of *N*-azidomyristoylated proteins

The concentration of RIPA buffer lysates was determined using the BioRad protein assay (**See 2.4.1**). The IRDye 800CW alkyne (Li-cor biosciences) was attached to *N*-azidomyristoylated by click chemistry using the protein reaction buffer kit (Invitrogen) as described in the supplied protocol. Equal amounts of lysate were treated in this way for all conditions tested before they were methanol: chloroform precipitated and the samples separated by SDS-PAGE (*Section 2.4.2*). Proteins were fixed with 10% acetic acid and 40% methanol for 15 min at RT before treating with 1 M KOH to remove O- and S-myristoylation. Gels were imaged by in-gel fluorescence (*Section 2.4.4*).

2.5.5 Enrichment of *N*-azidomyristoylated proteins

Washed *T. cruzi* epimastigotes were resuspended in urea lysis buffer and the parasites biologically inactivated by three freeze thaw cycles. The optimal lysis of parasites was achieved by subjecting the lysate to sonication (6, 3 second pluses at 10 micron) before the insoluble protein was pelleted (10,000 $\times$ g, 10 min at 4 $^{\circ}$C). Treated and untreated parasites prepared for qualitative analysis were separately enriched by click chemistry using the protein enrichment kit (Invitrogen), as recommended by the manufacturer with some minor modifications. Before the samples were reductively alkylated with iodoacetamide, the enrichments were incubated with 1 M hydroxylamine (pH 7.0) for 30 min to remove S-myristoylated proteins (Armah and Mensa-Wilmot, 1999).

2.6 Mass spectrometry and data processing

2.6.1 Mass spectrometry

All trypsin digestion and mass spectrometry was carried by the FingerPrints proteomic service at the University of Dundee (http://proteomics.lifesci.dundee.ac.uk). The following protocol has been provided by Dr Abdel Atrih. The beads were washed 5 times with 60 mM ammonium bicarbonate then re-suspended in 200 μl ammonium bicarbonate (60 Mm) containing 25 μl of trypsin (0.1 μg/μl). Digestion was carried out overnight at 30 °C and resulting peptides were desalted using C18 cartridges. Analysis of peptides was performed on a LTQ Orbitrap Velos Pro (Thermo Scientific) mass spectrometer coupled with a Dionex Ultimate 3000 RS (Thermo Scientific). LC buffers were the following: buffer A (2% acetonitrile and 0.1% formic acid in Milli-Q water (v/v)) and buffer B (80% acetonitrile and 0.08% formic acid in Milli-Q water (v/v). Aliquots of 15 μL of each sample were loaded at 5 μL/min onto a trap column (100 μm × 2 cm, PepMap nanoViper C18 column, 5 μm, 100 Å, Thermo Scientific) equilibrated in 98% buffer A. The trap column was washed for 3 min at the same flow rate and then the trap column was switched in-line with a Thermo Scientific, resolving C18 column (75 μm × 50 cm, PepMap RSLC C18 column, 2 μm, 100 Å). The peptides were eluted from the column at a constant flow rate of 300 nl/min with a linear gradient from 98% buffer A to 40% buffer B in 68 min, and then to 98% buffer B by 70 min. The column was then washed with 98% buffer B for 15 min and re-equilibrated in 98% buffer A for 34 min. LTQ Orbitrap Velos Pro was used in data dependent mode. A scan cycle comprised MS1 scan (m/z range from 335-1800) in the LTQ Orbitrap Velos Pro followed by 15 sequential dependant MS2 scans (the threshold value was set at 5000 and the minimum injection time was set at 200 ms) in LTQ with collision induced dissociation. The resolution of the Orbitrap Velos was set at to 60,000. To ensure mass

accuracy, the mass spectrometer was calibrated on the first day that the runs were performed.

2.6.2 Matrix assisted laser desorption ionisation time of flight spectrometry (MALDI-TOF)

The purity and mass of recombinant proteins were determined by MALDI-TOF on a AB Sciex Voyager DE-STR MALDI-TOF system. This was carried out by the Fingerprints proteomic service (http://proteomics.lifesci.dundee.ac.uk).

2.6.3 Tryptic mass fingerprinting

Coomassie stained SDS-PAGE gels were digested in-gel with Trypsin gold (Promega) and analysed by LC-MS/MS. In-solution digestion of immobilised proteins was also performed with trypsin gold and the peptides recovered and analysed by LC-MS/MS. LC-MS/MS spectra were acquired on an LTQ Orbitrap XL (Thermo Fisher).

2.6.4 Polymyxin acylase digestion

After tryptic digestion of the alkyne agarose, the resin was extensively washed with 20% acetonitrile to remove peptides remaining from the trypsin digestion and then washed with 100 µM phosphate buffer (pH 8.0). Digestion of alkyne agarose resin or *N*-azidomyristoylated proteins was carried out overnight at 37 °C in phosphate buffer pH 8.0. Peptides on resin were analysed by Mass spectrometry (*Section 2.6.1*), whilst click chemistry was carried out on whole proteins (*Section 2.5.5*)

2.6.5 *N*-myristoylome data processing

Thermo Xcalibur raw files were processed with MaxQuant version 1.3.0.5 which incorporates the Andromeda search engine (Cox and Mann, 2008; Cox *et al*., 2011). This software package allows SILAC ratios and relative label free intensities to be calculated for the SILAC and label free experiments respectively. For LFQ analysis, a 2 min window for matching peptides between runs was allowed to account for possible differences in retention times between the HPLC separations prior to MS identification (Cox *et al*., 2014). Experimental spectra were searched against a custom *T. cruzi* proteomic database consisting of 30,048 entries comprising sequences from CL Brenner, Silvio X10/1 and the Marinkelli strains that are deposited in UniProt and a database consisting of common laboratory contaminants. Peptide assignments were made using a MS tolerance of 6 ppm and carbamidomethylation as a fixed modification due to the reductive alkylation of samples with iodoacetamide. *N*-acetyl, *N*-pyroglutamate and the oxidation of methionine were counted as variable modifications for the experiment. To account for incomplete digestion, a maximum of two missed trypsin cleavage sites were allowed and the false discovery rates for both peptide and protein identifications were calculated to be <0.01 by performing a decoy search against a reversed sequence database.

2.6 Recombinant protein expression and characterisation

2.6.1 Expression of recombinant protein

Competent cells were transformed with the pET15b-TEV plasmids containing the Silvio X10/7A ORFs encoding *Tc*NMT. The pET15b-TEV-*Tc*NMT-CLBren plasmid was obtained from Dr Scott Cameron (University of Dundee).

2.6.2 Preparation of *E. coli* cell lysates

E. coli cell pellets were harvested by centrifugation (5020 g, 30 min at 4 °C). The pellets from 2 L cultures, were resuspended in 50 ml of cell lysis buffer (25 mM Tris, 500 mM NaCl, 10 mM imidazole, pH 8.5, EDTA free protease inhibitor tablets (Roche), lysozyme and DNaseI (Sigma)). Cells were lysed with a continuous flow cell disruptor at 4 °C (Constant Systems) by passing the sample through the cell disruptor twice at 30 kpsi. Confirmation of cell lysis was achieved by examination using a light microscope. Insoluble protein was separated from the soluble by centrifugation (40,000 × g, 30 min, 4 °C) and the soluble protein passed through a 0.2 μm polyethersulphone filter (Sartorius).

2.6.3 Protein purification

All buffers prepared for protein purification were filtered through a 0.2 μM polyamide membrane (Sartorius) and de-gassed before use. The columns used in all chromatographic separations were obtained from GE Healthcare and all purifications carried out on an ÄKTA purifier system equipped with a sample-loading pump using Unicorn 5.11.

2.6.4 Nickel affinity chromatography

Clarified *E. coli* lysates were loaded onto a 5 ml HisTrap HP nickel affinity chromatography column that had been pre-equilibrated with His binding buffer (25 mM Tris, 500 mM NaCl, 10 mM imidazole, 1 mM TCEP, pH8.5) at a constant flow rate of 5 ml min^{-1}. To remove unbound proteins, the column was washed with 10 column volumes (CV) of His-binding buffer, or until a stable reading at 280 nm was achieved. Histidine rich proteins were then eluted with 0.5 M imidazole diluted in his buffer, over

20 CV and protein containing fractions collected. If a more precise separation was required, the gradient was paused manually to allow a greater separation of merged protein peaks, after which the gradient was resumed. Fractions were analysed by SDS-PAGE to determine which fractions contained the protein of interest.

2.6.5 Anion exchange chromatography

Samples containing high concentrations of salt (>100 mM NaCl) were dialysed into anion exchange buffer containing 25 mM Tris, 25 mM NaCl at pH8.5, using a 10 kDa MWCO Slide-A-Lyzer cassette. The semi-purified protein samples were loaded onto a 1 ml HiTrap Q HP column (GE Healthcare), and eluted with a gradient of NaCl (0-500 mM). The purity of each fraction was determined by SDS-PAGE analysis.

2.6.6 Preparative size exclusion chromatography

Fractions containing the protein of interest were pooled and if required, concentrated to a volume less than 10 ml with a Vivaspin™ (20 k MWCO) centrifugal concentrator device. The sample was loaded onto a Superdex 75 26/60 pre-equilibrated in 25 mM Tris, 150 mM NaCl, 1 mM TCEP with a flow rate of 1.5 ml min^{-1}. The protein containing eluent, as determined by absorbance at 280 nm was collected and the purity analysed by SDS-PAGE. Fractions containing the protein of interest were pooled and concentrated to ~1 mg ml^{-1} and the enzyme activity determined. Active *Tc*NMT was diluted with glycerol to a final concentration of 10% v/v, flash frozen in liquid nitrogen and stored at -80 $^{\circ}$C.

2.6.7 Analytical size exclusion chromatography

For analytical separation, a Superdex 200 30/10 GL pre equilibrated was used to separate the BioRad, gel filtration protein standards (1.5 ml min^{-1}). The elution volumes of each standard were used construct a calibration curve for the column. Under the same conditions, 50 µl of ~1 mg ml^{-1} purified enzyme was separated, and the calibration curve used to calculate the MW of the sample.

2.6.8 Crystallography

Purified recombinant His$_6$-*Tc*NMT was concentrated to ~18 mg ml^{-1} in a Sartorius™ Vivaspin™ 6 Centrifugal Concentrator (10 k MWCO). Concentrated protein was incubated with a 2-fold excess of myristoyl-CoA and DDD85646 on ice for 30 min prior to dialysing into 25 mM Tris-HCl, 25 mM NaCl pH8.5 in a Pierce Slide-A-Lyzer cassette with a 10 k MWCO for 30 mins at 4 °C. The protein concentration was confirmed to be 16 mg ml^{-1} and then screened against the JCSG plus, JBScreen classics HTS I and JBScreen classics HTS II (Molecular dimensions and Jenna Bioscience) by vapour diffusion in a 96 well sitting drop format. Drops containing 1 µl of protein solution (Apoenzyme or enzyme co-incubated with MCoA and DDD85646) and 1 µl of reservoir solution were incubated at 25 °C and signs of crystallisation monitored at regular intervals after 12 hours. Crystals mounted containing the reservoir solution as a cryoprotectant and the diffraction tested on a Rigaku M007HF X-ray generator equipped with Varimax Cu-VHF optics, a Saturn 944HG$^+$ CCD detector and an AFC-11 4-axis partial χ goniometer.

2.6.9 Production of polyclonal antisera

Polyclonal anti-*Tc*NMT antisera were raised in adult male Wistar rates using the recombinantly expressed and purified His_6-*Tc*NMT from CL-Brenner. Purified protein was concentrated to 1 mg ml^{-1}, and emulsified in Freund's complete adjuvant for the initial immunisation or incomplete adjuvant for subsequent boosters. Antisera were raised exactly as described for *Leishmania major* glyoxalase I antisera (Greig *et al*., 2009). Five weeks post immunisation; blood was harvested from the rats and clotted at 37 °C for 1 h. Cells were harvested by centrifugation ($3000 \times g$, 15 min, 4 °C) and the antisera containing supernatant was removed and flash-frozen in the presence of sodium azide 0.05% (w/v) before storing at -20 °C. Immunisation protocols were approved by the University Welfare and Ethical Use of Animals Committee and were performed under the Animals (Scientific procedures) Act 1986 in accordance with the European Communities Council Directive (86/609/EEC).

2.7 Enzyme activity

2.7.1 Monitoring the activity of NMT using a coupled enzyme assay

The enzymatic activity of recombinant *Tc*NMT was monitored using a modified coupled enzyme spectrophotometric assay, with the pH of the reaction having been lowered from 8.0 to 7.4 (Boisson and Meinnel, 2003) . The assay buffer contained 50 mM Tris, 0.5 mM EDTA, 0.5 mM EGTA, 1.25 mM DTT, 0.1% Triton X-100, 40 mM pyruvic acid, 0.125 U ml^{-1} pyruvate dehydrogenase, 0.2 mM thiamine pyrophosphate and 2.5 mM NAD^+, adjusted to pH 7.4 with HCl. All enzyme activity measurements were made using a UV-1601 spectrophotometer equipped with a peltier device (SHIMADZU) set to 30 °C using quartz cuvettes.

The formation of NADH$^+$ from the coupled enzyme reaction was monitored at 340 nm and converted to a rate (s^{-1}), by dividing the change in absorbance by the molar extinction coefficient of NADH$^+$ and the enzyme concentration used in the assay. The rates were calculated for the linear regions of the spectra, which typically occurred between 50-100 seconds after starting the reaction. The specific activity of TcNMT was determined in the presence of 700 μM TbCAP5.5 peptide (GCGGSKVKPQPPQAK [biotin]) (Frearson et al., 2010) and 40 μM MCoA (Sigma) by varying the enzyme concentration in the reaction.

2.7.2 Determining kinetic parameters and inhibition of TcNMT

K_m and K_m^{app} values were determined for a biotinylated peptide substrate derived from amino acids 2-15 of the $T.$ $brucei$ and $T.$ $cruzi$ CAP5.5 proteins (TcCAP5.5 GCCASKEKQPRPGAK[biotin], TbCAP5.5 GCGGSKVKPQPPQAK [biotin], custom synthesised by Pepceuticals); and MCoA. In the case of K_m^{app} values were determined using GraFit5. The concentration of DDD85646 able to produce a 50% reduction in enzyme activity (IC$_{50}$) was determined by varying the concentration of inhibitor in the presence the TbCAP5.5 peptide at 200 μM. This data was fitted to the Morrison equation for tight binding inhibition (equation 1) to calculate the apparent dissociation constant (K_i^{app}) of the inhibitor from the enzyme complex. The true Ki was calculated from using equation 2.

(Eq. 1)

$$\frac{v_i}{v_o} = \frac{([E]_T + [I]_T + K_i^{app}) - \sqrt{([E]_T + [I]_T + K_i^{app})^2 - 4[E]_T[I]_T}}{2[E]_T}$$

(Eq. 2)

$$K_i = \frac{K_i^{app}}{\left(1 + \frac{[S]}{K_m}\right)}$$

2.8 Microscopy

2.8.1 Preparation of slides

Parasites washed twice in PBS were resuspended at a concentration of 1×10^6 parasites

ml^{-1}. Parasites (20 µl) adhered to poly-L-lysine covered glass slides for 15 minutes at

RT. Slides were fixed either in 100% methanol at -20 $^\circ$C overnight, or PBS containing

1% formaldehyde for 10 minutes at room temperature.

2.8.2 Localisation of eGFP fusion proteins

Formaldehyde fixed parasites expressing eGFP fusion proteins mounted with

SlowFade® Gold containing DAPI (Invitrogen) and a 1.5 glass coverslip fixed in place.

2.8.3 Giemsa staining

To determine confirm the life cycle stage of a parasite, methanol fixed parasites were

stained with Giemsa stain for 15 min at room temperature. Excess giemsa was removed

by washing the slide with H_2O for several minutes leaving the stained nuclear and

kinetoplast DNA to be visualised by light microscopy.

2.8.4 Fluorescence microscopy

Parasites for localisation studies were imaged with a DeltaVision elite deconvolution

microscope equipped with filters for the following fluorophores; DAPI, GFP, FITC,

Texas Red and Alexa 488. Images were acquired using the 100 x oil objective and processed using softWoRx deconvolution software to remove out of focus light from the image. Minor alterations were made to the brightness and or contrast of individual images. Merged images were produced in ImageJ by combining separate images as individual colour channels.

2.9 Bioinformatic analysis

2.9.1 Proteome wide prediction of *N*-myristoylation in the trypanosomatids

The reference proteomes of *Trypanosoma cruzi*, *Trypanosoma brucei* and *Leishmania major* were downloaded from UniProt (Accessions: UP000008313, UP000008524 UP000000542). The *T. cruzi* sequences were based on the predicted proteome for the Silvio X10/1 parasite. Sequences not annotated to start with the amino acids MG were filtered out of the dataset and the *N*-myristoylation status of these proteins predicted using the program Myristoylator (http://web.expasy.org/myristoylator/).

2.9.2 Bioinformatic analysis of experimental *N*-myristoylome

N-myristoylated proteins found to be enriched in all biological replicates or just in the LFQ or SILAC experiments were analysed using a variety of prediction programs. These high confidence proteins were searched against the Pfam sequence database to identify potential functional domains present in these proteins. Only significant matches from the "A database" were annotated as potential functional domains in addition to their significance value. Identified proteins were submitted to the SOSUI server for the prediction of transmembrane domains (http://harrier.nagahama-i-

bio.ac.jp/sosui/). The predicted isoelectric point of these proteins was calculated by the

compute pI/Mw tool (Expasy).

Chapter 3

Biochemical and genetic validation of

N-myristoyltransferase from

Trypanosoma cruzi

A

	420	440	460	480

T. cruzi NMT (X10_1) AAGGTACTCCAGAAAAACAAGAACACTGAAGAAAAAGAGCAGGGGTCGGAGGAGAAGAATAATGATCATAAGAGCCAAGCGGAGGAGCATTACCTC
Translation +1 K V L Q K N K N T E E K E Q G G S E E K N N D H K S Q A E E H Y L

S150 AAGGTACTCCAGAAAAACAAGAACACTGAAGAAAAAGAGCAGGGGTCGGAGGAGAAGAATAATGATCATAAGAGCCAAGCGGAGGAGCATTACCTC
Translation +1 K V L Q K N K N T E E K E Q G S E E K N N D H K S Q A E E H Y L
Trace data

P150 AAGGTACTCCAGAAAAACAAGAACACTGAAGAAAAAGAGCAGGGGCCGGAGGAGAAGAATAATGATCATAAGAGCCAAGCGGAGGAGCATTACCTC
Translation +1 K V L Q K N K N T E E K E Q G G P E E K N N D H K S Q A E E H Y L
Trace data

Figure 3.1 Sequencing and analysis of *T. cruzi N-myristoyltransferase*
(**A**) Sequencing analysis of the S150 and P150 clones encoded by the C-T SNP at position 448 (red box) in the nucleic acid sequence. (**B**) Alignment the NMT poly-peptides from *T. cruzi, T. brucei, L. major, H. sapiens, P. falciparum and S. cerevisae*.

B

```
                20                  40                  60
                |                   |                   |
TcNMT      ---------- ---------- ---------- ---------- ---------- ---------- ---------- -
TbNMT      ---------- ---------- ---------- ---------- ---------- ---------- ---------- -
PfNMT      MNDDKKDFVG RDLYQL---- ---------- ---------- ---------- ---------- ---------- 16
ScNMT      MSEEDK---- ---------- ---------- ---------- ---------- ---------- ---------- 6
HsNMT1     MADESETAVK PPAPPLPQMM EGNGNGHEHC S-DCENEEDN SYNRGGLSPA NDTGAKKKKK KQKKKKEK-- 67
HsNMT2     MAEDSESAAS QQSLEL---- ----DDQDTC GIDGDNEEET EHAKG--SPG GYLGAKKKKK KQKRKKEKPN 60
Consensus  MA**S**AV* *****LPQMM EGNG*****C *ID**NEE** ****GGLSP* ***GAKKKKK KQK*KKEKPN

                80                 100                 120                 140
                |                   |                   |                   |
TcNMT      ---------- ---------- ---------- ---------- ---------- MAEEGSGLHQ FWNTQPVPQS 20
TbNMT      ---------- ---------- ---------- ---------- ---------- MTDKAFTEHQ FWSTQPVRQP 20
PfNMT      ---------- ---------- ---------- ---------- -------IRN AKDKIKIDYK FWYTQPVPKI 39
ScNMT      ---------- ---------- ------AKK LENLLKLLQL NNDDTSKFTQ EQKKAMKDHK FWRTQPVPKDF 49
HsNMT1     --GSETDSAQ D-------QP VKMNSLPAER IQEIQKAIEL FSVGQGPAKT MEEASKRSYQ FWDTQPVPKL 128
HsNMT2     SGGTKSDSAS DSQEIKIQQP SKNPSVPMQK LQDIQRAMEL LSACQGPARN IDEAAKHRYQ FWDTQPVPKL 130
Consensus  SGG***DSA* DSQEIKIQQP *K**S*PA*K LQ*IQKA*EL *S**QGPARN M*EKAK*D*Q FWDTQPVPKL

               160                 180                 200
                |                   |                   |
TcNMT      STDAADTVG- PLEAAGTVDD VPTDPVAIAS TLEWWSPDMD NKDDVRAIYE LLRDNYVEDV ESMFRFNYSE 89
TbNMT      GAPDADKVG- FIMES-SLDA VPAEPYSLPS TFEWWSPDVA NPEDLRGVHE LLRDNYVEDS ESMFRFNYSE 88
PfNMT      NDEFDENVNE PFISDNKVED VRKEEYKLPS GYAWCVCDIT KENDRSDIYN LLTDNYVEDD DNVFRFNYSS 109
ScNMT      DEKVVEE--G PIDKPKTPED ISDKPLPLLS SFEWCSIDVD NKKQLEDVFV LLNENYVEDR DAGFRFNYTK 117
HsNMT1     G-EVVNTHG- PVEP--DKDN IRQEPYTLPQ GFTWDALDLG DRGVLKELYT LLNENYVEDD DNMFRFDYSP 194
HsNMT2     D-EVITSHG- AIEP--DKDN VRQEPYSLPQ GFMWDTLDLS DAEVLKELYT LLNENYVEDD DNMFRFDYSP 196
Consensus  **EV**TVG* PIEP****DD VRQEPYSLPS GFEW*S*D*D NKEDL***Y* LLN*NYVEDD DNMFRFNYS*

               220                 240                 260                 280
                |                   |                   |                   |
TcNMT      DFLRWALTPP GYHSSWHVAV RRKRDQMLMG FVSGIPVTMR MGVPKKVLQK NKNTEEKEQG PEEKNNDHKS 159
TbNMT      EFLRWALMPP GYHQSWHVGV RLKSNKSVLG FVAGVPITMR LGTPKMVLEK R---EHGEDG GEEVIND--- 152
PfNMT      EFLLWALSSP NYVKNWHIGV KYESTNKLVG FISAIPIDMC VN-------- ---------- ---------- 151
ScNMT      EFFNWALKSP GWKKDWHIGV RVKETQKLVA FISAIPVTLG VRG------- ---------- ---------- 160
HsNMT1     EFLLWALRPP GWLPQWHCGV RVVSSRKLVG FISAIPANIH I--------- ---------- ---------- 235
HsNMT2     EFLLWALRPP GWLLQWHCGV RVSSNKKLVG FISAIPANIR I--------- ---------- ---------- 237
Consensus  EFLLWALRPP G**K*WH*GV RVKS**KLVG FISAIP*TMR *G*PK*VL*K *KNTE**E*G *EE**NDHKS

               300                 320                 340
                |                   |                   |
TcNMT      QAEEHYLEPR KICEINFLCV HKLLRAKRLA PILIKEVTRR VHLMNIWQAV YTAGRLLPTP FATADYYHRS 229
TbNMT      -----YLEPQ TICEINFLCV HKKLRQRRLG PILIKEVTRR VNLMNIWHAV YTSGTLLPTP FAKGHYFHRS 217
PfNMT      ------KNII KMAEVNFLCV HKSLRSKRLA PVLIKEITRR INLESIWQAI YTAGVYLPKP ISTARYFHRS 215
ScNMT      -------KQV PSVEINFLCV HKQLRSKRLT PVLIKEITRR VNKCDIWHAL YTAGIVLPAP VSTCRYTHRP 223
HsNMT1     -----YDTEK KMVEINFLCV HKKLRSKRVA PVLIREITRR VHLEGIFQAV YTAGVVLPKP VGTCRYWHRS 300
HsNMT2     -----YDSVK KMVEINFLCV HKKLRSKRVA PVLIREITRR VNLEGIFQAV YTAGVVLPKP IATCRYWHRS 302
Consensus  QAEEHY*EPK KMVEINFLCV HKKLRSKRLA PVLIKEITRR VNLE*IWQAV YTAGVVLPKP *ATCRY*HRS

               360                 380                 400                 420
                |                   |                   |                   |
TcNMT      LNPEKLVAVG FSVIPQQYQK FQNPLSMIKR FYELPAKPKT RGLRPMEPKD APQVANLLRK KLATCDVAPV 299
TbNMT      LNSQKLVDVK FSGIPPHYKR FQNPVAVMER LYRLPDKTKT RGLRLMEPAD VPQVTQLLLK RLASFDVAPV 287
PfNMT      INVKKLIEIG FSCLNTRLT- ----MSRAIK LYRIDDTLNI KNLRLMKKKD IDGLQKLLNE HLKQYNLHAI 280
ScNMT      LNWKKLYEVD FTGLPDGHTE EDMIAENA-- ---LPAKTKT AGLRKLKKED IDQVFELFKR YQSRFELIQI 288
HsNMT1     LNPRKLIEVK FSHLSRNMT- ----MQRTMK LYRLPETPKT AGLRPMETKD IPVVHQLLTR YLKQFHLTPV 365
HsNMT2     LNPRKLVEVK FSHLSRNMT- ----LQRTMK LYRLPDVTKT SGLRPMEPKD IKSVRELINT YLKQFHLAPV 367
Consensus  LNP*KLVEVK FS*LPRN*T* FQNP**R*MK LYRLPDKTKT *GLRPMEPKD IPQV**LLN* YLKQF*LAPV

               440                 460                 480
                |                   |                   |
TcNMT      FTDEEVAHYT LPRE------ GVLMSYVVER EVSGGGGGGR VDSSRGRQND AET------- ---HKQITDF 353
TbNMT      FNEEEVAHYF LPRE------ GVVFSYVVES PV----GPGK DEENAGKASK GTPTGTKCVT GGCEKVITDF 347
PfNMT      FSKEDVAHWF TPID------ QVIYTVVNEE ---------- ---------- ---------- ---NGEIKDL 311
ScNMT      FTKEEFEHNF IGEESLPLDK QVIFSYVVEQ P--------- ---------- ---------- ---DGKITDF 326
HsNMT1     MSQEEVEHWF YPQE------ NIIDTFVVEN A--------- ---------- ---------- ---NGEVTDF 397
HsNMT2     MDEEEVAHWF LPRE------ HIIDTFVVES P--------- ---------- ---------- ---NGKLTDF 399
Consensus  F**EEVAHWF LPRESLPLDK *VI**YVVES PVSGGGG*G* *****G**** ***TGTKCVT GGCNG*ITDF

               500                 520                 540                 560
                |                   |                   |                   |
TcNMT      FSFFSLPSSI IGSSKHSVLN AAYVFYSANT ---------- -------TIS LVHLMSDLLI VAHQQGFDVC 406
TbNMT      FSFYSLPSTI IGNSNHSLLK VAYVYYTAAT ---------- -------SVS ITQLVNDLLI IVKLNGFDVC 400
PfNMT      ISFYSLPSKV LGNNKYNILN AAFSFYNITT ---------- -------TTT FKNLIQDAIC LAKRNNFDVF 364
ScNMT      FSFYSLPFTI LNNTKYKDLG IGYLYYYATD ADFQFKDRFD PKATKALKTR LCELIYDACI LAKNANMDVF 396
HsNMT1     LSFYTLPSTI MNHPTHKSLK AAYSFYNVHT ---------- -------QTP LLDLMSDALI LAKMKGFDVF 450
HsNMT2     LSFYTLPSTV MHHPAHKSLK AAYSFYNIHT ---------- -------ETP LLDLMSDALI LAKSKGFDVF 452
Consensus  FSFYSLPSTI *GN*KHKSLK AAYSFYNA*T ADFQFKDRFD PKATKALTT* LLDLMSDALI LAK**GFDVF

               580                 600
                |                   |
TcNMT      NVVNIMDNGD YLSELKFGRG DGNLHYYFYN WSYPIVQP-- ---------- -SDVGLFML 452
TbNMT      NVVDIYDNGT YLKELKFSPG DGNLYYYFYN WSYPSIPA-- ---------- -NEVGLVMV 446
PfNMT      NALEVMDNYS VFQDLKFGEG DGSLKYYLYN WKCASCHP-- ---------- -SKIGIVLL 410
ScNMT      NALTSQDNTL FLDDLKFGPG DGFLNFYLFN YRAKPITGGL NPDNSNDIKR RSNVGVVML 455
HsNMT1     NALDLMENKT FLEKLKFGIG DGNLQYYLYN WKCPSMGA-- ---------- -EKVGLVLQ 496
HsNMT2     NALDLMENKT FLEKLKFGIG DGNLQYYLYN WRCPGTDS-- ---------- -EKVGLVLQ 498
Consensus  NALD*MDN*T FLE*LKFG*G DGNLQYYLYN W*CPSI**GL NPDNSNDIKR RSKVGLV*L
```
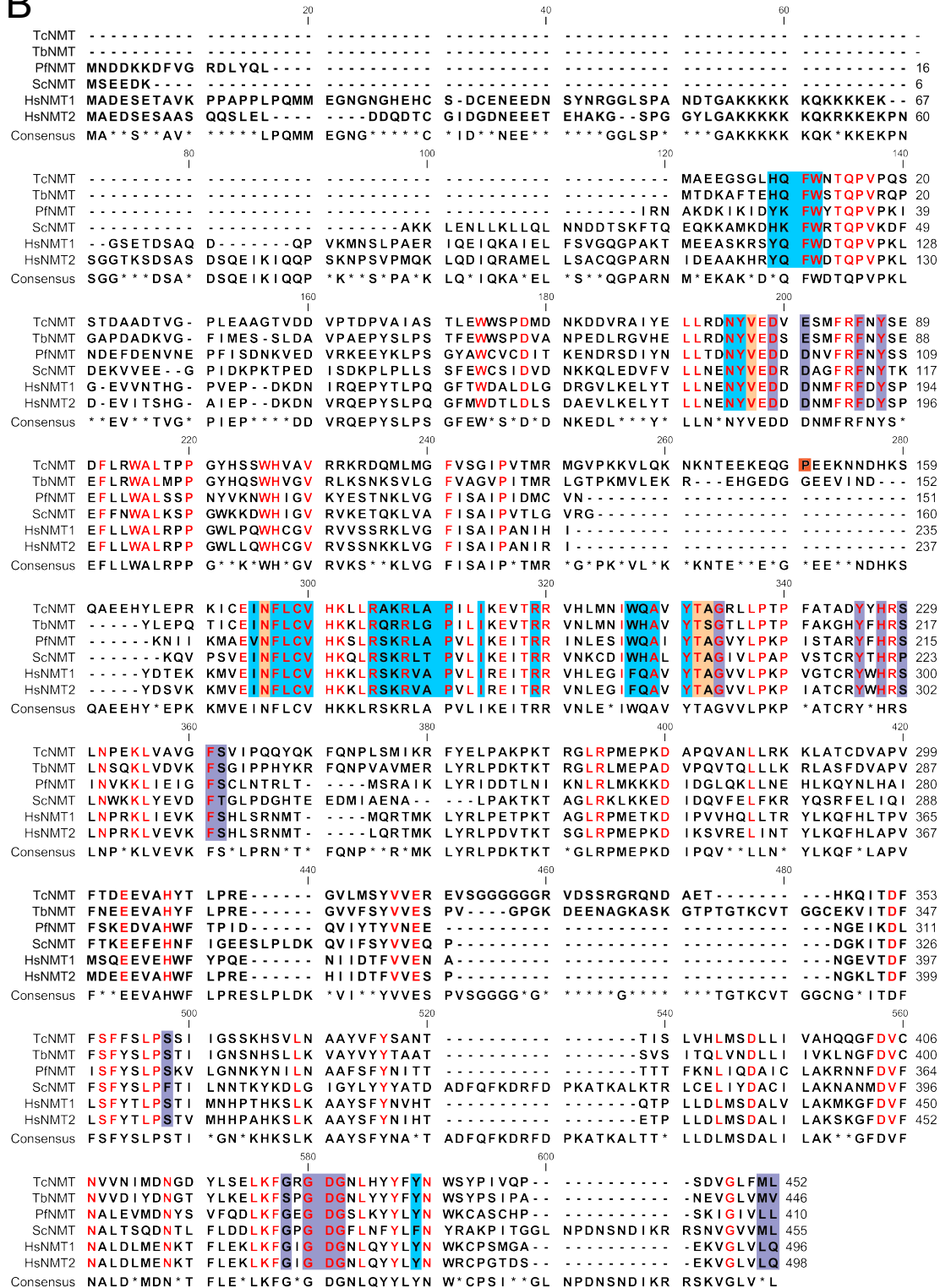
Figure 3.1 Sequencing and analysis of *T. cruzi N-myristoyltransferase*
(**A**) Sequencing analysis of the S150 and P150 clones encoded by the C-T SNP at position 448 (red box) in the nucleic acid sequence. (**B**) Alignment the NMT polypeptides from *T. cruzi, T. brucei, P. falciparum, S. cerevisae* and *H. sapiens.* Amino acids in red are conserved in all sequences, black are not conserved. Residues involved in the binding of Myr-CoA or peptide analogs are highligted in blue and purple respectivley, with those in peach involved in the binding of both. These were inffered from the S. cerevisiae structure (*Bhatnagar et al., 1998*). The orange shows theposition of Pro150 used this study.

3.1 Sequencing the *N*-myristoyltransferase gene from *T. cruzi* Silvio X10/7A

In recent years, the genomes of several *T. cruzi* strains have been published, including that of Silvio X10/1, isolated from the blood of a 19-year-old male in Brazil (Silveira *et al.*, 1979). A putative open reading frame (ORF) corresponding to *N*-myristoyltransferase was first identified in the X10/1 genome by BLAST (http://tritrypdb.org), using the sequence from *Saccharomyces cerevisiae* as a search template (ENA: AAA34815). A single nucleotide sequence of 1359 bp was identified on an unassembled contig (TriTrypDB: TCSYLVIO_006126) in the X10/1 genome against which PCR primers were designed. These primers were used to amplify the corresponding ORF from genomic DNA (gDNA), isolated from the cloned cell line, Silvio X10/7 clone A1 (X10/7A1). The resulting products from three independent PCR reactions were cloned into the pCR™-Blunt II-TOPO vector and multiple plasmids from each reaction sequenced in duplicate to minimise the likelihood of sequencing errors. Initial analysis these data revealed there to be two single nucleotide polymorphisms (SNPs) in the NMT ORF from X10/7A1 parasites. Each SNP was found to be present only in 50% of the sequencing reactions and were found to be mutually exclusive, suggesting the SNPs are present on different alleles. Although one SNP produced a change at the protein coding level by altering Ser150 to Pro (**Figure 3.1 A**), the second was silent. Multiple sequence alignments of the translated ORFs from *T. brucei*, *L. major*, *S. cerevisiae*, *H. sapiens*, *P. falciparum*, *T. cruzi* CL-Brenner and X10/1, revealed a lack of amino acid conservation at this position (**Figure 3.1 B**). The sequence containing Pro150 was used for the remainder of the studies as in both of the CL-Brener sequences there is a proline at this position. From this multiple sequence alignment the conservation of the NMT primary sequence was calculated throughout eukaryotes. Overall, sequence identify of NMT is broadly conserved across the trypanosomatids (**53-58% identity**), but a higher level of divergence is observed in
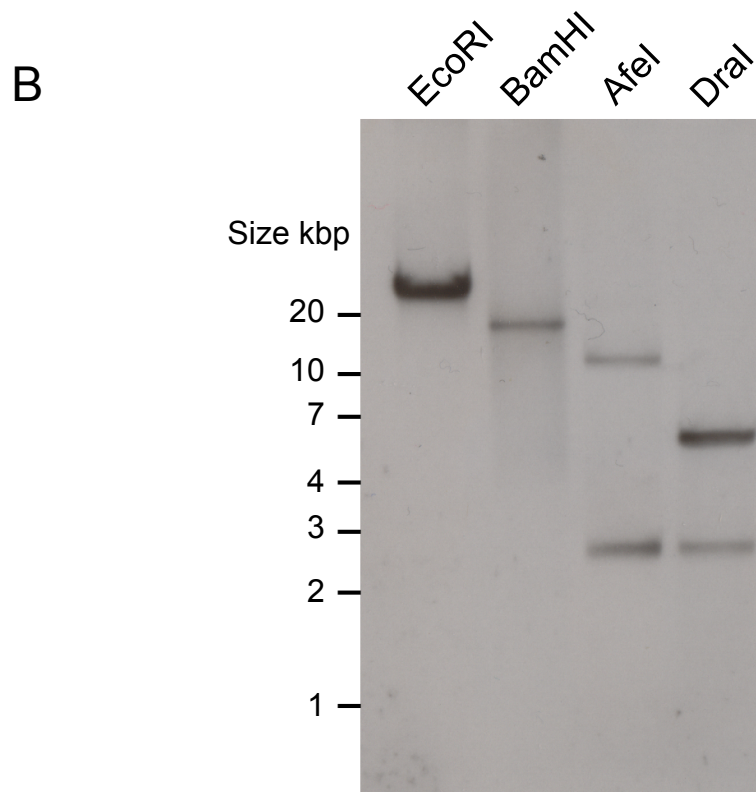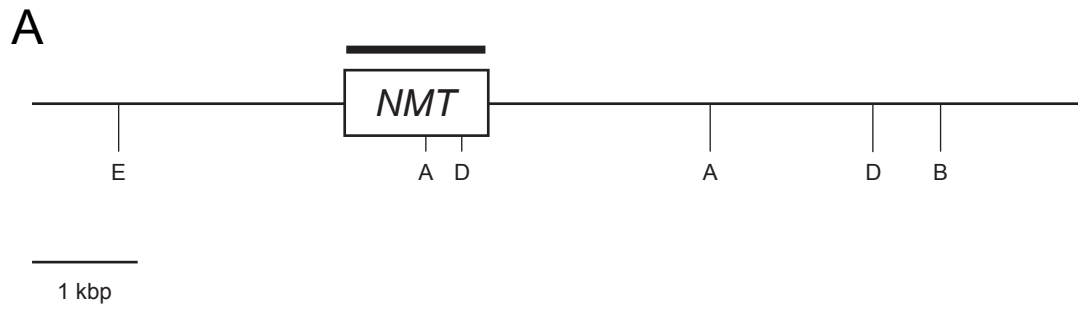
Figure 3.2 Analysis of *TcNMT* copy number

(**A**) Theoretical map of the *TcNMT* locus digested with EcoRI, BamHI, AfeI and DraI. The gene specific probe is marked as a black bar above the open reading frame. (**B**) Southern blot analysis of EcoRI, BamHI, AfeI and DraI digested gDNA (5 µg) from *T. cruzi* X10/7A. The blot was probed with the *NMT* open reading frame.

comparison with the *P. falciparum, H. sapiens and S. cerevisiae* enzymes (**31-34% identity**). Despite these homologs catalysing the same chemical reaction, there is diversity in the primary amino acid sequence of the enzyme from different species.

3.2 Determining the copy number of *TcNMT* in Silvio X10/7A

Sequence analysis of the original genome strain CL-Brenner found it to be a hybrid of two lineages and upon closer inspection, 2 putative NMT's sharing 99% sequence identity at the amino acid level have been annotated (TriTrypDB: TcCLB.506525.80 and TcCLB.511283.90). Prior to carrying out genetic validation, the copy number of *NMT* in X10/7A parasites was assessed by Southern blot. Isolated gDNA from this clone was digested using AfeI or DraI (**Figure 3.2 B,** *lanes 3+4*). These restriction endonucleases are both known to cut once within *NMT* ORF from sequencing of the X10/7A1 ORF and the X10/1 genome sequence (**Figure 3.2 A**). The digoxigenin (DIG) labelled *TcNMT* ORF hybridised to two fragments in both the AfeI and DraI digestions. The resulting fragment sizes produced by AfeI matched the predicted sizes from the X10/1 genome. The lower fragment of DraI digested gDNA was approximately 1 kbp smaller than expected, suggesting the presence of a SNP downstream of the *NMT* ORF in the X10/7A genome. Digestion with EcoRI or BamHI, both thought to cut outwith the coding sequence, yielded a single band, the sizes of which could not be predicted due to limited sequence assembley of Silvio X10/1. Together, these results suggest that this gene is present as a single copy per haploid genome. However, from these data we cannot rule out the possibility of aneuploidy in this parasite and that the chromosome encoding *TcNMT* has been duplicated.
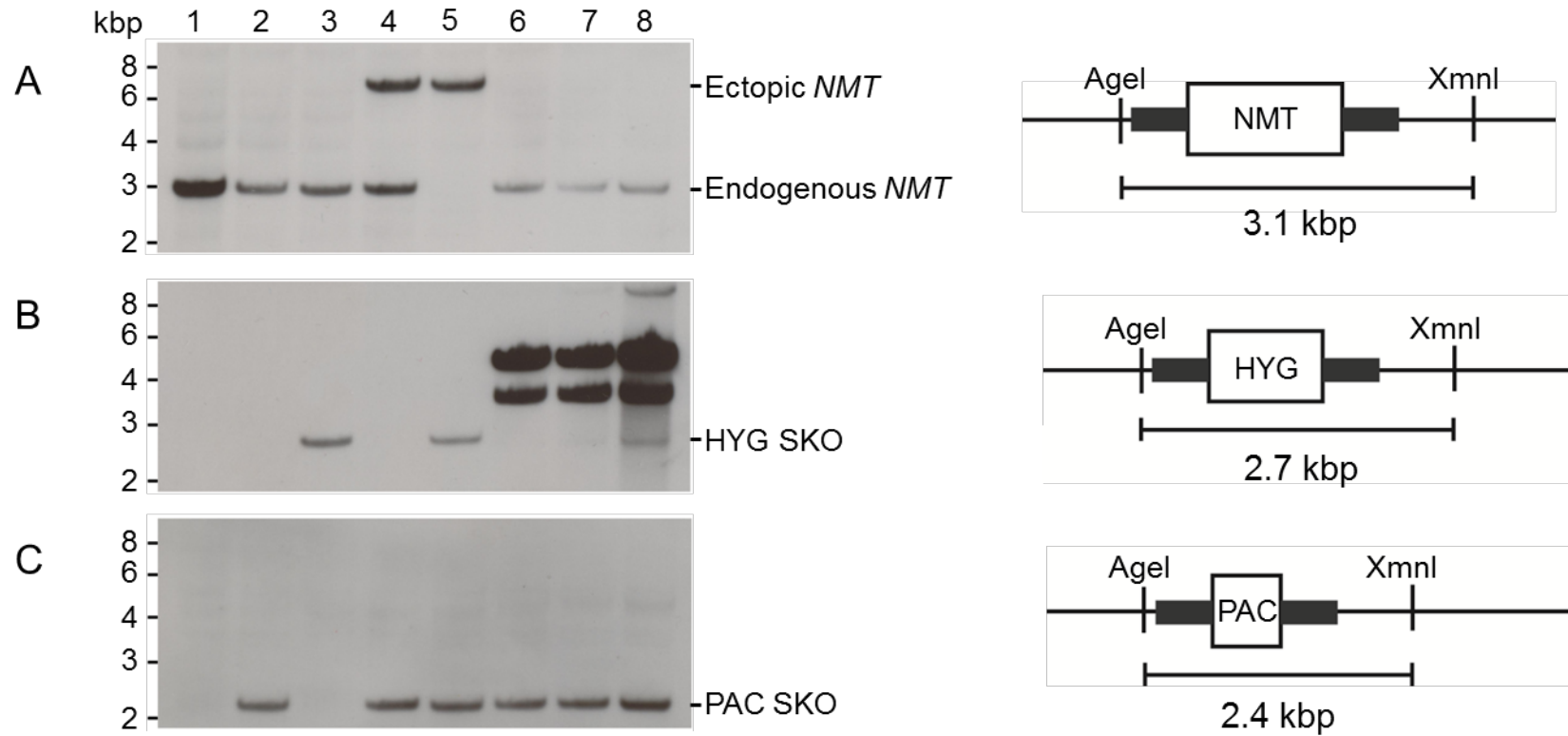
Figure 3.3 Analysis of WT, SKO and rescued *NMT* DKO cell lines
Southern blot analysis of AgeI and XmnI digested gDNA (5 µg) from WT cells (lane 1), SKO^{PAC} cells (lane 2), SKO^{HYG} cells (lane 3), SKO^{PAC} cells constitutively overexpressing *NMT* (lane 4), DKO$^{PAC+HYG}$ cells constitutively overexpressing *NMT* (lane 5) and failed *NMT* DKO$^{PAC+HYG}$ cells (lanes 6-8). Maps show the predicted fragment sizes for the WT and the correct replacement with the drug resistance markers when digested with AgeI and XmnI. Southern blots were probed with ORFs for (**A**) *TcNMT,* (**B**) *HYG* and (**C**) *PAC*.

3.3 Generation of a rescued *NMT* double knockout cell line

Having determined that *NMT* is a single copy gene, the genetic requirement for *NMT* in the epimastigote stage of this parasite was determined using a classical, multi-step gene replacement strategy (Wyllie *et al*., 2013). *TcNMT* specific, gene replacement constructs were generated using the 449 bp immediately up and downstream of the *NMT* ORF to flank the *hygromycin B phosphotransferase* (*HYG*) and *puromycin N-acetyltransferase* (*PAC*) drug selectable markers (Chang *et al*., 2002). The resulting *HYG* and *PAC* knockout constructs were individually transfected into epimastigotes and after ~6 weeks of selection with the appropriate drug, resistant parasites were recovered and cloned on semi-solid agar plates. Southern blot analysis was used to assess if these constructs were able to replace a single allelic copy of *TcNMT*. Probing the membrane with the *NMT* ORF revealed a single band present in WT and both drug resistant parasites indicating the retention of at least one allele (**Figure 3.3 A *lanes 1-3***). The *HYG* and *PAC* probes were both found to hybridise to a single band in their respective drug resistant cell lines (**Figures 3.3 B, *lane 3* and 3.3 C, *lane* 2**). The apparent sizes of these hybridised fragments correlated with the expected sizes for the correct replacement of a single allele by homologous recombination (**Figure 3.3 B + C right panel**), confirming these parasites to be genuine single knockouts (SKO).

Attempts were then made to replace the second allele in SKO^{PAC} parasites using the *HYG* replacement construct that had been used to generate the SKO^{HYG} cell line. Three independent transfections were carried out, but parasites resistant to both hygromycin B and puromycin were only recovered from two out of the three transfections. No parasites were observed in the third, even after 3 months. Clonal populations of these parasites were analysed by Southern blot and were all found to retain a copy of *NMT* at the WT size, suggesting that it might not be possible to generate a *NMT* null mutant, at least in the absence of a rescue construct (**Figure 3.3 A,**

lanes 6-8). Probing these failed DKO parasites (FDKO) for the *HYG* gene revealed it to be massively amplified in all FDKO cells in comparison with correct integration observed in the SKO*^{HYG}* cell line (Figure 3.3B lanes 6-8). However, a single band corresponding to the correct replacement of a single allele of *NMT* was detected in one out of three FDKO clones, despite the retention of a native copy of *Tc*NMT (**Figure 3.3 A+ B, *lane 8***). Probing with *PAC* revealed that this result was not due to the replacement of the *PAC* allele with the *HYG* knockout construct (**Figure 3.3 C, *lane 8***). These results indicate some form of genomic rearrangement has taken place, which may have led to aneuploidy in this particular clone.

The ability to generate a DKO in the presence of *NMT* overexpression was then investigated. Firstly, a constitutively expressed ectopic copy of *TcNMT* was targeted to the ribosomal spacer of the SKO*^{PAC}* cell line and was confirmed to have integrated at one site within the genome. It was then possible to replace this last endogenous copy of *TcNMT* only in the presence of the ectopic copy. Collectively with the identification of the genomic abnormality in a FDKO clone, this provides strong evidence that *TcNMT* is an important gene for the growth and survival of *T. cruzi* epimastigotes.

3.4 Analysis of failed double knockout parasites

With the evidence suggesting *TcNMT* is essential for the epimastigote stage of the parasite, the nature the *HYG* bands in the false DKO cell was studied. To determine if the intense nature of the detected bands was due to the formation of episomes, a diagnostic PCR reaction was carried out. Primers designed against the *T. cruzi trypanothione reductase* (*TcTryR*) ORF, or to read out from the *HYG* ORF (*HYG*^{OUT}) were used to amplify from equal amounts of gDNA isolated from WT, DKO^{OE} and the FDKO parasites. To provide a control for this diagnostic amplification, PCR reactions

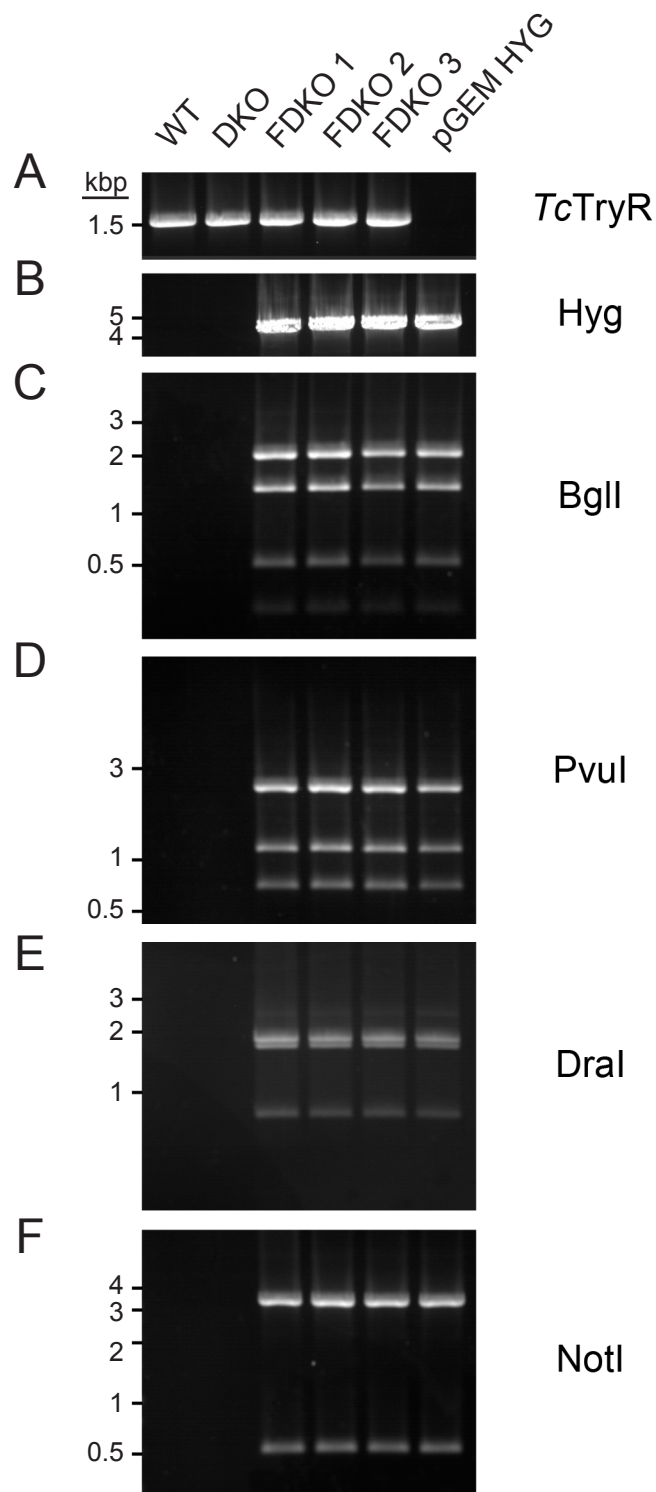**Figure 3.4 Diagnostic PCR and digestion of failed DKO parasites**
(**A**) Diagnostic PCR using primers for *TcTryR* from WT, DKO and failed DKO (FDKO) gDNA in addition to the pGEM-*HYG* plasmid. (**B**) PCR product using primers that read out from the *HYG* resistance gene. (**C-F**) Diagnostic digestion of **B** with the following restriction endonucleases (**C**) BglI, (**D**) PvuI, (**E**) DraI and (**F**) NotI.

of pGEM®-5Zf-*NMT-HYG* were also set up for both sets of primers. As expected, a single band at approximately 1.5 kbp was observed in PCRs from gDNA and was absent from the HYG-knockout plasmid, as it does not contain the *Tc*TryR ORF (**Figure 3.4 A**). The size of this band matches the predicted size of 1479 bp for the predicted *TcTryR* ORF from the Silvio X10/1 genome (**TriTryp: TCSYLVIO_004807**). In theory, amplification with the HYG^{OUT} primers would only produce a PCR product in cells where the *HYG* ORF was present as an extra-chromosomal episome, or had integrated with a head to tail concatemer. PCR products with a size of ~4.5 kbp were observed in FDKO parasites and the *HYG* knockout plasmid used as a positive control, but not in the WT and DKO^{OE} cell lines (**Figure 3.4 B**). To ensure that this was not simply due to a pipetting error, PCR reactions were repeated with the same results. These PCR products were then ligated into the TOPO® XL plasmid for sequencing, but despite multiple clones and TOPO® reactions, it was not possible to obtain sequencing data.

To assess if the product sizes from FDKO and control the PCR reactions matched by chance, these PCR products were digested with several restriction endonucleases (**Figure 3.4 C-F**). Analysing these digestions by gel electrophoresis revealed all of the fragment sizes in FDKO PCR products to match those produced by the PCR of the *HYG* knockout construct. In summary, these results suggest that the bands observed in Figure 3B are most likely to be episomal and they appear to have retained the pGEM5ZF backbone used in the construct generation. This is despite ensuring the vector was fully linearized prior to transfecting into the epimastigotes.
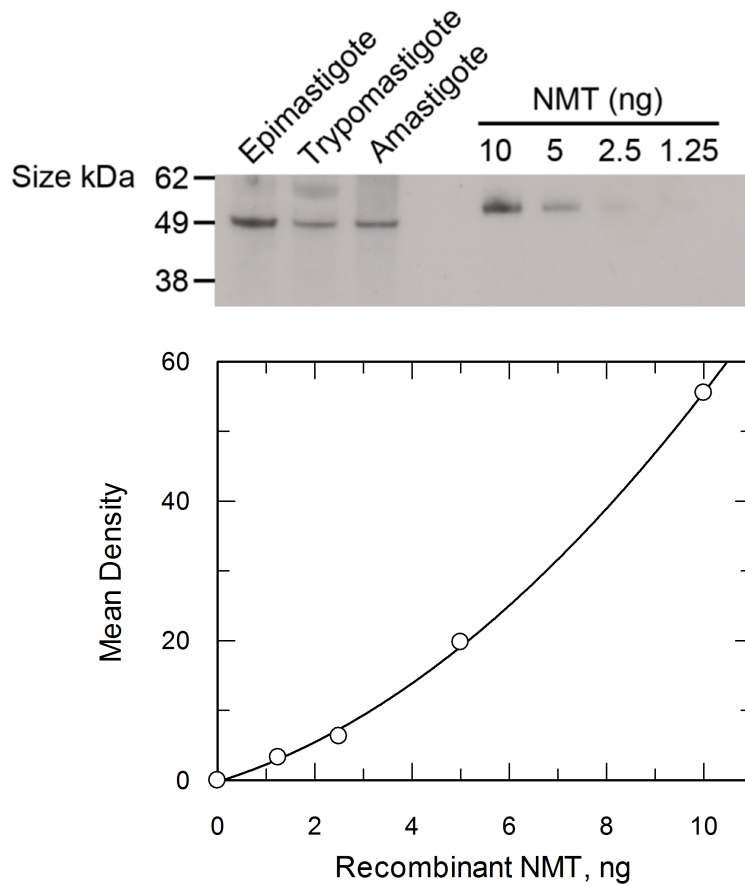
Figure 3.5 Levels of NMT expression throughout the lifecycle
Whole cell lysates (1×10^7 parasites per lane) of epimastigotes, trypmoastigotes and amastigotes were probed by immunoblot with a specific polyclonal antiserum raised against the recombinant protein. Known amounts of recombinant protein were used as standards for the quantification cellular NMT levels in the different lifecycle stage. The larger apparent mass of the recombinant protein is due to the presence of an N-terminal His_6 tag.

3.5 Expression of *Tc*NMT throughout the *T. cruzi* lifecycle

As the genetic tools available for use in *T. cruzi* are severely limited, it has not yet been possible to assess genetic essentiality in the disease relevant stages. To ensure that the enzyme is expressed in these clinically relevant stages, whole cell lysates of epimastigotes, trypomastigotes and amastigotes were probed with a specific polyclonal antiserum raised against the purified recombinant protein from *T. cruzi* CL-Brener. This antiserum was produced in collaboration with Dr Susan Wyllie, Dr Han Ong and Dr Scott Cameron at the University of Dundee. A single band at ~53 kDa was detected in all stages and was close to the theoretical mass of 51.3 kDa for the native enzyme (**Figure 3.5, top panel**). The amount of *Tc*NMT present in each stage was estimated by densitometry analysis using the intensities for known amounts of recombinant X10/7A1 protein, to produce the standard curve (**Figure 3.5, bottom panel**). The purified protein appeared marginally larger than the native enzyme due to the presence of an *N*-terminal His_6 tag. Using published cell volumes for the epimastigote, trypomastigote and amastigote, the cellular concentration of *Tc*NMT was calculated and was broadly similar throughout the life cycle at 1.2, 2.1 and 2.5 μM, respectively. In summary, the data show that NMT is continuously expressed in all forms of the parasite at a similar concentration. However, while NMT is expressed in the stages pertinent to the disease, we cannot extrapolate the importance of this enzyme during these infective stages.

3.6 Expression, purification and characterisation of recombinant *Tc*NMT

With the results of the genetic validation suggesting that this gene is essential in *T. cruzi* epimastigotes, the recombinant expression of NMT was undertaken in order to confirm it encoded a fully functional *N*-myristoyltransferase. *Tc*NMT was expressed as a fusion protein containing an N-terminal His_6 tag linked via a TEV protease cleavable peptide
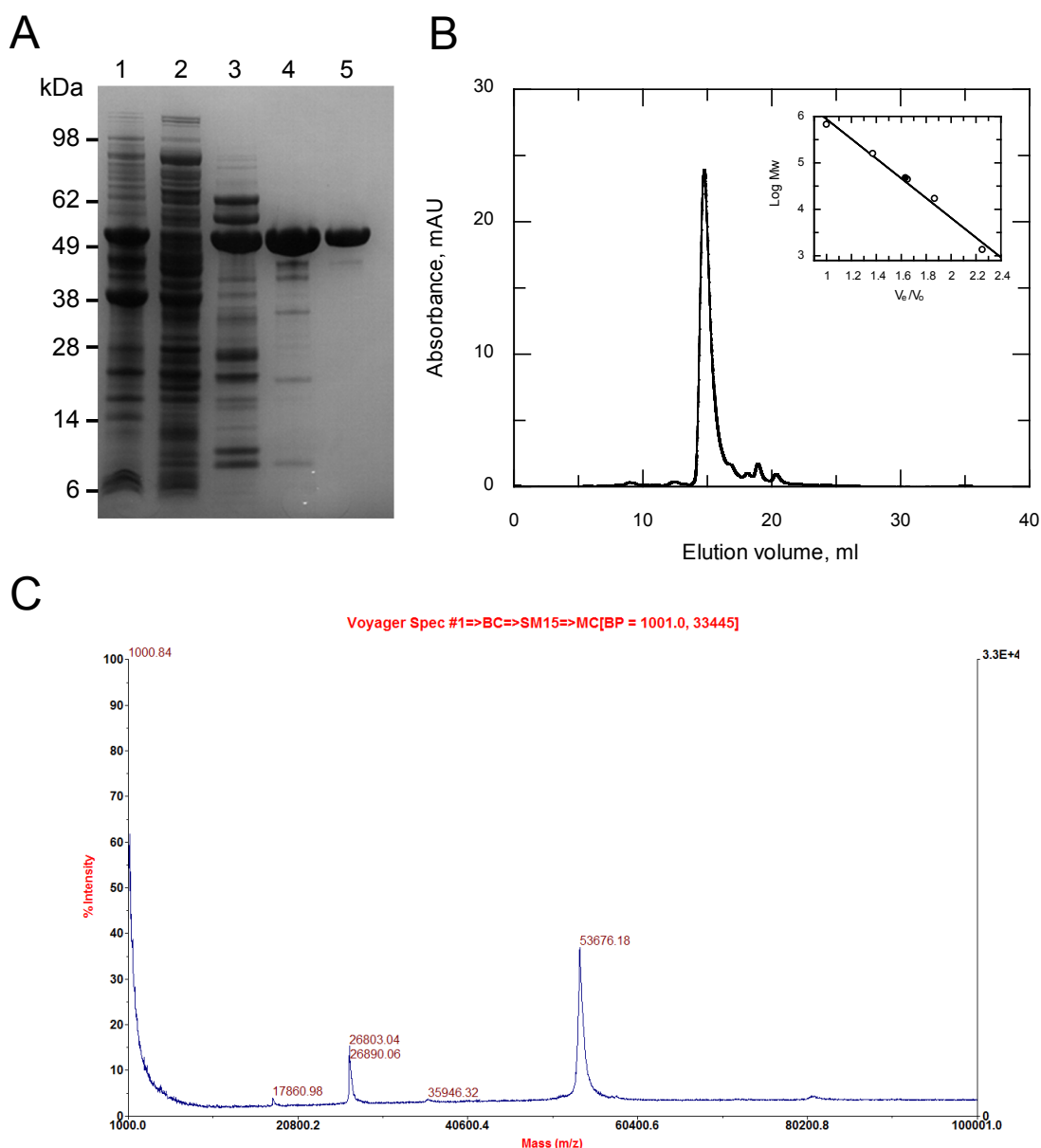
Figure 3.6 Recombinant expression and biophysical characterisation of *Tc*NMT
(**A**) SDS-PAGE of recombinant *Tc*NMT purification. Lane 1, insoluble fraction of induced Rosetta™ 2 (DE3) pLysS [pET15b-TEV-*TcNMT*]; lane 2, soluble fraction of induced Rosetta™ 2 (DE3) pLysS [pET15b-TEV-*TcNMT*]; lane 3, pooled fractions from Ni^{2+} affinity purification; lane 4, pooled fractions from anion exchange chromatography; lane 5, pooled fractions from size exclusion chromatography. (**B**) Analtical size exclusion profile for His_6-*Tc*NMT. The inset shows a plot of V_e/V_0 against the log molecular mass (Mw) of a standard protein mixture (open circles), where V_e is the elution volume and V_0 is the void volume of the column. The closed circle represents the elution volume of NMT. (**C**) MALDI-TOF spectra of recombinantly purified His_6-*Tc*NMT from Figure 5A lane 5.

sequence in *E. coli*. This strategy has successfully been used for the recombinant expression of the *T. brucei* and *L. major* homologs (Frearson *et al*., 2010; Price *et al*., 2003). The recombinant protein was produced using auto-induction medium in Rosetta 2 (DE3) pLysS cells, which express multiple tRNAs that are rarely used in *E. coli* (Studier, 2005). Following a three step chromatographic separation (nickel-affinity, anion exchange and size exclusion), the recombinant protein was purified to relative homogeneity as determined by SDS-PAGE, with an apparent Mw of ~49 kDa (**Figure 3.6 A**). The removal of the His$_6$ tag reduced the typical yield from ~2.5 mg L^{-1} to ~1 mg L^{-1} of culture, so the activity of the tagged and untagged forms was tested (***Section 3.7***).

Analysis of the sample by MALDI-TOF showed the purified fusion protein to be ~134 Da heavier than the theoretical mass of the protein with the N-terminal methionine excised (**Figure 3.6 C**). Assuming the initial methionine is excised in *E. coli* the mass difference may be explained by a combination of post-translational modifications that may occur in *E. coli,* but were not investigated for the purposes of this study. Alternatively, the methionine may still be present and the 15 Da discrepancy caused by a calibration error. Virtually all NMT's studied to date are reported to be monomeric however, the bovine brain form that has been shown to form oligomers ranging from 126-391 kDa as determined by size exclusion chromatography (Glover and Felsted, 1995). To determine the oligomeric structure of *Tc*NMT the purified recombinant enzyme was separated by analytical size exclusion chromatography against a series of protein markers of known mass (**Figure 3.6 B**). The majority of the recombinant enzyme eluted in a single peak with an apparent Mw of 47.4 kDa which is a similar order of magnitude to the mass as determined by mass spectrometry. Thus, *Tc*NMT from X10/7A1 was purified to homogeneity, with the His$_6$-fusion protein existing as a monomer *in vitro*. Purification of the CL-Brener enzyme used in the
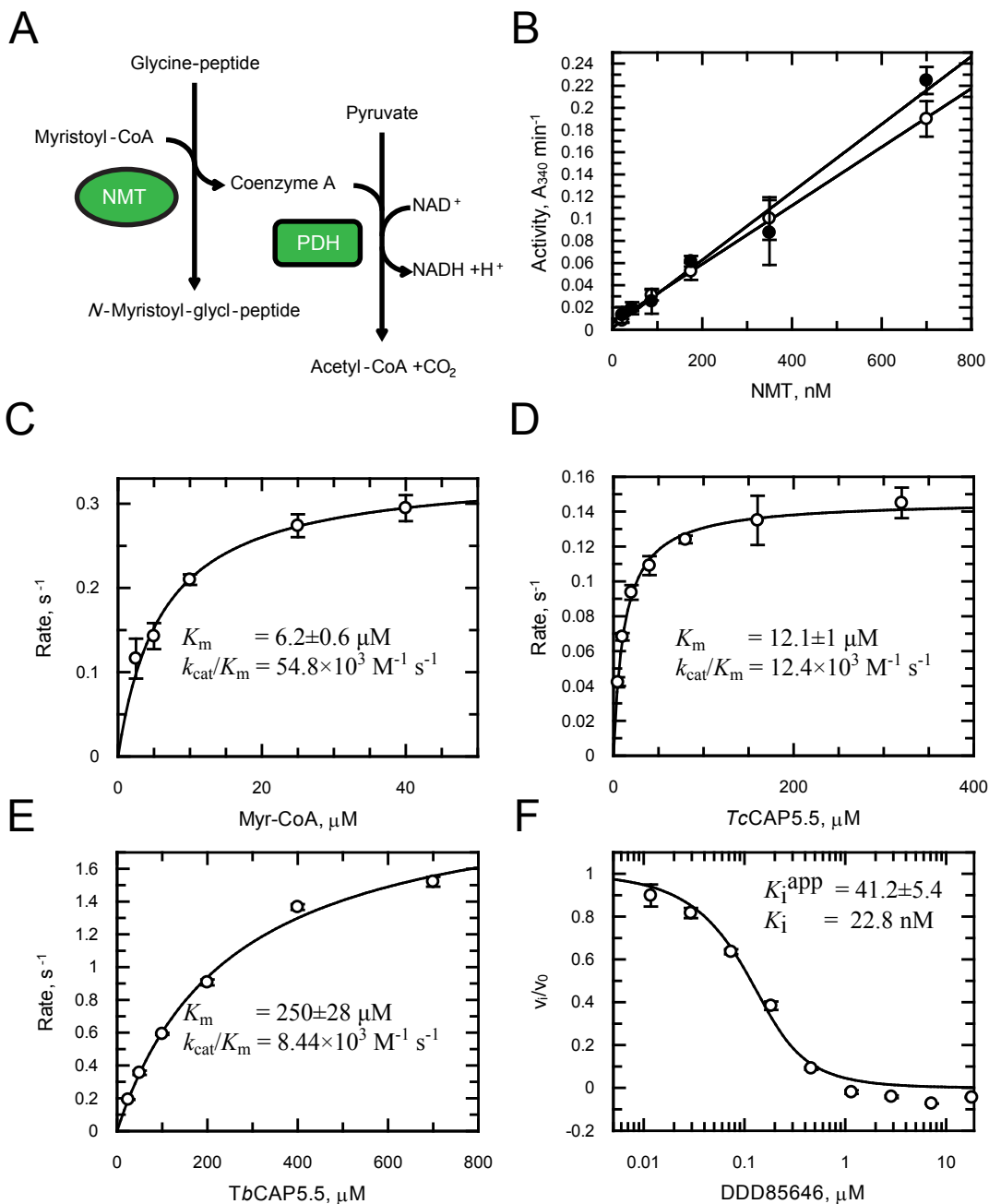
Figure 3.7 Kinetic characterisation of *Tc*NMT and its inhibition by DDD85646
(**A**) Diagram of the continuous coupled enzyme assay. Reaction is monitored in real time by the reduction of NAD^+ to $NADH^+$ at 340 nm. (**B**) Specific activity of *Tc*NMT (closed circles) and His$_6$-*Tc*NMT (open circles) measured by continuous spectrophotometric assay. (**C**) Determination of Myr-CoA K_m^{app}. (**D**) Determination of *Tc*CAP5.5 K_m. (**E**) Determination of *Tb*CAP5.5 K_m. (**F**) Inhibition of recombinant *Tc*NMT by DDD85646 in a dose dependant manner. The K_i^{app} and K_i were determined in the presence of 200 μM *Tb*CAP5.5. All measurements are made in triplicatte and are presented as the mean of 3 experiments ± standard deviation.

generation of polyclonal antisera was carried out in an identical manner and was also found to be monomeric.

3.7 Kinetic characterisation of NMT and inhibitor studies

The enzymatic products of NMT are not directly quantifiable in real time. However there are many assays available for the characterisation of these enzymes using a variety of techniques, such as coupled enzyme assays, scintillation proximity, enzyme-linked immunosorbent (ELISA) and HPLC methods (Boisson and Meinnel, 2003; Goncalves *et al*., 2012a; Panethymitaki *et al*., 2006; Rampoldi *et al*., 2012; Towler *et al*., 1988). For the characterisation of the *T. cruzi* enzyme, we modified a previously published coupled enzyme spectrophotometric assay by lowering the pH to 7.4 and coupling the activity of the recombinant enzyme to pyruvate dehydrogenase (Boisson and Meinnel, 2003). The resulting reduction of NADH to $NADH^+$ is monitored in real time at 340 nm (**Figure 3.7 A**). The activity of recombinant *Tc*NMT was first measured using a synthetic peptide based upon amino acids 2-15 of the *T. brucei* cytoskeleton associated protein CAP5.5, which is known to be *N*-myristoylated (Frearson *et al*., 2010; Hertz-Fowler *et al*., 2001b). The activity of the coupling enzyme was only observed in the presence of myristoyl-CoA, *Tc*NMT and the peptide substrate. When substrates were individually omitted from the reaction or NMT had been heat inactivated, no detectable activity was observed.

The specific activities for the His_6-tagged and untagged recombinant proteins were determined presence of 100 μM *Tb*CAP5.5 and 40 μM myristoyl-CoA (Myr-CoA) by varying the concentration of enzyme present. The presence of the tag did alter the activity of the enzyme by decreasing the specific activity from x μmol min^{-1} mg^{-1} to x μmol min^{-1} mg^{-1} (**Figure 3.7 B**). The remainder of the kinetic characterisation was

carried out on the His$_6$-TcNMT enzyme, as there was not significant loss in activity due to the presence of the tag.

The K_m's of TbCAP5.5 and TcCAP5.5 were determined using 150 nM NMT with this assay by taking the linear region of activity, which occurred between 60-110 seconds after initiation (**Figure 3.7 D+E**). Both substrates were able to accept myristic acid, however, the K_m values of 250 ±28 and 12.1 ±1 µM for TbCAP5.5 and TcCAP5.5 were significantly different to each other. Whilst this is probably due to the differences in the peptide substrates, both substrates had a similar catalytic efficiency k_{cat}/K_m. Due to reasons of cost and practicality, it was not possible to determine a true K_m for Myr-CoA under saturating concentrations of peptide substrate TbCAP5.5, so the apparent K_m (K_m^{app}) was determined with 700 µM of the peptide (**Figure 3.7 C**). The enzyme concentration was decreased (15 nM) to allow a longer linear region for quantification, as this assay starts to approach the limits of detection especially with K_m values in the single digit µM range. The K_m^{app} for Myr-CoA was found to be 6.2 ± 0.6 µM, which is in a similar range to other reported K_m values for different homologs.

Having demonstrated that the recombinant protein encoded a fully functional N-myristoyltransferase, the activity of the enzyme was determined in the presence of the *T. brucei* NMT inhibitor DDD85646 (**Figure 3.7 F**). This activity was determined for various concentrations of DDD85646 with fixed concentrations of enzyme and substrate (150 nM NMT, 40 µM Myr-CoA and 200 µM TbCAP5.5). The dose response curve suggested that the IC_{50} (the concentration of inhibitor required to reduce the activity to half the maximum) of DDD85646 was 75 nM which is in the region of tight binding inhibition. The data were alternatively fitted to the Morrison equation for tight binding inhibition to allow an apparent K_i ($K_i^{app} = 41.2$ nM) to be calculated for the inhibitor enzyme complex. It is known that there is a proportional relationship between the K_i^{app}

and the K_i. This was used to calculate the true K_i for DDD85646 to be 22.8 nM. This confirms that DDD85646 is able to inhibit the enzymatic activity of TcNMT via a tight binding mechanism, similar to that reported against the *T. brucei* enzyme (Frearson *et al.*, 2010).

3.8 Crystallisation of TcNMT

The differing substrate selectivities across these enzymes in eukaryotes have made them promising targets for rational based drug design (***Section 1.4.3***). This process can be greatly aided by the availability of structural data for these enzymes. A search of the protein data bank found crystal structures of the enzymes from *L. major*, *Plasmodium vivax*, *S. cerevisiae*, *L. donovani* and *C. albicans,* but not *T. cruzi*. With the aim of producing a crystal structure of the *T. cruzi* homolog, purified His_6-TcNMT was subjected to crystallisation trials in the presence in the absence and presence of Myr-CoA and the TbNMT inhibitor DDD85646. Within 24 hours, a single crystal had grown in 0.1 M Na/K phosphate pH 6.2, 25 % (v/v) 1,2-propanediol and 10 % (v/v) glycerol at 18.3 °C for the liganded recombinant protein. With the help of Dr Scott Cameron the diffraction of this crystal was tested, however it failed to produce an x-ray diffraction pattern. The initial hit conditions were then optimised by varying the concentrations of 1,2-propanediol and glycerol present in the reservoir solution. In addition, the protein concentration was decreased in an attempt to slow down the crystallisation process and after 5 months, a single crystal was found in 0.1 M Na/K phosphate pH 6.2, 27.5% 1,2-propanediol, 11 % Glycerol at 18.3 °C. Once again, the ability of the crystal to diffract x-rays was tested by Dr Scott Cameron and diffraction to ~4.5 Å was observed. Despite this success, a dataset was not collected on this crystal in favour of using it for crystal seeding experiments, all of which failed to produce further

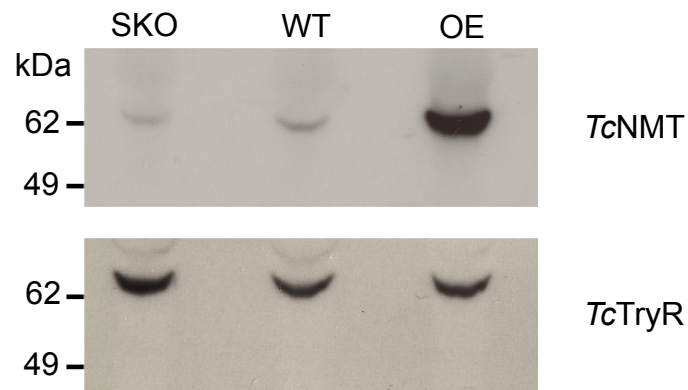**Figure 3.8 Modulation of NMT expression**
Western blot analysis of transgenic NMT parasite cell lines. Duplicate blots of epimastigotes (1×10^7 per lane) were probed with specific polyclonal antierum raised against TcNMT or TcTryR. Densitometry analysis was used to quantify the relative expression changes of TcNMT in SKO, WT and NMT^{OE} cells using TcTryR as the loading control.

crystals for analysis. The failure to grow crystals except in the presence of Myr-CoA and DDD85646 may suggest the presence of ligands may be an important factor for obtaining diffraction quality crystals.

3.9 Altered expression levels of *Tc*NMT in transgenic parasites

To facilitate NMT inhibition studies in the parasite, WT and transgenic-NMT cell lines were probed by western blot for *Tc*NMT expression to determine if the transgenic parasites had modulated levels of NMT in comparison with the WT. The NMT^{SKO} line was generated as described earlier whilst cells constitutively overexpressing NMT were generated by transfecting pTREX-*NMT* into WT parasites. Southern blot analysis of this cell line revealed the construct to have stably integrated twice within the genome however, the exact location of each integration was not determined. A single band with an apparent Mw of ~53 kDa was detected in the lysates of WT, NMT^{SKO} and NMT^{OE} parasites when probed with specific polyclonal antisera (**Figure 3.8**). Although a large excess of NMT was detected in NMT^{OE} parasites in comparison with the WT, the difference between the WT and NMT^{SKO} cells was less obvious. A duplicate blot was probed for the presence of TryR to act as a loading control across the different cell lines (**Figure 3.8**). This was chosen for the loading control as the expression of *Tc*TryR is unlikely to be affected by the modulation of NMT, as they are in unrelated pathways and different on chromosomes. By quantifying, the intensities of the *Tc*NMT and normalising the values to *Tc*TryR a 63% reduction in NMT was detected in the NMT^{SKO} compared to the WT, whilst a 7.6-fold increase was observed in the NMT^{OE}. In summary, these results have highlighted that it is possible to generate *T. cruzi* with modulated levels of expression by the deletion of a single allele, or by the genomic integration of a constitutive overexpression vector.
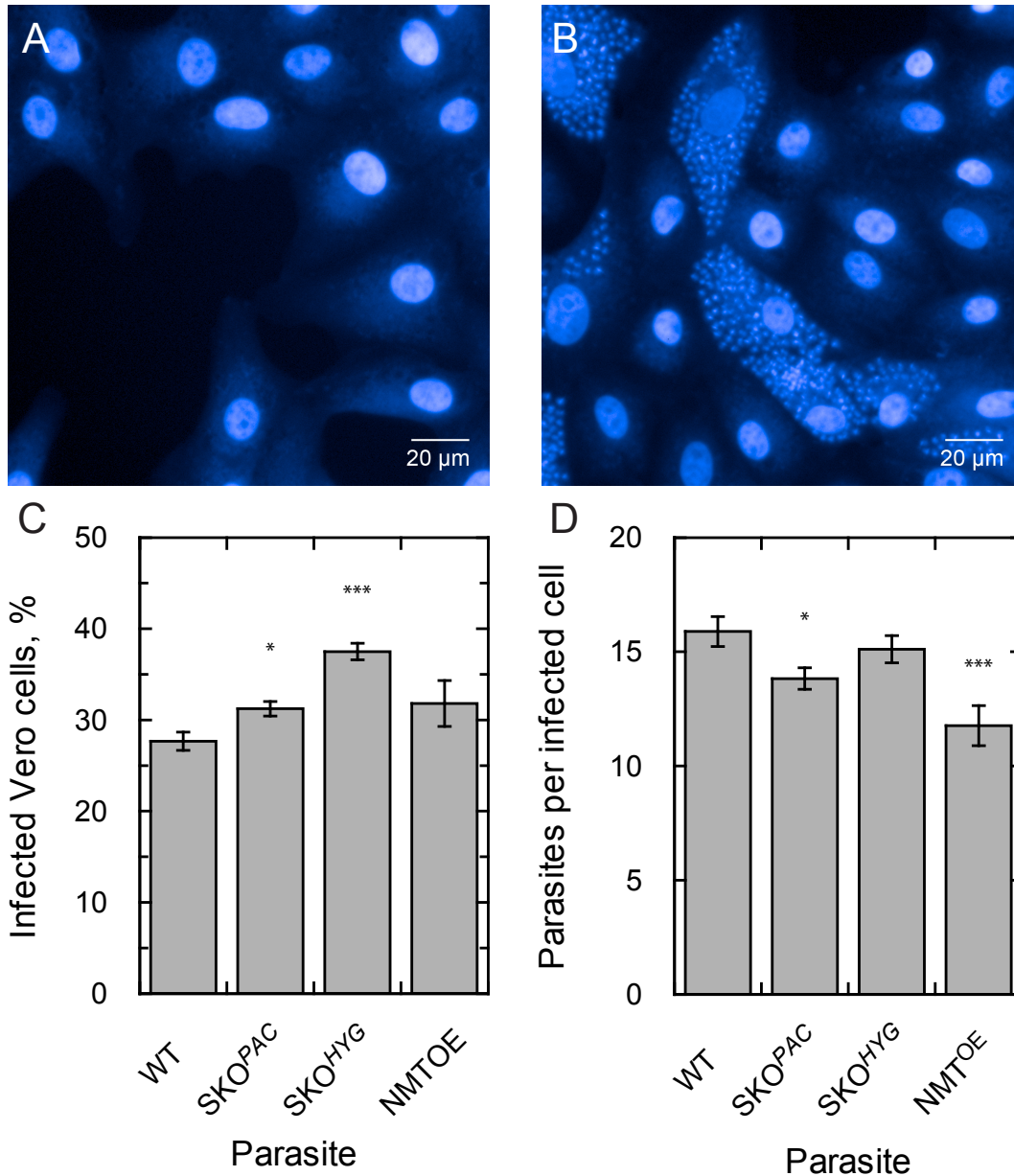
Figure 3.9 Infectivity of transgenic *T. cruzi* parasites
(**A**) Uninfected Vero cells stained with Hoechst 33342. (**B**) Typical view of infected Vero cells stained with Hoescht 33342. (**C**) The percentage of Vero cells infected with transgenic SKO^{PAC}, SKO^{HYG} and NMT^{OE} parasites in comparison with the WT. The infectivity of SKO^{PAC} and SKO^{HYG} were confirmed to be statistically significant (*P < 0.01) using an unpaired Students *t* test. (**D**) The mean number of amastigotes per infected Vero cell. Differences in the mean number of SKO^{PAC} and NMT^{OE} amastigotes in comparison to the WT were confirmed to be statistically significant using an unparied Students *t* test (*P < 0.05, ***P < 0.001). A total of 24 measurements were made for each paramater. The data is shown as the means ± S.E.M.

3.10 Infectivity of transgenic *T. cruzi* parasites

With the absence of full genetic validation in the clinically relevant stages, the ability of these transgenic parasites to infect a mammalian cell and progress through the complete lifecycle were compared. The University of Dundee's Drug Discovery Unit (DDU) has developed a *T. cruzi* high-throughput screening assay for assessing drug efficacy in Vero cells using image analysis software for quantification. As initial Vero cell infections revealed an un-even distribution of infected cells, the high content assay was used to remove bias and assess the infectivity of these transgenic parasites. A mixture of metacyclic trypomastigotes and epimastigotes obtained from late stage cultures were used to infect Vero cell monolayers overnight, before removing non-invaded parasites. After obtaining pure trypomastigote populations by cycling them through Vero cells (3 times), fresh infections were set up with a parasite to Vero cell ratio of 5:1. Infected cells were fixed with formaldehyde after 3 days and stained with DAPI. With the help of Dr Manu De Rycker (DDU, University of Dundee), the infections were imaged using a high content microscope where the percentage of infected cells, and the number of parasites per infected cell were quantified. Due to the size differences between mammalian and amastigote nuclei, the software is able to determine these parameters using these principles as described previously (Nohara *et al*., 2010). Typical images of un-infected and infected Vero cells (**Figure 3.9 A + B**). The deletion of a single allele of NMT led to a minor, but statistically significant, increase in the percentage of infected cells when compared to the WT, whereas the NMT^{OE} had no effect (**Figure 3.9 C**). Vero cells infected with SKO^{PAC} and NMT^{OE} parasites were found to have a marginally reduced, but statistically significant, parasite load compared to the WT parasites (**Figure 3.9 D**). Despite the statistically significant differences observed between some of these cell lines, the measured changes do not appear greatly alter the biological relevance, as all parasite cell lines showed a similar infection profile.
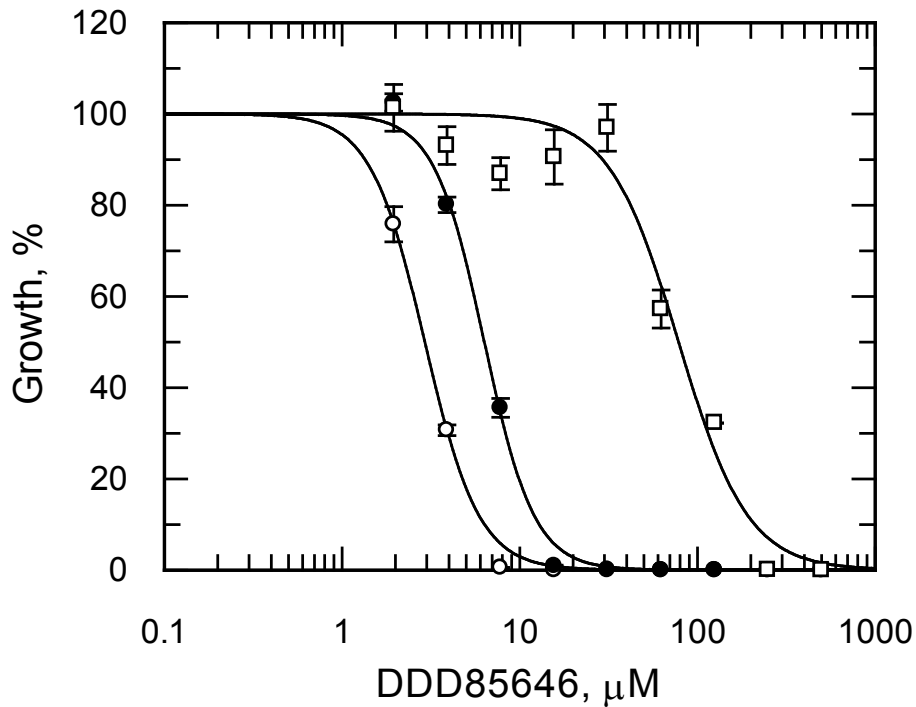
Figure 3.10 Potency of DDD85646 against transgenic NMT parasites
EC_{50} values were determined against SKO^{PAC} (open circles), WT (closed circles) and NMT^{OE} (open squares) parasites after a 5 day incubation with various concentrations of DDD85646 in RTH/FCS. EC_{50} values of 2.9 ± 0.04, 6.3 ± 0.1 and 78.6 ± 4.2 μM were determined against SKO^{PAC}, WT and NMT^{OE} cell lines respectivley. Shifts in potency were determined to be statistically significant with respect to WT cells (P=0.0001) using an unpaired Students t test.

3.11 DDD85646 versus *T. cruzi* epimastigotes

With the knowledge that the *Tb*NMT inhibitor DDD85646 was a highly potent inhibitor of the *T. cruzi* recombinant enzyme, the activity of this compound was determined against the parasite. The concentration of drug required to inhibit the growth of *T. cruzi* epimastigotes by 50% (EC_{50}) was found to be 6.3 ± 0.1 µM against WT parasites (**Figure 3.10**). To determine whether this anti-proliferative effect was mediated via NMT, EC_{50} values were also determined against cell lines containing modulated levels of NMT that were generated previously. The SKO parasites became approximately 2-fold more sensitive to treatment with DDD85646 ($EC_{50} = 2.9 \pm 0.04$ µM) in comparison with WT parasites. Conversely, a ~12-fold reduction in sensitivity to DDD85646 was observed with the overexpression of NMT (NMT^{OE}, $EC_{50} = 78.6 \pm 4.6$ µM). The potency shifts determined for transgenic parasites in comparison with WT were confirmed to be statistically significant for both cell lines using an unpaired Students *t* test ($P < 0.0001$). In combination with the data from **Figure 3.8**, the sensitivity of parasites to treatment with this inhibitor correlated with the cellular concentration of NMT present in the parasite. This would suggest that the reduction in parasite proliferation is a result of the specific targeting of *Tc*NMT in the cell by DDD85646.

3.12 Detection of cellular *N*-myristoylation

Due to the presence of multiple NAD^{+}-reducing enzymes in the parasite, the coupled enzyme spectrophotometric assay used for the kinetic characterisation of *Tc*NMT is not suitable for monitoring cellular *N*-myristoylation. Previous studies in *T. cruzi* and *T. brucei* have monitored the incorporation of [^{3}H]-myristic acid into proteins via NMT using autoradiography, which can require exposures to film over several weeks. More
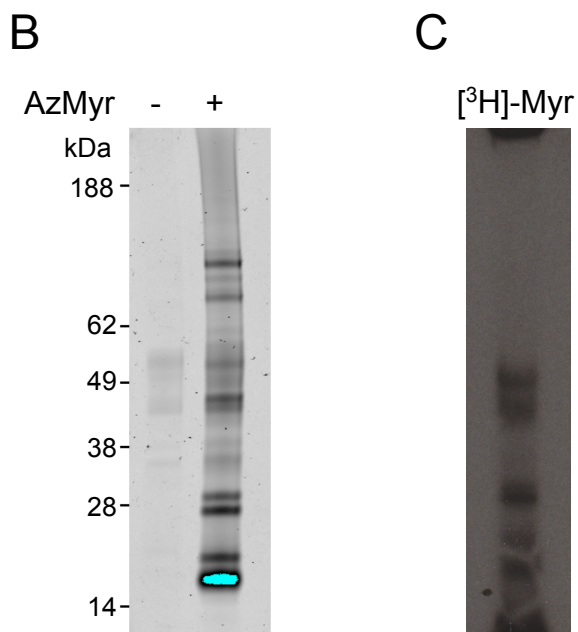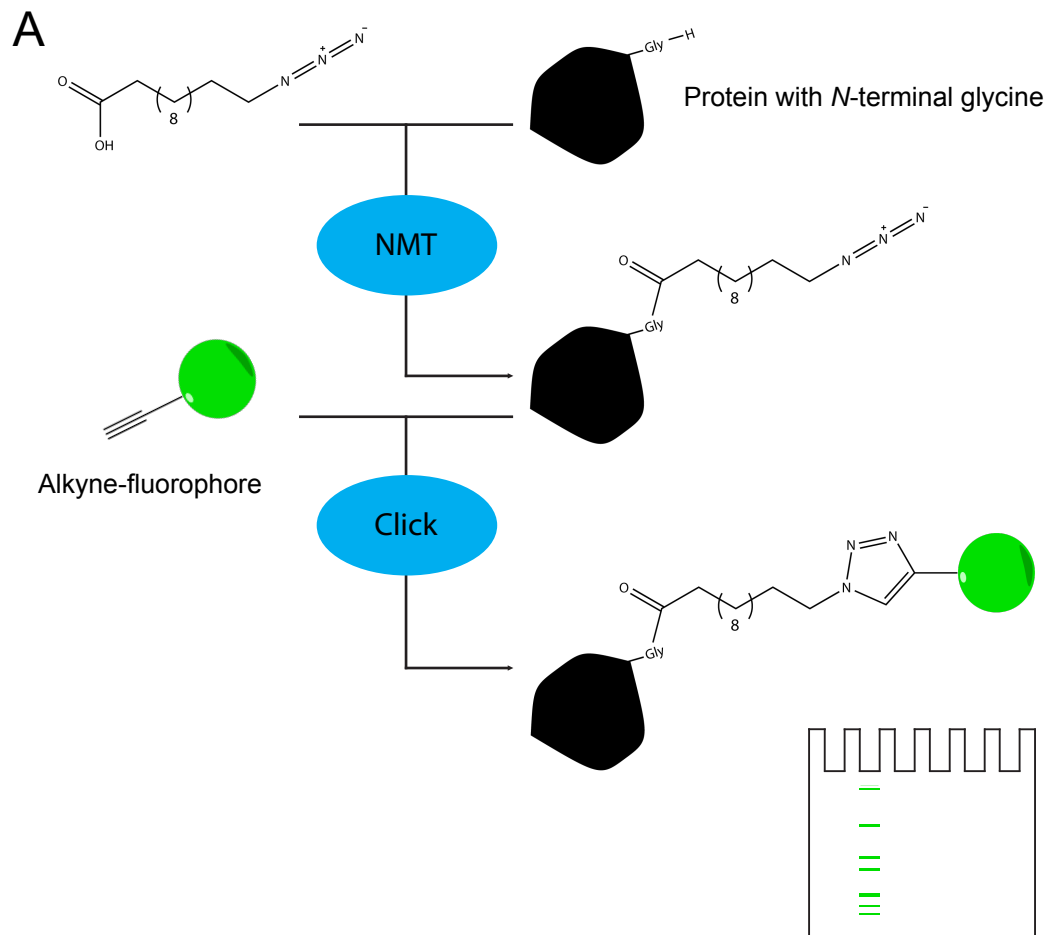
Figure 3.11 Detection of *N*-myristoylation

(**A**) Parasites take up the myristic acid analog azidomyristate and attach it to a molecule of CoA. Azidomyristate is incorporated onto the *N*-terminal glycine of specific proteins via cellular NMT. A fluorecently labelled alkyne is attached to *N*-azidomyristoyalted proteins by click chemistry. Labelled proteins visualised after separating by SDS-PAGE using in-gel fluorescence. (**B**) Detection of *N*-azidomyristoylated proteins with click chemistry. (**C**) Detection of *N*-myristoyation with [³H]-myristic acid with an exposure time of 2 weeks.

recently, the development of myristic acid analogs compatible with click chemistry has shortened this detection process to a few minutes (**Figure 3.11 A**) (Hang *et al*., 2007). To determine if the myristic acid analog 12-azidododecanoic acid (azidomyristate) was a comparable substrate to [^{3}H]-myristic acid in *T. cruzi*, the two detection methodologies were directly compared. Epimastigotes were labelled with 50 μM azidomyristate or 100 μCi ml^{-1} or myristic acid for 6 hours and samples subsequently processed and separated by SDS-PAGE and treated with 0.2 M KOH to remove *O*- and *S*-myristoylation. A single faint band was detected in cells without azidomyristate above 49 kDa (**Figure 3.11 B,** *lane 1*), whilst >10 bands were observed in treated with a range of sizes (**Figure 3.11 B,** *lane 2*). In comparison, parasites labelled with [^{3}H]-myristic acid displayed a slightly different pattern of *N*-myristoylation with bands at higher masses most notably absent (**Figure 3.11 C**). However, the base-insensitive incorporation of azidomyristate into the epimastigote proteome suggests that these bands are *N*-myristoylated proteins.

3.13 Inhibition of *N*-myristoylation in *T. cruzi* epimastigotes

The direct inhibition of *N*-myristoylation in cells treated with this compound would confirm DDD85646 as a true *Tc*NMT inhibitor. With this in mind, the incorporation of the myristic acid analog azidomyristate into the epimastigote proteome was measured using click chemistry in the presence of the inhibitor (**Figure 3.11 B**). Parasites were pre-incubated with DDD85646 at concentrations ranging from ~2-15 times the EC$_{50}$ value of WT cells to allow equilibration of the inhibitor into the parasite. A single prominent band was detected at ~49 kDa in epimastigotes not labelled with azidomyristate, whilst multiple bands were observed in labelled cells in the absence of any drug (**Figure 3.12 A lanes 1+2**). Increasing the inhibitor concentration produced a
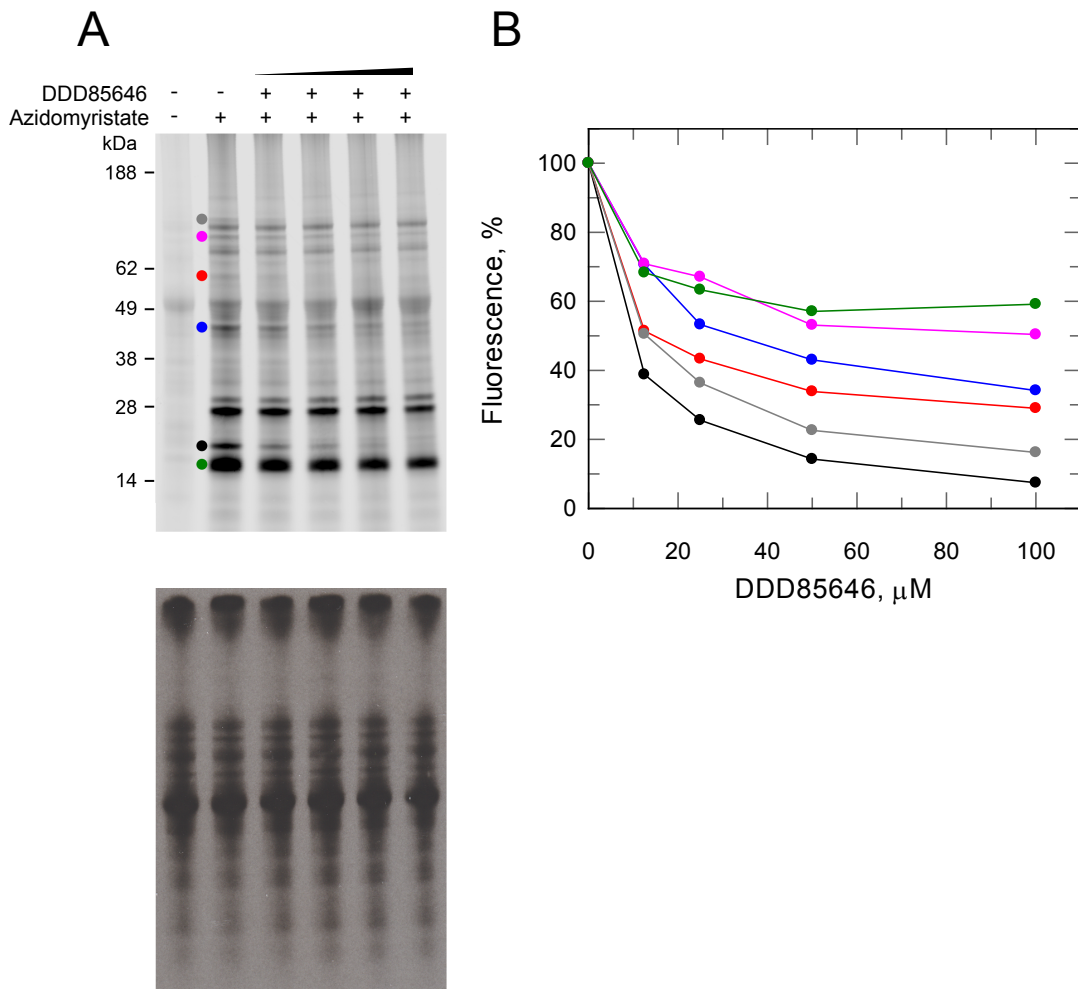
Figure 3.12 Specific inhibition of *N*-myristoylation in epimastigotes
Mid-log epimastigotes were pre-incubated with various concentrations of
DDD85646 ($0\text{-}15 \times EC_{50}$) and labelled with azidomyristate for 5h. (**A**)
N-myristoyalted proiteins were detected after click chemistry ligation of an
alkyne dye onto *N*-azidomyristoylated proteins (upper panel) and nascent
protein synthesis was assessed by L-[^{35}S]-methionine labelling of parasites by
autoradiography (lower panel). Coloured circles highlight bands sensitive to
treatment with DDD85646 that were quantified for panel B. (**B**) Reduced fluo-
rescence intensities as a function of DDD85646 concentration.

dose-dependent depletion of six *N*-azidomyristoylated proteins that were detected and quantified by in-gel fluorescence (**Figure 3.12 A, top panel lanes 3-6 and B**). The remaining bands were insensitive to DDD85646 treatment over incubation period of 5.5 h, the cause of which is not known. Parasites labelled with [^{35}S] L-methionine confirmed that this effect was due to the direct inhibition of *N*-myristoylation in the parasite and not due to the interruption of nascent protein synthesis (**Figure 3.12 A bottom panel**). These data provide the most conclusive evidence that DDD85646 acts via the chemical inhibition of *Tc*NMT and cellular *N*-myristoylation.

3.14 An alternative mechanism of DDD85646 in *T. cruzi* epimastigotes

The evidence so far has shown DDD85646 to be a specific inhibitor of *N*-myristoylation in this parasite. Morphological studies of *T. brucei* bloodstream form (BSF) parasites treated with this inhibitor showed a "Big Eye" phenotype caused by a massively enlarged flagellar pocket (Frearson *et al*., 2010). To determine if this effect was observed in *T. cruzi* epimastigotes treated with 10 times the EC_{50} of the WT and stained with Giemsa prior to viewing by light microscopy. After 72 hours, parasites appeared to have multiple flagella; however the nuclei and kinetoplasts of the parasites were not clearly resolved (**Figure 3.13 A + B**). To investigate the hypothesis that the multiple flagella observed in drug treated parasites were as result of a cell cycle defect, treated cells were fixed at 24 h intervals and stained with DAPI to view nucleic acid containing organelles. Slides were blinded prior to determining the parasites' kinetoplast (K) and nuclei (N) numbers for control and DDD85646 treated epimastigotes (2 and 10 times the EC_{50}). Representative fluorescence and light microscopy images for 1K1N, 2K2N and 3K3N parasites are shown (**Figure 3.13 C-E**). The accumulation of 2K2N WT and NMT^{OE} parasites was recorded at 2 times the EC_{50} revealing an increase in WT 2K2N
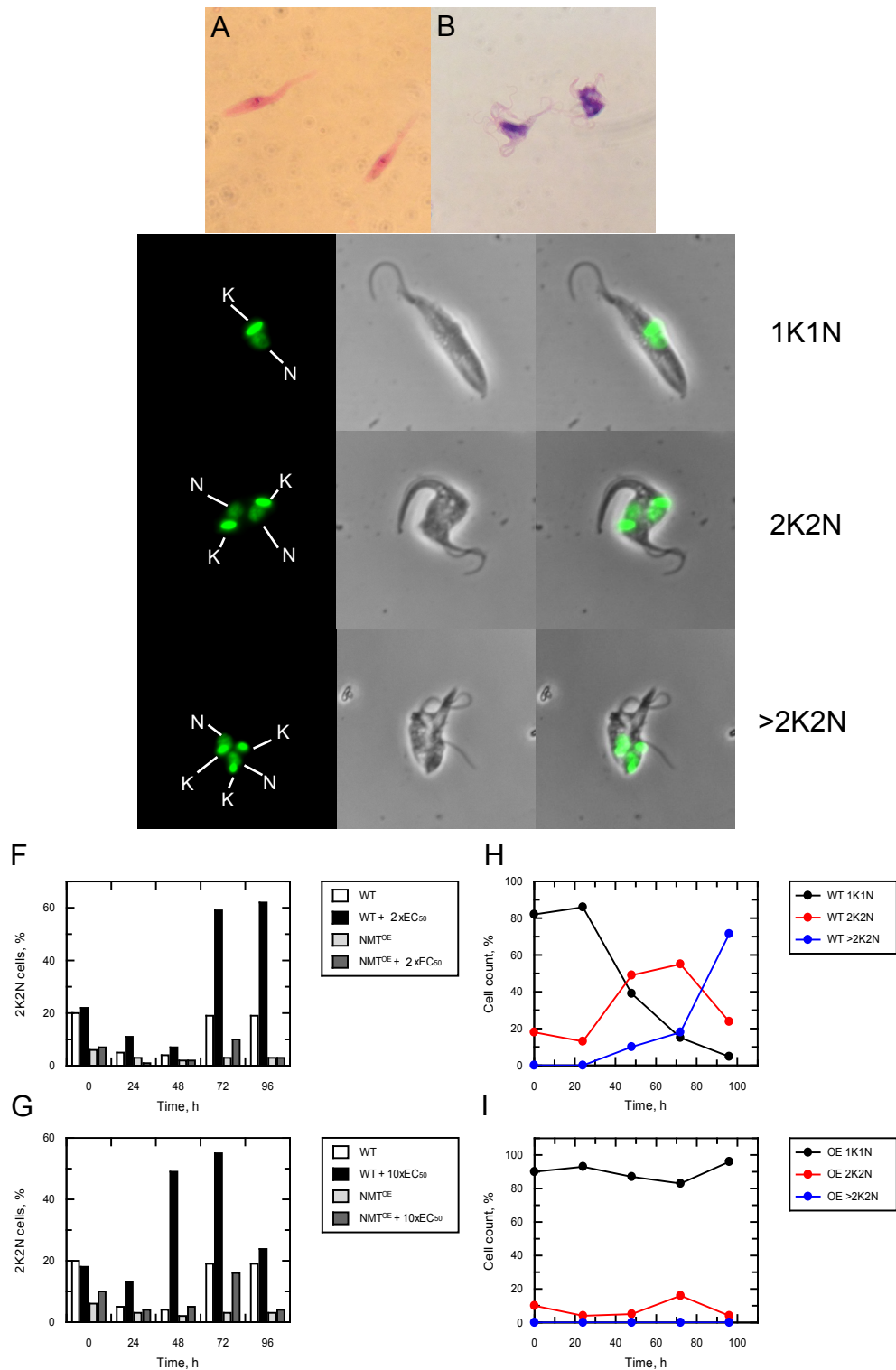
Figure 3.13 Inhibition of cytokinesis in |*T. cruzi* epimastigotes treated with DDD85646

Comparison of Geimsa staned epimastigotes treated with DMSO (**A**) or 10 × EC$_{50}$ of DDD85646 (**B**) after 48 hours. Representative images of 1K1N (**C**), 2K2N (**D**) and 3K3N (**E**) DAPI stained epimastigotes due to treatment with DDD85646. Time resolved, accumulation of 2K2N parasites for WT and NMT^{OE} parasites treated with 2 (**F**) and 10 × EC$_{50}$ (**G**) of DDDD85646. Population profiles of 1K1N, 2K2N and >2K2N epimastigotes for incubations at 2 (**H**) and 10 × EC$_{50}$ (**I**) of DDD85646.

numbers at 72 h, with overexpression of NMT counteracting the build-up of these multinucleated cells (**Figure 3.13 F**). This relationship also was evident in parasites treated with 10 times the EC_{50} of DDD85646, with the accumulation of 2K2N parasites appearing at 48 hours after addition of the drug in WT cells (**Figure 3.13 G**). The drop in 2K2N WT parasites after 72 h at 10 times the EC_{50} was accompanied with an increase in cells containing greater than 2K2N (**Figure 3.13 H**) with the overexpression of NMT once again rescuing this phenotype (**Figure 3.13 I**). Together, these results show the DDD85646 phenotype in *T. cruzi* epimastigotes is both dose-dependent and related to the expression levels of NMT and the morphological studies show the inhibition of *N*-myristoylation is associated with a failure to complete cytokinesis. Due to poor selectivity of DDD85646 between host cell and intracellular parasites, it is not possible to determine if this drug acts via the same mechanism in the clinically relevant amastigote stage.

Chapter 4

Characterising the *N*-myristoylome

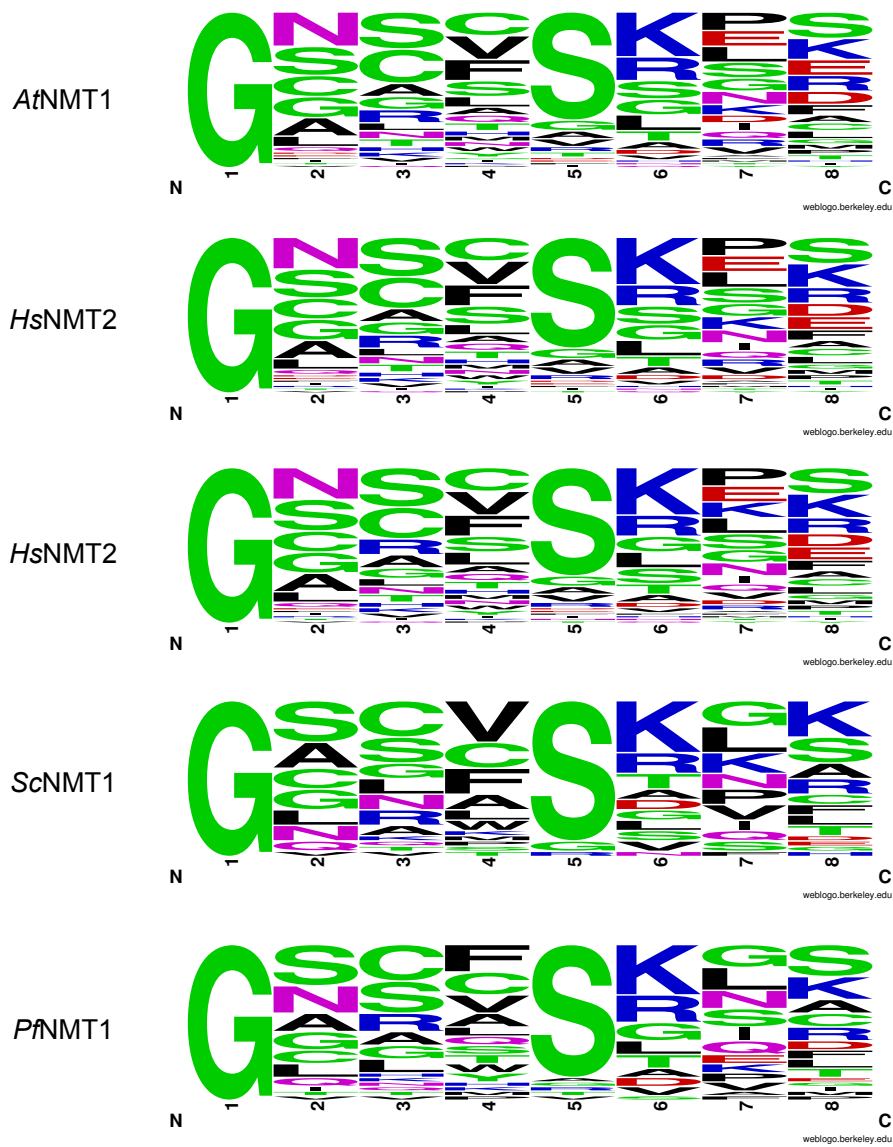**Figure 4.1 Peptide substrate specificities of NMT homologs**

Frequency Logo plots were generated for peptides capable of acting as substrates for *At*NMT, *Hs*NMT1, *Hs*NMT2, *Sc*NMT1 and *Pf*NMT1. Substrate specificities for these peptides was determined by a high-throughput assay and all substrates compared with each homolog. The data for these plots were published by Traverso *et al* 2010.

Table 4.1 Proteins predicted to be *N*-myristoylated with a high confidence using the program Myristoylator (ExPASy) from the *T. cruzi* reference proteome

UniProt Accession	Myr Score	Protein names
K4DUN8	0.978	Calpain cysteine peptidase, putative,cysteine peptidase, Clan CA, family C2, putative
K4E5Y1	0.990	Cytoskeleton-associated protein CAP5.5, cysteine peptidase, Clan CA, family C2
K4DSW1	0.982	Dynein heavy chain, putative
K4DT87	0.982	Dynein heavy chain, putative
K4E5P0	0.974	Fatty acyl CoA synthetase 2, putative
K4EC28	0.986	Flagellar calcium-binding protein, putative
K4E7U1	0.986	Flagellar calcium-binding protein, putative
K4DYY3	0.981	Golgi reassembly stacking protein, putative
K4E5W8	0.986	Mitotic centromere-associated kinesin (MCAK), putative
K4E5P4	0.880	Monoglyceride lipase, putative
K4E595	0.894	Nitrate reductase, putative
K4DN46	0.976	Palmitoyltransferase (EC 2.3.1.-)
K4E583	0.933	Phosphatase 2C, putative
K4DSR7	0.989	Protein kinase, putative
K4E6Q0	0.867	Protein kinase, putative
K4DTB6	0.990	Protein phosphatase 2C, putative
K4DV91	0.948	Serine/threonine-protein phosphatase (EC 3.1.3.16)
K4E2R8	0.985	Succinate dehydrogenase flavoprotein subunit
K4DRJ8	0.955	Trans-sialidase, putative
K4DSE2	0.987	Trans-sialidase, putative
K4DRN7	0.929	Trans-sialidase, putative
K4DQ44	0.968	Trans-sialidase, putative (Fragment)
K4DMQ6	0.968	Trans-sialidase, putative (Fragment)
K4DL99	0.968	Trans-sialidase, putative (Fragment)
K4DV27	0.982	Uncharacterized protein
K4DTI6	0.905	Uncharacterized protein
K4DUS5	0.865	Uncharacterized protein
K4DWR5	0.988	Uncharacterized protein
K4E6H0	0.980	Uncharacterized protein
K4EAU1	0.983	Uncharacterized protein
K4DNW0	0.988	Uncharacterized protein
K4E2Y2	0.910	Uncharacterized protein
K4DUB6	0.989	Uncharacterized protein
K4E7W3	0.990	Uncharacterized protein
K4EC81	0.968	Uncharacterized protein
K4E955	0.989	Uncharacterized protein
K4E3U8	0.990	Uncharacterized protein
K4DYQ2	0.989	Uncharacterized protein
K4DZT0	0.984	Uncharacterized protein
K4E362	0.928	Uncharacterized protein
K4DJS2	0.990	Uncharacterized protein
K4E4Y5	0.989	Uncharacterized protein
K4E1X7	0.975	Uncharacterized protein
K4DZU1	0.856	Uncharacterized protein
K4DTG5	0.955	Uncharacterized protein
K4E8V8	0.976	Uncharacterized protein
K4E943	0.989	Uncharacterized protein
K4DWF7	0.988	Uncharacterized protein
K4E8S3	0.912	Uncharacterized protein
K4DUB9	0.987	Uncharacterized protein
K4DTV5	0.963	Uncharacterized protein
K4E818	0.988	Uncharacterized protein
K4E5N2	0.990	Uncharacterized protein
K4DLH0	0.969	Uncharacterized protein
K4DSW4	0.990	Uncharacterized protein
K4DW97	0.869	Uncharacterized protein
K4DJU7	0.980	Uncharacterized protein
K4DUK6	0.986	Uncharacterized protein
K4DXT8	0.990	Zinc finger protein, putative

4.1 Bioinformatic prediction of the *T. cruzi N*-myristoylome

Studies by Traverso have compared the differential peptide substrate specificities of NMT homologs from both higher and lower eukaryotes (Traverso *et al*., 2013). The data from this study have been re-plotted to better illustrate these sometimes, subtle differences between the human, *S. cerevisiae*, *P. falciparum* and *A. thaliana* NMT homologs (**Figure 4.1**). Whilst the majority of substrates are recognised across all NMTs, this trend most notably diverges between the substrates of higher and lower eukaryotes. This is exemplified with a lower percentage of peptides containing asparagine in position 2 for lower eukaryotic NMT's, whilst serine at position 5 becoming slightly more common. Despite this underlying substrate diversity, two programs, which predict the *N*-myristoylation of proteins, have been developed, using the substrate specificities from higher eukaryotes. Previous work from Debbie Smiths lab (University of York) has predicted the *N*-myristoylome of the three-trypanosomatid parasites *L. major*, *T. brucei* and *T. cruzi* using a purely bioinformatic approach (Mills *et al*., 2007). Following their analysis, they predicted *L. major* and *T. brucei* to have approximately 60 *N*-myristoylated proteins, whist *T. cruzi* was predicted to have ~123 which they reasoned was due to their use of the hybrid strain CL-Brenner which is known to have multiple gene isoforms (El-Sayed *et al*., 2005).

To assess if this was true for a non-hybrid strain, the reference proteome containing the predicted proteins from Silvio X10/1 (Taxon: 5693) was analysed with Myristoylator (Expasy) for potentially *N*-myristoylated proteins. This reference proteome consists of 10,805 sequences of which ~6.1% did not contain an *N*-terminal methionine. These sequences were removed from the dataset and classified as missannotated or fragmented proteins. Of the remaining sequences, 5.6% had a glycine following the initial methionine (subsequently referred to as ΔMG) and these sequences were analysed for *N*-myristoylation. Out of 568 sequences, 98 were predicted to be *N*-
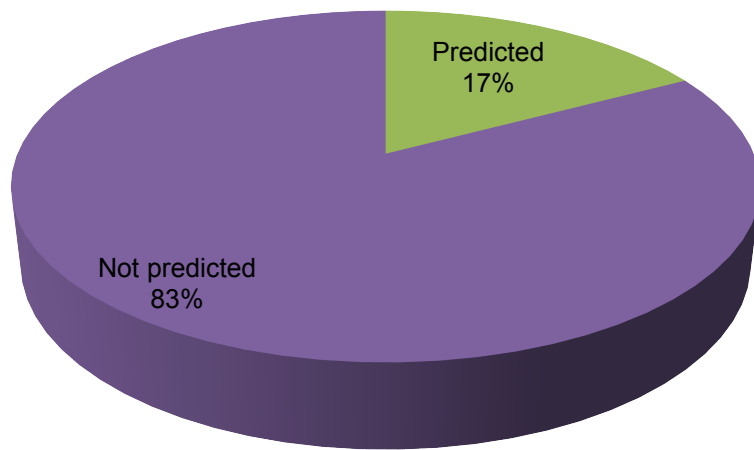
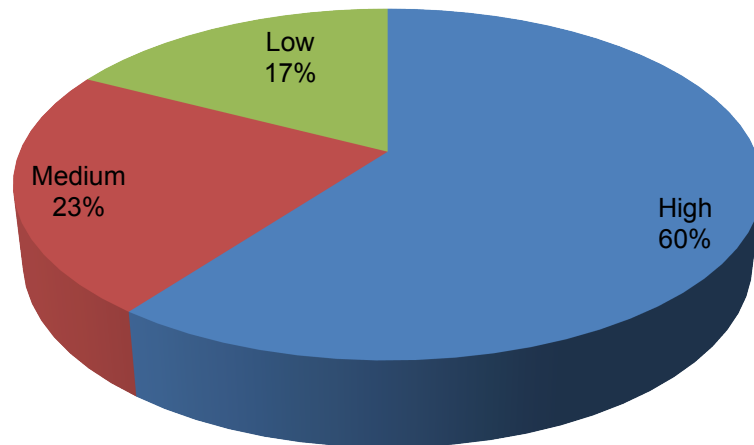**Figure 4.2 Theoretical *N*-myristoylome**
(**A**) Percentage of proteins predicted to be *N*-myristoylated with Myristoylator. (**B**) Confidence of *N*-myristoylation predictions for the 98 proteins, categorised into high, medium and low confidence groups. Myristoylator scores of 0.85 of greater are classed as high confidence, between 0.4-0.85 were medium and less than 0.4 are low confidence.

myristoylated with varying levels of confidence (**Figure 4.2 A, B**). Analysis of this non-hybrid strain predicted 59 proteins to be *N*-myristoylated with a high confidence, similar to the number predicted for *T. brucei* 927 and *L. major*. Both CAP5.5 and FCaBP, which are both known substrates for *Tc*NMT were present in the bioinformatic predictions with a high confidence (**Table 4.1**). However, the known *N*-myristoylated protein, phosphoinositide-specific phospholipase C (**UniProt accessions: Q9TZN8, O96101, Q4DUP6**) (**Martins *et al*., 2010; Okura *et al*., 2005**) was not present in the theoretical *N*-myristoylome due to its complete absence from the reference proteome. Despite the apparent incompleteness of the reference proteome, this bioinformatic approach has identified two known substrates of NMT with high confidence in addition to many uncharacterised proteins. Whilst it is ultimately desirable to identify proteins that actually undergo *N*-myristoylation in the parasite, rather than rely upon predictions, this set of proteins can be used for future comparison with my experimentally determined *N*-myristoylome.

4.2 Lifecycle *N*-myristoylation

In the previous chapter (***Section 3.12***), epimastigotes were demonstrated to be able to utilise the myristic acid analog AzMyr to label specific proteins in the parasite. Having also demonstrated that NMT is continuously expressed throughout the life cycle, *N*-myristoylation in these clinically relevant stages was assessed using by click chemistry and in-gel fluorescence. First *N*-myristoylation in the epimastigote and trypomastigote was compared side by side and whilst the majority of bands were identified in both stages, the relative intensities of several of these differed (**Figure 4.3A, upper panel**). Coomassie staining of the gel also revealed minor differences in the proteome between these two stages (**Figure 4.3A, lower panel**). Whilst the presence of *N*-myristoylation
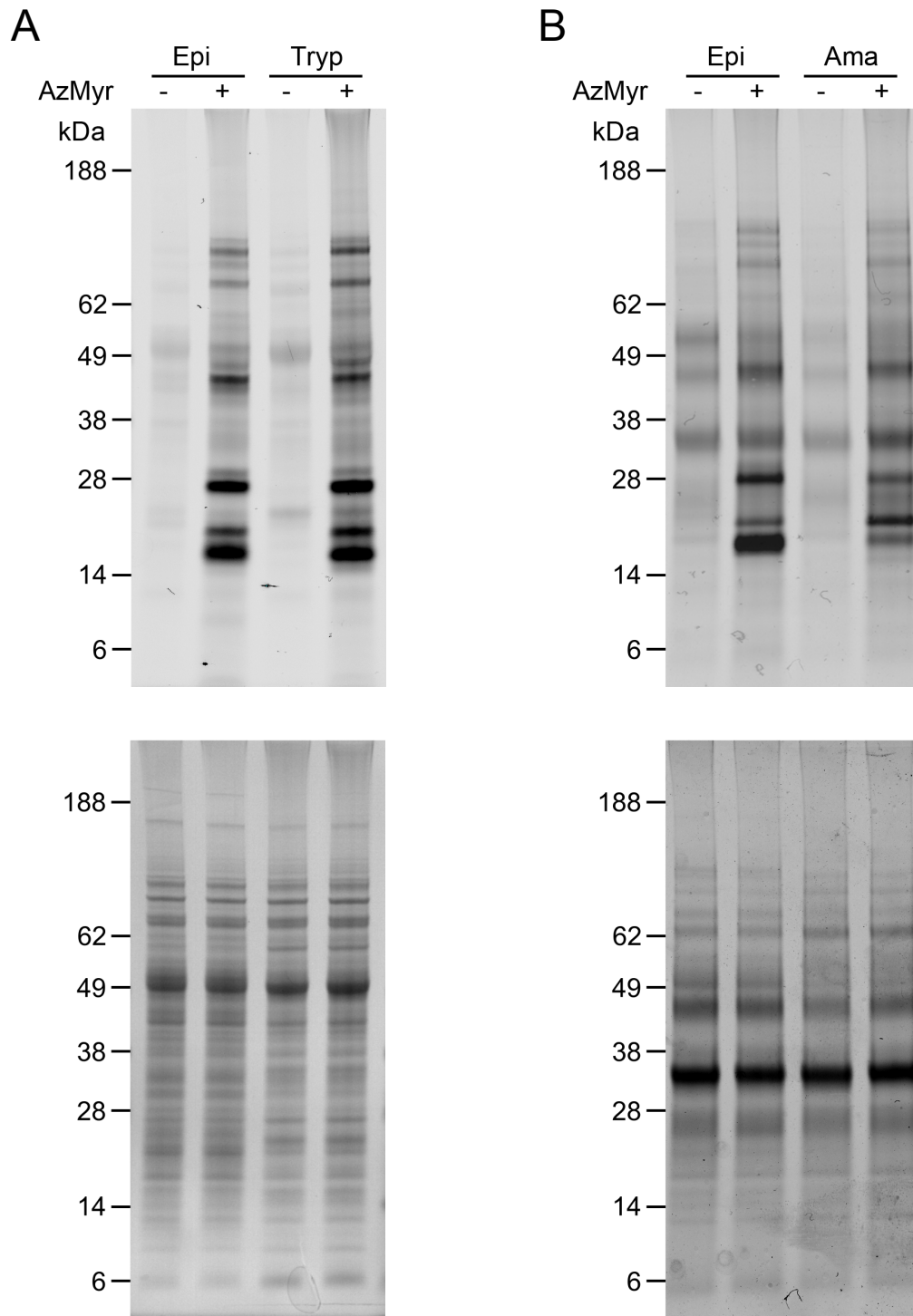
Figure 4.3 Lifecycle *N*-myristoylation
Comparison of *N*-myristoylation in epimastigotes, trypomastigotes and amastigotes after AzMyr labelling (upper panel). Coomassie stainied gel (lower panel). Comparison of epimastigotes vs trypomastigotes (**A**). Comparison of epimastigotes and amastigotes (**B**).

in the non-dividing trypomastigote stage was not entirely unexpected, as they undergo protein synthesis, the result both demonstrates a stage-specific regulation of this modification and shows it to be a dynamic process that is independent of cell division. Similarly, amastigotes were able to incorporate AzMyr with a similar efficiency to the epimastigote and trypomastigote forms (**Figure 4.3B**). However, the bands were not as distinct as the comparison of the epimastigote and trypomastigote, which may be due to possible proteolytic degradation, for instance the band at 49 kDa decreases to ~35 kDa. Despite this, the pattern of *N*-myristoylation appears to highly similar between the two epimastigote experiments. Together with the data from the previous chapter (***Section 3.5***), this demonstrates that the enzyme is functional throughout the lifecycle of the parasite.

4.3 Turnover of *N*-myristoylated proteins

A literature review has revealed a scarcity of information relating to the de-myristoylation of proteins, with only two characterised enzymes having been reported to carry out this process (Burnaevskiy *et al*., 2013; Misumi *et al*., 1995). Additionally the cytoplasmic fraction of brain synaptosomes has also been reported to de-myristoylate the myristoylated alanine-rich c kinase substrate (MARKS) *in vitro*; however, the identity of this enzyme or complex has not yet been elucidated (Manenti *et al*., 1995). The 26S proteasome inhibitor MG132 was used to probe if de-myristoylation in *T. cruzi* is enzyme specific or if it is related to the proteasome mediated turnover of *N*-myristoylated proteins. In a pulse chase labelling experiment, epimastigotes were labelled with AzMyr as described earlier (**Figure 3.11B**) for 4 hours to allow the incorporation of the analog into the proteome. Parasites were washed into medium supplemented with myristic acid to outcompete any residual AzMyr in the cell
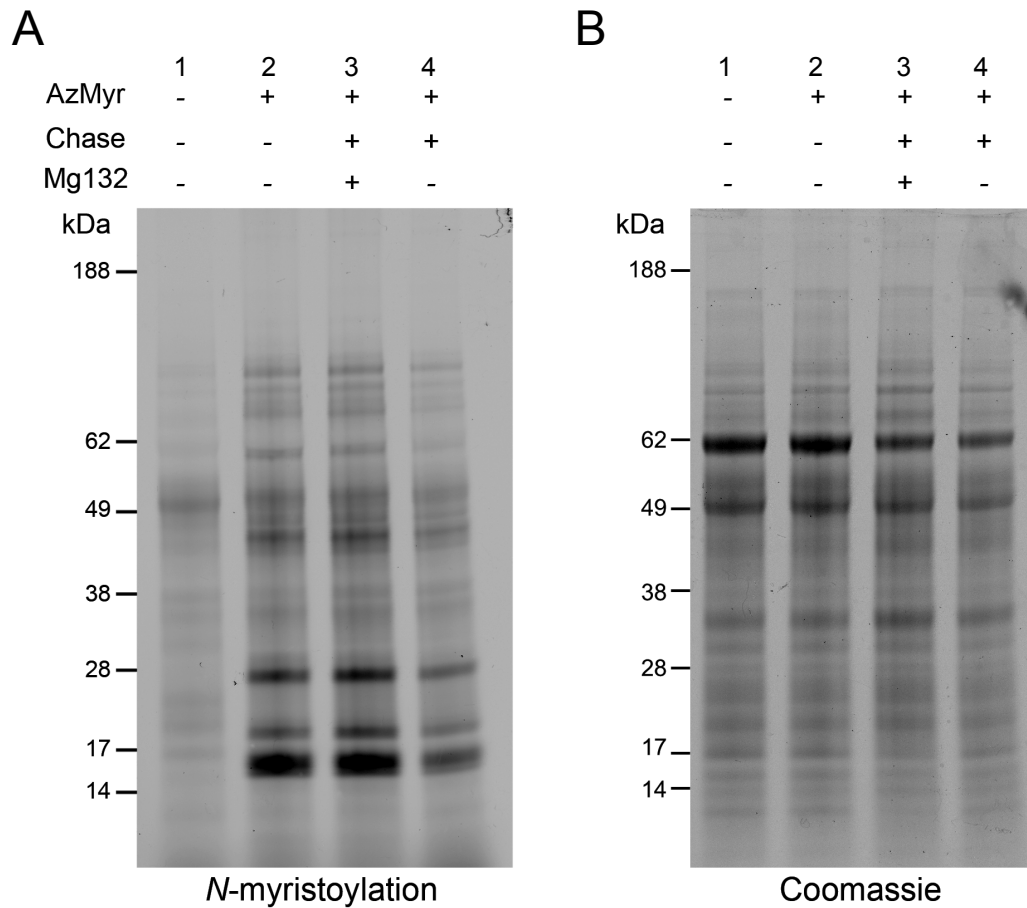
Figure 4.4 Turnover of *N*-myristoylated proteins
The depletion of *N*-azidomyristoylated proteins was monitored in the presence and absence of the proteasome inhibitor MG132. Epimastigotes were labelled for 2 h with AzMyr and a lysate prepared (lane 2). Following the labelling period, cells were incubated in the presence and absence of MG132 (Lanes 3 + 4 respectivley). *N*-myristoylated proteins were visualised using click chemistry and in-gel fluorecence (**A**). Loading was revealed by coomassie blye staining of the gel after imaging (**B**).

and then treated with or without MG132 for a further 4 hours. *N*-myristoylation was assessed by click chemistry and in-gel fluorescence as before. As previously observed, there was only one significant band detected in control cells in the absence of AzMyr (**Figure 4.4A,** *lane 1*). The shorter labelling pulse used in this experiment did not significantly alter the number *N*-myristoylated bands identified when compared to the prior experiment using a 6-h labelling, also detecting ~10 bands (**Figure 4.4A,** *lane 2*). In parasites chased with myristic acid and treated with MG132, the fluorescence intensities of the bands remained broadly unchanged in comparison with labelled parasites (**Figure 4.4A,** *lanes 2+3*). However, in the presence of myristic acid and the absence of MG132, the band intensities decreased proportionally with the length of chase, when compared to inhibitor-treated cells (**Figure 4.4A,** *lanes 3+4*). The gel was then stained with coomassie blue and analysed by fluorescence for equal loading. Whilst there were minor differences in loading between lanes, this was not able to account for the decrease in *N*-myristoylated proteins detected in the absence of MG132 (**Figure 4.4B**). Collectively the data show that the loss of myristoylated protein is primarily coupled to proteolytic turnover via the 26 S proteasome, because treatment with MG132 was able to abolish this effect.

4.4 *N*-myristoylation is co-translational

N-myristoylation has been described to occur both co- and post-translation (***Section 1.4.1***). The stage at which myristic acid is incorporated into the *T. cruzi* proteome was determined by detecting AzMyr labelling in the presence and absence cycloheximide, an inhibitor of nascent protein synthesis (Ennis and Lubin, 1964). Epimastigotes pre-incubated with cycloheximide before the addition of AzMyr were unable to incorporate the label to the same level as the seen in the untreated control (**Figure 4.5 A, top**).
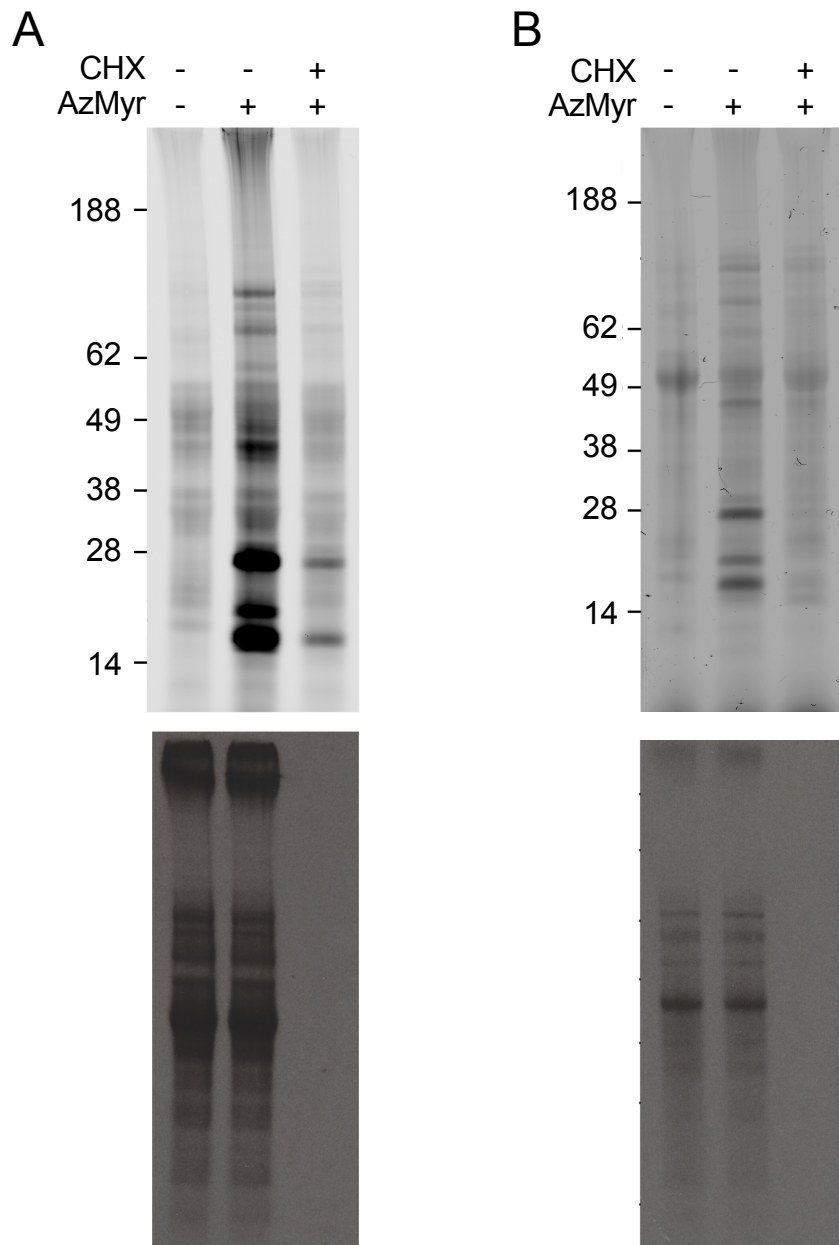
Figure 4.5 Effect of cycloheximide on *N*-myristoylation
Epimastigotes (**A**) and trypomastigotes (**B**) were treated with azidomyristate in the presence and absence of cycloheximide. Detecting the incorporation of azidomyristate by click chemistry using in-gel fluorescence (upper pannels) or the incorporation of L-[^{35}S]-methionine by autoradiography (lower pannels).

Whilst the labelling of several bands were abolished to below the detection limit, two prominent bands were observed in the cycloheximide treated cells suggesting that either nascent protein synthesis was not completely inhibited, or that a subset of proteins are modified post-translationally. Assessment of the former hypothesis was carried out in parallel with the click chemistry labelling experiment by measuring the incorporation of L-[^{35}S]-methionine. The pre-incubation with cycloheximide was able to almost completely, interrupt nascent protein synthesis (**Figure 4.5 B, bottom**). The same observations were also made in the trypomastigote stage of the parasite, where the incomplete inhibition of *N*-myristoylation did not correlate with the abolition of protein synthesis (**Figure 4.5 B**). Whilst the data support the theory that the *N*-myristoylation of some proteins may occur post-translationally, it is clear that the majority of proteins are co-translationally, *N*-myristoylated in this parasite. A repeat of this experiment in the presence and absence of an NMT inhibitor would confirm if this modification is carried out by NMT.

4.5 Growth of *T. cruzi* epimastigotes in azidomyristate

In the previous chapter, the enzyme *N*-myristoyltransferase was validated as a potential drug target against *T. cruzi* and the results outlined in this chapter has shown this process occurs throughout all stages of the parasite. In an attempt to reconcile the mechanism of action of DDD85646 against epimastigotes as well as identifying new potential drug targets, the experimental identification of the parasites *N*-myristoylome was carried out using a click chemistry, enrichment approach. Two studies in the related parasite *T. brucei* have found myristic acid analogues to be toxic to the cell (Doering *et al*., 1994; Doering *et al*., 1991). Although no noticeable defect was observed in *T. cruzi* after labelling for 6 h with AzMyr, the toxicity was determined
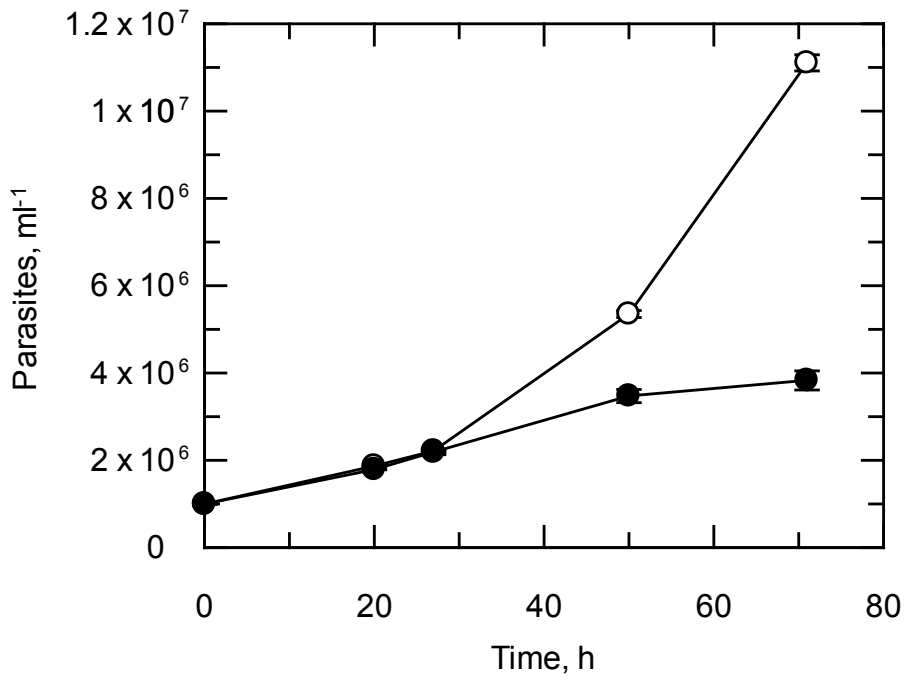
Figure 4.6 Proliferation of *T. cruzi* parasites in the presence of AzMyr
The doubling of epimastigotes cultured in the absence (Open circles) and presence
(closed circles) of 50 μM AzMyr was monitored for 72 h. Parasites were cultured
in RTH/FCS and counted with a Neubauer haemocytometer. Data is plotted as the
mean of three independent cultures ± standard deviation.

against the epimastigote stage over an extended time-period by monitoring the proliferation of the parasites was monitored in the presence of 50 μM AzMyr over 72 h (**Figure 4.6**). Growth was unaffected over the first 27 h, but was slowed thereafter, indicating the toxic effect of this analog against the parasite. Nonetheless, 20 h exposure would allow an almost complete single population doubling of the parasites, which in theory would allow the labelling of any proteins that may be related to the cell cycle.

4.6 Label free analysis of the *N*-myristoylome

There have been vast improvements in the field of proteomics over the past decade, allowing the identification of specific proteins from complex mixtures, or peptides covering several orders of magnitude in abundance, see review (Yates *et al*., 2009). Despite these advances, it is still common practice to carry out an enrichment step prior to identifying the digested peptides by mass spectrometry, as this can increase the number of proteins identified from a highly complex mixture. As all stages of the parasite were able to incorporate AzMyr into the *N*-myristoylome, this analog was used to label and directly capture these proteins from epimastigotes onto an alkyne-functionalised resin using click chemistry (**Figure 4.7**). Since the number and intensities of the bands measured by in-gel fluorescence varied very little between the lifecycle stages, the epimastigote *N*-myristoylome was chosen as they are readily cultured to high densities and the relative toxicity could be determined. In addition, as epimastigotes undergo cell division this could lead to the identification of proteins that may be related to the cell cycle, which are unlikely to be affected in the non-dividing trypomastigote stage.
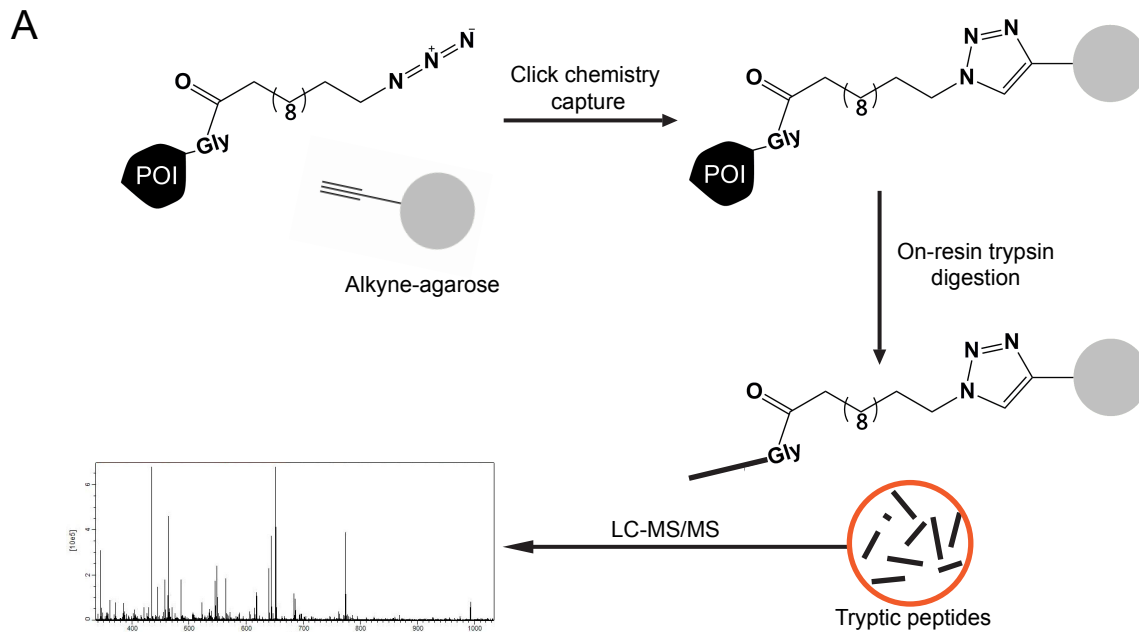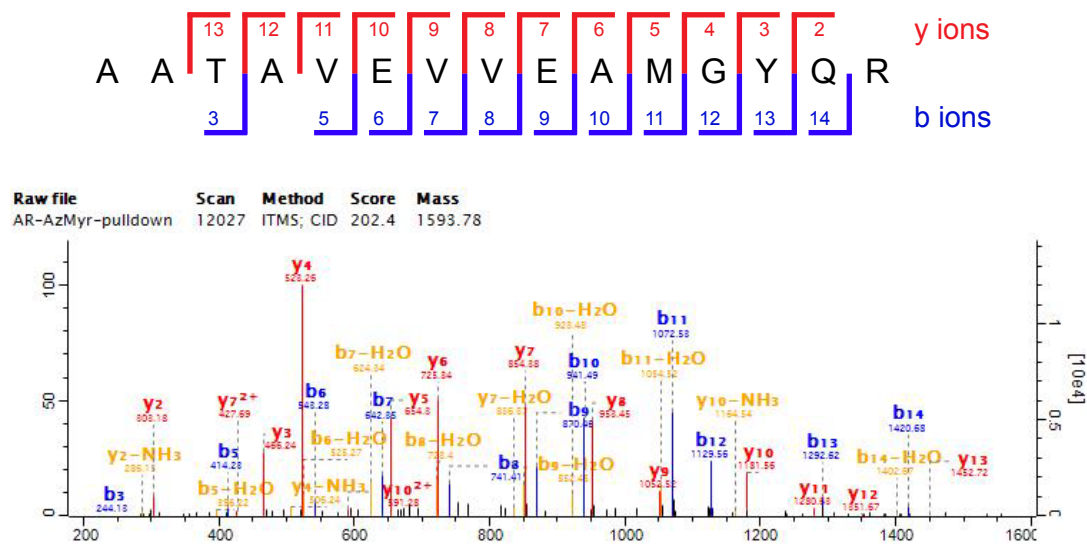
Figure 4.7 Enrichement strategy for identifying the *N*-myristoylome
(**A**) *N*-azidomyristoylated proteins from whole cell lysates were directly captured onto an alkyne-agarose resin using click chemistry. Stringent washing of the resin under denaturing conditions was designed to remove non-specific contaminanting proteins. The captured proteins were digested on-resin with trypsin yielding tryptic peptides for identification by LC-MS/MS. The *N*-azidomyristoylated peptide is retained on the agarose and could not be identified by mass spec. (**B**) An annotated example of a MS/MS spectrum matching a the peptide AATAVEVVEAMGYQAR from the uncharacterised protein Q4DLX6. Matching b and y ions have been annotated on the peptide sequence.

Parasites cultured in normal RTH/FBS medium were labelled with azidomyristate or myristic acid over 20 h, based on the previous experiment showing that no adverse growth effects were observed up to this point (**Figure 4.6**). Whole cell lysates of both labelled and unlabelled parasites were enriched by click chemistry onto an alkyne agarose resin overnight. This allows *N*-azidomyristoylated proteins to be captured in labelled cells and to filter out non-specific interactions in the unlabelled sample. After enriching equal amounts of the lysates, samples were stringently washed to remove non-specifically interacting proteins. Hydroxylamine treatment of the resin removed *S*-myristoylated proteins prior and subsequent to reductive alkylation of the immobilised proteins with iodoacetamide, blocked cysteine residues for analysis by mass spectrometry. Additional, high stringency washes were included to remove any remaining contaminant proteins. Proteins were digested on-resin and the recovered peptides were analysed by liquid chromatography coupled to tandem mass spectrometry (LC-MS/MS) (**Figure 4.7A**). A representative, high-confidence peptide identification resulting from the LC-MS/MS experiments is shown mapped with the detected b and y ions matching the theoretical tandem mass spectra of the peptide (**Figure 4.7B**).

The enrichments were analysed by comparison of the label free quantitation intensities (LFQ) calculated by MaxQuant (Luber *et al*., 2010). This method relies upon the measurement of the precursor ion intensities of identified peptides between two independent mass spec runs, in this case between the control and AzMyr labelled enrichments. Owing to the incompleteness of the reference proteome (***Section 4.1***) tryptic MS/MS spectra were searched against the complete *T. cruzi* proteome consisting of 30,047 sequences from Cl-Brenner, Silvio X10/1 and Marinkellei sequences to maximise the number of hits. Protein identifications were required to have a minimum of two matched peptides, one of which was required to be unique. Using these criteria 424, 372 and 106 proteins were identified from three biological replicates. LFQ values
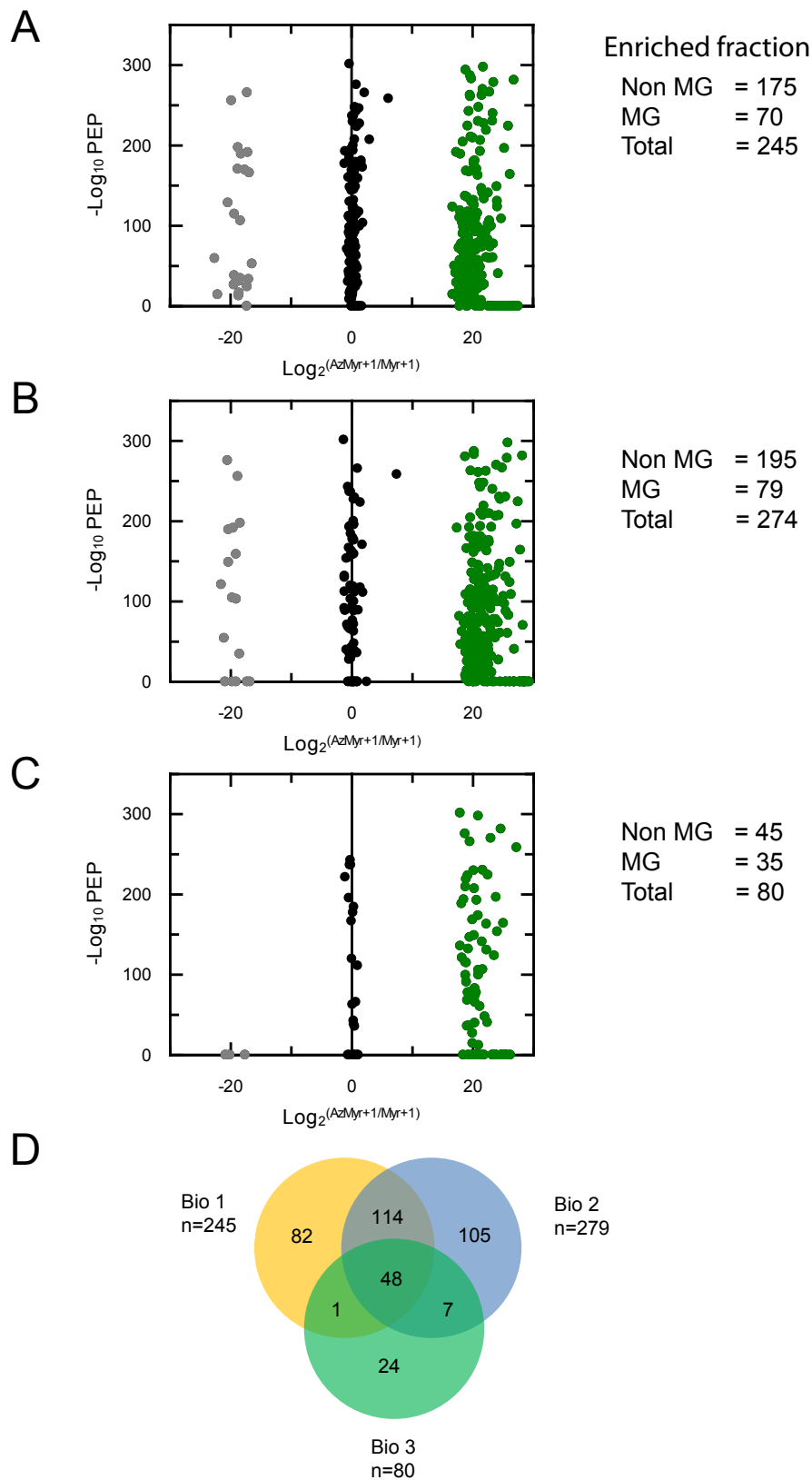
Figure 4.8 Label-free enrichment of the epimastigote *N*-myristoylome
LFQ analysis of the enrichment of N-azidomyristoylated from three independant biological replicates (**A, B and C**). Log$_2$ LFQ ratio changes are plotted against the -Log$_{10}$ of posterior error of probability (PEP). Green circles represent enriched proteins (>10 Log$_2$) from each replicate. Black circles are proteins that are unenriched or negativeley enriched. (**D**) Number of proteins common to all three label-free enrichment experiments.

Table 4.2 List of enriched proteins from 3 label-free experiments.

UniProt Accession	First 2 aa's	Protein names
Q4DZP2	MG	60S ribosomal protein L18
Q4D7Y8	MG	ADP-ribosylation factor 1, putative
Q4DZM9	MG	ADP-ribosylation factor-like protein, putative
Q4CW64	MG	Calpain-like cysteine peptidase, putative
Q4CV42	MG	Calpain-like cysteine peptidase, putative
Q4E2W1	ML	Cystathionine beta-synthase (EC 4.2.1.22)
Q4E5Z7	MA	Cytochrome c oxidase copper chaperone, putative
K4E5Y1	MG	Cytoskeleton-associated protein CAP5.5, putative,cysteine peptidase,
K4DT87	MG	Dynein heavy chain, putative
K4E5P0	MG	Fatty acyl CoA synthetase 2, putative
K4E1L2	MG	Fatty acyl CoA synthetase, putative
K4EAZ1	VC	Flagellar calcium-binding protein, putative (Fragment)
K4DY43	MS	Gim5A protein, putative,glycosomal membrane protein, putative
K4E595	MG	Nitrate reductase, putative
K4E583	MG	Phosphatase 2C, putative
Q4D0B9	MG	Proteasome regulatory ATPase subunit 2, putative
K4DTB6	MG	Protein phosphatase 2C, putative
Q4E4N2	MG	Protein phosphatase, putative
Q4DRI6	MG	Putative uncharacterized protein
Q4E5H8	MS	Ribosomal protein
Q4DFP3	ME	Uncharacterized protein
Q4E2Z0	MG	Uncharacterized protein
K4DWR5	MG	Uncharacterized protein
Q4DPA5	MG	Uncharacterized protein
K4E955	MG	Uncharacterized protein
K4DJS2	MG	Uncharacterized protein
K4E1X7	MG	Uncharacterized protein
K4DXD3	MG	Uncharacterized protein
K4E189	MG	Uncharacterized protein
K4E8V8	MG	Uncharacterized protein
K4E943	MG	Uncharacterized protein
Q4DLX6	MG	Uncharacterized protein
K4DWF7	MG	Uncharacterized protein
Q4DVL2	MG	Uncharacterized protein
Q4D708	MG	Uncharacterized protein
Q4DXG4	MG	Uncharacterized protein
Q4DDD2	MG	Uncharacterized protein
K4DQN8	MG	Uncharacterized protein
K4DZS1	MG	Uncharacterized protein
K4E5N2	MG	Uncharacterized protein
Q4CWV8	ML	Uncharacterized protein
K4E0P3	MM	Uncharacterized protein
K4E0J9	MR	Uncharacterized protein
K4DX27	MS	Uncharacterized protein
K4E681	MS	Uncharacterized protein
K4E3X3	MY	Uncharacterized protein
K4EE92	KG	Uncharacterized protein (Fragment)
Q4D6T7	MA	Universal minicircle sequence binding protein (UMSBP)

from all experiments were all increased by 1 intensity value to avoid the generation of infinite values when LFQ enrichment ratios (LFQ^{AzMyr}/LFQ^{Myr}) were calculated. This artefact is produced where a protein is identified in one experiment but not another. Log_2 LFQ changes for each replicate were plotted against $-Log_{10}$ posterior error of probability (PEP) and proteins with >10-fold enrichment selected for further analysis (**Figures 4.8 ABC**). Using this cut-off, 245, 274 and 80 proteins were deemed to be enriched, with 48 proteins consistently found to be enriched across all replicates (**Figure 4.8D, Table 4.2**). Whilst replicates one and two share the highest similarity with each other, the percentage of $^\Delta$MG proteins identified were both lower than observed in the third experiment (28.6%, 28.8% and 43.8% respectively). Combining the proteins across the three experiments greatly increased the specificity from 24-36% to ~71% (**Table 4.2**). The use of hydroxylamine rather than KOH precludes the elimination of O-myristoylated proteins from the dataset. Whilst LFQ analysis has provided a relatively robust identification of the parasite's *N*-myristoylome, a further two experiments were carried out using stable isotope labelling to rule out errors in the handling and processing of the sample.

4.7 SILAC *N*-myristoylome

Despite the many merits offered by label-free proteomic quantitation, it is not suitable for the accurate quantification of expression changes for several reasons. The development of stable isotope labelling of amino acids in cell culture (SILAC) can rule out many of the experimental errors associated with the parallel preparation of samples (Ong *et al*., 2002). Ultimately, allowing for a higher accuracy in the calculated expression changes than currently offered by relative label-free quantitation. The RTH/FBS medium used for the general culturing of epimastigotes is highly undefined
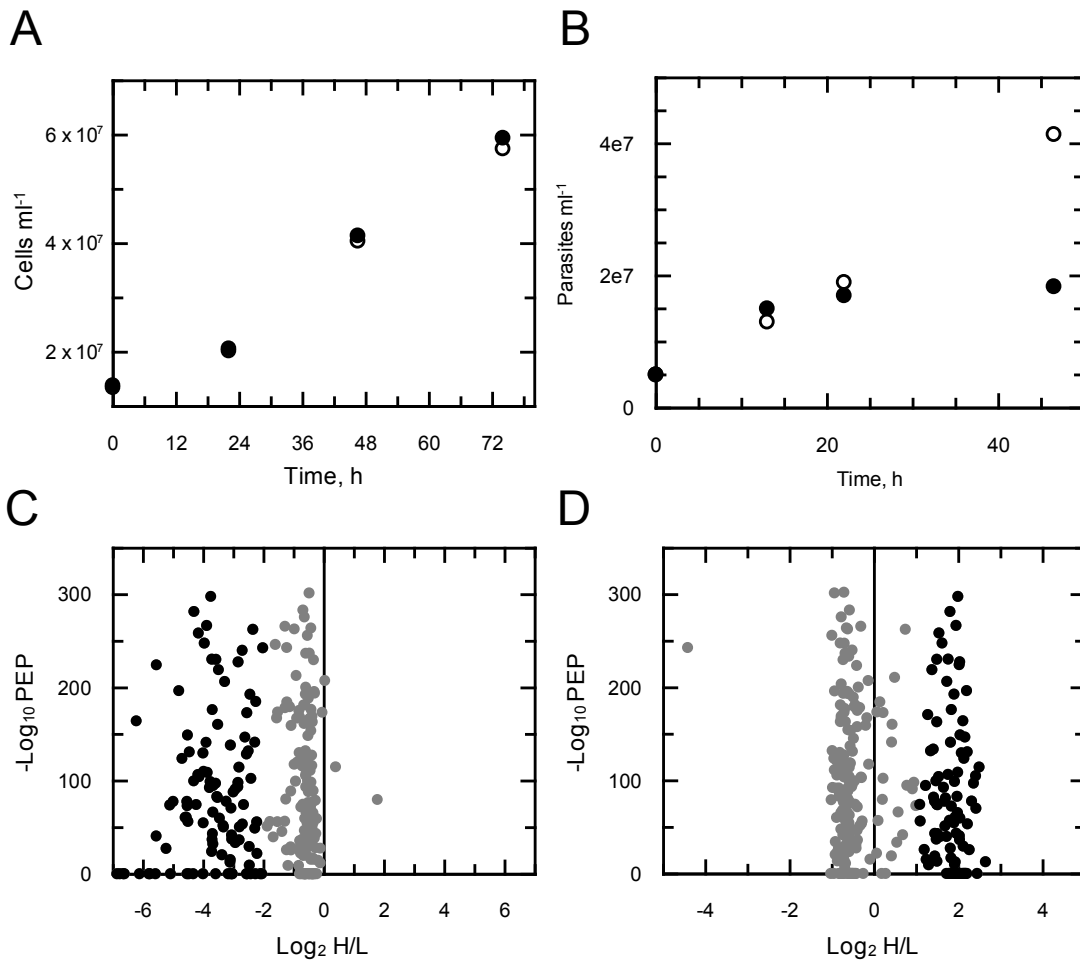
Figure 4.9 SILAC *N*-myristoylome

(**A**) Growth of *T. cruzi* epimastigotes in SDM-79 heavy (closed circles) and light (open circles) media. (**B**) Growth of epimastigotes in the presence (closed) and absence (open) of 50 μM AzMyr in SDM-79 medium. (**C+D**) Enrichment of *N*-azidomyristoylated proteins from light and heavy labelled epimastigotes. (**C**) AzMyr labelling of light parasites. (**D**) AzMyr labelling of heavy parasites. Enriched proteins are marked by black circles.

due to the presence of trypticase (a pancreatic digest) and FBS, which both contain unknown concentrations of amino acids, thus making it unsuitable for use with SILAC. Previous work from our lab has demonstrated that these parasites can be cultured in the more chemically defined SDM-79 medium, which is more commonly used for the culture of procyclic forms of *T. brucei* (Greig *et al*., 2009). Recently, a version of this medium compatible with SILAC has successfully used for studies in *T. brucei* (Urbaniak *et al*., 2012; Urbaniak *et al*., 2013). Initial attempts to adapt epimastigotes for growth in this medium were not very successful, however supplementing the media with 100 μM putrescine aided the growth of these parasites since *T. cruzi* is auxotrophic for polyamines (Hunter *et al*., 1994). Cells were labelled in light or heavy isotopically labelled mediums for 10 population doublings to allow for the complete incorporation of heavy labelled amino acids into protein. Growth studies of parasites in the heavy SDM-79 medium revealed the cells became more sensitive to azidomyristate, so the labelling period was shortened to 12-h (**Figure 4.9B**). Parasites were counted and mixed in a 1:1 ratio prior to washing away unincorporated label and lysates from 4×10^9 cells were processed as described for label-free click chemistry. Two independent SILAC enrichments were carried out with the labels swapped between each experiment. Whilst the heavy to light ratios H/L for the first experiment were almost centred over a Log_2 value of 0 indicating equal mixing, the second biological replicate of including the label swap was not (**Figures 4.9C+D**). MaxQuant is able to calculate the normalised SILAC ratios based upon the principle that the abundance of the majority of protein for any given treatment should be unaffected and thus will be normally distributed around a Log_2 of zero. Applying this normalisation approach to the second set of data, failed to normalise the data and produced a standard distribution with no enrichment. Proteins with log2 values less than 2 in the first experiment or greater than 1 in the second experiment were deemed to be enriched. From the 108 and 85 enriched proteins

Table 4.3 List of proteins enriched from 2 SILAC labelled samples and their predicted starting amino acids.

UniProt Accession	First 2 aa's	Protein names
Q4D7Y8	MG	ADP-ribosylation factor 1, putative
Q4DPJ1	MG	ADP-ribosylation factor, putative
Q4DZM9	MG	ADP-ribosylation factor-like protein, putative
K4DUN8	MG	Calpain cysteine peptidase, putative,cysteine peptidase
Q4CW64	MG	Calpain-like cysteine peptidase, putative
Q4CV42	MG	Calpain-like cysteine peptidase, putative
K4E5Y1	MG	Cytoskeleton-associated protein CAP5.5, putative,cysteine
K4DT87	MG	Dynein heavy chain, putative
K4E5P0	MG	Fatty acyl CoA synthetase 2, putative
K4E8Y0	MP	I/6 autoantigen, putative
K4E595	MG	Nitrate reductase, putative
K4EEE5	MS	Oxidoreductase, putative
K4E583	MG	Phosphatase 2C, putative
K4E1B3	MG	PIF1 helicase-like protein
Q4DZR8	MC	Procyclic form surface glycoprotein, putative
Q4D0B9	MG	Proteasome regulatory ATPase subunit 2, putative
K4DTB6	MG	Protein phosphatase 2C, putative
Q4E4N2	MG	Protein phosphatase, putative
Q4DRI6	MG	Putative uncharacterized protein
K4DTV7	MR	Surface protease GP63, putative
Q4DP22	MK	Thioredoxin, putative
K4DVP7	MY	Trans-sialidase, putative
K4DVI8	MG	Ubiquitin carboxyl-terminal hydrolase (EC 3.4.19.12)
K4DP88	MF	Uncharacterized protein
K4DV27	MG	Uncharacterized protein
K4E6H6	MG	Uncharacterized protein
Q4E2Z0	MG	Uncharacterized protein
K4DWR5	MG	Uncharacterized protein
K4E6H0	MG	Uncharacterized protein
Q4DPA5	MG	Uncharacterized protein
K4E955	MG	Uncharacterized protein
Q4CZT4	MG	Uncharacterized protein
K4EC97	MG	Uncharacterized protein
K4DJS2	MG	Uncharacterized protein
K4E1X7	MG	Uncharacterized protein
K4DXD3	MG	Uncharacterized protein
K4E189	MG	Uncharacterized protein
K4E8V8	MG	Uncharacterized protein
K4E943	MG	Uncharacterized protein
Q4DLX6	MG	Uncharacterized protein
K4DWF7	MG	Uncharacterized protein
Q4DVL2	MG	Uncharacterized protein
Q4DXG4	MG	Uncharacterized protein
Q4DDD2	MG	Uncharacterized protein
K4DQN8	MG	Uncharacterized protein
K4E818	MG	Uncharacterized protein
K4DZS1	MG	Uncharacterized protein
K4E5N2	MG	Uncharacterized protein
Q4DEK1	MK	Uncharacterized protein
Q4CWV8	ML	Uncharacterized protein
K4E0P3	MM	Uncharacterized protein
K4E948	MP	Uncharacterized protein
K4E6B5	MP	Uncharacterized protein
K4EBF6	MR	Uncharacterized protein
Q4DDT2	MR	Uncharacterized protein
K4E0J9	MR	Uncharacterized protein
K4DX27	MS	Uncharacterized protein
Q4DEA8	MS	Uncharacterized protein
Q4DQE0	MW	Uncharacterized protein
K4E3X3	MY	Uncharacterized protein
K4EE92	KG	Uncharacterized protein (Fragment)
Q4DDN8	MP	Vesicle-associated membrane protein, putative
K4DXT8	MG	Zinc finger protein, putative

identified from the two replicates, 63 were found in both experiments (**Figure 4.9, Table 4.3**). Similar to the label-free experiments the enrichment of ΔMG containing proteins were 44 and 65 % respectively. After combining the two replicates this value marginally increased to 67 **%**. Despite the different labelling conditions used in the enrichment of the *N*-myristoylome for SILAC and label-free analyses, 37 proteins were found to be consistently enriched (**Table 4.3**). It was noted that the flagellar calcium binding protein is absent. This is due to there not being enough H/L counts to accurately quantify the abundance of heavy and light peptides. Proteins present in both types of experiment are most likely to form the core *N*-myristoylome of the parasite.

4.8 Polymyxin acylase digestion

The data so far have identified **48 and 63** proteins in the label free and isotopically labelled experiments. Whilst the direct immobilisation approach used in the enrichment was intended to reduce the number of contaminating proteins, by allowing high stringency washing. The immobilised *N*-azidomyristoyl-glycine peptide is always retained on the resin after digestion. There are two known enzymes that can carry out de-myristoylation, polymyxin acylase isolated from *Pseudomonas sp*. M-6-3 and factor invasion plasmid antigen J (IPAJ) from *Shigella flexneri* (Burnaevskiy *et al*., 2013; Misumi *et al*., 1995). In an attempt to identify the myristoylated peptides that are covalently attached to the resin, post-tryptic resin was treated with polymyxin acylase and the extracted peptides identified by LC-MS/MS from both SILAC enrichments. However, whilst peptides were recovered from both replicates (6 and 9 respectively), only two contained an N-terminal glycine that also matched the *N*-myristoylome (**Table S1**). The rest of these peptides did not match proteins enriched in all replicates and their identification was probably a result of carryover from the initial experiments, despite

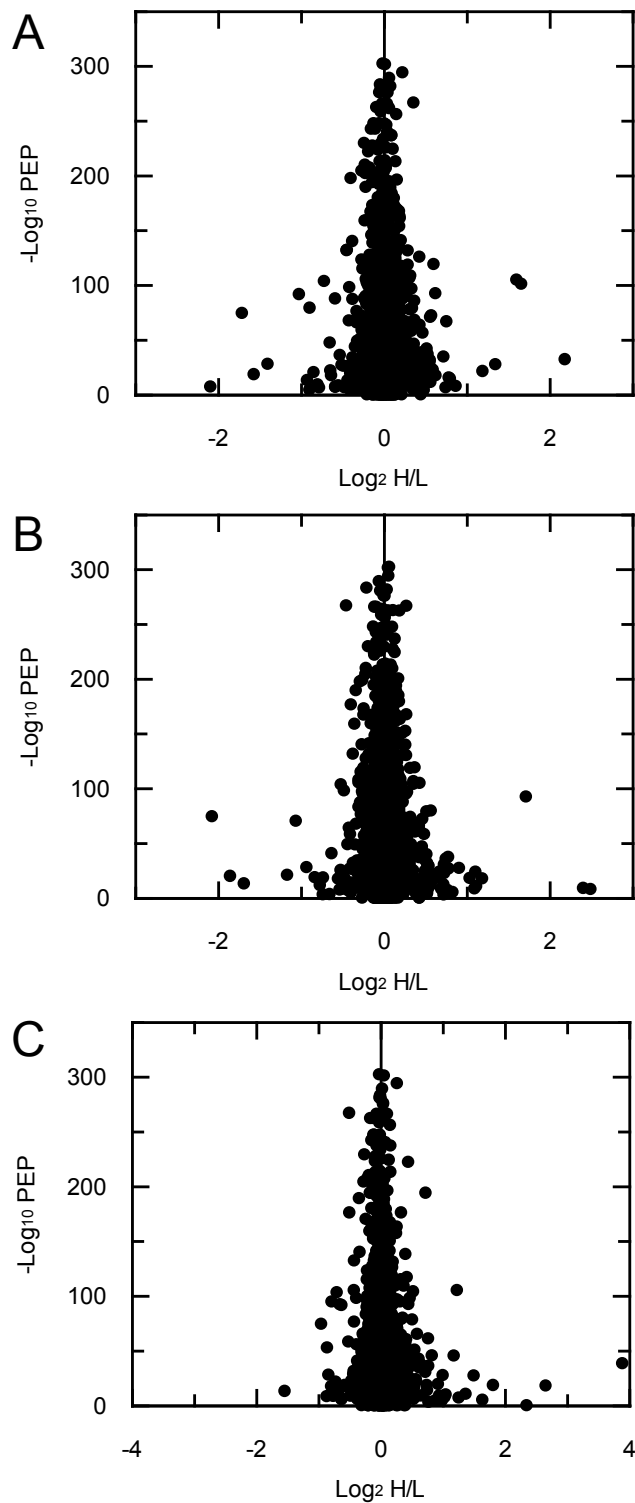**Figure 4.10 Proteomic analysis of AzMyr treated parasites**
Epimastigotes grown in heavy and light SDM-79 medium and treated with and without AzMyr for 12 h. Parasites were mixed in a 1:1 ratio, and proteomic analysis was carried out on whole cell lysates after in-gel digestion. (**A**) DMSO treated light and heavy parasites. (**B**) AzMyr treated heavy parasites. (**C**) AzMyr treated light parasites.

extensive washing. These data shows that polymyxin acylase is not efficient at de-acylating, click-immobilised acyl peptides. One possible reason is that the presence of the resin inhibits the activity of this enzyme by steric hindrance.

4.9 Proteomic analysis of azidomyristate treated parasites

Earlier in this thesis (*Section 4.5*), incubation with azidomyristate was shown to have a negative effect on the proliferation of these parasites after 12-27 h. To see if these labelling conditions were producing large scale proteomic changes and thus artificially be altering the *N*-myristoylome, whole cell lysates of SILAC parasites that had been treated with or without azidomyristate and then mixed in a 1:1 ratio were analysed by tryptic mass fingerprinting. Datasets were processed as described for the *N*-myristoylome with minor modifications for Myr and AzMyr see below to look for large changes in H/L protein ratios. Labelling of parasites with AzMyr did not appear to produce any large changes in the detected proteome by mass spectrometry (**Figure 4.10 A-C**). Whilst complete coverage of the *T. cruzi* proteome was not achieved, more than 1000 proteins were identified across the two biological replicates and the control sample. Subsequently the combined proteomic dataset was searched for the presence myristate and azidomyristate modified peptides (Mass changes of +211.2 Da and +223.1 Da respectively). This analysis identified **4** peptides across the three replicates to be *N*-myristoylated and **2** to be *N*-azidomyristoylated (**Table S2**). Comparing these proteins with mapped, modified peptides with those proteins identified from the click chemistry enrichments found **1** to be common to both datasets, identified as the calpain-like cysteine peptidase peptide GCGASSKPSTVEYK (Q4CW64). This finding validates the logic underpinning the enrichment process carried out prior to identifying the *N*-myristoylome (*Sections 4.6 and 4.7*) whilst confirming the *N*-myristoyl-peptide

Table 4.4 List of proteins enriched in all SILAC and label-free experiments. Those highlighted in red are not predicted to start with MG a requirement for co-translational *N*-myristoylation. Proteins with homologs that are known to be *N*-myristoylated are indicated.

UniProt	Protein names	*N*-myristoylated in	Ref
Q4D7Y8	ADP-ribosylation factor 1	*C. albicans, S. cerevisiae*	(Liu *et al*., 2009; Lodge *et al*., 1997)
Q4DZM9	ADP-ribosylation factor-like protein	*T. brucei*	
Q4CW64	Calpain-like cysteine peptidase	*L. major*	(Tull *et al*., 2004)
Q4CV42	Calpain-like cysteine peptidase	*L. major*	(Tull *et al*., 2004)
K4E5Y1	Cytoskeleton-associated protein CAP5.5	*T. brucei*	(Hertz-Fowler *et al*., 2001)
K4DT87	Dynein heavy chain, putative		
K4E5P0	Fatty acyl CoA synthetase 2, putative		
K4EAZ1	Flagellar calcium binding protein	*T. cruzi, T. brucei*	(Godsel and Engman, 1999)
K4E595	Nitrate reductase, putative		
K4E583	Phosphatase 2C, putative		
Q4D0B9	Proteasome regulatory ATPase subunit 2, putative	*S. cerevisiae*	(Kimura *et al*., 2012)
K4DTB6	Protein phosphatase 2C, putative		
Q4E4N2	Protein phosphatase, putative		
Q4DRI6	Putative uncharacterized protein		
Q4E2Z0	Uncharacterized protein		
K4DWR5	Uncharacterized protein		
Q4DPA5	Uncharacterized protein		
K4E955	Uncharacterized protein		
K4DJS2	Uncharacterized protein		
K4E1X7	Uncharacterized protein		
K4DXD3	Uncharacterized protein		
K4E189	Uncharacterized protein		
K4E8V8	Uncharacterized protein		
K4E943	Uncharacterized protein		
Q4DLX6	Uncharacterized protein		
K4DWF7	Uncharacterized protein	*S. cerevisiae* (FRQ1)	
Q4DVL2	Uncharacterized protein		
Q4DXG4	Uncharacterized protein		
Q4DDD2	Uncharacterized protein		
K4DQN8	Uncharacterized protein		
K4DZS1	Uncharacterized protein		
K4E5N2	Uncharacterized protein		
Q4CWV8	Uncharacterized protein		
K4E0P3	Uncharacterized protein		
K4E0J9	Uncharacterized protein		
K4DX27	Uncharacterized protein		
K4E3X3	Uncharacterized protein		
K4EE92	Uncharacterized protein (Fragment)		
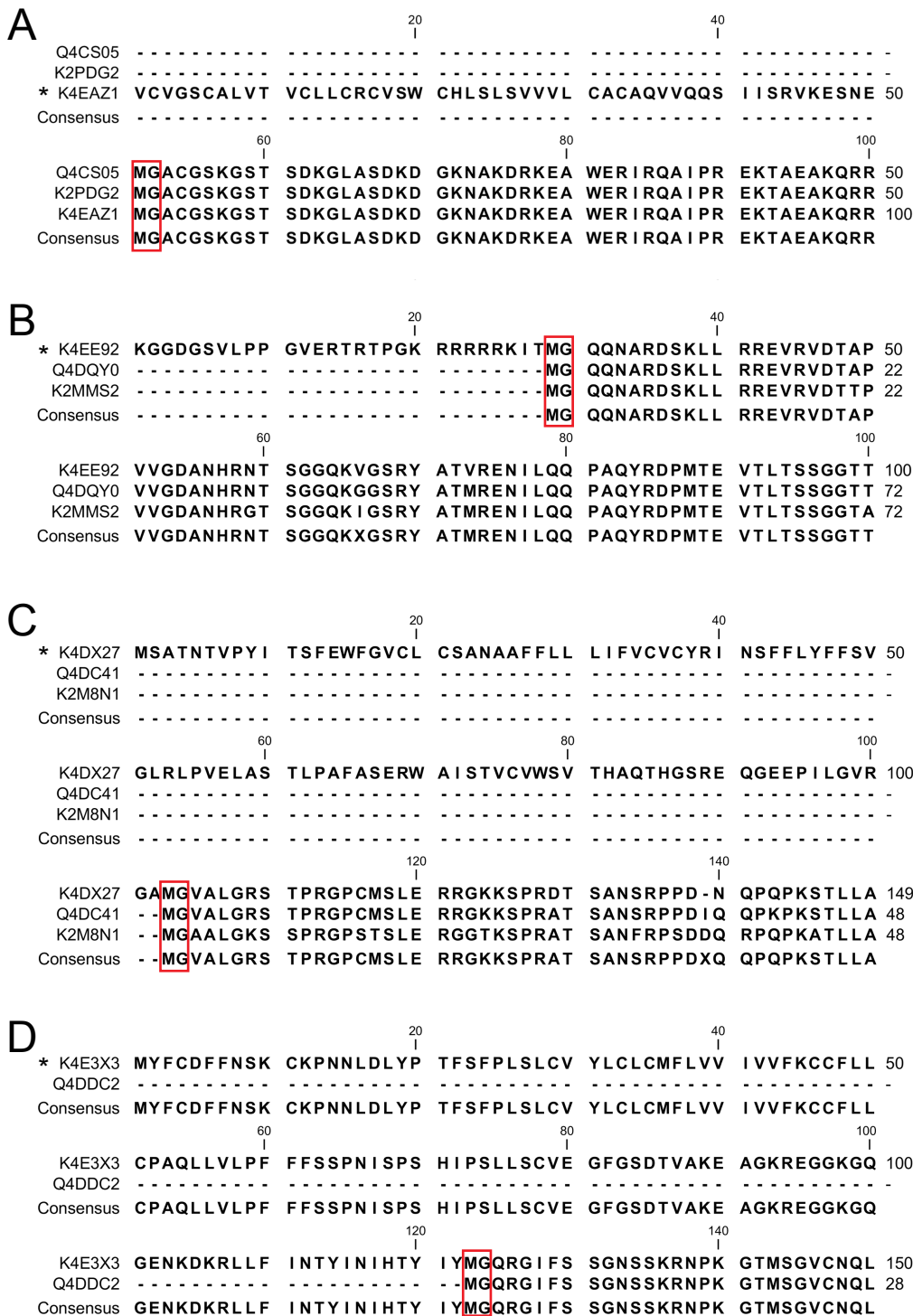
Figure 4.11 Multiple sequence alignments of homologous proteins identified by BLAST. Possible alternative start sites are highlighted by the red boxes. (**A**) Alignment of the misannotated flagellar calcium binding protein (*) with other *T. cruzi* species. (**B-D**) Alignment of multiple uncharacterised proteins with alternative annotated *T. cruzi* isoforms. (*) indicates the top ranked protein identified from all biological replicates.

of several proteins, something that we were unable to achieve with the secondary digestion with polymyxin acylase (*Section 4.8*). Combined with the enrichment experiments, we have also experimentally identified 1705 proteins of the Silvio X10/7A epimastigote proteome.

4.10 Bioinformatic analyses of consistently enriched proteins

Earlier in this chapter, 48 and 63 proteins were consistently enriched by pulling down *N*-azidomyristoylated proteins. Although these experiments were carried out under differing labelling conditions and these lists should be considered separately, combining these lists finds 38 proteins to be consistently enriched across all 5 biological replicates (**Table 4.4**). For the purpose of this list, the known *N*-myristoylated protein the flagellar calcium binding protein has been included in this list as whilst it was identified in all 5 replicates, it could not be accurately quantified in the SILAC experiments due to the stringency settings. In this combined *N*-myristoylome, 82% of proteins were annotated to start with MG. A closer inspection of this list found there to be incorrectly annotated sequences associated with UniProt accession numbers such as the uncharacterised protein fragment K4EE92 and the flagellar calcium binding protein which were predicted to start with lysine and valine respectively. With the current understanding of protein synthesis, this should not be possible as there is no initiator methionine annotated. As a result, these sequences were BLAST searched against other *T. cruzi* sequences to identify the possibility that the start sites of these sequences had been missannotated (**Figure 4.11 A+B**). Both proteins were found to have downstream MG sequences after alignment suggesting that these proteins, one of which is already known to be *N*-myristoylated, undergo *N*-myristoylation. To see if the other 5 non-MG sequences were also missannotated, alignments with other the other *T. cruzi* strains
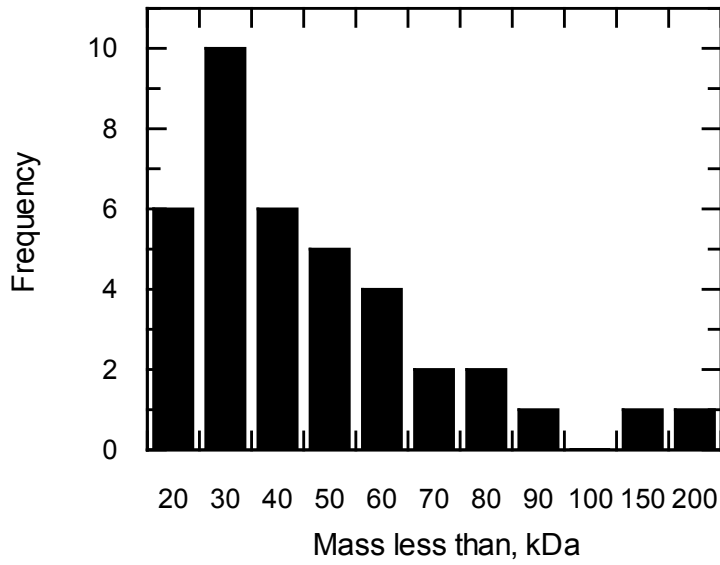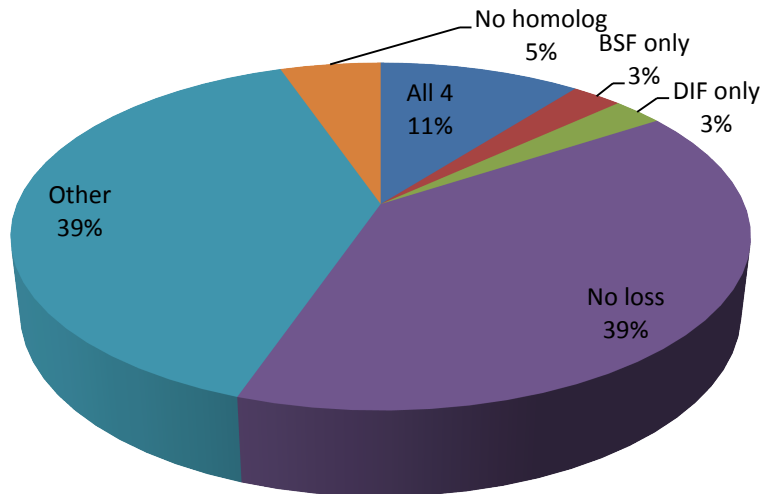
Figure 4.12 Bioinformatic analysis of proteins enriched in all 5 biological replicates
(**A**) Frequency distribution of theoretical Mw's of *N*-myristoylated proteins enriched in all 5 biological replicates. (**B**) Frequency LOGO plot of the experimentally determined *N*-myristoylation motif of *T. cruzi* NMT from all enriched proteins predicted to start with MG. (**C**) Loss of fitness experiments in *T. brucei* for the homologs of the the consistently enriched proteins identified in *T. cruzi*. Data obtained from the supplimentary materials of Alsford *et al.*, 2011. BSF is bloodstream form, DIF is differentiation and other corresponds a difference observed in atleast, two out of the 4 stages assessed.

suggested that 2 additional proteins appear to be missannotated, as they both were predicted to have downstream MG sequences (**Figure 4.11 C-D**). The incorrect annotation of start codons has previously been reported in *T. brucei* using a transcriptomics approach (Kolev *et al*., 2010). The remaining 3 sequences were not predicted to be missannotated by this method. One possible explanation is that these non-MG proteins may have GPI anchors that have incorporated AzMyr, as this type of modification requires base treatment to remove. To test this, the sequences were analysed using the big-PI Predictor (http://mendel.imp.ac.at/sat/gpi/gpi_server.html), but, these sequences were predicted not to have this modification. Another explanation is that these proteins are modified post-translation with proteolytic cleavage exposing an internal glycine for modification, or the incomplete removal of *S*-myristoylated proteins from the dataset. Finally, these proteins may just have a natural affinity for the agarose resin used for the enrichments, explaining their consistent identification. In summary, this increases the number of *N*-myristoylated proteins in the epimastigote to **35.**

The theoretical masses of the constantly enriched proteins, correlated well with the size distribution of the *N*-myristoylated proteins detected by in-gel fluorescence (**Figures 3.11 B and 4.12A**) with the majority of enriched proteins have a mass less than 60 kDa. Due to the use of two different experimental approaches to identify *N*-myristoylated proteins and the differences between the complete and reference proteomes. It has not been possible to directly compare, the theoretical and experimental *N*-myristoylomes. To determine the accuracy of Myristoylator and the NMT predictor to predict the *N*-myristoylome of *T. cruzi*, the enriched proteins were run through the programs. Incorrectly annotated proteins had their downstream MG sequences used in place of their annotated start sequence. Both Myristoylator and the NMT predictor (Eukaryota setting) produced similar numbers of high confidence predictions whilst the fungi setting predicted a lower number. However, unanimous predictions were only

Table 4.5 The analysis of experimentally verifie4d N-myristoylated proteins present in all 5 biological replicates using Myristoylator and both settings of the NMT predictor. Proteins not predicted to start with MG are highlighted in red. Number of proteins predicted at each confidence level listed below.

UniProt accession	Myristoylator	NMT predictor (Eukaryota)	NMT predictor (Fungi)
Q4D7Y8	High	No	No
Q4DZM9	Medium	Twilight	Yes
Q4CW64	High	Yes	Yes
Q4CV42	High	Yes	Yes
K4E5Y1	High	Yes	Yes
K4DT87	High	Yes	Yes
K4E5P0	High	Twilight	Yes
K4EAZ1	High	Yes	Yes
K4E595	High	Yes	Yes
K4E583	High	No	No
Q4D0B9	Low	No	No
K4DTB6	High	No	No
Q4E4N2	No prediction	No	No
Q4DRI6	High	Twilight	Twilight
Q4E2Z0	Low	Yes	No
K4DWR5	High	Yes	Twilight
Q4DPA5	High	Yes	Yes
K4E955	High	Yes	Yes
K4DJS2	High	Yes	Yes
K4E1X7	High	Yes	Twilight
K4DXD3	No prediction	No	No
K4E189	No prediction	No	No
K4E8V8	High	Yes	Yes
K4E943	High	Yes	Twilight
Q4DLX6	No prediction	Twilight	No
K4DWF7	High	Yes	Yes
Q4DVL2	No prediction	Twilight	Twilight
Q4DXG4	No prediction	Twilight	Twilight
Q4DDD2	High	Yes	Yes
K4DQN8	No prediction	Twilight	Twilight
K4DZS1	No prediction	Yes	Yes
K4E5N2	High	Yes	Yes
Q4CWV8	No MG	No MG	No MG
K4E0P3	No MG	No MG	No MG
K4E0J9	No MG	No MG	No MG
K4DX27	No prediction	No	No
K4E3X3	No prediction	No	No
K4EE92	No prediction	Yes	No
High confidence	21	19	16
Med/low/twilight	3	7	7
No prediction	11	9	12

made in **51%** of cases, of which 14% of this subproteome was consistently predicted not to undergo this modification (**Table 4.5**). Taking into account all confidence level predictions, the NMT predictor (Eukaryota setting) had the highest rate of predictions that were consistent with the experimental evidence.

A consensus *N*-myristoylation sequence was generated using the 35 proteins that started, or were predicted to start with an MG using WEBLOGO (http://weblogo.berkeley.edu/logo.cgi) (**Figure 4.12B** http://weblogo.berkeley.edu/). Analysis of this motif revealed several amino acids were tolerated at positions 2-4 with serine being the most common at position 5, followed by K, R or S at position 6. Similarly, a diversity of amino acids were tolerated after this position. Below is the consensus sequence for the *N*-myristoylome of the epimastigote.

G-X-X-X-S-(K/R/S)-X-X-X

The most tolerated amino acids at position 7 suggests that the substrate specificity of *Tc*NMT may be more similar to that of higher eukaryotes due to the presence of a basic residue at position 6 and proline at position 7 (**Figure 4.1**). It is also worth noting that similar to higher eukaryotes, a marginally higher percentage of substrates did not have serine at position 5 in *T. cruzi*. However, rather than having a positively charged amino acid in the second position, *Tc*NMT substrates were found to have a glutamine and serine was found to be under-represented in comparison with all eukaryotes. Further work is required to ascertain if this is the case.

Just over two thirds (**69%**) of the proteins identified that form the *T. cruzi N*-myristoylome are currently annotated as uncharacterised. These proteins were searched against the Pfam database (*version 27.0*), in an attempt to assign putative functions for these proteins (Finn *et al*., 2014). Only Pfam A matches were counted for this analysis (**See Table S3**). Functional domains that were assigned to already annotated proteins

appeared to match their respective annotations, with the exception of the dynein heavy chain which appears to be an uncharacterised protein by blast searching. For example, the flagellar calcium binding protein was predicted to have 2 calcium binding EF hands, despite experimental evidence from a crystal structure showing there to be 4 EF hands (Wingard *et al*., 2008). Interestingly, the Pfam prediction for the uncharacterised and missannotated protein K4EE92 identified an AMP-activated kinase (AMPK) ß subunit domain, something that is known to be *N*-myristoylated and to plays a role in the regulation and localisation of the enzyme in mammalian cells (Oakhill *et al*., 2010). BLAST searching also identified putative functions for enriched proteins such as K4DWF7 that has homology to the *N*-myristoylated frequinin homolog (FRQ1) in yeast (20% identity). The small myristoylated proteins 1, 2 and 3 (SMP) were also identified, proteins that are known to be *N*-myristoylated in *Leishmania major* (Tull *et al*., 2010; Tull *et al*., 2004). As this modification is known to help promote membrane interactions, the solubility of these proteins was predicted using the Sosui server. While the majority of proteins were predicted to be soluble, four proteins were predicted to have transmembrane helices, but these were for uncharacterised proteins with no Pfam prediction. This would require further experimental work to determine the accuracy of these predictions however, the acylation of transmembrane proteins has been reported in the literature previously (Moriya *et al*., 2013).

Studies with NMT inhibitors in *T. brucei* have found these molecules to be highly potent against the parasites. The process of genetic validation in *T. cruzi* is an extremely lengthy process taking approximately 3 months to produce a cloned SKO cell line. To see if any *N*-myristoylated proteins may be important, the homologs in *T. brucei* were identified from a genome-wide RNAi phenotypic screen (Alsford *et al*., 2011). Of the **35** proteins in the *N*-myristoylome, homologs could only be identified for 33 (**Figure 4.12 C**). A small proportion of homologs (**4 out of 36**) were identified to
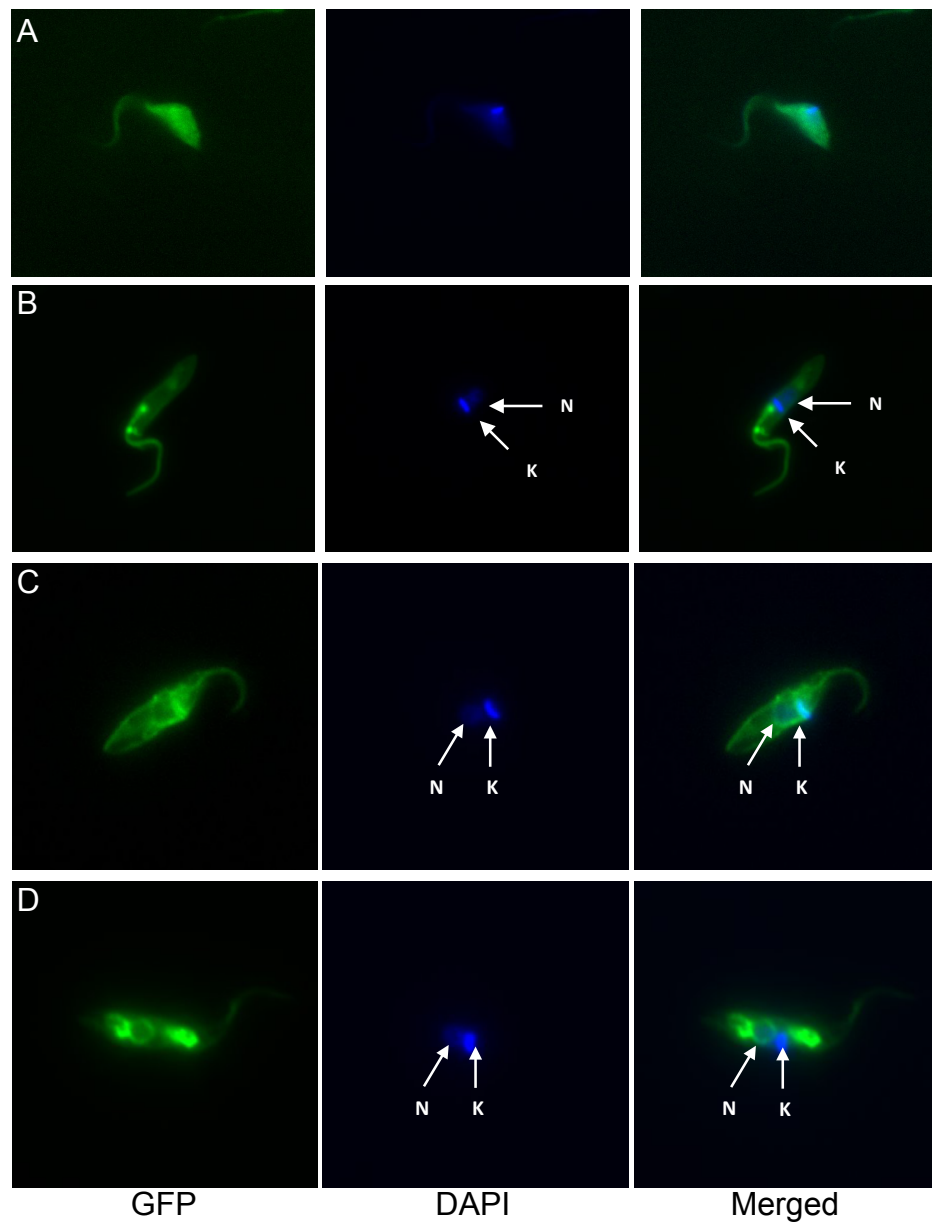
GFP   DAPI   Merged

Figure 4.13 Localisation of G and G2A, GFP fusion proteins
The *N*-terminal 24 aminod acids of *N*-myristoylated proteins were fused to the
N-terminus of eGFP. (**A**) FCaBP-G2A. (**B**) FCaBP. (**C**) ARF1-G2A. (**D**) ARF1.

produce a growth defect by RNAi in all 4 stages assessed suggesting that these homologs may be the most *N*-myristoylated proteins in *T. brucei*. The stages assessed by their study were the differentiation between procyclic and bloodstream form parasites, PCF parasites and BSF parasites at 3 and 6 days post-induction of the RNAi library. Overall, the majority of proteins enriched in all experiments had a growth phenotype in at least one of the assessed stages indicating that the homologs of the *T. cruzi N*-myristoylome and three unexplained proteins appear to be important for the proliferation of *T. brucei* parasites. Whilst these gene products appear to be biologically important for *T. brucei*, further work is required to assess their importance in *T. cruzi*. However, they provide a starting point for the assessment of future drug targets in this parasite.

4.11 Localisation studies

With the identification of more than 30 *N*-myristoylated proteins in these parasites with conflicting predictions, as determined using the currently the available programs, six proteins were chosen to see if the *N*-terminal 24 aa were enough to influence the localisation of GFP in these parasites as has previously been observed for the flagellar calcium binding protein (Godsel and Engman, 1999; Maric *et al*., 2011). Several proteins were selected from the *N*-myristoylome to determine if the first 24 aa were able to influence the localisation of eGFP in comparison with their G2A mutants. The protein phosphatase 2C that was predicted not to be *N*-myristoylated, AFR1, the RPT2 homolog, a putative nitrate reductase, and an uncharacterised protein were selected in addition to the FCaBP to act as provide a control. The first 72 bp if these genes were amplified by PCR and cloned into pTEX containing a c-terminal eGFP coding sequence. The mutants containing alanine at position 2 were made by altering the

nucleotide a position 5 from G-C in the primers leading to a G2A change at the protein level and ligated into the pTEX-eGFP plasmid. After selection, parasites were analysed by fluorescence microscopy and the GFP distribution assessed. Despite transfection of the 6 localisation constructs and their G2A mutants, fluorescent parasites were only recovered for the Arf1, RPT2 FCaBP and an uncharacterised protein. Analysis of the GFP distribution of the FCaBP-eGFP and G2A mutant revealed a similar localisation as to what has already been reported in the literature (**See Figure 4.13 A+B**) (Godsel and Engman, 1999). Similarly, a differential localisation pattern was observed between the ARF1 and G2A mutant fusion proteins (**Figure 4.13 C+D**). The ARF1G2A mutant was observed to have a more diffuse distribution that also appears to associate with outer membrane of the cell. Conversely, the wild-type ARF1 fusion protein showed a perinuclear localisation in addition to localising to an unknown vesicle posterior to the nucleus and kinetoplast. Studies of *T. brucei* ARF1 find the WT sequence to localise to the golgi complex, while the G2A mutant abolished this localisation (Price *et al*., 2007a). This difference may be due to only having used a truncated sequence for the localisation of the *T. cruzi* sequence. Meanwhile the failure of the RPT2 and uncharacterised proteins to differentially localise, in comparison with their respective G2A mutants requires further investigation, but most likely suggests that there are additional factors that play a role in the localisation of these proteins. Alternatively, the overexpression of these fusion proteins may lead to their miss localisation. This could be caused by a higher rate of protein expression than possible for NMT to myristoylate, leading to an accumulation of the un-modified fusion protein.

Chapter 5

Discussion

5.1 NMT as a drug target in *T. cruzi*

5.1.1 Genetic validation

There are very few instances reported in the literature of the genetic validation of drug targets in *T. cruzi* (Caler *et al*., 1998; Ekanayake *et al*., 2011; Manning-Cela *et al*., 2001; Xu *et al*., 2009). This, in part, is due to a scarcity of genetic tools available for use in this parasite, unlike the related parasite *T. brucei*, which has a large range of constructs for the conditional overexpression, in-situ tagging and down-regulation of specific genes. Despite the absence of an RNAi pathway in *T. cruzi* that could be used to knock-down specific genes (DaRocha *et al*., 2004; Ullu *et al*., 2004), there is a range of overexpression vectors available for use (Bouvier *et al*., 2013; Kelly *et al*., 1992; Ma *et al*., 2012; Martinez-Calvillo *et al*., 1997; Taylor and Kelly, 2006; Vazquez and Levin, 1999; Xu *et al*., 2009). Only two of these vectors could potentially be any use in generating a conditional knockout, which is considered the gold standard for genetic essentiality studies. Despite the availability of the tetracycline inducible expression vector pTcINDEX for almost a decade, it has yet to become widely adopted within the community with only 3 out of the 26 citations to this vector having actually used it in their studies to generate an overexpression cell line. Personally, we were unable to generate a pTcINDEX-*TcNMT* rescue plasmid despite multiple attempts by several members of the lab. Therefore, the benchmark adopted for the genetic essentiality in *T. cruzi* is the same used in *Leishmania* parasites, which also have a similar lack of genetic tools available (Price *et al*., 2003; Tovar *et al*., 1998; Wyllie *et al*., 2013), to generate conditional null parasites (Beverley, 2003). The alternative approach taken by researchers is to switch to *T. brucei* and assess the RNAi phenotype in this parasite.

In the studies presented here, it was not possible to generate a *Tc*NMT null mutant in the absence of constitutive NMT expression, a trait that has been observed in

Leishmania (Price *et al*., 2003). There was also evidence of a genomic rearrangement in *T. cruzi* false DKO cells, adding further evidence that this gene is essential in the epimastigote. A similar genomic rearrangement has been observed when attempting to generate a trypanothione reductase null mutant in *Leishmania* parasites, which retained an endogenous copy of the gene despite the correct replacement of the two alleles (Tovar *et al*., 1998). Although overexpression of NMT (>10-fold) in *Leishmania major* has been demonstrated to be lethal (Price *et al*., 2003), in *T. cruzi* the observed ~8-12-fold overexpression was not, as determined by western blot and drug sensitivity assays. The activity of the overexpressed *Tc*NMT in the parasite was inferred by the decreased potency of DDD85646. It may be that *T. cruzi* tolerates a greater range of NMT expression in this parasite than *Leishmania.* In summary, the genetic replacement studies in this parasite demonstrated that *TcNMT* is an essential gene for the proliferation of these parasites in axenic culture. This is in-line with the results of genetic studies carried out in other organisms (Lodge *et al*., 1994; Price *et al*., 2003; Weinburg *et al*., 1995; Yang *et al*., 2005).

5.1.2 Biochemical validation

The characterisation of recombinant *Tc*NMT found it to be highly similar to the reported values of the homologs in other species, with respect to the size, oligomeric structure and kinetic behaviour. The turnover rates (k_{cat}) for both the *Tb* and *Tc*CAP5.5 were similar to reported values for substrates of other homologs, admittedly at the lower end of the range (Boisson and Meinnel, 2003; Panethymitaki *et al*., 2006; Seaton and Smith, 2008). During the kinetic characterisation of this enzyme, DDD85646, which was originally designed to inhibit the *T. brucei* enzyme, was also found to be a potent inhibitor of *T. cruzi* NMT *in vitro*. Using the coupled enzyme assay, it was found to

have a K_i of 22.8 nM, some 23-fold less potent than its reported value of 1 nM against *Tb*NMT (Frearson *et al*., 2010). Using the same scintillation proximity assay used to determine the *Tb*NMT K_i, this value decreases to 12.7 nM (value provided by Dr Leah Torrie DDU, University of Dundee) (Roberts *et al*., 2014). The differences in values may be explained by the different assay buffers or the temperature at which the assays were carried out. While DDD85646 is potent against the purified enzyme, it does not maintain the same level of activity against the epimastigote stage. Although a decreased potency from the enzyme to the cellular level has been documented for several organisms, the notable exception to this rule is in *T. brucei,* where BSF parasites are only 3-fold less sensitive to DDD85646 (Devadas *et al*., 1997; Frearson *et al*., 2010; Wright *et al*., 2014). Meanwhile, the 276-fold decrease observed from *Tc*NMT to epimastigotes is at the extreme end of the scale. This reduction could be explained in several ways.

1. *T. cruzi* may display differential sensitivity to NMT inhibition as the parasite progresses throughout its life cycle. Several examples of varying potencies against different developmental stages have already been documented in this parasite, with inhibition values ranging 2-250-fold (Ciccarelli *et al*., 2012; Frank *et al*., 2013; Lane *et al*., 1996). Another instance of this behaviour is the differential requirement of the NTR gene in *T. cruzi*, as it is not important in the epimastigote, but becomes essential in producing infective trypomastigotes (Wilkinson *et al*., 2008). To investigate if this is the mechanism, more potent and selective compounds against *Tc*NMT are required to be able to test in the intracellular amastigote. As mentioned previously, this is due to DDD85646 being highly potent against the host Vero cells used for the assay.

2. One hypothesis is that *T. cruzi* may have greatly elevated levels of NMT expression than *T. brucei,* which may act in tandem with the reduced potency of

DDD85646. An initial trial of the antiserum generated against *Tc*NMT found it to recognise purified recombinant *Tb*NMT, however, against whole cell lysates the antiserum was found to be non-specific. To assess the concentration of NMT in *T. brucei* and *Leishmania* parasites, specific antibodies would need to be generated against each recombinant protein.

3. The overexpression of specific transporters in *T. brucei* produced cell lines that are resistant to suramin and melarsoprol (Shahi *et al*., 2002), two current drugs used in the treatment of HAT. Higher activities of P-glycoprotein efflux pumps (PGP) have been associated with resistance generated *in vitro* to benznidazole in *T. cruzi* (Campos *et al*., 2013). PGP overexpression has also been identified in two antimony resistant *Leishmania spp*. cell lines when compared to the parental cell line (Moreira *et al*., 2013). Interestingly, in the same study, PGP was not overexpressed in resistant *Leishmania infantum* and was not detected in *Leishmania braziliensis* parasites, which were found to have an increase in the transcript of an ABC transporter called MRPA. In three out of the four strains used in their study, the uptake of antimony was found to be lower than WT parasites. Overall, this suggests that the modulation expression of transport proteins is only one of many possible mechanisms that leads to an increased resistance of *Leishmania spp*. to a drug (Callahan *et al*., 1994; Coelho *et al*., 2003; El Fadili *et al*., 2005; Gourbal *et al*., 2004; Maharjan *et al*., 2008). To assess the contributions of the uptake and efflux of this compound in *T. cruzi*, further studies would be required using radiolabelling or metabolomic strategies to determine the kinetics of drug uptake and efflux. This can also be assessed by comparing the levels of PGP in *T. cruzi* with other trypanosomatid parasites by western blot. Alternatively, if a resistant cell line were generated, its genome

and transcriptome could be sequenced to find alternate transport proteins that may be involved in the generation of resistance.

4. The inhibitor DDD85646 which was originally designed to target *Tb*NMT is only 2-fold less potent against the human enzyme, despite there being a 200-fold difference in potency at the cellular level (Frearson *et al*., 2010). This indicates the different biology between human cells and *T. brucei* BSF parasites plays a role in the differential potency. The RNAi mediated depletion of NMT led to an impairment in the endocytic pathway in these parasites, a process that is known to involve the *N*-myristoylated protein ARF1 (Price *et al*., 2010; Price *et al*., 2007a). In this organism, both endo and exocytosis occur at a small invagination in the membrane near the base of the flagellum known as the flagellar pocket equivalent to 5% of the surface area (Engstler *et al*., 2004). *T. bruc*ei has been reported to turn over the entirety of the variant surface glycoprotein coat that is anchored into the plasma membrane within 12 min. This is between 3-5 times quicker than a macrophage or fibroblast is able to turnover its plasma membrane (Engstler *et al*., 2004). However, treating *T. brucei* with DDD85646 led to a massively enlarged flagellar pocket, a different phenotype than observed by the depletion of NMT alone, in which multi-flagellated and rounded parasites were observed in addition to the long and slender forms (Frearson *et al*., 2010; Price *et al*., 2003). The protein ADP-ribosylation factor 1 (ARF1) is known to play a role in endocytosis and trafficking in this parasite, the depletion of which by RNAi led to an accumulation of multi-nucleated parasites and parasites with the big eye phenotype (Price *et al*., 2007b). The different phenotypes may be explained by

differing levels of NMT inhibition, as chemical inhibition may be more efficient at inhibiting *N*-myristoylation than the depletion of the enzyme by RNAi. The authors concluded that the effect of this compound is partly due to the higher rate of endocytosis in *T. brucei* BSF parasites. This may be a viable explanation of the observed drop in potency from *T. brucei* to *T. cruzi*.

5.2 *T. cruzi N*-myristoylome

5.2.1 *N*-myristoylation in *T. cruzi*

The pattern of *N*-myristoylation in this parasite appears to be consistent with other eukaryotes, in particular, lower eukaryotes. The notable exception to this behaviour was the identification that post-translational *N*-myristoylation may occur in this parasite. Although further work is required to validate if this is the case, an alternative explanation may provide the answer. The fold decrease observed in cycloheximide treated cells was roughly proportional with the length of labelling with AzMyr. However, in L-[^{35}S]-methionine labelled epimastigotes, longer exposures found that virtually all protein synthesis was abolished, thus potentially ruling out this theory. This could be further investigated by comparing the band intensities in cycloheximide-treated and un-treated parasites at several time points, to determine if they remain similar.

Several studies have reported *N*-myristoylated proteins for every stage of the *T. cruzi* life cycle (Godsel and Engman, 1999; Martins *et al*., 2010; Okura *et al*., 2005). Whilst the results of this work show that there are multiple *N*-myristoylated proteins expressed in each lifecycle stage, the majority of definable bands were observed in both. The choice to purify amastigotes liberated from infected vero cell monolayers may have artificially selected for a specific population of parasites. If I were to repeat this study

again, I would label vero cell monolayers with azidomyristate and purify the intracellular population of parasites, as this would provide the most robust *N*-myristoylome of the amastigote.

5.2.2 The theoretical and experimental *N*-myristoylomes

Even with the minimal use of the reference *T. cruzi* proteome (UniProt) in this study, a number of artefacts have been identified including the misannotation of this predicted, reference proteome (Silvio X10/1). Comparison with the reference *T. brucei brucei* (927) proteome revealed that there were significantly more proteins not annotated to start with methionine (6.1 vs 0.19%) in *T. cruzi* X10/1. Meanwhile, no mis annotations of this type were identified in the *L. major* proteome. In summary, this reference proteome requires more accurate curation before it can reach its potential as a resource for bioinformatic studies of protein modifications or putative targeting sequences. This could readily be achieved if the genome of Silvio X10/1 was fully assembled and a splice leader mapping transcriptomic study carried out, as has been reported in *T. brucei* where they found a diversity of alternatively spiced transcripts depending upon lifecycle stage (Nilsson *et al*., 2010).

The consensus *N*-myristoylation motif that has been observed in eukaryotes to date has been used to generate several prediction programs to date. The program Myristoylator was found to have the lowest false positive rate of 2.1% in comparison with PROSITE and a similar rate to the NTM predictor (2.7%). The authors of this study note that their false negative rate was marginally higher than the NMT predictor due to use of different set of rules (Bologna *et al*., 2004). The choice to use Myristoylator in this study over the NMT predictor was purely due to a higher compatibility with the workflow and being able to use UniProt accession codes for the analysis. Previous work by Mills and colleagues used only the high confidence predictions for the

predicted *N*-myristoylome of *Leishmania* with Blast results for the other trypanosomatid parasites (Mills *et al*., 2007). The lower number of *N*-myristoylated proteins predicted in Silvio X10/1 was congruent with their hypothesis of overrepresentation of proteins due to multiple isoforms in the hybrid strain CL-Brener. Known *N*-myristoylated proteins from the trypanosomatid parasites were identified in both the high and medium confidence predictions.

Studies of *N*-myristoylation in other organisms have utilised a variety of techniques to identify proteins comprising the *N*-myristoylomes of their respective species. This ranges from bioinformatic predictions, screening of cDNA libraries, cell free approaches, such as in vitro transcription and translation using tritiated myristic acid and the enrichment of bio-orthogonal labelled proteins (Cordero *et al*., 2009; Mills *et al*., 2007; Suzuki *et al*., 2006; Suzuki *et al*., 2010; Takamitsu *et al*., 2014). In theory, the bio-orthogonal labelling strategy coupled to the direct pull-down approach opted for in this study, should have yielded a very clean enrichment of proteins. However, in practice, this was not observed and percentage of proteins starting with MG varied ~2-fold, with increasing specificity observed in the later enrichments, especially with the use of SILAC labelled parasites. Several factors may have contributed to this low level of enrichment.

1. Individual replicates were carried out on separate days over the period of several months. Although the experimental protocol was adhered to on each occasion, minor differences in the timings and sample handling or wash buffers cannot be ruled out. It is not possible to assess the individual contributions of these factors.

2. Despite the copper-catalysed azide-alkyne cycloaddition being highly specific, there are instances of non-specific interaction of the alkyne, such as the alkyne

hydrothiolation reaction, were a alkyne reacts with a thiol (Hoogenboom, 2010). The most likely source of this reaction in these experiments is the presence of free radicals in lysates or exposure to UV light (Lowe, 2014). However, it is not possible to determine the relative contribution of this to the enriched proteomic datasets that we collected.

3. Despite the low occurrence of non-specific interactions advertised for the agarose slurry supplied with the kit, the lack of repeatability for the majority of proteins identified, suggests that this may be a significant contributing factor.

4. Base treatment of *N*-azidomyristoylated proteins in *T. cruzi* did not produce a noticeable difference in the number or intensity of the bands seen by in-gel fluorescence. Hydroxylamine treatment of the resin was designed to remove *S*-azidomyristoylated proteins.   The incomplete removal of this form of myristoylation or the presence of myristate in the GPI anchors of less abundant proteins may explain the identification of proteins not conforming to the typical myristoylation motif.

5. Fifth, stage-specific, alternative splicing events, similar to reports in *T. brucei,* may account for some, but not all proteins identified that do not have an *N*-terminal glycine (Nilsson *et al*., 2010).   A similar splice leader trapping transcriptomic study in this parasite would help identify if this is the case, particularly for the consistently enriched proteins that do not conform to the traditional rule of *N*-myristoylation.

The use of multiple biological replicates refined the list of identified proteins, with the vast majority of the remaining sequences conforming to the universal rules of *N*-myristoylation, or could be alternatively explained by several of the points discussed above. Despite the introduction of SILAC in kinetoplastid organisms in the past couple of years (Brotherton *et al*., 2013; Chawla *et al*., 2011; Guther *et al*., 2014; Silverman *et*

al., 2008; Urbaniak *et al*., 2012; Urbaniak *et al*., 2013) it has yet to be widely adopted, especially in *T. cruzi*, where to my knowledge, this is the first reported use. The identification of multiple known *N*-myristoylated proteins validates the quantification approach taken. Both the label free and SILAC approaches had their merits, such as reduced chances of including contaminants, while label free is more physiologically relevant and the myristic acid analog was found to be less toxic. The increased toxicity of AzMyr observed in the SILAC medium and with the longer doubling period when compared to RTH/FBS this may have hampered the labelling of low-turnover proteins. This in turn, may have reduced the number of enriched proteins and thus quantifiable peptides, despite these enrichments identifying the highest percentage of $^{\Delta}$MG proteins.

In retrospect, the ideal strategy would have been to incorporate some form of cleavable linker for the selective release of enriched proteins, an approach successfully used in *P. falciparum* (Wright *et al*., 2014). Despite a variety of options available, all have drawbacks. For instance, disulphides linkers were not suitable, as there are reports of protein complexes stabilised by disulphide bridges and this type of linker would not be compatible with the reductive alkylation required for mass spectrometry (Bischerour *et al*., 2003; Newhall and Jones, 1983; Toichi *et al*., 2013). An alternative option would be the incorporation of a protease cleavable tag such as TEV, but this option was not selected as could have further complicated the identification of peptides by mass spectrometry due to off-target cleavage of the protein in addition to the tag. This artefact would not be a problem if a trypsin cleavable linker was used. Lastly, enrichment could be achieved with a biotin-functionalised azidomyristate. However, probing *T. cruzi* lysates with streptavidin shows there to be a number of biotinylated proteins in this parasite complicating the analysis by having to remove the biotinylated proteins from the proteomics data. In addition to identifying the biotinylated proteins of *T. cruzi*, there would also be many non-specific proteins that bind to streptavidin coated

beads. This is seen frequently with pull-downs; but, the use of isotopically labelled parasites would have helped to circumvent this problem.

The original aim of the predicted *N*-myristoylome was to provide a reference to highlight the differences between theory and experimental evidence. To ensure the maximal number of proteins identified from the enrichment experiments, the complete proteome was used ruling out the direct comparison of the experimental and theoretical results. Although proteins with annotated functions were evident in the hypothetical and observed *N*-myristoylomes, the bioinformatic predictions for the experimental subproteome, reveals the lack of consensus between the predicted and observed proteins, only achieving this for **~50**% of proteins. The individual performances of the prediction programs revealed Myristoylator to have the highest number of high confidence predictions matching the observed dataset. The best results were obtained by considering the results from the three predictors, requiring one high confidence prediction to be counted as a positive result. Using this approach, 70% of the experimentally determined *N*-myristoylome was predicted to be *N*-myristoylated with a high confidence. In taking an Occam's razor view to the experimental *N*-myristoylome, the experimental approach has been highly effective at identifying the *N*-myristoylated proteins in this parasite, with **~90**% of proteins identified or predicted to have a glycine at position 2. This is the most comprehensive experimental *N*-myristoylome identified in *T. cruzi*, surpassing the previous study by Cordero (Cordero *et al*., 2009), which reported multiple accession codes for protein isoforms with the same function. This significantly reduces the number of predicted proteins from 27 down to 8 unique proteins. Despite this study identifying multiple proteins from enriched membrane fractions, the assignment of *N*-myristoylation as a modification of these proteins was based upon the bioinformatic prediction and not on experimental observation; however, several proteins were cross-identified in the dataset presented here. This in tandem with

the identification of known *N*-myristoylated proteins increases the confidence that the enriched proteins undergo myristoylation in this parasite.

5.2.3 Comparison of *N*-myristoylomes

Protein myristoylation has been studied since 1985, however while there are many known *N*-myristoylated proteins in eukaryotes, only the *N*-myristoylomes of *Arabidopsis thaliana* and *Plasmodium falciparum* have been experimentally defined (Boisson *et al*., 2003; Wright *et al*., 2014). It has long been known that NMT homologs have divergent peptide substrate specificities, even between closely related species. This is further complicated by differences in the *N*-termini of *N*-myristoylated proteins between the species, which was highlighted in the kinetic characterisation of *Tc*NMT with peptides derived from *Tb*CAP5.5 and *Tc*CAP5.5. This complex nature of species-specific substrate recognition made the experimental identification of the *T. cruzi N*-myristoylome the clear choice. Taking into account proteins enriched in all of the biological experiments, a similar number of proteins were identified as to the reported *N*-myristoylome of *P. falciparum*. The list of *N*-myristoylated proteins common to both studies was very low with only the ADP-ribosylation factor 1, ADP-ribosylation factor like proteins, protein phosphatase 2C and a kinase regulatory subunit present in both. There are several possible explanations for the apparent differences in the *N*-myristoylomes of these parasites.

1. The labelling of *P. falciparum* was carried out in parasites cultured in red blood cells. Thus, the *N*-myristoylome has been determined in the erythrocytic cycle, the clinically relevant stage of the disease (Kooij *et al*., 2006). Both transcriptomic and quantitative proteomic studies have shown there to be stage specific regulation of both protein and mRNA expression throughout the life cycle of the parasite (Bozdech *et al*., 2003; Le Roch *et al*., 2004; Nirmalan *et al*.,

2004). It may be that the homologs of the *Plasmodium* proteins are expressed only in the clinically relevant stages. This lifecycle-dependant change in protein and transcript levels has also been reported in *T. cruzi* (Atwood, III *et al.*, 2005; Minning *et al.*, 2003; Minning *et al.*, 2009). Despite minor differences in *N*-myristoylation by in-gel fluorescence across the lifecycle, it could be that there are many more changes below the detection level of this technique. To directly compare the *N*-myristoylomes of these parasites, the *N*-myristoylomes of the clinically relevant trypomastigote and amastigote stages need to be elucidated.

2. Despite only a few, known proteins identified to be common to both *P. falciparum* and *T. cruzi* proteins implicated in similar process have been identified. In both parasites, regulatory subunits of their respective proteasomes have been identified to be *N*-myristoylated, but not the same subunits. Although one would expect homologs of proteins between species to have similar functions, this is not always the case. An example of this is the proteasome regulatory ATPase subunit 2, RPT2, in both *S. cerevisiae* and *T. brucei,* which have both been found to be essential. However, reconstitution of *Sc*RPT2 into a *Tb*RPT2 deficient cell line failed to rescue the lethal phenotype in *T. brucei*, showing the incompatibity of these homologs (Li *et al.*, 2002). It may that the different homologs identified may play similar roles in the different parasites. Genetic studies in *T. cruzi* would help to identify if *N*-myristoylation is important for the function of these proteins by knocking out the *T. cruzi* genes in the presence of a G2A mutant, or the homolog from another organism.

3. In contrast to *P. falciparum*, the labelling efficacy of the *N*-myristoylome in *T. cruzi*, and the chemical capture of these proteins was not assessed. It has not been possible to determine if the identified sub-proteomes have been affected by the turnover of these proteins, or differential expression levels. The direct

inhibition of *N*-myristoylation in epimastigotes by DDD85646 demonstrated differential rates of AzMyr incorporation in these (**Figure 3.12**). In particular, the band at ~20 kDa was found to be significantly affected by the inhibition of *Tc*NMT. A pulse-chase labelling strategy could allow the turnover of these proteins to be assessed in *T. cruzi* and this technique could be used to compare turnover rates with other parasites. In particular, *T. brucei* has been shown to be highly sensitive to NMT inhibition (Brand *et al.*, 2012; Frearson *et al.*, 2010) and it may be that the proteins with the highest turnover rates, in *T. brucei* produce the observed big eye phenotype.

4. These differences in the *N*-myristoylomes of these parasites may simply reflect the divergent nature of this process in the different parasites. If this is the case, then the *N*-myristoylomes may provide a promising list of species-specific drug targets to be assessed in the individual parasites. This would require the extremely time consuming process of the biochemical and genetic validation of these proteins individually.

5.3 Prospective mechanisms of DDD85646 against *T. cruzi* epimastigotes

This study has shown that by inhibiting *N*-myristoylation in *T. cruzi*, proliferation of epimastigotes also became impaired. Despite using the same inhibitor as reported for *T. brucei*, the resulting phenotypes whilst initially appearing similar by light microscopy were found to be markedly different. It has been postulated that the "Big-Eye" phenotype observed in *T. brucei* is related to the interruption of endocytosis, as the phenotype was similar when clathrin is knocked down in this parasite (Allen *et al.*, 2003; Frearson *et al.*, 2010). A point worth bearing in mind is that in *T. cruzi* epimastigotes, the site of endocytosis is a small invagination known as the cytostome

(Porto-Carreiro *et al.*, 2000) rather than the flagellar pocket, which may explain the lack of the big eye phenotype in drug treated parasites. The DDD85646 mediated inhibition of cytokinesis and the identification of the *N*-myristoylome in this study has allowed for a unique perspective into the mechanism by which this compound affects the division of these parasites. A literature review of the proteins identified in this study suggests that the cytokinesis defect may be caused by one or several proteins from this study.

FRQ1 and its interaction partner

The frequinin homolog in yeast FRQ1 is a small *N*-myristoylated calcium-binding protein that was found to associate with phosphatidylinositol-4-OH kinase (PIK1) (Hendricks *et al.*, 1999). Domain deletion experiments found that the *N*-terminus of PIK1 which contains a lipid kinase domain was required for the association of FRQ1, in a calcium independent manner. The presence of both myristoylated and non-myristoylated Frq1 was found to increase the activity of PIK1 *in vitro*. Nevertheless, studies in *S. cerevisiae* found the *N*-myristoylation of FRQ1 to be important for rescuing growth, as the G2A mutant was unable to restore proliferation. This demonstrates that the *N*-myristoylation is essential for its biological function. Gene knockout studies in *S. cerevisiae* found Frq1 to be essential for the growth of the organism, as proliferation ceased after 3-4 divisions in Frq1 null mutants (Hendricks *et al.*, 1999). Similarly, the RNAi mediated depletion of this homolog in *T. brucei* revealed a growth phenotype in all lifecycle stages assessed (Alsford *et al.*, 2011). This would indicate that correct function of this gene product is essential for the proliferation of the both organisms and thus could be essential in *T. cruzi*.

As discussed above, FRQ1 plays a role in the activation of the kinase Pik1. A null mutant *S. cerevisiae* strain is rendered completely inviable (Flanagan *et al.*, 1993).

The authors of the same study also note that the overexpression of Pik1 makes them more sensitive to growth arrest by the yeast growth inhibitory pheromone that is known to be involved with mating of yeast. However, a second study found this effect to be marginal and not reproducible (Flanagan *et al*., 1993). In addition, this enzyme was found to sediment with the nucleus rather than the cytoplasm which they attribute to the isolation methods used (Garcia-Bustos *et al*., 1994). It was noted by this study that the phenotypes for PI-PLC and Pik1 overlapped as both produce cytokinesis defects (Flick and Thorner, 1993; Payne and Fitzgerald-Hayes, 1993; Yoko-o T *et al*., 1993). Loss of gene function studies in *S. pombe* were consistent with Pik1 playing an essential role in this yeast but was not found to localise to the nucleus in this strain (Park *et al*., 2009). The use of fission yeast in this latter study more closely resembles the replication events that occur in *T. cruzi*. Loss of Pik1 was associated with an increase in the presence of bi-nucleated cells. Pik1 is known to interact with several proteins in both *Saccharomyces sp*. One is CdC4 a contractile ring protein required for cytokinesis in the pombe strain (Desautels *et al*., 2001). Interestingly, the overexpression of Pik1 was lethal in *S. pombe* in some cases with further studies indicating that an inability to associate with cdc4 was the largest contributing factor.

Clearly, the roles that FRQ1 and Pik1 play in the regulation of cytokinesis in cell division are not yet fully understood. Nevertheless, without further functional studies of these homologs in *T. cruzi*, it is not possible to ascertain the relative contributing factors of the individual components to the observed cytokinesis defect.

CAP5.5

There are two forms of CAP5.5 in *T. brucei*, CAP5.5 and CAP5.5V both are differentially expressed in bloodstream and procyclic stages (Olego-Fernandez *et al*.,

2009). The RNAi mediated depletion of CAP5.5 in the procyclic form was found to produce abnormal cytokinesis artefacts leading to the accumulation of 2K1N, 2K2N and 1K0N parasites (Olego-Fernandez *et al*., 2009). Nuclear mis-positioning was also identified in 2K2N cells in relation to the position of the cleavage furrow that forms part of the cytokinesis event. This relationship was also maintained in bloodstream form parasites when the variant protein was depleted (Olego-Fernandez *et al*., 2009). Closer analysis of these abnormal parasites by electron microscopy have indicated that the abnormal morphologies are accompanied by a loss in microtubule organisation (Olego-Fernandez *et al*., 2009). The authors of this study postulate several possible mechanisms to account for the formation of zoids 1K1N parasites, but fail to provide a suitable hypothesis for the accumulation >2K2N cells. Regardless of this, it is hard to dispute that "646" treated epimastigotes resemble the CAP5.5 RNAi phenotype in *T. brucei*, making this a credible cause for this phenotype.

ARF1 and ARL1

The depletion of ARF1 in *T. brucei* BSF parasites leads to an accumulation of multi-nucleated parasites, with the predominant big eye phenotype is present in 86% of parasites 24 h after induction of RNAi (Price *et al*., 2007a). At the same time point, almost no change was observed in the number of multi-nucleated parasites. Despite the same producing one aspect of the phenotype in *T. brucei*, is not as extreme as observed in *T. cruzi,* which after 48 hours the number of normal parasites decreases by 25 and 50% respectively in the two parasites (Price *et al*., 2007a). Given the longer doubling time of epimastigotes (16-20 h) it would be expected that a higher percentage of *T. brucei* parasites would display this abnormal nuclear phenotype at this stage, rather than the opposite way around. A similar phenotype is also observed by the depletion of the

ARF1-related protein ADP-ribosylation factor like-protein 1 (ARL1). Similar to ARF1, ~25% of cells display the abnormal phenotype (Price *et al*., 2005). Similarly, in *T. cruzi* there is an increase in 2K2N parasites followed by a decrease, prior to an increase in abnormal parasites (>2K2N) rising to ~70% at 96h of DDD85646 treatment. This effect is not limited to *T. brucei* as an ARF activating protein is also implicated in cytokinesis of a species of *Dictyostelium* (Dias *et al*., 2013).

While the individual depletion of these homologs provides a convenient explanation for the mechanism of DDD85646 observed in these studies, these proteins listed above account for ~10% of the *N*-myristoylome. Therefore, it is just as likely that the effect cause by this compound is due to the cumulative miss-localisation of multiple proteins, some of which have yet to be characterised. The contribution of these proteins to the observed phenotype could be assessed by the individual overexpression of each protein in the presence of DDD85646 to determine which if any, abolish the phenotype. This would be under the assumption that the overexpression of these proteins is not lethal, which is the case with TbARF1, but not for the G2A mutant (Price *et al*., 2007a). Although this work has been carried out on the epimastigote stage, it may provide an insight as to the mechanism of NMT inhibition in the clinically relevant amastigote stage, which also undergoes cell division. As mentioned above and in our publication, DDD85646 does not have a high enough selectivity for the intracellular parasite over the host Vero cell (Roberts *et al*., 2014). To elucidate the mechanism of action in the clinically relevant stages, NMT inhibitors with both a higher potency and a greater selectivity for the *T. cruzi* enzyme first need to be identified. To assess if the cytokinesis defect was also present in the amastigote stage, immune fluorescence on infected Vero cells with an antibody targeting an amastigote-specific surface protein

may answer this question.   An alternate approach is that the intracellular amastigotes could be purified by anion exchange chromatography and analysed by scanning and transmission electron microscopy.

5.4 The suitability of NMT as a drug target in *T. cruzi*

Having found genetic, biochemical and mechanistic evidence to show that *N*-myristoylation is an essential process in these parasites, it is clear that NMT is a drug target in the clinically irrelevant stage. However, more potent and selective inhibitors need to be developed to determine it essentiality in the mammalian stages of the lifecycle. The development of better inhibitors would be greatly aided by a crystal structure of the enzyme and DDD85646-NMT complex. A new inhibitor-screening program to identify new starting points for the development of *Tc*NMT specific inhibitors would help achieve this, in addition to comparing the potency of WT and SKO parasites. Without useful genetic tools or more potent tool compounds, it is not possible to draw reliable conclusions about the essentiality or druggability of this enzyme in the mammalian lifecycle. Nonetheless on the basis that this process has been shown to be important in all eukaryotes studied in to date (***Sections 1.4.2 and 1.4.3***) it is highly likely that *N*-myristoylation is essential in both the amastigote and trypomastigote stages also, with the essentiality in the trypomastigote being the easiest to assess.

In *T. brucei*, the inhibition of *N*-myristoylation has been associated with the formation of a big-eye phenotype, similar to results obtained by the interruption of clathrin (Allen *et al*., 2003). However, no extensive investigations into the mechanism of action of this drug were ever undertaken in this parasite. RNAi studies in *T. brucei* of homologs found to be enriched in all experiments found the depletion of more than

50% to affect the proliferation of these parasites, suggesting that they are important in proliferation. Several of these proteins were found to negatively affect proliferation in all four stages assessed, raising the possibility that these proteins could be potential drug targets in the future. Targeting an enzyme responsible for the modification of multiple essential proteins has many benefits of allowing for based drug design. Whilst this can aid the development of highly potent inhibitors, this target-based drug discovery approach has the drawback of an increased risk of resistance arising. Alternatively, the use of compounds with multiple targets can reduce this risk, but not necessarily entirely abolish it. In summary, it is likely that *N*-myristoyltransferase is a drug target throughout the lifecycle of the parasite, but more work is required to determine its druggability in the clinical stages.

5.5 Future work

The work undertaken in this study has opened the possibility of the *N*-myristoylome for drugs to treat Chagas disease. The need for more potent and selective inhibitors that target *T. cruzi* NMT has been highlighted at several stages in this research. The continuous spectrophotometric assay that has been used through the study has routinely generated robust kinetics data for both the kinetic characterisation of the enzyme and its inhibition by DDD85646. Further optimisation of this assay into a 96 well or 384 well assay would allow a compound library to be screened against the recombinant enzyme and may provide a new starting point for the development of potent new inhibitors of *Tc*NMT. This would be carried out in tandem with the optimisation of crystallisation conditions for the enzyme, with the aim of solving the structure to aid rational drug design. This would be followed up by the assessment of NMT in the clinically relevant amastigote stage and mechanism of action studies to determine if NMT inhibition

merely inhibits cytokinesis, or if it is lethal in the amastigote. It is evident that the *N*-myristoylome is important for the proliferation of these parasites, at least in axenic culture. The homologs of several *N*-myristoylated proteins have been implicated to be important in the growth of *T. brucei* parasites. The genetic and biochemical assessment of these proteins may provide a range of alternative targets for drug development against *T. cruzi*. Lastly, a high quality omic study needs to be carried out in one parasite strain (comprising a proteome, a genome and a transcriptome) in order to provide a useful resource to the trypanosome community.

Reference List

(1998). Chagas disease: Central American initiative launched. *Tropical Disease Research news* , 6.

(2002). Chagas disease after organ transplantation--United States, 2001. *MMWR Morb. Mortal. Wkly. Rep. 51*, 210-212.

(2006). Chagas disease after organ transplantation--Los Angeles, California, 2006. *MMWR Morb. Mortal. Wkly. Rep. 55*, 798-800.

Alarcon de, N.B., Diaz-Bello, Z., Colmenares, C., Ruiz-Guevara, R., Mauriello, L., Zavala-Jaspe, R., Suarez, J.A., Abate, T., Naranjo, L., Paiva, M., Rivas, L., Castro, J., Marques, J., Mendoza, I., Acquatella, H., Torres, J. and Noya, O. (2010). Large urban outbreak of orally acquired acute Chagas disease at a school in Caracas, Venezuela. *Journal of Infectious Diseases 201*, 1308-1315.

Ali, S.T., Moir, A.J., Ashton, P.R., Engel, P.C. and Guest, J.R. (1990). Octanoylation of the lipoyl domains of the pyruvate dehydrogenase complex in a lipoyl-deficient strain of *Escherichia coli*. *Molecular Microbiology 4*, 943-950.

Allen, C.L., Goulding, D. and Field, M.C. (2003). Clathrin-mediated endocytosis is essential in *Trypanosoma brucei*. *EMBO Journal 22*, 4991-5002.

Almeida, E.A., Lima, J.N., Lages-Silva, E., Guariento, M.E., Aoki, F.H., Torres-Morales, A.E. and Pedro, R.J. (2010). Chagas' disease and HIV co-infection in patients without effective antiretroviral therapy: prevalence, clinical presentation and natural history. *Transactions of the Royal Society of Tropical Medicine and Hygiene 104*, 447-452.

Alsford, S., Turner, D.J., Obado, S.O., Sanchez-Flores, A., Glover, L., Berriman, M., Hertz-Fowler, C. and Horn, D. (2011). High-throughput phenotyping using parallel sequencing of RNA interference targets in the African trypanosome. *Genome Research 21*, 915-924.

Altcheh, J., Moscatelli, G., Moroni, S., Garcia-Bournissen, F. and Freilij, H. (2011). Adverse events after the use of benznidazole in infants and children with Chagas disease. *Pediatrics 127*, e212-e218.

Ameisen, J.C., Idziorek, T., Billaut-Mulot, O., Loyens, M., Tissier, J.P., Potentier, A. and Ouaissi, A. (1995). Apoptosis in a unicellular eukaryote (*Trypanosoma cruzi*): implications for the evolutionary origin and role of programmed cell death in the control of cell proliferation, differentiation and survival. *Cell Death and Differentiation 2*, 285-300.

Ames, J.B., Hendricks, K.B., Strahl, T., Huttner, I.G., Hamasaki, N. and Thorner, J. (2000). Structure and calcium-binding properties of Frq1, a novel calcium sensor in the yeast *Saccharomyces cerevisiae*. *Biochemistry 39*, 12149-12161.

Ammerman, N.C., Beier-Sexton, M. and Azad, A.F. (2008). Growth and maintenance of Vero cell lines. *Curr. Protoc. Microbiol. 11*, A.4E.1-A.4E.7.

Andrade, J.P., Marin Neto, J.A., Paola, A.A., Vilas-Boas, F., Oliveira, G.M., Bacal, F., Bocchi, E.A., Almeida, D.R., Fragata Filho, A.A., Moreira, M.C., Xavier, S.S., Oliveira Junior, W.A. and Dias, J.C.

(2011). I Latin American Guidelines for the diagnosis and treatment of Chagas' heart disease: executive summary. *Arq Bras. Cardiol. 96*, 434-442.

Anez, N., Carrasco, H., Parada, H., Crisante, G., Rojas, A., Gonzalez, N., Ramirez, J.L., Guevara, P., Rivero, C., Borges, R. and Scorza, J.V. (1999). Acute Chagas' disease in western Venezuela: a clinical, seroparasitologic, and epidemiologic study. *American Journal of Tropical Medicine and Hygiene 60*, 215-222.

Apt, W., Aguilera, X., Arribada, A., Gomez, L., Miles, M.A. and Widmer, G. (1987). Epidemiology of Chagas' disease in northern Chile: isozyme profiles of Trypanosoma cruzi from domestic and sylvatic transmission cycles and their association with cardiopathy. *American Journal of Tropical Medicine and Hygiene 37*, 302-307.

Apt, W., Arribada, A., Zulantay, I., Rodriguez, J., Saavedra, M. and Munoz, A. (2013). Treatment of Chagas' disease with itraconazole: electrocardiographic and parasitological conditions after 20 years of follow-up. *Journal of Antimicrobial Chemotherapy 68*, 2164-2169.

Apt, W., Arribada, A., Zulantay, I., Solari, A., Sanchez, G., Mundaca, K., Coronado, X., Rodriguez, J., Gil, L.C. and Osuna, A. (2005). Itraconazole or allopurinol in the treatment of chronic American trypanosomiasis: the results of clinical and parasitological examinations 11 years post-treatment. *Annals of Tropical Medicine and Parasitology 99*, 733-741.

Armah, D.A. and Mensa-Wilmot, K. (1999). *S*-myristoylation of a glycosylphosphatidylinositol-specific phospholipase C in *Trypanosoma brucei*. *Journal of Biological Chemistry 274*, 5931-5938.

Atwood, J.A., III, Weatherly, D.B., Minning, T.A., Bundy, B., Cavola, C., Opperdoes, F.R., Orlando, R. and Tarleton, R.L. (2005). The *Trypanosoma cruzi* proteome. *Science 309*, 473-476.

Bahia, M.T., de Andrade, I.M., Martins, T.A., do Nascimento, A.F., Diniz, L.F., Caldas, I.S., Talvani, A., Trunz, B.B., Torreele, E. and Ribeiro, I. (2012). Fexinidazole: a potential new drug candidate for Chagas disease. *PLoS Neglected Tropical Diseases 6*, e1870.

Basso, B. (2013). Modulation of immune response in experimental Chagas disease. *World Journal of Experimental Medicine 3*, 1-10.

Bastos, C.J., Aras, R., Mota, G., Reis, F., Dias, J.P., de Jesus, R.S., Freire, M.S., de Araujo, E.G., Prazeres, J. and Grassi, M.F. (2010). Clinical outcomes of thirteen patients with acute chagas disease acquired through oral transmission from two urban outbreaks in northeastern Brazil. *PLoS Neglected Tropical Diseases 4*, e711.

Bell, A.S., Mills, J.E., Williams, G.P., Brannigan, J.A., Wilkinson, A.J., Parkinson, T., Leatherbarrow, R.J., Tate, E.W., Holder, A.A. and Smith, D.F. (2012). Selective inhibitors of protozoan protein *N*-myristoyltransferases as starting points for tropical disease medicinal chemistry programs. *PLoS Neglected Tropical Diseases 6*, e1625.

Bern, C., Montgomery, S.P., Katz, L., Caglioti, S. and Stramer, S.L. (2008). Chagas disease and the US blood supply. *Current Opinion in Infectious Diseases 21*, 476-482.

Beverley, S.M. (2003). Protozomics: Trypanosomatid parasite genetics comes of age. *Nature Reviews Genetics 4*, 11-19.

Bhatnagar, R.S., Futterer, K., Farazi, T.A., Korolev, S., Murray, C.L., Jackson-Machelski, E., Gokel, G.W., Gordon, J.I. and Waksman, G. (1998). Structure of *N*-myristoyltransferase with bound myristoylCoA and peptide substrate analogs. *Nature Structural Biology 5*, 1091-1097.

Bhatnagar, R.S., Schall, O.F., Jackson-Machelski, E., Sikorski, J.A., Devadas, B., Gokel, G.W. and Gordon, J.I. (1997). Titration calorimetric analysis of AcylCoA recognition by myristoylCoA:protein *N*-myristoyltransferase. *Biochemistry 36*, 6700-6708.

Bischerour, J., Leh, H., Deprez, E., Brochon, J.C. and Mouscadet, J.F. (2003). Disulfide-linked integrase oligomers involving C280 residues are formed in vitro and in vivo but are not essential for human immunodeficiency virus replication. *Journal of Virology 77*, 135-141.

Boisson, B., Giglione, C. and Meinnel, T. (2003). Unexpected protein families including cell defense components feature in the *N*-myristoylome of a higher eukaryote. *Journal of Biological Chemistry 278*, 43418-43429.

Boisson, B. and Meinnel, T. (2003). A continuous assay of myristoyl-CoA:protein *N*-myristoyltransferase for proteomic analysis. *Analytical Biochemistry 322*, 116-123.

Bologna, G., Yvon, C., Duvaud, S. and Veuthey, A.L. (2004). *N*-Terminal myristoylation predictions by ensembles of neural networks. *Proteomics 4*, 1626-1632.

Bouvier, L.A., Camara, M.L., Canepa, G.E., Miranda, M.R. and Pereira, C.A. (2013). Plasmid vectors and molecular building blocks for the development of genetic manipulation tools for *Trypanosoma cruzi*. *Plos One 8*, e80217.

Bozdech, Z., Llinas, M., Pulliam, B.L., Wong, E.D., Zhu, J. and DeRisi, J.L. (2003). The transcriptome of the intraerythrocytic developmental cycle of *Plasmodium falciparum*. *PLoS Biology 1*, E5.

Brand, S., Cleghorn, L.A.T., McElroy, S.P., Robinson, D.A., Smith, V.C., Hallyburton, I., Harrison, J.R., Norcross, N.R., Spinks, D., Bayliss, T., Norval, S., Stojanovski, L., Torrie, L.S., Frearson, J.A., Brenk, R., Fairlamb, A.H., Ferguson, M.A.J., Read, K.D., Wyatt, P.G. and Gilbert, I.H. (2012). Discovery of a novel class of orally active trypanocidal *N*-myristoyltransferase inhibitors. *Journal of Medicinal Chemistry 55*, 140-152.

Brandariz, S., Schijman, A., Vigliano, C., Arteman, P., Viotti, R., Beldjord, C. and Levin, M.J. (1995). Detection of parasite DNA in Chagas' heart disease . *Lancet 346*, 1370-1371.

Brannigan, J.A., Smith, B.A., Yu, Z.Y., Brzozowski, A.M., Hodgkinson, M.R., Maroof, A., Price, H.P., Meier, F., Leatherbarrow, R.J., Tate, E.W., Smith, D.F. and Wilkinson, A.J. (2010). N-Myristoyltransferase from Leishmania donovani: Structural and Functional Characterisation of a Potential Drug Target for Visceral Leishmaniasis. *Journal of Molecular Biology 396*, 985-999.

Brener, Z. (1973). Biology of *Trypanosoma cruzi*. *Annual Review of Microbiology 27*, 347-382.

Brotherton, M.C., Bourassa, S., Leprohon, P., Legare, D., Poirier, G.G., Droit, A. and Ouellette, M. (2013). Proteomic and genomic analyses of antimony resistant *Leishmania infantum* mutant. *Plos One 8*, e81899.

Brun, R. and Schonenberger, M. (1979). Cultivation and in vitro cloning of procyclic culture forms of *Trypanosoma brucei* in a semi-defined medium. *Acta Tropica 36*, 289-292.

Buckner, F.S., Wilson, A.J. and Van Voorhis, W.C. (1999). Detection of live Trypanosoma cruzi in tissues of infected mice by using histochemical stain for beta-galactosidase. *Infection and Immunity 67*, 403-409.

Burnaevskiy, N., Fox, T.G., Plymire, D.A., Ertelt, J.M., Weigele, B.A., Selyunin, A.S., Way, S.S., Patrie, S.M. and Alto, N.M. (2013). Proteolytic elimination of N-myristoyl modifications by the *Shigella* virulence factor IpaJ. *Nature 496*, 106-+.

Buss, J.E., Kamps, M.P. and Sefton, B.M. (1984). Myristic acid is attached to the transforming protein of *Rous sarcoma* virus during or immediately after synthesis and is present in both soluble and membrane-bound forms of the protein. *Molecular and Cellular Biology 4*, 2697-2704.

Caler, E.V., de Avalos, S.V., Haynes, P.A., Andrews, N.W. and Burleigh, B.A. (1998). Oligopeptidase B-dependent signaling mediates host cell invasion by *Trypanosoma cruzi*. *EMBO Journal 17*, 4975-4986.

Callahan, H.L., Roberts, W.L., Rainey, P.M. and Beverley, S.M. (1994). The *PGPA* gene of *Leishmania major* mediates antimony (SbIII) resistance by decreasing influx and not by increasing efflux. *Molecular and Biochemical Parasitology 68*, 145-149.

Campos, M.C., Castro-Pinto, D.B., Ribeiro, G.A., Berredo-Pinho, M.M., Gomes, L.H., da Silva Bellieny, M.S., Goulart, C.M., Echevarria, A. and Leon, L.L. (2013). P-glycoprotein efflux pump plays an important role in *Trypanosoma cruzi* drug resistance. *Parasitology Research 112*, 2341-2351.

Cancado, J.R. (2002). Long term evaluation of etiological treatment of Chagas disease with benznidazole. *Rev. Inst. Med. Trop Sao Paulo 44*, 29-37.

Caradonna, K.L., Engel, J.C., Jacobi, D., Lee, C.H. and Burleigh, B.A. (2013). Host metabolism regulates intracellular growth of *Trypanosoma cruzi*. *Cell Host. Microbe 13*, 108-117.

Cevallos, A.M. and Hernandez, R. (2014). Chagas' disease: pregnancy and congenital transmission. *Biomed. Res. Int. 2014*, 401864.

Chang, T.H., Milne, K.G., Guther, M.L.S., Smith, T.K. and Ferguson, M.A.J. (2002). Cloning of *Trypanosoma brucei* and *Leishmania major* genes encoding the GlcNAc-phosphatidylinositol de-*N*-acetylase of glycosylphosphatidylinositol biosynthesis that is essential to the African sleeping sickness parasite. *Journal of Biological Chemistry 277*, 50176-50182.

Chawla, B., Jhingran, A., Panigrahi, A., Stuart, K.D. and Madhubala, R. (2011). Paromomycin affects translation and vesicle-mediated trafficking as revealed by proteomics of paromomycin -susceptible -resistant *Leishmania donovani*. *Plos One 6*, e26660.

Chin-Hong, P.V., Schwartz, B.S., Bern, C., Montgomery, S.P., Kontak, S., Kubak, B., Morris, M.I., Nowicki, M., Wright, C. and Ison, M.G. (2011). Screening and treatment of chagas disease in organ transplant recipients in the United States: recommendations from the chagas in transplant working group. *Am. J. Transplant. 11*, 672-680.

Chuenkova, M.V. and PereiraPerrin, M. (2009). *Trypanosoma cruzi* targets Akt in host cells as an intracellular antiapoptotic strategy. *Sci. Signal. 2*, ra74.

Ciccarelli, A.B., Frank, F.M., Puente, V., Malchiodi, E.L., Batlle, A. and Lombardo, M.E. (2012). Antiparasitic Effect of Vitamin B12 on *Trypanosoma cruzi*. *Antimicrobial Agents and Chemotherapy 56*, 5315-5320.

Clayton, J. (2010). Chagas disease: pushing through the pipeline. *Nature 465*, S12-S15.

Coelho, A.C., Beverley, S.M. and Cotrim, P.C. (2003). Functional genetic identification of PRP1, an ABC transporter superfamily member conferring pentamidine resistance in *Leishmania major*. *Molecular and Biochemical Parasitology 130*, 83-90.

Combs, T.P., Nagajyothi, Mukherjee, S., de Almeida, C.J., Jelicks, L.A., Schubert, W., Lin, Y., Jayabalan, D.S., Zhao, D., Braunstein, V.L., Landskroner-Eiger, S., Cordero, A., Factor, S.M., Weiss, L.M., Lisanti, M.P., Tanowitz, H.B. and Scherer, P.E. (2005). The adipocyte as an important target cell for *Trypanosoma cruzi* infection. *Journal of Biological Chemistry 280*, 24085-24094.

Cordero, E.M., Nakayasu, E.S., Gentil, L.G., Yoshida, N., Almeida, I.C. and da Silveira, J.F. (2009). Proteomic analysis of detergent-solubilized membrane proteins from insect-developmental forms of *Trypanosoma cruzi*. *Journal of Proteome Research 8*, 3642-3652.

Cox, J., Hein, M.Y., Luber, C.A., Paron, I., Nagaraj, N. and Mann, M. (2014). Accurate proteome-wide label-free quantification by delayed normalization and maximal peptide ratio extraction, termed MaxLFQ. *Mol. Cell Proteomics 13*, 2513-2526.

Cox, J. and Mann, M. (2008). MaxQuant enables high peptide identification rates, individualized p.p.b.-range mass accuracies and proteome-wide protein quantification. *Nature Biotechnology 26*, 1367-1372.

Cox, J., Neuhauser, N., Michalski, A., Scheltema, R.A., Olsen, J.V. and Mann, M. (2011). Andromeda: a peptide search engine integrated into the MaxQuant environment. *Journal of Proteome Research 10*, 1794-1805.

da Silveira, A.B., Lemos, E.M., Adad, S.J., Correa-Oliveira, R., Furness, J.B. and d'Avila, R.D. (2007). Megacolon in Chagas disease: a study of inflammatory cells, enteric nerves, and glial cells. *Hum. Pathol. 38*, 1256-1264.

DaRocha, W.D., Otsu, K., Teixeira, S.M.R. and Donelson, J.E. (2004). Tests of cytoplasmic RNA interference (RNAi) and construction of a tetracycline-inducible T7 promoter system in *Trypanosoma cruzi*. *Molecular and Biochemical Parasitology 133*, 175-186.

De Carvalho, T.U. and de, S.W. (1986). Infectivity of amastigotes of *Trypanosoma cruzi*. *Rev. Inst. Med. Trop. Sao Paulo 28*, 205-212.

deAndrade, A.L.S.S., Zicker, F., deOliveira, R.M., Silva, S.A.E., Luquetti, A., Travassos, L.R., Almeida, I.C., deAndrade, S.S., deAndrade, J.G. and Martelli, C.M.T. (1996). Randomised trial of efficacy of benznidazole in treatment of early *Trypanosoma cruzi* infection. *Lancet 348*, 1407-1413.

Denny, P.W., Gokool, S., Russell, D.G., Field, M.C. and Smith, D.F. (2000). Acylation-dependent protein export in *Leishmania*. *Journal of Biological Chemistry 275*, 11017-11025.

Desautels, M., Den Haese, J.P., Slupsky, C.M., McIntosh, L.P. and Hemmingsen, S.M. (2001). Cdc4p, a contractile ring protein essential for cytokinesis in *Schizosaccharomyces pombe*, interacts with a phosphatidylinositol 4-kinase. *Journal of Biological Chemistry 276*, 5932-5942.

Desmeules, P., Grandbois, M., Bondarenko, V.A., Yamazaki, A. and Salesse, C. (2002). Measurement of membrane binding between recoverin, a calcium-myristoyl switch protein, and lipid bilayers by AFM-based force spectroscopy. *Biophysical Journal 82*, 3343-3350.

Devadas, B., Freeman, S.K., Zupec, M.E., Lu, H.F., Nagarajan, S.R., Kishore, N.S., Lodge, J.K., Kuneman, D.W., McWherter, C.A., Vinjamoori, D.V., Getman, D.P., Gordon, J.I. and Sikorski, J.A. (1997). Design and synthesis of novel imidazole-substituted dipeptide amides as potent and selective inhibitors of *Candida albicans* myristoylCoA:protein *N*-myristoyltransferase and identification of related tripeptide inhibitors with mechanism-based antifungal activity. *Journal of Medicinal Chemistry 40*, 2609-2625.

Devadas, B., Lu, T., Katoh, A., Kishore, N.S., Wade, A.C., Mehta, P.P., Rudnick, D.A., Bryant, M.L., Adams, S.P. and Li, Q. (1992). Substrate specificity of *Saccharomyces cerevisiae* myristoyl-CoA: protein *N*-myristoyltransferase. Analysis of fatty acid analogs containing carbonyl groups, nitrogen heteroatoms, and nitrogen heterocycles in an *in vitro* enzyme assay and subsequent identification of inhibitors of human immunodeficiency virus I replication. *Journal of Biological Chemistry 267*, 7224-7239.

Devadas, B., Zupec, M.E., Freeman, S.K., Brown, D.L., Nagarajan, S., Sikorski, J.A., McWherter, C.A., Getman, D.P. and Gordon, J.I. (1995). Design and syntheses of potent and selective dipeptide inhibitors of *Candida albicans* myristoyl-CoA:protein *N*-myristoyltransferase. *Journal of Medicinal Chemistry 38*, 1837-1840.

Dias, E., Laranja, F.S., Miranda, A. and Nobrega, G. (1956). Chagas' disease; a clinical, epidemiologic, and pathologic study. *Circulation 14*, 1035-1060.

Dias, J.C. (2007). Southern Cone Initiative for the elimination of domestic populations of *Triatoma infestans* and the interruption of transfusional Chagas disease. Historical aspects, present situation, and perspectives. *Memorias do Instituto Oswaldo Cruz 102 Suppl 1*, 11-18.

Dias, J.C.P. (1984). Acute Chagas' disease. *Memorias do Instituto Oswaldo Cruz 79*, S85-S91.

Dias, M., Blanc, C., Thazar-Poulot, N., Ben, L.S., Cosson, P. and Letourneur, F. (2013). *Dictyostelium* ACAP-A is an ArfGAP involved in cytokinesis, cell migration and actin cytoskeleton dynamics. *Journal of Cell Science 126*, 756-766.

Diaz-de-Toranzo, E.G., Castro, J.A., Franke de Cazzulo, B.M. and Cazzulo, J.J. (1988). Interaction of benznidazole reactive metabolites with nuclear and kinetoplastic DNA, proteins and lipids from Trypanosoma cruzi. *Experientia 44*, 880-881.

Diniz, L.F., Caldas, I.S., Guedes, P.M., Crepalde, G., de, L.M., Carneiro, C.M., Talvani, A., Urbina, J.A. and Bahia, M.T. (2010). Effects of ravuconazole treatment on parasite load and immune response in dogs experimentally infected with *Trypanosoma cruzi*. *Antimicrobial Agents and Chemotherapy 54*, 2979-2986.

Docampo, R., Mason, R.P., Mottley, C. and Muniz, R.P.A. (1981). Generation of free radicals induced by nifurtimox in mammalian tissues. *Journal of Biological Chemistry 256*, 10930-10933.

Docampo, R. and Moreno, S.N.J. (1984). Free radical metabolites in the mode of action of chemotherapeutic agents and phagocytic cells on *Trypanosoma cruzi*. *Reviews of Infectious Diseases 6*, 223-238.

Docampo, R. and Moreno, S.N.J. (1986). Free-radical metabolism of antiparasitic agents. *Federation Proceedings 45*, 2471-2476.

Docampo, R. and Stoppani, A.O. (1979). Generation of superoxide anion and hydrogen peroxide induced by nifurtimox in *Trypanosoma cruzi*. *Archives of Biochemistry and Biophysics 197*, 317-321.

Doering, T.L., Lu, T., Werbovetz, K.A., Gokel, G.W., Hart, G.W., Gordon, J.I. and Englund, P.T. (1994). Toxicity of myristic acid analogs toward African trypanosomes. *Proceedings of the National Academy of Sciences of the United States of America 91*, 9735-9739.

Doering, T.L., Raper, J., Buxbaum, L.U., Adams, S.P., Gordon, J.I., Hart, G.W. and Englund, P.T. (1991). An analog of myristic acid with selective toxicity for African trypanosomes. *Science 252*, 1851-1854.

Doyle, P.S., Chen, C.K., Johnston, J.B., Hopkins, S.D., Leung, S.S., Jacobson, M.P., Engel, J.C., McKerrow, J.H. and Podust, L.M. (2010). A nonazole CYP51 inhibitor cures Chagas' disease in a mouse model of acute infection. *Antimicrobial Agents and Chemotherapy 54*, 2480-2488.

Doyle, P.S., Zhou, Y.M., Engel, J.C. and McKerrow, J.H. (2007). A cysteine protease inhibitor cures Chagas' disease in an immunodeficient-mouse model of infection. *Antimicrobial Agents and Chemotherapy 51*, 3932-3939.

Ekanayake, D.K., Minning, T., Weatherly, B., Gunasekera, K., Nilsson, D., Tarleton, R., Ochsenreiter, T. and Sabatini, R. (2011). Epigenetic regulation of transcription and virulence in *Trypanosoma cruzi* by O-linked thymine glucosylation of DNA. *Molecular and Cellular Biology 31*, 1690-1700.

El Fadili, K., Messier, N., Leprohon, P., Roy, G., Guimond, C., Trudel, N., Saravia, N.G., Pavadopoulou, B., Legare, D. and Ouellette, M. (2005). Role of the ABC transporter MRPA (PGPA) in antimony resistance in *Leishmania infantum* axenic and intracellular amastigotes. *Antimicrobial Agents and Chemotherapy 49*, 1988-1993.

El-Sayed, N.M., Myler, P.J., Bartholomeu, D.C., Nilsson, D., Aggarwal, G., Tran, A.N., Ghedin, E., Worthey, E.A., Delcher, A.L., Blandin, G., Westenberger, S.J., Caler, E., Cerqueira, G.C., Branche, C., Haas, B., Anupama, A., Arner, E., Aslund, L., Attipoe, P., Bontempi, E., Bringaud, F., Burton, P., Cadag, E., Campbell, D.A., Carrington, M., Crabtree, J., Darban, H., da Silveira, J.F., de Jong, P., Edwards, K., Englund, P.T., Fazelina, G., Feldblyum, T., Ferella, M., Frasch, A.C., Gull, K., Horn, D., Hou, L.H., Huang, Y.T., Kindlund, E., Ktingbeil, M., Kluge, S., Koo, H., Lacerda, D., Levin, M.J., Lorenzi, H., Louie, T., Machado, C.R., McCulloch, R., McKenna, A., Mizuno, Y., Mottram, J.C., Nelson, S., Ochaya, S., Osoegawa, K., Pai, G., Parsons, M., Pentony, M., Pettersson, U., Pop, M., Ramirez, J.L., Rinta, J., Robertson, L., Salzberg, S.L., Sanchez, D.O., Seyler, A., Sharma, R., Shetty, J., Simpson, A.J., Sisk, E., Tammi, M.T., Tarteton, R., Teixeira, S., Van Aken, S., Vogt, C., Ward, P.N., Wickstead, B., Wortman, J., White, O., Fraser, C.M., Stuart, K.D. and Andersson, B. (2005). The genome sequence of *Trypanosoma cruzi*, etiologic agent of Chagas disease. *Science 309*, 409-415.

Engel, J.C., Doyle, P.S., Hsieh, I. and McKerrow, J.H. (1998a). Cysteine protease inhibitors cure an experimental *Trypanosoma cruzi* infection. *Journal of Experimental Medicine 188*, 725-734.

Engel, J.C., Doyle, P.S., Palmer, J., Hsieh, I., Bainton, D.F. and McKerrow, J.H. (1998b). Cysteine protease inhibitors alter Golgi complex ultrastructure and function in *Trypanosoma cruzi*. *Journal of Cell Science 111*, 597-606.

Engstler, M., Thilo, L., Weise, F., Grunfelder, C.G., Schwarz, H., Boshart, M. and Overath, P. (2004). Kinetics of endocytosis and recycling of the GPI-anchored variant surface glycoprotein in *Trypanosoma brucei*. *Journal of Cell Science 117*, 1105-1115.

Ennis, H.L. and Lubin, M. (1964). Cycloheximide: aspects of inhibition of protein synthesis in mammalian cells. *Science 146*, 1474-1476.

Farazi, T.A., Waksman, G. and Gordon, J.I. (2001). Structures of *Saccharomyces cerevisiae N*-myristoyltransferase with bound myristoylCoA and peptide provide insights about substrate recognition and catalysis. *Biochemistry 40*, 6335-6343.

Fearon, M.A., Scalia, V., Huang, M., Dines, I., Ndao, M. and Lagace-Wiens, P. (2013). A case of vertical transmission of Chagas disease contracted via blood transfusion in Canada. *Can. J. Infect. Dis. Med. Microbiol. 24*, 32-34.

Feasey, N., Wansbrough-Jones, M., Mabey, D.C. and Solomon, A.W. (2010). Neglected tropical diseases. *British Medical Bulletin 93*, 179-200.

Fernandes, M.C., Flannery, A.R., Andrews, N. and Mortara, R.A. (2013). Extracellular amastigotes of *Trypanosoma cruzi* are potent inducers of phagocytosis in mammalian cells. *Cellular Microbiology 15*, 977-991.

Ferreira, A.V., Segatto, M., Menezes, Z., Macedo, A.M., Gelape, C., de Oliveira, A.L., Nagajyothi, F., Scherer, P.E., Teixeira, M.M. and Tanowitz, H.B. (2011). Evidence for *Trypanosoma cruzi* in adipose tissue in human chronic Chagas disease. *Microbes and Infection 13*, 1002-1005.

Figueiredo, R.C., Rosa, D.S. and Soares, M.J. (2000). Differentiation of *Trypanosoma cruzi* epimastigotes: metacyclogenesis and adhesion to substrate are triggered by nutritional stress. *Journal of Parasitology 86*, 1213-1218.

Filardi, L.S. and Brener, Z. (1987). Susceptibility and natural resistance of *Trypanosoma cruzi* strains to drugs used clinically in Chagas disease. *Transactions of the Royal Society of Tropical Medicine and Hygiene 81*, 755-759.

Finn, R.D., Bateman, A., Clements, J., Coggill, P., Eberhardt, R.Y., Eddy, S.R., Heger, A., Hetherington, K., Holm, L., Mistry, J., Sonnhammer, E.L., Tate, J. and Punta, M. (2014). Pfam: the protein families database. *Nucleic Acids Research 42*, D222-D230.

Flanagan, C.A., Schnieders, E.A., Emerick, A.W., Kunisawa, R., Admon, A. and Thorner, J. (1993). Phosphatidylinositol 4-kinase: gene structure and requirement for yeast cell viability. *Science 262*, 1444-1448.

Flick, J.S. and Thorner, J. (1993). Genetic and biochemical characterization of a phosphatidylinositol-specific phospholipase C in *Saccharomyces cerevisiae*. *Molecular and Cellular Biology 13*, 5861-5876.

Frank, F.M., Ciccarelli, A.B., Bollini, M., Bruno, A.M., Batlle, A. and Lombardo, M.E. (2013). Trypanocidal activity of thioamide-substituted imidazoquinolinone: electrochemical properties and biological effects. *Evid. Based. Complement Alternat. Med. 2013*, 945953.

Frearson, J.A., Brand, S., McElroy, S.P., Cleghorn, L.A.T., Smid, O., Stojanovski, L., Price, H.P., Guther, M.L.S., Torrie, L.S., Robinson, D.A., Hallyburton, I., Mpamhanga, C.P., Brannigan, J.A., Wilkinson, A.J., Hodgkinson, M., Hui, R., Qiu, W., Raimi, O.G., van Aalten, D.M.F., Brenk, R.,

Gilbert, I.H., Read, K.D., Fairlamb, A.H., Ferguson, M.A.J., Smith, D.F. and Wyatt, P.G. (2010). *N*-myristoyltransferase inhibitors as new leads to treat sleeping sickness. *Nature 464*, 728-732.

Frearson, J.A., Wyatt, P.A., Gilbert, I.H. and Fairlamb, A.H. (2007). Target assessment for antiparasitic drug discovery. *Trends in Parasitology 23*, 589-595.

Galbiati, F., Volonte, D., Meani, D., Milligan, G., Lublin, D.M., Lisanti, M.P. and Parenti, M. (1999). The dually acylated NH2-terminal domain of gi1alpha is sufficient to target a green fluorescent protein reporter to caveolin-enriched plasma membrane domains. Palmitoylation of caveolin-1 is required for the recognition of dually acylated g-protein alpha subunits in vivo. *Journal of Biological Chemistry 274*, 5843-5850.

Garcia, S., Ramos, C.O., Senra, J.F., Vilas-Boas, F., Rodrigues, M.M., Campos-de-Carvalho, A.C., Ribeiro-Dos-Santos, R. and Soares, M.B. (2005). Treatment with benznidazole during the chronic phase of experimental Chagas' disease decreases cardiac alterations. *Antimicrobial Agents and Chemotherapy 49*, 1521-1528.

Garcia-Bustos, J.F., Marini, F., Stevenson, I., Frei, C. and Hall, M.N. (1994). PIK1, an essential phosphatidylinositol 4-kinase associated with the yeast nucleus. *EMBO Journal 13*, 2352-2361.

Gascon, J., Bern, C. and Pinazo, M.J. (2010). Chagas disease in Spain, the United States and other non-endemic countries. *Acta Tropica 115*, 22-27.

Gaunt, M.W., Yeo, M., Frame, I.A., Stothard, J.R., Carrasco, H.J., Taylor, M.C., Mena, S.S., Veazey, P., Miles, G.A.J., Acosta, N., de Arias, A.R. and Miles, M.A. (2003). Mechanism of genetic exchange in American trypanosomes. *Nature 421*, 936-939.

Girones, N. and Fresno, M. (2003). Etiology of Chagas disease myocarditis: autoimmunity, parasite persistence, or both? *Trends in Parasitology 19*, 19-22.

Glover, C.J. and Felsted, R.L. (1995). Identification and characterization of multiple forms of bovine brain *N*-myristoyltransferase. *Journal of Biological Chemistry 270*, 23226-23233.

Goad, L.J., Berens, R.L., Marr, J.J., Beach, D.H. and Holz, G.G.Jr. (1989). The activity of ketoconazole and other azoles against *Trypanosoma cruzi*: biochemistry and chemotherapeutic action in vitro. *Molecular and Biochemical Parasitology 32*, 179-189.

Godsel, L.M. and Engman, D.M. (1999). Flagellar protein localization mediated by a calcium-myristoyl/palmitoyl switch mechanism. *EMBO Journal 18*, 2057-2065.

Goncalves, V., Brannigan, J.A., Thinon, E., Olaleye, T.O., Serwa, R., Lanzarone, S., Wilkinson, A.J., Tate, E.W. and Leatherbarrow, R.J. (2012a). A fluorescence-based assay for *N*-myristoyltransferase activity. *Analytical Biochemistry 421*, 342-344.

Goncalves, V., Brannigan, J.A., Whalley, D., Ansell, K.H., Saxty, B., Holder, A.A., Wilkinson, A.J., Tate, E.W. and Leatherbarrow, R.J. (2012b). Discovery of *Plasmodium vivax N*-myristoyltransferase inhibitors: screening, synthesis, and structural characterization of their binding mode. *Journal of Medicinal Chemistry 55*, 3578-3582.

Gourbal, B., Sonuc, N., Bhattacharjee, H., Legare, D., Sundar, S., Ouellette, M., Rosen, B.P. and Mukhopadhyay, R. (2004). Drug uptake and modulation of drug resistance in *Leishmania* by an aquaglyceroporin. *Journal of Biological Chemistry 279*, 31010-31017.

Greig, N., Wyllie, S., Patterson, S. and Fairlamb, A.H. (2009). A comparative study of methylglyoxal metabolism in trypanosomatids. *FEBS Journal 276*, 376-386.

Guhl, F. (2007). Chagas disease in Andean countries. *Memorias do Instituto Oswaldo Cruz 102 Suppl 1*, 29-38.

Gupta, S. and Garg, N.J. (2013). TcVac3 induced control of *Trypanosoma cruzi* infection and chronic myocarditis in mice. *Plos One 8*, e59434.

Guther, M.L., Urbaniak, M.D., Tavendale, A., Prescott, A. and Ferguson, M.A. (2014). High-confidence glycosome proteome for procyclic form *Trypanosoma brucei* by epitope-tag organelle enrichment and SILAC proteomics. *Journal of Proteome Research 13*, 2796-2806.

Gutierrez, F.R., Guedes, P.M., Gazzinelli, R.T. and Silva, J.S. (2009). The role of parasite persistence in pathogenesis of Chagas heart disease. *Parasite Immunol. 31*, 673-685.

Hang, H.C., Geutjes, E.J., Grotenbreg, G., Pollington, A.M., Bijlmakers, M.J. and Ploegh, H.L. (2007). Chemical probes for the rapid detection of fatty-acylated proteins in mammalian cells. *Journal of the American Chemical Society 129*, 2744-2745.

Hasslocher-Moreno, A.M., do Brasil, P.E., de Sousa, A.S., Xavier, S.S., Chambela, M.C. and Sperandio da Silva, G.M. (2012). Safety of benznidazole use in the treatment of chronic Chagas' disease. *Journal of Antimicrobial Chemotherapy 67*, 1261-1266.

Hemmige, V., Tanowitz, H. and Sethi, A. (2012). *Trypanosoma cruzi* infection: a review with emphasis on cutaneous manifestations. *Int. J. Dermatol. 51*, 501-508.

Hendricks, K.B., Wang, B.Q., Schnieders, E.A. and Thorner, J. (1999). Yeast homologue of neuronal frequenin is a regulator of phosphatidylinositol-4-OH kinase. *Nature Cell Biology 1*, 234-241.

Herriott, R.M. (1935). Acetylation of tyrosiine in pepsin. *J. Gen. Physiol 19*, 283-299.

Hertz-Fowler, C., Ersfeld, K. and Gull, K. (2001a). CAP5.5, a life-cycle-regulated, cytoskeleton-associated protein is a member of a novel family of calpain-related proteins in *Trypanosoma brucei*. *Molecular and Biochemical Parasitology 116*, 25-34.

Hertz-Fowler, C., Ersfeld, K. and Gull, K. (2001b). CAP5.5, a life-cycle-regulated, cytoskeleton-associated protein is a member of a novel family of calpain-related proteins in Trypanosoma brucei (vol 116, pg 25, 2001). *Molecular and Biochemical Parasitology 117*, 119.

Heuckeroth, R.O., Glaser, L. and Gordon, J.I. (1988). Heteroatom-substituted fatty acid analogs as substrates for *N*-myristoyltransferase: an approach for studying both the enzymology and function of protein acylation. *Proceedings of the National Academy of Sciences of the United States of America 85*, 8795-8799.

Heuckeroth, R.O., Jackson-Machelski, E., Adams, S.P., Kishore, N.S., Huhn, M., Katoh, A., Lu, T., Gokel, G.W. and Gordon, J.I. (1990). Novel fatty acyl substrates for myristoyl-CoA:protein *N*-myristoyl-transferase. *Journal of Lipid Research 31*, 1121-1129.

Hofflin, J.M., Sadler, R.H., Araujo, F.G., Page, W.E. and Remington, J.S. (1987). Laboratory acquired Chagas disease. *Transactions of the Royal Society of Tropical Medicine and Hygiene 81*, 437-440.

Hoft, D.F., Farrar, P.L., Kratz-Owens, K. and Shaffer, D. (1996). Gastric invasion by *Trypanosoma cruzi* and induction of protective mucosal immune responses. *Infection and Immunity 64*, 3800-3810.

Hoogenboom, R. (2010). Thiol-yne chemistry: a powerful tool for creating highly functional materials. *Angew. Chem. Int. Ed Engl. 49*, 3415-3417.

Howard, E.J., Xiong, X., Carlier, Y., Sosa-Estani, S. and Buekens, P. (2014). Frequency of the congenital transmission of *Trypanosoma cruzi*: a systematic review and meta-analysis. *BJOG. 121*, 22-33.

Hunter, K.J., Le Quesne, S.A. and Fairlamb, A.H. (1994). Identification and biosynthesis of N^1,N^9-*bis*(glutathionyl)aminopropylcadaverine (homotrypanothione) in *Trypanosoma cruzi*. *European Journal of Biochemistry 226*, 1019-1027.

Huprikar, S., Bosserman, E., Patel, G., Moore, A., Pinney, S., Anyanwu, A., Neofytos, D., Ketterer, D., Striker, R., Silveira, F., Qvarnstrom, Y., Steurer, F., Herwaldt, B. and Montgomery, S. (2013). Donor-derived *Trypanosoma cruzi* infection in solid organ recipients in the United States, 2001-2011. *Am. J. Transplant. 13*, 2418-2425.

Irigoin, F., Inada, N.M., Fernandes, M.P., Piacenza, L., Gadelha, F.R., Vercesi, A.E. and Radi, R. (2009). Mitochondrial calcium overload triggers complement-dependent superoxide-mediated programmed cell death in *Trypanosoma cruzi*. *Biochemical Journal 418*, 595-604.

Islam, N.N., Igarashi, K., Tachibana, T., Ooshima, H. and Azuma, M. (2008). Synthesis and degradation of acyl peptide using enzyme from *Pseudomonas aeruginosa*. *J. Biosci. Bioeng. 105*, 282-287.

Iwaki, T., Iefuji, H., Hiraga, Y., Hosomi, A., Morita, T., Giga-Hama, Y. and Takegawa, K. (2008). Multiple functions of ergosterol in the fission yeast *Schizosaccharomyces pombe*. *Microbiology 154*, 830-841.

Jackson, Y., Alirol, E., Getaz, L., Wolff, H., Combescure, C. and Chappuis, F. (2010). Tolerance and safety of nifurtimox in patients with chronic Chagas disease. *Clinical Infectious Diseases 51*, e69-e75.

Jimenez, V., Paredes, R., Sosa, M.A. and Galanti, N. (2008). Natural programmed cell death in *T. cruzi* epimastigotes maintained in axenic cultures. *J. Cell Biochem. 105*, 688-698.

Jyomoto, T., Azuma, M., Islam, N.N., Fujinami, R., Takao, T., Ogawa, T., Tabuchi, M., Igarashi, K., Kato, J. and Ooshima, H. (2006). Purification and characterization of enzyme responsible for *N*-myristoylation of octapeptide in aqueous solution without ATP and coenzyme a from *Pseudomonas aeruginosa*. *J. Biosci. Bioeng. 102*, 193-197.

Kelly, J.M., Ward, H.M., Miles, M.A. and Kendall, G. (1992). A shuttle vector which facilitates the expression of transfected genes in *Trypanosoma cruzi* and *Leishmania*. *Nucleic Acids Research 20*, 3963-3969.

Kinoshita-Yanaga, A.T., Toledo, M.J., Araujo, S.M., Vier, B.P. and Gomes, M.L. (2009). Accidental infection by *Trypanosoma cruzi* follow-up by the polymerase chain reaction: case report. *Rev. Inst. Med. Trop. Sao Paulo 51*, 295-298.

Kishore, N.S., Wood, D.C., Mehta, P.P., Wade, A.C., Lu, T., Gokel, G.W. and Gordon, J.I. (1993). Comparison of the acyl chain specificities of human myristoyl-CoA synthetase and human myristoyl-CoA:protein *N*-myristoyltransferase. *Journal of Biological Chemistry 268*, 4889-4902.

Koder, R.L., Haynes, C.A., Rodgers, M.E., Rodgers, D.W. and Miller, A.F. (2002). Flavin thermodynamics explain the oxygen insensitivity of enteric nitroreductases. *Biochemistry 41*, 14197-14205.

Kolev, N.G., Franklin, J.B., Carmi, S., Shi, H., Michaeli, S. and Tschudi, C. (2010). The transcriptome of the human pathogen *Trypanosoma brucei* at single-nucleotide resolution. *PLoS Pathogens 6*, e1001090.

Kooij, T.W., Janse, C.J. and Waters, A.P. (2006). *Plasmodium* post-genomics: better the bug you know? *Nature Reviews Microbiology 4*, 344-357.

Lane, J.E., Ribeiro-Rodrigues, R., Suarez, C.C., Bogitsh, B.J., Jones, M.M., Singh, P.K. and Carter, C.E. (1996). In vitro trypanocidal activity of tetraethylthiuram disulfide and sodium diethylamine-N-carbodithioate on *Trypanosoma cruzi*. *American Journal of Tropical Medicine and Hygiene 55*, 263-266.

Le Roch, K.G., Johnson, J.R., Florens, L., Zhou, Y., Santrosyan, A., Grainger, M., Yan, S.F., Williamson, K.C., Holder, A.A., Carucci, D.J., Yates, J.R., III and Winzeler, E.A. (2004). Global analysis of transcript and protein levels across the *Plasmodium falciparum* life cycle. *Genome Research 14*, 2308-2318.

Lee, B.Y., Bacon, K.M., Bottazzi, M.E. and Hotez, P.J. (2013). Global economic burden of Chagas disease: a computational simulation model. *Lancet Infectious Diseases 13*, 342-348.

Lee, S.C. and Shaw, B.D. (2008). Localization and function of ADP ribosylation factor A in Aspergillus nidulans. *FEMS Microbiology Letters 283*, 216-222.

Ley, V., Andrews, N.W., Robbins, E.S. and Nussenzweig, V. (1988). Amastigotes of *Trypanosoma cruzi* sustain an infective cycle in mammalian cells. *Journal of Experimental Medicine 168*, 649-659.

Li, Z., Zou, C.B., Yao, Y., Hoyt, M.A., McDonough, S., Mackey, Z.B., Coffino, P. and Wang, C.C. (2002). An easily dissociated 26 S proteasome catalyzes an essential ubiquitin-mediated protein degradation pathway in *Trypanosoma brucei*. *Journal of Biological Chemistry 277*, 15486-15498.

Lodge, J.K., Jackson-Machelski, E., Toffaletti, D.L., Perfect, J.R. and Gordon, J.I. (1994). Targeted gene replacement demonstrates that myristoyl-CoA: protein *N*-myristoyltransferase is essential for viability of *Cryptococcus neoformans*. *Proceedings of the National Academy of Sciences of the United States of America 91*, 12008-12012.

Lorente, S.O., Gomez, R., Jimenez, C., Cammerer, S., Yardley, V., de Luca-Fradley, K., Croft, S.L., Perez, L.M.R., Urbina, J., Pacanowska, D.G. and Gilbert, I.H. (2005). Biphenylquinuclidines as inhibitors of squalene synthase and growth of parasitic protozoa. *Bioorganic and Medicinal Chemistry 13*, 3519-3529.

Lowe, A.B. (2014). Thiol-ene "click" reactions and recent applications in polymer and materials synthesis: a first update. *Polymer Chemistry 5*, 4820-4870.

Lu, S.X. and Hrabak, E.M. (2013). The myristoylated amino-terminus of an *Arabidopsis* calcium-dependent protein kinase mediates plasma membrane localization. *Plant Molecular Biology 82*, 267-278.

Luber, C.A., Cox, J., Lauterbach, H., Fancke, B., Selbach, M., Tschopp, J., Akira, S., Wiegand, M., Hochrein, H., O'Keeffe, M. and Mann, M. (2010). Quantitative proteomics reveals subset-specific viral recognition in dendritic cells. *Immunity. 32*, 279-289.

Ma, Y.F., Weiss, L.M. and Huang, H. (2012). A method for rapid regulation of protein expression in *Trypanosoma cruzi*. *International Journal for Parasitology 42*, 33-37.

Magee, A.I. and Courtneidge, S.A. (1985). Two classes of fatty acid acylated proteins exist in eukaryotic cells. *EMBO Journal 4*, 1137-1144.

Magee, A.I., Koyama, A.H., Malfer, C., Wen, D. and Schlesinger, M.J. (1984). Release of fatty acids from virus glycoproteins by hydroxylamine. *Biochimica et Biophysica Acta 798*, 156-166.

Maharjan, M., Singh, S., Chatterjee, M. and Madhubala, R. (2008). Role of aquaglyceroporin (AQP1) gene and drug uptake in antimony-resistant clinical isolates of *Leishmania donovani*. *American Journal of Tropical Medicine and Hygiene 79*, 69-75.

Manenti, S., Sorokine, O., Van, D.A. and Taniguchi, H. (1995). Demyristoylation of myristoylated alanine-rich C kinase substrate. *Biochemical Society Transactions 23*, 561-564.

Manning-Cela, R., Cortes, A., Gonzalez-Rey, E., Van Voorhis, W.C., Swindle, J. and Gonzalez, A. (2001). LYT1 protein is required for efficient in vitro infection by *Trypanosoma cruzi*. *Infection and Immunity 69*, 3916-3923.

Marcon, G.E., de Albuquerque, D.M., Batista, A.M., Andrade, P.D., Almeida, E.A., Guariento, M.E., Teixeira, M.A. and Costa, S.C. (2011). *Trypanosoma cruzi*: parasite persistence in tissues in chronic chagasic Brazilian patients. *Memorias do Instituto Oswaldo Cruz 106*, 85-91.

Maric, D., McGwire, B.S., Buchanan, K.T., Olson, C.L., Emmer, B.T., Epting, C.L. and Engman, D.M. (2011). Molecular determinants of ciliary membrane localization of *Trypanosoma cruzi* flagellar calcium-binding protein. *Journal of Biological Chemistry 286*, 33109-33117.

Marin-Neto, J.A., Rassi, A., Jr., Avezum, A., Jr., Mattos, A.C., Rassi, A., Morillo, C.A., Sosa-Estani, S. and Yusuf, S. (2009). The BENEFIT trial: testing the hypothesis that trypanocidal therapy is beneficial for patients with chronic Chagas heart disease. *Memorias do Instituto Oswaldo Cruz 104 Suppl 1*, 319-324.

Marques, A., Nakayasu, E. and Almeida, I. (2011). Purification of extracellular and intracellular amastigotes of *Trypanosoma cruzi* from mammalian host-infected cells. *Protocol Exchange dx.doi.org/10.1038/protex.2011.265*.

Martin, D.D., Ahpin, C.Y., Heit, R.J., Perinpanayagam, M.A., Yap, M.C., Veldhoen, R.A., Goping, I.S. and Berthiaume, L.G. (2012). Tandem reporter assay for myristoylated proteins post-translationally (TRAMPP) identifies novel substrates for post-translational myristoylation: PKCε, a case study. *FASEB Journal 26*, 13-28.

Martin, D.D., Vilas, G.L., Prescher, J.A., Rajaiah, G., Falck, J.R., Bertozzi, C.R. and Berthiaume, L.G. (2008). Rapid detection, discovery, and identification of post-translationally myristoylated proteins during apoptosis using a bio-orthogonal azidomyristate analog. *FASEB Journal 22*, 797-806.

Martin, D.L., Goodhew, B., Czaicki, N., Foster, K., Rajbhandary, S., Hunter, S. and Brubaker, S.A. (2014). *Trypanosoma cruzi* survival following cold storage: possible implications for tissue banking. *Plos One 9*, e95398.

Martinez-Calvillo, S., Lopez, I. and Hernandez, R. (1997). pRIBOTEX expression vector: a pTEX derivative for a rapid selection of *Trypanosoma cruzi* transfectants. *Gene 199*, 71-76.

Martins, V.D., Okura, M., Maric, D., Engman, D.M., Vieira, M., Docampo, R. and Moreno, S.N.J. (2010). Acylation-dependent export of *Trypanosoma cruzi* phosphoinositide-specific phospholipase C to the outer surface of amastigotes. *Journal of Biological Chemistry 285*, 30906-30917.

Mattoo, A.K., Callahan, F.E., Mehta, R.A. and Ohlrogge, J.B. (1989). Rapid in vivo acylation of acyl carrier protein with exogenous fatty Acids in *Spirodela oligorrhiza*. *Plant Physiol 89*, 707-711.

Maurer-Stroh, S. and Eisenhaber, F. (2004). Myristoylation of viral and bacterial proteins. *Trends in Microbiology 12*, 178-185.

Maya, J.D., Cassels, B.K., Iturriaga-Vasquez, P., Ferreira, J., Faundez, M., Galanti, N., Ferreira, A. and Morello, A. (2007). Mode of action of natural and synthetic drugs against *Trypanosoma cruzi a*nd their interaction with the mammalian host. *Comparative Biochemistry and Physiology A-Molecular & Integrative Physiology 146*, 601-620.

Mejia, A.M., Hall, B.S., Taylor, M.C., Gomez-Palacio, A., Wilkinson, S.R., Triana-Chavez, O. and Kelly, J.M. (2012). Benznidazole-resistance in *Trypanosoma cruzi* is a readily acquired trait that can arise independently in a single population. *Journal of Infectious Diseases 206*, 220-228.

Mejia-Jaramillo, A.M., Fernandez, G.J., Palacio, L. and Triana-Chavez, O. (2011). Gene expression study using real-time PCR identifies an NTR gene as a major marker of resistance to benznidazole in *Trypanosoma cruzi*. *Parasites & Vectors 4*.

Mills, E., Price, H.P., Johner, A., Emerson, J.E. and Smith, D.F. (2007). Kinetoplastid PPEF phosphatases: dual acylated proteins expressed in the endomembrane system of *Leishmania*. *Molecular and Biochemical Parasitology 152*, 22-34.

Minning, T.A., Bua, J., Garcia, G.A., McGraw, R.A. and Tarleton, R.L. (2003). Microarray profiling of gene expression during trypomastigote to amastigote transition in *Trypanosoma cruzi*. *Molecular and Biochemical Parasitology 131*, 55-64.

Minning, T.A., Weatherly, D.B., Atwood, J., III, Orlando, R. and Tarleton, R.L. (2009). The steady-state transcriptome of the four major life-cycle stages of *Trypanosoma cruzi*. *BMC Genomics 10*, 370.

Misumi, S., Tsuruta, M., Furuishi, K. and Shoji, S. (1995). Determination of *N*-myristoyl peptide sequence both by MALDI TOF MASS and with an *N*-myristoyl cleaving enzyme (polymyxin acylase). *Biochemical and Biophysical Research Communications 217*, 632-639.

Molina, I., Prat, J., Salvador, F., Trevino, B., Sulleiro, E., Serre, N., Pou, D., Roure, S., Cabezos, J., Valerio, L., Blanco-Grau, A., Sanchez-Montalva, A., Vidal, X. and Pahissa, A. (2014). Randomized trial of posaconazole and benznidazole for chronic Chagas' disease. *New England Journal of Medicine 370*, 1899-1908.

Molina-Berrios, A., Campos-Estrada, C., Lapier, M., Duaso, J., Kemmerling, U., Galanti, N., Leiva, M., Ferreira, J., Lopez-Munoz, R. and Maya, J.D. (2013). Benznidazole prevents endothelial damage in an experimental model of Chagas disease. *Acta Tropica 127*, 6-13.

Moncayo, A. (2003). Chagas disease: current epidemiological trends after the interruption of vectorial and transfusional transmission in the Southern Cone countries. *Memorias do Instituto Oswaldo Cruz 98*, 577-591.

Moreira, A.A.B., De Souza, H.B.W.T., Amato Neto, V., Matsubara, L., Pinto, P.L.S., Tolezano, J.E., Nunes, E.V. and Okumura, M. (1992). Evaluation of the therapeutic activity of itraconazole in human and experimental chronic infection by Trypanosoma cruzi AVALIACAO DA ATIVIDADE TERAPEUTICA DO ITRACONAZOL NAS INFECCOES CRONICAS, EXPERIMENTAL E HUMANA, PELO TRYPANOSOMA CRUZI. *Revista do Instituto de Medicina Tropical de Sao Paulo 34*, 177-180.

Moreira, D.S., Monte Neto, R.L., Andrade, J.M., Santi, A.M., Reis, P.G., Frezard, F. and Murta, S.M. (2013). Molecular characterization of the MRPA transporter and antimony uptake in four New World Leishmania *spp.* susceptible and resistant to antimony. *International journal for parasitology. Drugs and drug resistance 3*, 143-153.

Moretti, E., Basso, B., Castro, I., Carrizo, P.M., Chaul, M., Barbieri, G., Canal, F.D., Sartori, M.J. and Carrizo, P.R. (2005). Chagas' disease: study of congenital transmission in cases of acute maternal infection. *Revista da Sociedade Brasiliera de Medicina Tropical 38*, 53-55.

Moriya, K., Nagatoshi, K., Noriyasu, Y., Okamura, T., Takamitsu, E., Suzuki, T. and Utsumi, T. (2013). Protein *N*-myristoylation plays a critical role in the endoplasmic reticulum rorphological change induced by overexpression of protein lunapark, an integral membrane protein of the endoplasmic reticulum. *Plos One 8*.

Murta, S.M., Krieger, M.A., Montenegro, L.R., Campos, F.F., Probst, C.M., Avila, A.R., Muto, N.H., de Oliveira, R.C., Nunes, L.R., Nirde, P., Bruna-Romero, O., Goldenberg, S. and Romanha, A.J. (2006). Deletion of copies of the gene encoding old yellow enzyme (TcOYE), a NAD(P)H flavin oxidoreductase, associates with in vitro-induced benznidazole resistance in Trypanosoma cruzi. *Molecular and Biochemical Parasitology 146*, 151-162.

Navin, T.R., Roberto, R.R., Juranek, D.D., Limpakarnjanarat, K., Mortenson, E.W., Clover, J.R., Yescott, R.E., Taclindo, C., Steurer, F. and Allain, D. (1985). Human and sylvatic *Trypanosoma cruzi* infection in California. *Am. J. Public Health 75*, 366-369.

Ndao, M., Beaulieu, C., Black, W.C., Isabel, E., Vasquez-Camargo, F., Nath-Chowdhury, M., Masse, F., Mellon, C., Methot, N. and Nicoll-Griffith, D.A. (2014). Reversible cysteine protease inhibitors show promise for a chagas disease cure. *Antimicrobial Agents and Chemotherapy 58*, 1167-1178.

Neal, R.A. and van Bueren, J. (1988). Comparative study of drug susceptibility of five strains of *Trypanosoma cruzi in vivo* and *in vitro*. *Transactions of the Royal Society of Tropical Medicine and Hygiene 82*, 709-714.

Newhall, W.J. and Jones, R.B. (1983). Disulfide-linked oligomers of the major outer membrane protein of chlamydiae. *Journal of Bacteriology 154*, 998-1001.

Nilsson, D., Gunasekera, K., Mani, J., Osteras, M., Farinelli, L., Baerlocher, L., Roditi, I. and Ochsenreiter, T. (2010). Spliced leader trapping reveals widespread alternative splicing patterns in the highly dynamic transcriptome of *Trypanosoma brucei*. *PLoS Pathogens 6*, e1001037.

Nimchuk, Z., Marois, E., Kjemtrup, S., Leister, R.T., Katagiri, F. and Dangl, J.L. (2000). Eukaryotic fatty acylation drives plasma membrane targeting and enhances function of several type III effector proteins from *Pseudomonas syringae*. *Cell 101*, 353-363.

Nirmalan, N., Sims, P.F. and Hyde, J.E. (2004). Quantitative proteomics of the human malaria parasite *Plasmodium falciparum* and its application to studies of development and inhibition. *Molecular Microbiology 52*, 1187-1199.

Nohara, L.L., Lema, C., Bader, J.O., Aguilera, R.J. and Almeida, I.C. (2010). High-content imaging for automated determination of host-cell infection rate by the intracellular parasite *Trypanosoma cruzi. Parasitol. Int. 59*, 565-570.

Norris, K.A. (1998). Stable transfection of *Trypanosoma cruzi* epimastigotes with the trypomastigote-specific complement regulatory protein cDNA confers complement resistance. *Infection and Immunity 66*, 2460-2465.

Oakhill, J.S., Chen, Z.P., Scott, J.W., Steel, R., Castelli, L.A., Ling, N., Macaulay, S.L. and Kemp, B.E. (2010). β-Subunit myristoylation is the gatekeeper for initiating metabolic stress sensing by AMP-activated protein kinase (AMPK). *Proceedings of the National Academy of Sciences of the United States of America 107*, 19237-19241.

Okura, M., Fang, J., Salto, M.L., Singer, R.S., Docampo, R. and Moreno, S.N. (2005). A lipid-modified phosphoinositide-specific phospholipase C (*Tc*PI-PLC) is involved in differentiation of trypomastigotes to amastigotes of *Trypanosoma cruzi. Journal of Biological Chemistry 280*, 16235-16243.

Olego-Fernandez, S., Vaughan, S., Shaw, M.K., Gull, K. and Ginger, M.L. (2009). Cell morphogenesis of *Trypanosoma brucei* requires the paralogous, differentially expressed calpain-related proteins CAP5.5 and CAP5.5V. *Protist 160*, 576-590.

Ong, S.E., Blagoev, B., Kratchmarova, I., Kristensen, D.B., Steen, H., Pandey, A. and Mann, M. (2002). Stable isotope labeling by amino acids in cell culture, SILAC, as a simple and accurate approach to expression proteomics. *Mol. Cell Proteomics 1*, 376-386.

Panethymitaki, C., Bowyer, P.W., Price, H.P., Leatherbarrow, R.J., Brown, K.A. and Smith, D.F. (2006). Characterization and selective inhibition of myristoyl-CoA : protein *N*-myristoyltransferase from *Trypanosoma brucei* and *Leishmania major*. *Biochemical Journal 396*, 277-285.

Parada, H., Carrasco, H.A., Anez, N., Fuenmayor, C. and Inglessis, I. (1997). Cardiac involvement is a constant finding in acute Chagas' disease: a clinical, parasitological and histopathological study. *Int. J. Cardiol. 60*, 49-54.

Park, J.S., Steinbach, S.K., Desautels, M. and Hemmingsen, S.M. (2009). Essential role for *Schizosaccharomyces pombe* pik1 in septation. *Plos One 4*, e6179.

Payne, W.E. and Fitzgerald-Hayes, M. (1993). A mutation in PLC1, a candidate phosphoinositide-specific phospholipase C gene from *Saccharomyces cerevisiae*, causes aberrant mitotic chromosome segregation. *Molecular and Cellular Biology 13*, 4351-4364.

Perinpanayagam, M.A., Beauchamp, E., Martin, D.D., Sim, J.Y., Yap, M.C. and Berthiaume, L.G. (2013). Regulation of co- and post-translational myristoylation of proteins during apoptosis: interplay of *N*-myristoyltransferases and caspases. *FASEB Journal 27*, 811-821.

Piacenza, L., Irigoin, F., Alvarez, M.N., Peluffo, G., Taylor, M.C., Kelly, J.M., Wilkinson, S.R. and Radi, R. (2007). Mitochondrial superoxide radicals mediate programmed cell death in *Trypanosoma cruzi*: cytoprotective action of mitochondrial iron superoxide dismutase overexpression. *Biochemical Journal 403*, 323-334.

Pinazo, M.J., Espinosa, G., Gallego, M., Lopez-Chejade, P.L., Urbina, J.A. and Gascon, J. (2010). Successful treatment with posaconazole of a patient with chronic Chagas disease and systemic lupus erythematosus. *Am. J. Trop Med. Hyg. 82*, 583-587.

Pinazo, M.J., Lacima, G., Elizalde, J.I., Posada, E.J., Gimeno, F., Aldasoro, E., Valls, M.E. and Gascon, J. (2014). Characterization of digestive involvement in patients with chronic *T. cruzi* infection in Barcelona, Spain. *PLoS Neglected Tropical Diseases 8*, e3105.

Porto-Carreiro, I., Attias, M., Miranda, K., de, S.W. and Cunha-e-Silva. (2000). *Trypanosoma cruzi* epimastigote endocytic pathway: cargo enters the cytostome and passes through an early endosomal network before storage in reservosomes. *European Journal of Cell Biology 79*, 858-869.

Price, H.P., Guther, M.L., Ferguson, M.A. and Smith, D.F. (2010). Myristoyl-CoA:protein *N*-myristoyltransferase depletion in trypanosomes causes avirulence and endocytic defects. *Mol Biochem. Parasitol. 169*, 55-58.

Price, H.P., Menon, M.R., Panethymitaki, C., Goulding, D., McKean, P.G. and Smith, D.F. (2003). Myristoyl-CoA : protein *N*-myristoyltransferase, an essential enzyme and potential drug target in kinetoplastid parasites. *Journal of Biological Chemistry 278*, 7206-7214.

Price, H.P., Panethymitaki, C., Goulding, D. and Smith, D.F. (2005). Functional analysis of functional analysis of TbARL1, an *N*-myristoylated Golgi protein essential for viability in bloodstream trypanosomes. *Journal of Cell Science 118*, 831-841.

Price, H.P., Stark, M. and Smith, D.F. (2007a). *Trypanosoma brucei* ARF1 plays a central role in endocytosis and Golgi-lysosome trafficking. *Molecular Biology of the Cell 18*, 864-873.

Price, H.P., Starkb, M., Smith, B. and Smith, D.F. (2007b). TbARF1 influences lysosomal function but not endocytosis in procyclic stage *Trypanosoma brucei*. *Molecular and Biochemical Parasitology 155*, 123-127.

Pugh, E.L. and Kates, M. (1994). Acylation of proteins of the archaebacteria *Halobacterium cutirubrum* and *Methanobacterium thermoautotrophicum*. *Biochimica et Biophysica Acta 1196*, 38-44.

Quijano-Hernandez, I. and Dumonteil, E. (2011). Advances and challenges towards a vaccine against Chagas disease. *Human Vaccines 7*, 1184-1191.

Rampoldi, F., Sandhoff, R., Owen, R.W., Grone, H.J. and Porubsky, S. (2012). A new, robust, and nonradioactive approach for exploring *N*-myristoylation. *Journal of Lipid Research 53*, 2459-2468.

Rassi, A., Jr., Rassi, A. and Marin-Neto, J.A. (2010). Chagas disease. *Lancet 375*, 1388-1402.

Rassi, A., Rassi, A. and Marin-Neto, J.A. (2010). Chagas disease. *Lancet 375*, 1388-1402.

Robbins, S.M., Quintrell, N.A. and Bishop, J.M. (1995). Myristoylation and Differential Palmitoylation of the Hck Protein-Tyrosine Kinases Govern Their Attachment to Membranes and Association with Caveolae. *Molecular and Cellular Biology 15*, 3507-3515.

Roberts, A.J., Torrie, L.S., Wyllie, S. and Fairlamb, A.H. (2014). Biochemical and genetic characterisation of *Trypanosoma cruzi N*-myristoyltransferase. *Biochemical Journal 459*, 323-332.

Roca, C., Pinazo, M.J., Lopez-Chejade, P., Bayo, J., Posada, E., Lopez-Solana, J., Gallego, M., Portus, M., Gascon, J. and Chagas-Clot, R.G. (2011). Chagas Disease among the Latin American Adult Population Attending in a Primary Care Center in Barcelona, Spain. *PLoS Neglected Tropical Diseases 5*.

Rocque, W.J., McWherter, C.A., Wood, D.C. and Gordon, J.I. (1993). A comparative analysis of the kinetic mechanism and peptide substrate specificity of human and *Saccharomyces cerevisiae* myristoyl-CoA:protein *N*-myristoyltransferase. *Journal of Biological Chemistry 268*, 9964-9971.

Rohloff, P., Rodrigues, C.O. and Docampo, R. (2003). Regulatory volume decrease in *Trypanosoma cruzi* involves amino acid efflux and changes in intracellular calcium. *Molecular and Biochemical Parasitology 126*, 219-230.

Roldan, M.D., Perez-Reinado, E., Castillo, F. and Moreno-Vivian, C. (2008). Reduction of polynitroaromatic compounds: the bacterial nitroreductases. *FEMS Microbiology Reviews 32*, 474-500.

Rudnick, D.A., McWherter, C.A., Rocque, W.J., Lennon, P.J., Getman, D.P. and Gordon, J.I. (1991). Kinetic and structural evidence for a sequential ordered Bi Bi mechanism of catalysis by *Saccharomyces cerevisiae* myristoyl-CoA:protein *N*-myristoyltransferase. *Journal of Biological Chemistry 266*, 9732-9739.

Sahin, A., Espiau, B., Tetaud, E., Cuvillier, A., Lartigue, L., Ambit, A., Robinson, D.R. and Merlin, G. (2008). The *Leishmania* ARL-1 and Golgi Traffic. *Plos One 3*.

Sakurai, N. and Utsumi, T. (2006). Posttranslational *N*-myristoylation is required for the anti-apoptotic activity of human tGelsolin, the C-terminal caspase cleavage product of human gelsolin. *Journal of Biological Chemistry 281*, 14288-14295.

Sardana, D., Zhu, C., Zhang, M.L., Gudivada, R.C., Yang, L. and Jegga, A.G. (2011). Drug repositioning for orphan diseases. *Briefings in Bioinformatics 12*, 346-356.

Sartori, A.M., Lopes, M.H., Benvenuti, L.A., Caramelli, B., di, P.A., Nunes, E.V., Ramirez, L.P. and Shikanai-Yasuda, M.A. (1998). Reactivation of Chagas' disease in a human immunodeficiency virus-infected patient leading to severe heart disease with a late positive direct microscopic examination of the blood. *American Journal of Tropical Medicine and Hygiene 59*, 784-786.

Sartori, A.M., Neto, J.E., Nunes, E.V., Braz, L.M., Caiaffa-Filho, H.H., Oliveira, O.C., Jr., Neto, V.A. and Shikanai-Yasuda, M.A. (2002). *Trypanosoma cruzi* parasitemia in chronic Chagas disease: comparison between human immunodeficiency virus (HIV)-positive and HIV-negative patients. *Journal of Infectious Diseases 186*, 872-875.

Schlesinger, M.J., Magee, A.I. and Schmidt, M.F.G. (1980). Fatty acid acylation of proteins in cultured cells. *Journal of Biological Chemistry 255*, 21-24.

Schmunis, G.A. (2007). Epidemiology of Chagas disease in non-endemic countries: the role of international migration. *Memorias do Instituto Oswaldo Cruz 102 Suppl 1*, 75-85.

Schofield, C.J. and Dias, J.C. (1999). The Southern Cone Initiative against Chagas disease. *Advances in Parasitology 42*, 1-27.

Seaton, K.E. and Smith, C.D. (2008). *N*-Myristoyltransferase isozymes exhibit differential specificity for human immunodeficiency virus type 1 Gag and Nef. *Journal of General Virology 89*, 288-296.

Selvakumar, P. and Sharma, R.K. (2007). Role of calpain and caspase system in the regulation of N-myristoyltransferase in human colon cancer (Review). *International Journal of Molecular Medicine 19*, 823-827.

Shahi, S.K., Krauth-Siegel, R.L. and Clayton, C.E. (2002). Overexpression of the putative thiol conjugate transporter *Tb*MRPA causes melarsoprol resistance in *Trypanosoma brucei*. *Molecular Microbiology 43*, 1129-1138.

Shrivastav, A., Varma, S., Saxena, A., DeCoteau, J. and Sharma, R.K. (2007). *N*-myristoyltransferase: a potential novel diagnostic marker for colon cancer. *J. Transl. Med. 5*, 58.

Silveira, F.T., Viana Dias, M.G., Pereira Pardal, P., Oliveira Lobâo, A. and Britto Melo, G. (1979). Nono caso-autóctone de doença de Chagas registrado no estado do Pará, Brasil (Nota prévia). *Hiléia Médica 1*, 61-62.

Silverman, J.M., Chan, S.K., Robinson, D.P., Dwyer, D.M., Nandan, D., Foster, L.J. and Reiner, N.E. (2008). Proteomic analysis of the secretome of *Leishmania donovani*. *Genome Biology 9*, R35.

Sogabe, S., Masubuchi, M., Sakata, K., Fukami, T.A., Morikami, K., Shiratori, Y., Ebiike, H., Kawasaki, K., Aoki, Y., Shimma, N., D'Arcy, A., Winkler, F.K., Banner, D.W. and Ohtsuka, T. (2002). Crystal structures of *Candida albicans N*-myristoyltransferase with two distinct inhibitors. *Chemistry & Biology 9*, 1119-1128.

Stevens, J.R., Noyes, H.A., Schofield, C.J. and Gibson, W. (2001). The molecular evolution of Trypanosomatidae. *Advances in Parasitology, Vol 48 48*, 1-56.

Studier, F.W. (2005). Protein production by auto-induction in high-density shaking cultures. *Protein Expression and Purification 41*, 207-234.

Suzuki, T., Ito, M., Ezure, T., Shikata, M., Ando, E., Utsumi, T., Tsunasawa, S. and Nishimura, O. (2006). *N*-Terminal protein modifications in an insect cell-free protein synthesis system and their identification by mass spectrometry. *Proteomics 6*, 4486-4495.

Suzuki, T., Moriya, K., Nagatoshi, K., Ota, Y., Ezure, T., Ando, E., Tsunasawa, S. and Utsumi, T. (2010). Strategy for comprehensive identification of human *N*-myristoylated proteins using an insect cell-free protein synthesis system. *Proteomics 10*, 1780-1793.

Takamitsu, E., Fukunaga, K., Iio, Y., Moriya, K. and Utsumi, T. (2014). Cell-free identification of novel *N*-myristoylated proteins from complementary DNA resources using bioorthogonal myristic acid analogues. *Analytical Biochemistry* .

Tarleton, R.L. (2003). Chagas disease: a role for autoimmunity? *Trends in Parasitology 19*, 447-451.

Taylor, M.C. and Kelly, J.M. (2006). pTcINDEX: a stable tetracycline-regulated expression vector for *Trypanosoma cruzi*. *BMC Biotechnology 6*, 32.

Thao, S., Chen, C.S., Zhu, H. and Escalante-Semerena, J.C. (2010). $N\varepsilon$-lysine acetylation of a bacterial transcription factor inhibits Its DNA-binding activity. *Plos One 5*, e15123.

Toichi, K., Yamanaka, K. and Furukawa, Y. (2013). Disulfide scrambling describes the oligomer formation of superoxide dismutase (SOD1) proteins in the familial form of amyotrophic lateral sclerosis. *Journal of Biological Chemistry 288*, 4970-4980.

Tovar, J. and Fairlamb, A.H. (1996). Extrachromosomal, homologous expression of trypanothione reductase and its complementary mRNA in *Trypanosoma cruzi*. *Nucleic Acids Research 24*, 2942-2949.

Tovar, J., Wilkinson, S., Mottram, J.C. and Fairlamb, A.H. (1998). Evidence that trypanothione reductase is an essential enzyme in *Leishmania* by targeted replacement of the *tryA* gene locus. *Molecular Microbiology 29*, 653-660.

Towler, D.A., Adams, S.P., Eubanks, S.R., Towery, D.S., Jackson-Machelski, E., Glaser, L. and Gordon, J.I. (1987). Purification and characterization of yeast myristoyl CoA:protein *N*-myristoyltransferase. *Proceedings of the National Academy of Sciences of the United States of America 84*, 2708-2712.

Towler, D.A., Adams, S.P., Eubanks, S.R., Towery, D.S., Jackson-Machelski, E., Glaser, L. and Gordon, J.I. (1988). Myristoyl CoA:protein *N*-myristoyltransferase activities from rat liver and yeast possess overlapping yet distinct peptide substrate specificities. *Journal of Biological Chemistry 263*, 1784-1790.

Traverso, J.A., Giglione, C. and Meinnel, T. (2013). High-throughput profiling of *N*-myristoylation substrate specificity across species including pathogens. *Proteomics 13*, 25-36.

Trochine, A., Creek, D.J., Faral-Tello, P., Barrett, M.P. and Robello, C. (2014). Benznidazole biotransformation and multiple targets in *Trypanosoma cruzi* revealed by metabolomics. *PLoS Neglected Tropical Diseases 8*, e2844.

Tull, D., Naderer, T., Spurck, T., Mertens, H.D., Heng, J., McFadden, G.I., Gooley, P.R. and McConville, M.J. (2010). Membrane protein SMP-1 is required for normal flagellum function in *Leishmania*. *Journal of Cell Science 123*, 544-554.

Tull, D., Vince, J.E., Callaghan, J.M., Naderer, T., Spurck, T., McFadden, G.I., Currie, G., Ferguson, K., Bacic, A. and McConville, M.J. (2004). SMP-1, a member of a new family of small myristoylated proteins in kinetoplastid parasites, is targeted to the flagellum membrane in *Leishmania*. *Molecular Biology of the Cell 15*, 4775-4786.

Ullu, E., Tschudi, C. and Chakraborty, T. (2004). RNA interference in protozoan parasites. *Cellular Microbiology 6*, 509-519.

Urbaniak, M.D., Guther, M.L. and Ferguson, M.A. (2012). Comparative SILAC proteomic analysis of *Trypanosoma brucei* bloodstream and procyclic lifecycle stages. *Plos One 7*, e36619.

Urbaniak, M.D., Martin, D.M. and Ferguson, M.A. (2013). Global quantitative SILAC phosphoproteomics reveals differential phosphorylation is widespread between the procyclic and bloodstream form lifecycle stages of *Trypanosoma brucei*. *Journal of Proteome Research 12*, 2233-2244.

Urbina, J.A., Concepcion, J.L., Caldera, A., Payares, G., Sanoja, C., Otomo, T. and Hiyoshi, H. (2004). In vitro and in vivo activities of E5700 and ER-119884, two novel orally active squalene synthase inhibitors, against *Trypanosoma cruzi*. *Antimicrobial Agents and Chemotherapy 48*, 2379-2387.

Urbina, J.A., Concepcion, J.L., Rangel, S., Visbal, G. and Lira, R. (2002). Squalene synthase as a chemotherapeutic target in *Trypanosoma cruzi* and *Leishmania mexicana*. *Molecular and Biochemical Parasitology 125*, 35-45.

Urbina, J.A. and Docampo, R. (2003). Specific chemotherapy of Chagas disease: controversies and advances. *Trends in Parasitology 19*, 495-501.

Urbina, J.A., Payares, G., Contreras, L.M., Liendo, A., Sanoja, C., Molina, J., Piras, M., Piras, R., Perez, N., Wincker, P. and Loebenberg, D. (1998). Antiproliferative effects and mechanism of action of SCH 56592 against Trypanosoma (Schizotrypanum) cruzi: In vitro and in vivo studies. *Antimicrobial Agents and Chemotherapy 42*, 1771-1777.

Urbina, J.A., Payares, G., Sanoja, C., Lira, R. and Romanha, A.J. (2003). *In vitro* and *in vivo* activities of ravuconazole on *Trypanosoma cruzi,* the causative agent of Chagas disease. *Int. J. Antimicrob. Agents 21*, 27-38.

Vazquez, M.P. and Levin, M.J. (1999). Functional analysis of the intergenic regions of TcP2 β gene *loci* allowed the construction of an improved *Trypanosoma cruzi* expression vector. *Gene 239*, 217-225.

Vazquez-Chagoyan, J.C., Gupta, S. and Garg, N.J. (2011). Vaccine development against *Trypanosoma cruzi* and Chagas disease. *Advances in Parasitology 75*, 121-146.

Vespa, G.N., Cunha, F.Q. and Silva, J.S. (1994). Nitric oxide is involved in control of *Trypanosoma cruzi*-induced parasitemia and directly kills the parasite in vitro. *Infection and Immunity 62*, 5177-5182.

Vickerman, K. (1976). The diversity of Kinetoplastid flagellates. In *Biology of the Kinetoplastida*, W.H. Lumsden and D.A. Evans, eds. (New York: Academic Press), pp. 1-34.

Vilas, G.L., Corvi, M.M., Plummer, G.J., Seime, A.M., Lambkin, G.R. and Berthiaume, L.G. (2006). Posttranslational myristoylation of caspase-activated p21-activated protein kinase 2 (PAK2) potentiates late apoptotic events. *Proceedings of the National Academy of Sciences of the United States of America 103*, 6542-6547.

Weinburg, R.A., McWherter, C.A., Freeman, K.S., Wood, D.C., Gordon, J.I. and Lee, S.C. (1995). Genetic studies reveal that myristoylCoA-protein *N*-myristoyltransferase is an essential enzyme in *Candida albicans*. *Molecular Microbiology 16*, 241-250.

Westenberger, S.J., Cerqueira, G.C., El-Sayed, N.M., Zingales, B., Campbell, D.A. and Sturm, N.R. (2006). *Trypanosoma cruzi* mitochondrial maxicircles display species- and strain-specific variation and a conserved element in the non-coding region. *BMC Genomics 7*, 60.

WHO Expert Committee. (1998). Control and surveillance of African trypanosomiasis. *World Health Organization Technical Report Series 881*, 1-113.

WHO Expert Committee. (2002). Control of Chagas disease. *World Health Organ Tech. Rep. Ser. 905*, 1-109.

Wilkinson, S.R., Taylor, M.C., Horn, D., Kelly, J.M. and Cheeseman, I. (2008). A mechanism for cross-resistance to nifurtimox and benznidazole in trypanosomes. *Proceedings of the National Academy of Sciences of the United States of America 105*, 5022-5027.

Wilkowsky, S.E., Barbieri, M.A., Stahl, P. and Isola, E.L. (2001). *Trypanosoma cruzi*: phosphatidylinositol 3-kinase and protein kinase B activation is associated with parasite invasion. *Experimental Cell Research 264*, 211-218.

Wingard, J.N., Ladner, J., Vanarotti, M., Fisher, A.J., Robinson, H., Buchanan, K.T., Engman, D.M. and Ames, J.B. (2008). Structural insights into membrane targeting by the flagellar calcium-binding protein (FCaBP), a myristoylated and palmitoylated calcium sensor in *Trypanosoma cruzi*. *Journal of Biological Chemistry 283*, 23388-23396.

World Health Organization. (1998). Chagas disease - Interruption of transmission, Uruguay. *Weekly Epidemiological Record 73*, 1-3.

World Health Organization. (2000a). Chagas disease, Brazil - Interruption of transmission. *Weekly Epidemiological Record 75*, 153-155.

World Health Organization. (2000b). Chagas disease, Chile - Certification of interruption of transmission. *Weekly Epidemiological Record 75*, 10-11.

World Health Organization. (2006). Human African trypanosomiasis (sleeping sickness): epidemiological update. *Weekly Epidemiological Record 81*, 71-80.

World Health Organization. (2012). Chagas disease (American trypanosomiasis) - fact sheet (revised in August 2012). *Weekly Epidemiological Record 87*, 519-522.

Wright, M.H., Clough, B., Rackham, M.D., Rangachari, K., Brannigan, J.A., Grainger, M., Moss, D.K., Bottrill, A.R., Heal, W.P., Broncel, M., Serwa, R.A., Brady, D., Mann, D.J., Leatherbarrow, R.J., Tewari, R., Wilkinson, A.J., Holder, A.A. and Tate, E.W. (2014). Validation of *N*-myristoyltransferase as an antimalarial drug target using an integrated chemical biology approach. *Nature Chemistry 6*, 112-121.

Wyllie, S., Patterson, S. and Fairlamb, A.H. (2013). Assessing the essentiality of *Leishmania donovani* nitroreductase and its role in nitro drug activation. *Antimicrobial Agents and Chemotherapy 57*, 901-906.

Wyllie, S., Patterson, S., Stojanovski, L., Simeons, F.R., Norval, S., Kime, R., Read, K.D. and Fairlamb, A.H. (2012). The anti-trypanosome drug fexinidazole shows potential for treating visceral leishmaniasis. *Sci. Transl. Med 4*, 119re1.

Xu, D., Brandan, C.P., Basombrio, M.A. and Tarleton, R.L. (2009). Evaluation of high efficiency gene knockout strategies for *Trypanosoma cruzi*. *BMC Microbiology 9*.

Yamey, G. (2002). The world's most neglected diseases - Ignored by the pharmaceutical industry and by public-private partnerships. *British Medical Journal 325*, 176-177.

Yang, S.H., Shrivastav, A., Kisinski, C., Sharma, R.K., Chen, M.H., Berthiaume, L.G., Peters, L.L., Chuang, P.T., Young, S.G. and Bergo, M.O. (2005). *N*-myristoyltransferase 1 is essential in early mouse development. *Journal of Biological Chemistry 280*, 18990-18995.

Yates, J.R., Ruse, C.I. and Nakorchevsky, A. (2009). Proteomics by mass spectrometry: approaches, advances, and applications. *Annu. Rev. Biomed. Eng 11*, 49-79.

Yoko-o T, Matsui, Y., Yagisawa, H., Nojima, H., Uno, I. and Toh-e A. (1993). The putative phosphoinositide-specific phospholipase C gene, PLC1, of the yeast *Saccharomyces cerevisiae* is important for cell growth. *Proc. Natl. Acad. Sci. U. S. A 90*, 1804-1808.

Young, C., Losikoff, P., Chawla, A., Glasser, L. and Forman, E. (2007). Transfusion-acquired *Trypanosoma cruzi* infection. *Transfusion 47*, 540-544.

Zha, J., Weiler, S., Oh, K.J., Wei, M.C. and Korsmeyer, S.J. (2000). Posttranslational *N*-myristoylation of BID as a molecular switch for targeting mitochondria and apoptosis. *Science 290*, 1761-1765.

Zhang, Y.Q., Gamarra, S., Garcia-Effron, G., Park, S., Perlin, D.S. and Rao, R. (2010). Requirement for ergosterol in V-ATPase function underlies antifungal activity of azole drugs. *PLoS Pathogens 6*, e1000939.

Zhao, C. and Ma, S. (2014). Recent advances in the discovery of *N*-myristoyltransferase inhibitors. *ChemMedChem, in press*.

Zingales, B., Andrade, S.G., Briones, M.R.S., Campbell, D.A., Chiari, E., Fernandes, O., Guhl, F., Lages-Silva, E., Macedo, A.M., Machado, C.R., Miles, M.A., Romanha, A.J., Sturm, N.R., Tibayrenc, M. and Schijman, A.G. (2009). A new consensus for *Trypanosoma cruzi* intraspecific nomenclature: second revision meeting recommends TcI to TcVI. *Memorias do Instituto Oswaldo Cruz 104*, 1051-1054.

Supplementary tables

Table S1 Table of peptides identified from polymyxin acylase treatment. Proteins highlighted in green are also consistently enriched.

Leading razor protein	First amino acid	PEP	SILAC exp
K4E0X7	D	0.041281	2
Q4CU61	E	1.43E-32	2
Q4DM59	G	0.057287	2
K4E583	G	0.000659	2
Q4DA14	G	0.030335	2
Q4DTH5	R	0.058326	2
Q4DHT7	A	0.037163	1
Q4CVR9	D	2.27E-35	1
P60712	D	5.02E-99	1
K4DVI8	G	1.73E-08	1
K4DPM9	G	0.00761	1
Q4DM75	M	1.15E-44	1
Q4D7R3	Q	0.058931	1
K4DT87	R	1.21E-11	1
Q4E469	T	0.006293	1

Table S2 N-myristoylated peptides identified from whole lysates

Accession	Sequence	PEP	Modification
K4E527	GEEFFVR	0.018545	*N*-azidomyristoylated
Q4DKH5	GVDDTMSSANMDDVWRTAR	0.049755	*N*-azidomyristoylated
Q4CW64	GCGASSKPSTVEYK	0.026783	*N*-myristoylated
K4E5P0	GGIISTIMDMR	0.03173	*N*-myristoylated
Q4CQA8	GSQAESEMHR	0.057294	*N*-myristoylated

Table S 3 Pfam searches of consistently enriched proteins identified from the *N*-myristoylome. Only significant A family matches were included

Accession	Protein ID	Pfam family	E value
Q4D7Y8	ADP-ribosylation factor 1, putative	Arf	4.00E-78
Q4DZM9	ADP-ribosylation factor-like protein, putative	Arf	6.60E-49
Q4CW64	Calpain-like cysteine peptidase, putative	DUF1935	1.10E-38
Q4CV42	Calpain-like cysteine peptidase, putative	DUF1935	7.50E-33
K4E5Y1	Cytoskeleton-associated protein CAP5.5	Peptidase_C2	3.20E-43
K4DT87	Dynein heavy chain, putative	NO	
K4E5P0	Fatty acyl CoA synthetase 2, putative	AMP-binding	1.60E-76
K4EAZ1	Flagellar calcium binding protein	EF-hand_7	6.50E-07
K4E595	Nitrate reductase, putative	Cyt-b5	4.10E-13
K4E583	Phosphatase 2C, putative	PP2C	1.10E-49
Q4D0B9	Proteasome regulatory ATPase subunit 2, putative	AAA	6.30E-42
K4DTB6	Protein phosphatase 2C, putative	PP2C	3.10E-72
Q4E4N2	Protein phosphatase, putative	PP2C	2.90E-55
Q4DRI6	Putative uncharacterized protein	Snf7	7.60E-28
Q4E2Z0	Uncharacterized protein	Cmc1	1.70E-06
K4DWR5	Uncharacterized protein	zf-C3HC4_3	5.50E-15
Q4DPA5	Uncharacterized protein	NO	
K4E955	Uncharacterized protein	NO	
K4DJS2	Uncharacterized protein	NO	
K4E1X7	Uncharacterized protein	NO	
K4DXD3	Uncharacterized protein	SpoIIE	8.00E-13
K4E189	Uncharacterized protein	NO	
K4E8V8	Uncharacterized protein	NO	
K4E943	Uncharacterized protein	NO	
Q4DLX6	Uncharacterized protein	Rhodanese	4.30E-13
K4DWF7	Uncharacterized protein	EF-hand_7	5.60E-08
Q4DVL2	Uncharacterized protein	NO	
Q4DXG4	Uncharacterized protein	NO	
Q4DDD2	Uncharacterized protein	NO	
K4DQN8	Uncharacterized protein	NO	
K4DZS1	Uncharacterized protein	NO	
K4E5N2	Uncharacterized protein	NO	
Q4CWV8	Uncharacterized protein		
K4E0P3	Uncharacterized protein		
K4E0J9	Uncharacterized protein		
K4DX27	Uncharacterized protein	NO	
K4E3X3	Uncharacterized protein	NO	
K4EE92	Uncharacterized protein (Fragment)	AMPKBI	2.60E-17

Appendix

Roberts AJ, Torrie LS, Wyllie S, Fairlamb AH. (2014) Biochemical and genetic characterisation of *Trypanosoma cruzi N*-myristoyltransferase. ***Biochemical journal.*** (2014) **459** (323–332).
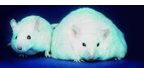
Biochemical and genetic characterization of *Trypanosoma cruzi* *N*-myristoyltransferase

Adam J. ROBERTS*, Leah S. TORRIE*, Susan WYLLIE* and Alan H. FAIRLAMB*[1]

*Division of Biological Chemistry and Drug Discovery, College of Life Sciences, University of Dundee, Dundee DD1 5EH, U.K.

Co- and post-translational N-myristoylation is known to play a role in the correct subcellular localization of specific proteins in eukaryotes. The enzyme that catalyses this reaction, NMT (*N*-myristoyltransferase), has been pharmacologically validated as a drug target in the African trypanosome, *Trypanosoma brucei*. In the present study, we evaluate NMT as a potential drug target in *Trypanosoma cruzi*, the causative agent of Chagas' disease, using chemical and genetic approaches. Replacement of both allelic copies of *TcNMT* (*T. cruzi* NMT) was only possible in the presence of a constitutively expressed ectopic copy of the gene, indicating that this gene is essential for survival of *T. cruzi* epimastigotes. The pyrazole sulphonamide NMT inhibitor DDD85646 is 13–23-fold less potent against recombinant *Tc*NMT than *Tb*NMT (*T. brucei* NMT), with K_i values of 12.7 and 22.8 nM respectively, by scintillation proximity or coupled assay methods. DDD85646 also inhibits growth of *T. cruzi* epimastigotes ($EC_{50} = 6.9$ μM), but is ~1000-fold less potent than that reported for *T. brucei*. On-target activity is demonstrated by shifts in cell potency in lines that over- and under-express NMT and by inhibition of intracellular N-myristoylation of several proteins in a dose-dependent manner. Collectively, our findings suggest that N-myristoylation is an essential and druggable target in *T. cruzi*.

Key words: Chagas' disease, click chemistry, drug target, N-myristoylation, *Trypanosoma cruzi*, validation.

INTRODUCTION

The protozoan parasite *Trypanosoma cruzi* is the causative agent of Chagas' disease, which is endemic in Latin American countries. There are an estimated 8–10 million infected individuals worldwide, with an annual death toll of ~10 000 per annum [1–3]. Migration from endemic countries has also led to the worldwide distribution of Chagas' disease [1]. The acute stage of this disease often has very mild and non-specific symptoms that occur 4–8 weeks post-infection, resulting in only 1–2% of all infected individuals being diagnosed in this stage [4]. Approximately 30% of infected individuals go on to develop the chronic disease, most often characterized by heart abnormalities, and to a lesser extent, mega-organ disease affecting the digestive tract [2]. To date, benznidazole and nifurtimox are the only approved drugs available for the treatment of Chagas' disease. Prolonged treatment with these nitroimidazoles during the acute stage cures up to 70% of individuals; however, the efficacy of these drugs significantly decreases in the chronic stage [5]. Both therapies have been associated with severe toxic side effects that can lead to the interruption or discontinuation of treatment in as many as 30% of cases [6,7]. At present, there are two drugs being clinically assessed for the treatment of asymptomatic chronic Chagas' disease, posaconazole (Merck; ClinicalTrials.gov Identifiers NCT01377480 and NCT01162967) and E1224 (Eisai; ClinicalTrials.gov Identifier NCT01489228). However, bearing in mind the high levels of drug candidate attrition in the clinical trials process, there remains an urgent need to identify new drug targets and better drugs to treat this disease.

The enzyme NMT (*N*-myristoyltransferase; EC 2.3.1.97) catalyses the co- and post-translational addition of myristic acid ($C_{14:0}$) on to the N-terminal glycine residue of specific proteins [8,9]. This irreversible modification plays an important role in the correct cellular localization and biological function of the modified proteins. This enzyme has been extensively studied in a number of organisms including the trypanosomatid parasites *Trypanosoma brucei* and *Leishmania major* [10–15]. In these parasitic organisms, NMT has been demonstrated to be essential for viability either by classical gene knockout with episomal rescue or by RNAi, indicating that the N-myristoylation of certain proteins is a key biological process. Moreover, in the African trypanosome, NMT is now pharmacologically validated with compounds such as DDD85646 that specifically inhibit the enzyme and are curative in the mouse model of stage one African sleeping sickness [13]. Amino acid sequence comparisons indicate that the *T. cruzi* enzyme is approximately 60% identical to those of *Leishmania* spp. and various African trypanosomes. Although metabolic labelling studies in the parasite have confirmed that multiple proteins are N-myristoylated [16], *T. cruzi* NMT has not been characterized biochemically or assessed for essentiality or druggability. With this in mind, in our present study, we utilize both genetic and chemical approaches to assess the essentiality of the enzyme in *T. cruzi*.

MATERIALS AND METHODS

Parasite and mammalian cell culture

T. cruzi epimastigotes from the Silvio strain (MHOM/BR/78/Silvio; clone X10/7) were grown at 28 °C in RTH/FBS [RPMI 1640 medium supplemented with trypticase, haemin, Hepes and 10% heat-inactivated FBS (PAA Laboratories; now GE Healthcare)] [17]. {The Silvio strain, originally isolated

Primer	Sequence
*Tc*NMT-pTREX_s	5′-gaattcATGGCAGAAGAGGGGTTCAGGTTTACATCAG-3′
*Tc*NMT-pTREX_as	5′-ctcgagCTATAGCATGAACAATCCCACGTCACTTGG-3′
*Tc*NMT-pET15b-TEV_s	5′-catATGGCAGAAGAGGGGTTCAGGTTTACATCAG-3′
*Tc*NMT-pET15b-TEV_as	5′-ggatccCTATAGCATGAACAATCCCACGTCACTTGG-3′
5′-UTR-NotI_s	5′-ataagaatgcggccgcGTGATCTTCTCAACAACAAAAATGGATGA-3′
5′-UTRHindIII/PmeI_as	5′-gtttaaacttacggaccgtcaagcttTCCTTCAAAAAGGCGATCAAGTCCA-AAATTAC-3′
3′-UTR-PmeI/BamHI_s	5′-gacggtccgtaagtttaaacggatccGATGCGGGCGGAATTTAGGAGAGA-AGT-3′
3′-UTR-NotI_as	5′-ataagtaagcggccgcCCGCATCCAGCAGATGGATTAATCACCGT-3′

from a 19-year-old male patient (Silvio B.S.) living in Pará, Brazil [18], is also incorrectly referred to as the Sylvio strain in the literature.} Clone Silvio X10/7A, used in subsequent experiments, was generated by limiting dilution. Stationary-phase epimastigote cultures containing metacyclic trypomastigotes were used to infect Vero cells. Trypomastigotes were recovered from Vero cell monolayers infected with Silvio X10/7A at 5–6 days post-infection [19]. For infectivity studies, Vero cells were infected with transgenic *T. cruzi* trypomastigotes using a multiplicity of infection of 5:1. Free-swimming trypomastigotes were washed off after 12 h and the infected cells were re-plated into 384-well plates (Corning® CellBIND®). After 72 h the cells were fixed in PBS containing 1 % formaldehyde before staining with 5 μg·ml^{-1} Hoechst 33342 in PBS containing 0.01 % Triton X-100. Plates were imaged using a high content microscope (Operetta, PerkinElmer), and the images captured were processed using an automated image analysis software (Columbus, PerkinElmer) to determine the percentage of infected cells and the mean number of parasites per infected Vero cell. Vero cells (*Cercopithecus aethiops* kidney cells; ATCC® CCL-81™) were cultured in DMEM (Dulbecco's modified Eagle's medium; Lonza) supplemented with 10 % heat-inactivated FBS at 37°C with 5 % CO_2 [20].

Cloning, expression and purification of recombinant *Tc*NMT (*T. cruzi* NMT)

The *NMT* ORF was identified from the Silvio X10/1 genome by BLAST, using the CL-Brenner sequence (TriTrypDB accession number TcCLB.511283.90) as a search template [21]. Primers designed against this sequence, *Tc*NMT-pET15b-TEV_s and *Tc*NMT-pET15b-TEV_as (Table 1), were used to amplify the *NMT* ORF from Silvio X10/7A genomic DNA using Pfu DNA polymerase (Promega). The resulting PCR product was cloned into Zero Blunt® TOPO® and sequenced. *Tc*NMT was excised from Zero Blunt® TOPO®-*Tc*NMT by digestion with the appropriate restriction enzymes and ligated directly into linearized pET15b-TEV.

The resulting pET15b-*Tc*NMT expression construct was transformed into Rosetta™ (DE3)pLysS competent cells and recombinant expression was carried out in auto-induction media [22] at 20°C for 48 h with agitation at 200 rev./min. The cells were harvested (20 min, 4°C and 5020 *g*), resuspended in lysis buffer {25 mM Tris, 500 mM NaCl, 25 mM imidazole, 1 mM TCEP [tris-(2-carboxyethyl)phosphine]/HCl, pH 8.5, DNAse I (Sigma) and cOmplete EDTA-free protease inhibitors (Roche)} and lysed at 30 000 psi (1 psi = 6.9 kPa) using a Constant Systems cell disruptor. Soluble protein was recovered by centrifugation

(30 min, 4°C and 40 000 *g*) and filtered (0.2 μm Sartorius) before loading on to a pre-equilibrated HisTrap HP 5 ml column (GE Healthcare). The protein was eluted using a gradient of 25–500 mM imidazole. Fractions containing NMT were identified by SDS/PAGE (4–12 % gel), pooled and dialysed into buffer A (25 mM Tris, 25 mM NaCl and 1 mM TCEP, pH 8.5). The dialysed protein was loaded on to a 5 ml HiTrap Q HP column (GE Healthcare) and eluted with a gradient of NaCl (25–500 mM) in buffer A. Pooled fractions containing NMT were further purified by size exclusion on a Superdex 75 26/60 column equilibrated in buffer B (25 mM Tris/HCl, 150 mM NaCl and 1 mM TCEP, pH 8.5). The purity and mass of the recovered recombinant NMT was assessed by SDS/PAGE and MALDI–TOF carried out by the FingerPrints Proteomics service at the University of Dundee. The oligomeric structure was characterized by size-exclusion chromatography using a Superdex 200 300/10 GL column (GE Healthcare) equilibrated with buffer B.

GENERATION OF KNOCKOUT, OVEREXPRESSION AND RECOVERY CONSTRUCTS

The primers used to generate constructs for genetic manipulation were designed using the *Tc*NMT X10/1 and flanking sequences in TriTrypDB as a template (Table 1). The accuracy of all assembled constructs was verified by sequencing. NMT gene replacement cassettes were generated by amplifying a region of DNA encompassing 449 bp of the 5′-UTR, the ORF and 449 bp of the 3′-UTR of *Tc*NMT from genomic DNA with primers 5′-UTR-NotI_s and 3′-UTR-NotI_as, using Pfu DNA polymerase. This sequence was then used as a template for the amplification of the individual regions used in the assembly of replacement cassettes containing the selectable drug resistance genes *PAC* (puromycin *N*-acetyltransferase) and *HYG* (hygromycin phosphotransferase), exactly as described previously [23]. To generate a construct for use as both a recovery and NMT-overexpressing vector in knockout and WT (wild-type) parasites, NMT was amplified from genomic DNA using the primers *Tc*NMT-pTREX_s and *Tc*NMT-pTREX_as and cloned into the constitutive expression vector pTREX [24] using the EcoRI and XhoI cloning sites.

Generation of transgenic *T. cruzi* cell lines

Transfections of *T. cruzi* epimastigotes were carried out using an Amaxa Nucleofector™ electroporator, as described previously [25]. A total of 5–10 μg of DNA was transfected into early-to mid-log epimastigotes (1×10^7), suspended in Human T-cell Nucleofector™ solution (100 μl; Lonza), using the program U-33. At 24 h following transfection, 10 μg·ml^{-1} puromycin (Sigma), 250 μg·ml^{-1} G418 (Gibco®) or 500 μg·ml^{-1} hygromycin (Roche) was added to cultures of transgenic parasites. Following drug selection, the parasites were cloned on to semi-solid agar plates [1 % Agar Noble (Difco™) and RTH/FBS] containing 20 μg·ml^{-1} puromycin, 500 μg·ml^{-1} G418 or 750 μg·ml^{-1} hygromycin, as appropriate. After 2–3 weeks at 28°C, colonies were picked and grown in fresh RTH/FBS plus the appropriate drug.

In vitro drug sensitivity assays

To examine the effects of test compounds on growth, triplicate epimastigote cultures were seeded with 1×10^5 cells·ml^{-1}. Parasites were grown in 10-ml cultures in the presence of drug for 120 h. Cells were fixed in PBS (137 mM NaCl, 2.7 mM KCl, 10 mM Na_2HPO_4 and 1.8 mM KH_2PO_4) containing

1 % formaldehyde and manually counted using a Neubauer haemocytometer. Data were processed using GraFit (version 5.0.4; Erithacus software) and fitted to a 2-parameter equation (eqn 1) to obtain the effective EC_{50}:

$$y = \frac{100}{1 + \left(\frac{[I]}{EC_{50}}\right)^m} \tag{1}$$

In this equation, [I] represents inhibitor concentration and m is the slope factor. The data are presented as the means $\pm$ S.D.

Quantification of cellular levels of NMT in lysates

Epimastigotes and trypomastigotes were harvested by centrifugation (15 min, 20°C, 1620 and 2000 g respectively) and washed twice in PBS. Amastigotes were purified from a mixed population of trypomastigotes and amastigotes released from an infected Vero cell monolayer [25a]. Briefly, parasites were collected by centrifugation (10 min, 20°C, 4000 g) and the pellet incubated for 3 h at 37°C overlaid with DMEM/FBS. Motile trypomastigotes released into the supernatant were removed and the pellet was resuspended in DMEM/FBS. This process was repeated twice to produce a pure population of amastigotes (~95 %). Cells (5×10^7) were resuspended in Laemmli buffer (Bio-Rad Laboratories) and heated at 95°C for 10 min. The equivalent of 1×10^7 cells were separated by SDS/PAGE on a 4–12 % NuPAGE® gel. Cellular proteins were transferred on to Protran™ nitrocellulose membrane (Whatman) by electrotransfer. Membranes were probed with primary rat antisera generated against either *Tc*NMT or *Tc*TryR (*T. cruzi* trypanothione reductase) [26] (both 1:500 dilution) before probing with an HRP (horseradish peroxidase)-conjugated rabbit anti-rat polyclonal secondary serum (1:10 000; Dako). *Tc*NMT-specific polyclonal antiserum was raised against the recombinant His$_6$–*Tc*NMT (CL-Brenner) in adult male Wistar rats, as described previously [27]. Immunization protocols were approved by the University Welfare and Ethical Use of Animals Committee and were performed under the Animals (Scientific Procedures) Act 1986 in accordance with the European Communites Council Directive (86/609/EEC). The blot was developed using ECL detection reagent kit (GE Healthcare) and exposed to Amersham Hyperfilm™ ECL (GE Healthcare). The developed film was scanned and the protein bands were quantified by densitometry with ImageJ (NIH).

Southern blot analyses of transgenic *T. cruzi* cell lines

The ORFs of *TcNMT*, *PAC* and *HYG* were amplified by PCR (using the primers described previously for the cloning of *TcNMT* and knockout constructs) using the PCR DIG Probe Synthesis Kit (Roche). The resulting DIG (digoxigenin)-labelled products were used as probes. Samples of genomic DNA (5 μg) from WT and transgenic cell lines were digested with appropriate restriction endonucleases, the digestion products were then separated on a 0.8 % agarose gel and transferred to a positively charged nylon membrane (Roche). The membrane was hybridized overnight in DIG Easy Hyb solution (Roche) at 42°C with the DIG-labelled probes (2 μl of PCR product). Following hybridization, membranes were washed twice in low stringency conditions (25°C, 5 min, 2× SSC buffer with 0.1 % SDS) and twice in high stringency conditions (68°C, 15 min, 0.5× SSC with 0.1 % SDS), where 1× SSC comprises 150 mM NaCl and 50 mM sodium acetate, pH 7.0. The bound probe was detected using the DIG immunological detection kit (Roche) as per the manufacturer's instructions.

Detection of cellular N-myristoylation

Mid-log epimastigotes were harvested by centrifugation and resuspended at 1×10^7 cells·ml^{-1} in fresh RTH/FBS. Various concentrations of DDD85646 (0, 12.5, 25, 50 and 100 μM) were added to epimastigote cultures 30 min before the addition of 50 μM Click-IT® myristic acid (Invitrogen) and cultures were then incubated for a further 5 h. Following incubation, cells were washed (three times in PBS), the resulting cell pellet was resuspended in lysis buffer (150 μl, 50 mM Tris/HCl, pH 7.4, 150 mM NaCl, 1 % sodium deoxycholate, 0.1 % SDS, 1 % Triton X-100 and a cOmplete mini EDTA-free protease inhibitor cocktail tablet) and incubated on ice for 1 h. Lysates were clarified by centrifugation (10 min, 4°C and 14 000 g) and quantified with the Bio-Rad Laboratories protein assay using BSA as a standard. IRDye® 800CW alkyne (LI-COR Biosciences) was ligated to Click-IT® myristic acid using the Click-IT® protein reaction buffer set (Invitrogen) and methanol/chloroform precipitated, according to the manufacturer's instructions. Treated lysates (12 μg) were separated by SDS/PAGE, fixed in 10 % acetic acid and 40 % methanol. The fixed gel was washed in 0.2 M NaOH for 1 h before washing briefly in H$_2$O and imaged by in-gel fluorescence using an Odyssey Sa infrared imaging system (LI-COR Biosciences). Quantification of band intensities was carried out using Image Studio Lite (version 3.1; LI-COR Biosciences). Cells not labelled with azidomyristate were used for a background fluorescence measurement to correct the values obtained for N-myristoylated proteins. Intensities are expressed as a percentage of the no drug control.

Metabolic labelling

Parasites were incubated in a methionine-free RTH/FBS medium that was supplemented with 10 μCi·ml^{-1} L-[^{35}S]methionine (PerkinElmer). After incubating with the same concentrations of inhibitor and azidomyristate as mentioned above, the parasites were washed three times in PBS and boiled in Laemmli buffer for 10 min. A total of 5×10^6 parasites per lane were separated by SDS/PAGE and stained with Coomassie Blue. The gel was incubated in EN^{3}HANCE™ solution (PerkinElmer) as per the manufacturer's protocol and then gel dried. The gel was exposed to BioMax MS film (Kodak) using a BioMax TranScreen LE (Kodak) for 8 h.

Kinetic analysis of *Tc*NMT

Kinetic analysis [$K_{m(app)}$ and k_{cat} values] of *Tc*NMT activity was performed at 30°C using a previously published coupled-enzyme spectrophotometric assay monitoring the increase in absorbance at 340 nm [28]. Each 0.25 ml assay contained 50 mM Tris, 0.5 mM EDTA, 0.5 mM EGTA, 1.25 mM DTT, 0.1 % Triton X-100, 40 mM pyruvic acid, 0.125 units·ml^{-1} pyruvate dehydrogenase, 0.2 mM thiamine pyrophosphate, 40 μM myristoyl-CoA and 2.5 mM NAD$^+$, adjusted to pH 7.4 with HCl. $K_{m(app)}$ values were determined for a biotinylated peptide substrate derived from amino acids 2–15 of *T. brucei* [13] and *T. cruzi* CAP5.5 (cytoskeleton-associated protein 5.5) (*Tc*CAP5.5 GCCASKEKQPRPGAK[biotin], *Tb*CAP5.5 GCGGSKVKPQPPQAK[biotin], custom synthesized by Pepceuticals) and for myristoyl-CoA (Sigma). The IC$_{50}$ value of DDD85646 for recombinant NMT was determined using this coupled-enzyme assay. The $K_{i(app)}$ was determined by fitting the resulting data to the Morrison equation (eqn 2), allowing the true K_i value to be determined using eqn 3. In a comparative study, the kinetic parameters of *Tc*NMT (5 nM per assay) were also
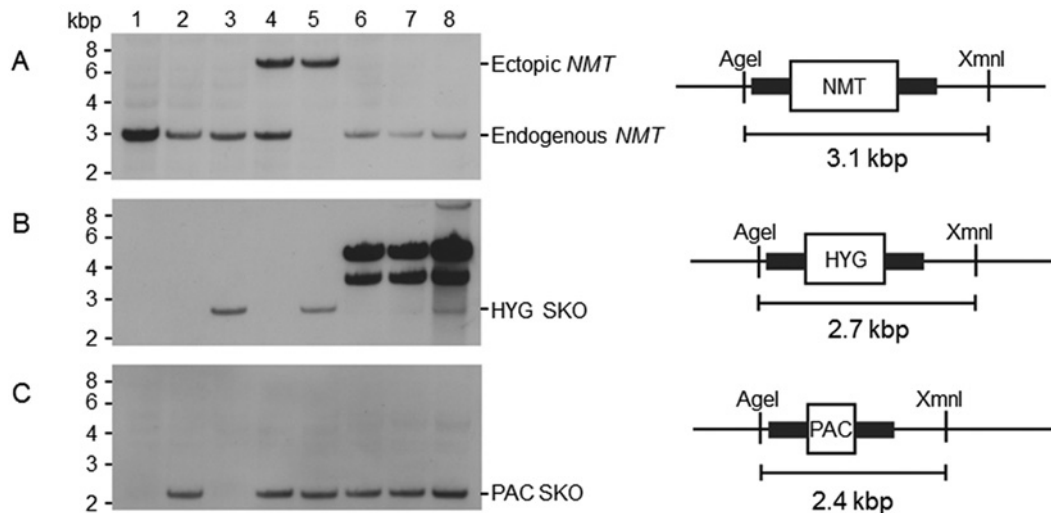
Figure 1   Genotypic analysis of WT, SKO and rescue DKO cell lines

Southern blot analysis of AgeI and XmnI digested genomic DNA (~5 μg) from WT *T. cruzi* (clone Silvio X10/7A) cells (lane 1), *NMT* SKO (*PAC*) cells (lane 2), *NMT* SKO (*HYG*) cells (lane 3), *NMT* SKO (*PAC*) cells constitutively expressing NMT (lane 4), *NMT* DKO (*PAC* and *HYG*) cells constitutively expressing NMT (lane 5) and 'pseudo' *NMT* DKO (*PAC* and *HYG*) cells (lanes 6–8). The maps show the predicted fragment sizes for the WT and for correct replacement with drug resistance markers. Southern blots were probed with (**A**) *NMT* ORF, (**B**) *HYG* and (**C**) *PAC*.

determined using a scintillation proximity method, as described previously [13,29]. The myristoyl-CoA $K_{m(app)}$ was determined using CAP5.5 at 600 μM or 50 μM in the coupled-enzyme and scintillation proximity assays respectively. The CAP5.5 $K_{m(app)}$ values were determined using either 40 μM or 125 nM in the coupled-enzyme or scintillation proximity assays.

$$\frac{v_i}{v_0} =$$

$$\frac{\left([E]_T - [I]_T - K_{i(app)}\right) + \sqrt{\left([E]_T - [I]_T - K_{i(app)}\right)^2 + 4[E]_T[I]_T}}{2[E]_T}$$

$$(2)$$

$$K_i = \frac{K_{i(app)}}{\left(1 + \dfrac{[S]}{K_m}\right)} \qquad (3)$$

RESULTS

Generation of an NMT 'rescued' DKO (double knockout) cell line

Restriction enzyme digestion and Southern blotting analysis of *T. cruzi* X10/7A DNA indicated that *NMT* is a single copy gene per haploid genome (results not shown). DNA sequencing of PCR products gave identical amino acid sequences apart from a serine or proline residue at position 150, probably due to allelic variation. The essentiality of NMT in *T. cruzi* epimastigotes was then assessed using a classical two-step gene replacement strategy where *NMT* is sequentially replaced by homologous recombination with drug resistance genes and drug selection (Figure 1). The first gene copy of *NMT* could be successfully replaced with either hygromycin (*HYG*) or puromycin (*PAC*) resistance genes resulting in two independent SKO (single knockout) cell lines (Figures 1B, lane 3, and 1C, lane 2). Loss of

a single allelic copy of *NMT* did not markedly alter the growth rate of SKO parasites. Several attempts were made to directly replace the remaining allelic copy of *NMT* in the SKO-*PAC* clone with *HYG*. In two out of three attempts, epimastigotes that were resistant to both hygromycin and puromycin were recovered following transfection. On the remaining occasion, no live parasites were recovered. Southern blot analysis of genomic DNA isolated from clones of putative DKO parasites revealed that in all cases an endogenous copy of *NMT* was retained (Figure 1A, lanes 6–8) along with a copy of *PAC* at the *NMT* locus (Figure 1C, lanes 6–8). Moreover, probing these blots with the *HYG* probe showed that this drug resistance gene had not integrated into the *T. cruzi* genome (Figure 1B, lanes 6 and 7). PCR of these failed DKO attempts suggest that the *HYG* resistance gene is present as a multicopy episome. In another of these clones, *HYG* was not only present as an episomal copy, but also integrated at the *NMT* locus with retention of a copy of *NMT* (Figures 1A and 1B, lane 8). We have not investigated whether the latter is due to amplification of all or part of the *NMT* chromosome resulting in aneuploidy, as has been observed in *Leishmania* spp. [30].

Owing to the failure to directly produce *NMT* DKO epimastigotes, a 'rescued' DKO cell line was generated. First, a constitutively expressed ectopic copy of *NMT* was targeted to the ribosomal locus of SKO-*PAC* parasites (Figure 1A, lane 4). Only then was it possible to replace the last allelic copy of *NMT* in cells, due to the presence of an episomal copy of the gene (Figure 1A, lane 5). These findings provide strong evidence that NMT is essential for growth and survival of *T. cruzi* epimastigotes *in vitro*.

Infectivity of transgenic parasites

The ability to infect Vero cells was quantified to determine whether the presence of an ectopic copy or the deletion of a single allele of *TcNMT* affected the virulence of these parasites. Representative images of uninfected and infected Vero cells are shown (Figures 2A and 2B respectively). The deletion of a single
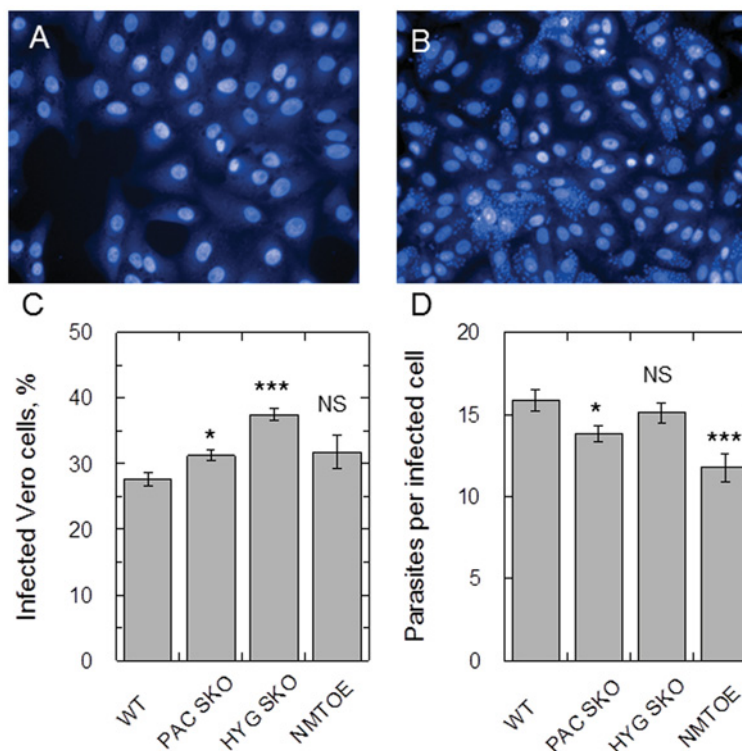
Figure 2 Infectivity of transgenic *T. cruzi* parasites

(**A**) Uninfected Vero cells stained with Hoechst 33342. (**B**) Vero cells infected with WT *T. cruzi*. (**C**) The percentage of Vero cells infected with WT, SKO-*PAC*, SKO-*HYG* and NMT^{OE} transgenic parasites. Differences in the percentage of WT compared with SKO-*PAC* and SKO-*HYG* parasites were confirmed to be statistically significant (*$P < 0.01$) using an unpaired Student's t test. (**D**) The mean number of amastigotes per infected Vero cell of WT, SKO-*PAC*, SKO-*HYG* or NMT^{OE} parasites. Differences in the percentage of WT compared with SKO-*PAC* and NMT^{OE} parasites were confirmed to be statistically significant ($P < 0.01$) using an unpaired Student's t test (*$P < 0.05$, ***$P < 0.001$). A total of 24 measurements were made for each parameter. Data are shown as means $\pm$ S.E.M. NS, not significant.

allele in both cases led to a very minor increase in the percentage of infected cells compared with the WT, whereas the presence of an ectopic copy [NMT^{OE} (NMT overexpressor)] had no effect (Figure 2C). Absolute numbers of parasites per infected Vero cell were also monitored (Figure 2D). Vero cells infected with SKO-*PAC* and NMT^{OE} parasites were found to have marginally reduced parasite loads compared with WT. Despite the statistical differences between some, but not all, cell lines, these changes are not relevant biologically as all lines showed similar infection profiles.

Expression of NMT in *T. cruzi* life-cycle stages

For technical reasons, it is not possible to genetically validate *NMT* in the clinically relevant non-dividing trypomastigote stage and intracellular amastigote stage by gene knockout. However, we were able to confirm that NMT is expressed in all stages of the parasite's life cycle by probing an immunoblot of crude lysates with a *Tc*NMT-specific antiserum (Figure 3). Single bands of approximately 53 kDa, close to the predicted molecular mass of NMT (51.4 kDa), were detected in all three lysates indicating that NMT is expressed at all stages of the parasite life cycle. The cellular concentration of NMT in each of these parasite stages was determined by densitometry and previously published cell volumes [31]. Using this information, NMT concentrations in each stage of the parasite were estimated to be within a 2-fold range; 1.2, 2.1 and 2.5 μM in the epimastigote, trypomastigote and amastigote respectively.

Sensitivity to DDD85646 shifts with NMT expression levels

The pyrazole sulphonamide DDD85646 has been shown to specifically inhibit *Tb*NMT (*T. brucei* NMT) *in vitro* and cure the stage 1 murine model of human African trypanosomiasis [13]. To establish whether this inhibitor can also chemically target the *T. cruzi* enzyme, the comparative sensitivity of WT epimastigotes and transgenic cell lines with different levels of NMT to DDD85646 was determined. In the first instance, altered levels of NMT expression in transgenic parasites were confirmed by Western blot, using *Tc*TryR as a loading control (Figure 4A). Cellular levels of NMT were analysed in WT parasites, the SKO cell line generated previously (SKO-*PAC*) and in an NMT overexpressing cell line (NMT^{OE}) which was generated by transfecting pTREX-NMT into WT epimastigotes. Densitometry revealed that SKO-*PAC* parasites contained NMT protein levels ~2.5-fold lower than the WT, with levels in the NMT^{OE} epimastigotes ~7.6-fold higher. Varying the cellular levels of NMT within these parasites was found to markedly alter their sensitivity to DDD85646 with WT, SKO-*PAC* and NMT^{OE} cell lines having EC$_{50}$ values of 6.3, 2.9 and 78.6 μM respectively (Figure 4B). The clear relationship observed between the levels of NMT expression and the sensitivity of the parasites for this compound confirms that *Tc*NMT is specifically targeted by DDD85646 and thus may be druggable in *T. cruzi*. There was no selectivity between the amastigote and Vero cells with DDD85646 [EC$_{50}$ values of $\geqslant 8.7 \pm 0.8$ μM and 6.7 ± 1 μM ($n = 4$) respectively]. The actual EC$_{50}$ value for the amastigote may be higher as the parasite cannot replicate in the absence of the host cell.
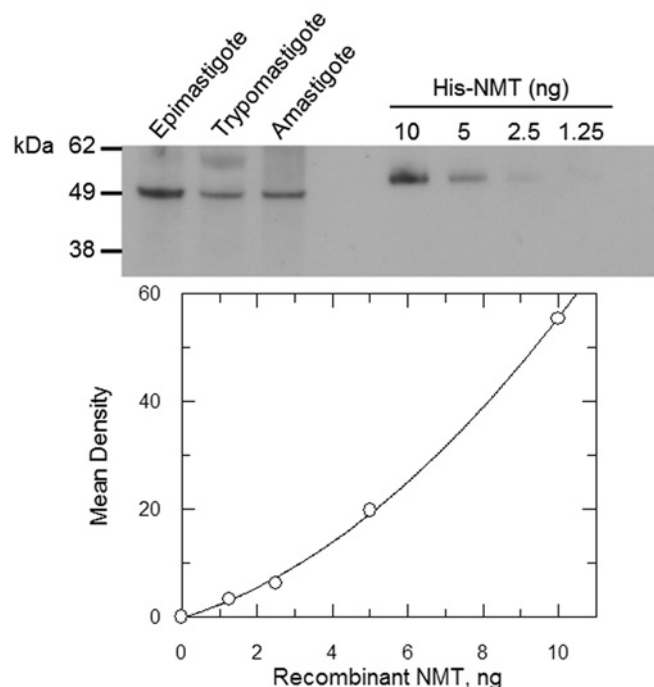
Figure 3   Cellular levels of NMT in *T. cruzi* life-cycle stages

Immunoblots of whole cell extracts (equivalent of 1×10^7 parasites in each lane) from *T. cruzi* epimastigotes, trypomastigotes and amastigotes were probed with *Tc*NMT-specific polyclonal antiserum. Known amounts of purified recombinant *Tc*NMT were loaded as standards for the quantification of the cellular levels of NMT. The difference in size between recombinant and cellular NMT is due to the His$_6$-tag on the recombinant protein.

DDD85646-mediated inhibition of N-myristoylation

To confirm DDD85646-mediated inhibition of N-myristoylation within *T. cruzi* epimastigotes, parasites were pre-treated with a range of inhibitor concentrations for 30 min. N-azidomyristoylated proteins were detected by in-gel fluorescence. It is evident that there is some non-specific interaction of the dye with an unlabelled 49 kDa protein (Figure 4A, upper panel, lane 1). Labelling parasites with this myristic acid analogue led to

the NMT-mediated incorporation of azidomyristate into multiple *T. cruzi* proteins (Figure 4A, upper panel, lane 2). In parasites treated with DDD85646, we observe that six bands were depleted in a dose-dependent manner which was confirmed by quantifying the fluorescent intensities of the bands (Figures 5A, upper panel, and 5B). The most prominent effect was observed for a ~20 kDa band, where the N-myristoylation of this protein decreased to 40% of the untreated control, at the lowest inhibitor concentration tested ($\sim 2 \times EC_{50}$). The remaining bands are insensitive over 5.5 h exposure to DDD85646 at the range of concentrations tested. Labelling parasites with L-[^{35}S]methionine revealed no inhibition of nascent protein synthesis (Figure 5A, lower panel), indicating that the observed inhibition of N-myristoylation is due to the direct inhibition of cellular NMT. These data further demonstrate the on-target activity of the inhibitor DDD85646 in *T. cruzi*.

Kinetic characterization of recombinant *Tc*NMT

In order to facilitate kinetic studies of *Tc*NMT, the recombinant enzyme was expressed and purified to homogeneity. *Escherichia coli* Rosetta™ (DE3)pLysS cells transformed with pET15b-TEV-*Tc*NMT produced soluble and active protein. *Tc*NMT was purified following three chromatographic steps to obtain a yield of 2.5 mg·l^{-1} (Figure 6A). Analysis of the recombinant protein by size-exclusion chromatography revealed that His$_6$–NMT elutes primarily as a monomer at ~47.4 kDa, close to the predicted molecular mass of 53.7 kDa (Figure 6B). This was confirmed by MS to be 53.7 kDa for the tagged recombinant protein by MALDI–TOF analysis.

Multiple assays already exist for the kinetic characterization of NMTs using HPLC, ELISA, scintillation proximity assay or spectrophotometric methodologies [9,29,32,33]. In the present study, we have compared the scintillation proximity assay with a modified version of a coupled-enzyme spectrophotometric assay [28]. The basic kinetic parameters of *Tc*NMT [$K_{m(app)}$ and k_{cat}] were measured in these assays for CAP5.5, a protein known to be N-myristoylated in *T. brucei* [34] (Table 2). Synthetic peptides based on the amino acids 2–15 of CAP5.5 from both *T. brucei* and *T. cruzi* were used as substrates in these assays. In the coupled-enzyme assay, the K_m value determined for *Tb*CAP5.5 was ~21-fold higher than observed for *Tc*CAP5.5, but the catalytic
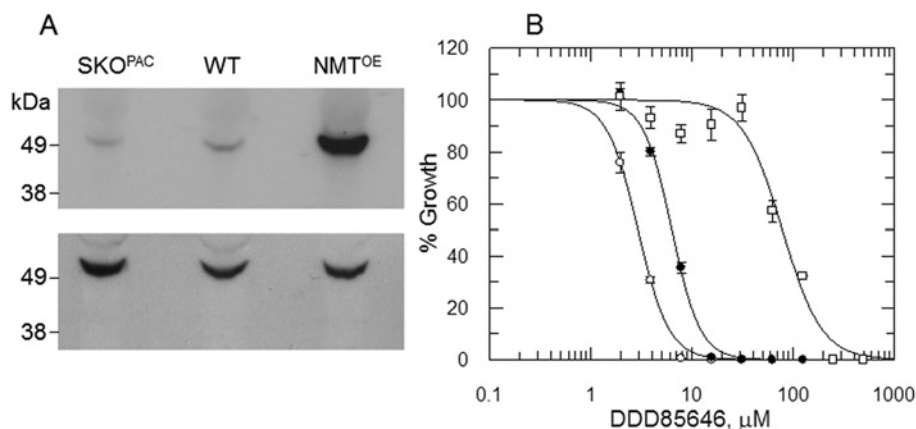

Figure 4   Effects of NMT modulation on DDD85646 susceptibility

(**A**) Immunoblots of whole cell extracts (equivalent of 1×10^7 parasites in each lane) of WT, NMT SKO and NMT-overexpressing epimastigotes were probed with *Tc*NMT-specific polyclonal antiserum. A duplicate blot was probed with antiserum against *Tc*TryR to act as a loading control. (**B**) EC$_{50}$ values were determined for DDD85646 against WT (closed circles), SKO (PAC) (open circles) and NMT-overexpressing parasites (open squares). EC$_{50}$ values of 6.3 ± 0.1, 2.9 ± 0.04 and 78.6 ± 4.6 μM were determined for DDD85646 against WT, SKO and NMT-overexpressing cell lines respectively. Data are shown as means $\pm$ S.D. for triplicate cultures.
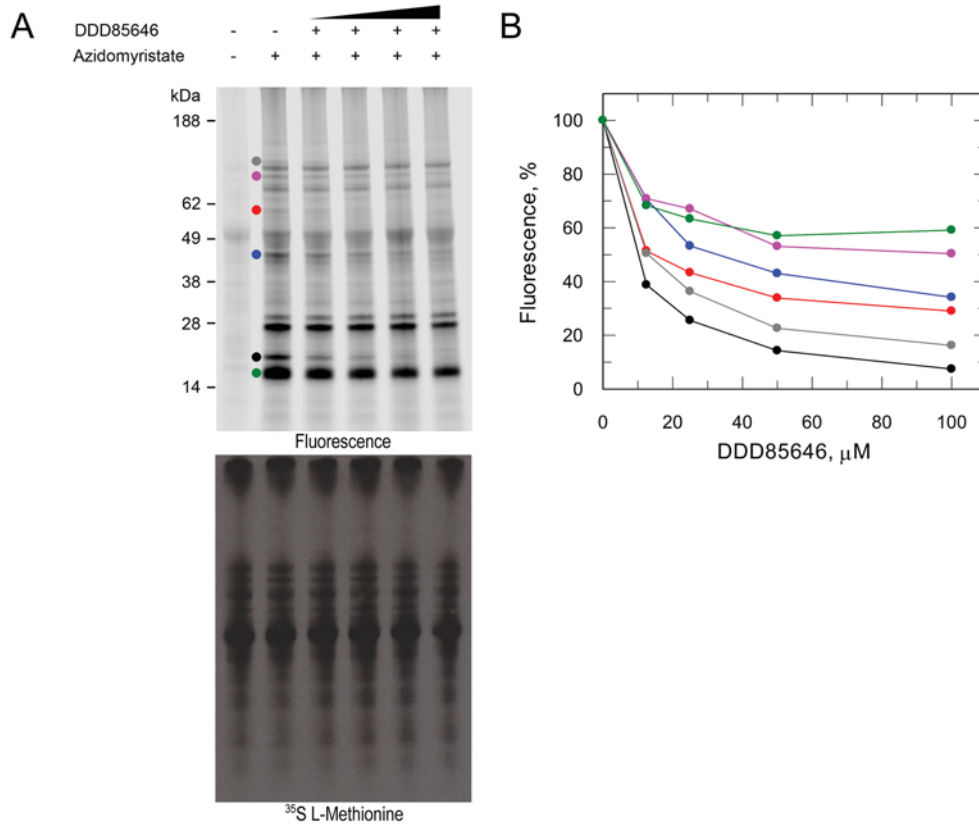
Figure 5   DDD85646-mediated inhibition of cellular N-myristoylation

Mid-log epimastigotes were pre-treated with varying concentrations of DDD85646 (0–15×EC$_{50}$) for 5.5 h. (**A**) N-myristoylated proteins were detected by click chemistry ligation of an alkyne fluorescent dye on to azidomyristate-labelled proteins (upper panel) and protein synthesis assessed by L-[^{35}S]methionine labelling of parasites (lower panel). Circles highlight bands that are sensitive to NMT inhibition that were quantified in (**B**). (**B**) Reduction in fluorescence intensity as a function of DDD85646 concentration.
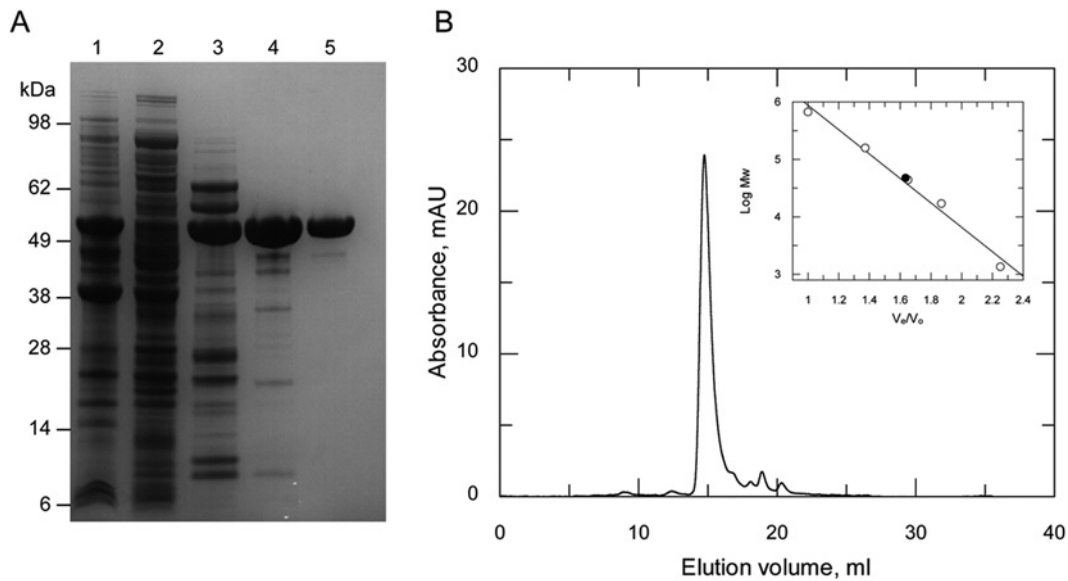

Figure 6   Purification of recombinant *Tc*NMT

(**A**) SDS/PAGE of purification of recombinant *Tc*NMT. Lane 1, insoluble fraction of Rosetta™ 2 (DE3)pLysS [pET15b-*Tc*NMT], induced; lane 2, soluble fraction of Rosetta™ 2 (DE3)pLysS [pET15b-*Tc*NMT], induced; lane 3, pooled fractions from Ni^{2+}-affinity chromatography; lane 4, pooled fractions from anion exchange chromatography (Q Sepharose); and lane 5, pooled fractions from size-exclusion chromatography. (**B**) Gel filtration profile of the His$_6$-tagged *Tc*NMT. The inset shows a plot of V_e/V_0 against the log molecular mass (Mw) of a standard protein mixture (open circles), where V_e is the elution volume and V_0 is the void volume of the column. The closed circle represents the elution volume of NMT.

Table 2   Kinetic characterization of recombinant *Tc*NMT

Data for the *Tb*NMT column are taken from [13,29]. n.d., not determined.

Parameter	Coupled-enzyme assay	Scintillation proximity assay	*Tb*NMT
$K_{m(app)}$ (μM)			
Myristoyl-CoA	6.2 ± 0.6	5.3 ± 1.0	1.78
*Tb*CAP5.5	250 ± 28	2.2 ± 0.2	11.3
*Tc*CAP5.5	12.1 ± 1	1.6 ± 0.15	–
k_{cat} (s^{-1})			
Myristoyl-CoA	0.34 ± 0.01	n.d.	–
*Tb*CAP5.5	2.11 ± 0.05	n.d.	–
*Tc*CAP5.5	0.15 ± 0.003	n.d.	–
k_{cat}/K_m (M$^{-1}\cdot$s^{-1})			
Myristoyl-CoA	54.8×10^3	–	–
*Tb*CAP5.5	8.44×10^3	–	–
*Tc*CAP5.5	12.4×10^3	–	–
Inhibition by DDD85646			
$K_{i(app)}$ (nM)	41.2 ± 5.4*	16.6 ± 4.4†	1.44
K_i (nM)	22.8	12.7	1.04

*Determined using 150 nM *Tc*NMT, 200 μM *Tb*CAP5.5 and 40 μM myristoyl-CoA.
†Determined using 5 nM *Tc*NMT. 0.5 μM *Tc*CAP5.5 and 0.125 μM myristoyl-CoA.

efficiencies (k_{cat}/K_m) of both substrates were found to be similar. For reasons of cost, it was not possible to determine the K_m values in the presence of saturating concentrations of myristoyl-CoA using the scintillation proximity assay, allowing only a $K_{m(app)}$ value to be determined for each peptide. Using this assay, the $K_{m(app)}$ values for the peptide substrates were very similar at 1.6 and 2.2 μM. In the coupled-enzyme assay (in the presence of 600 μM *Tb*CAP5.5), the $K_{m(app)}$ value of the myristoyl-CoA substrate was 6.2 ± 0.6 μM, which is not statistically different from the value of 5.3 ± 1.0 μM determined in the scintillation proximity assay (in the presence of 50 μM *Tc*CAP5.5) ($P = 0.252$) Student's t test.

Inhibition of recombinant *Tc*NMT by DDD85646

DDD85646 is a potent inhibitor of *T. brucei* recombinant NMT [$K_{i(app)} = 1.44$ nM] and inhibits the growth of *T. brucei* bloodstream parasites *in vitro* at similar concentrations (EC$_{50}$ = 2.1 nM) [13]. In comparison, we noted that DDD85646 was far less potent against *T. cruzi* epimastigotes (EC$_{50}$ = 6.3 μM) (Figure 4B). Since we have demonstrated that DDD85646 specifically inhibits *Tc*NMT *in vitro*, the drop-off in cellular potency could be in part explained by differences in active site architecture leading to a decreased affinity for the inhibitor. To test this hypothesis, the K_i value of DDD85646 was determined against the *T. cruzi* recombinant enzyme using both the scintillation proximity assay and coupled assay (Table 2). Under both sets of assay conditions, the K_i of DDD85646 was calculated to be $\sim$12.7–22.8 nM, which is 13–23-fold less potent than against the *T. brucei* enzyme. In contrast with *T. brucei*, there is a drop-off in culture potency of two orders of magnitude between target and cell activity.

DISCUSSION

The paucity of validated drug targets in *T. cruzi* has severely hampered the search for better and more effective treatments for Chagas' disease. Previous studies have shown that the enzyme encoded by the *NMT* gene is essential for the survival of many eukaryotic organisms [10,12,35,36], including the related trypanosomatids *L. major* and *T. brucei* [12]. Metabolic labelling studies in *T. cruzi* have already revealed that N-myristoylation

occurs in this parasite and plays a role in the correct cellular localization of the flagellar calcium-binding protein [16,37]. The genetic studies investigated in the present study indicate that *TcNMT* is an essential gene in the epimastigote stage of the parasite, since we were unable to directly replace both endogenous copies of *NMT*, except in the presence of an ectopic copy of the gene. Although we have carried out genetic validation of *Tc*NMT in the epimastigote stage of the parasite, there is clear evidence to show that the enzyme is also present in the clinically relevant stages. Therefore it is likely that N-myristoylation is also an essential cellular process during the trypomastigote and amastigote stages of development.

The comparative profiling of NMT substrate specificities from multiple organisms has revealed that there are subtle species-specific differences in the N-myristoylation motif of protein substrates recognized by each homologue. These differences have already been exploited to generate inhibitors which are up to 560-fold more potent against a fungal enzyme than the human enzyme [38]. Several high-throughput inhibitor-screening programmes have been carried out in recent years with the aim of identifying both potent and selective inhibitors of NMT from the target species [13,39,40]. One such campaign led to the development of DDD85646, a highly potent inhibitor of *T. brucei* and human NMT [13]. Despite selectivity at the target level being only 2-fold, this increases to 200-fold at the cellular level. The reason for biological selectivity is not fully understood and may involve pleiotropic biological effects. Depletion of NMT by RNAi in this parasite leads to impairment of the endocytic pathway [41], a process that is known to involve the N-myristoylated protein *Tb*ARF1 (*T. brucei* ARF1) [42]. Endocytosis and exocytosis in *T. brucei* occurs exclusively from a specialized invagination of the plasma membrane known as the flagellar pocket. Owing to the high endocytic/exocytic rate, the entire plasma membrane of the parasite is turned over in approximately 12 min, considerably faster than that of mammalian macrophages or fibroblasts [43]. Treatment of *T. brucei* with DDD85646 causes a massively enlarged flagellar pocket or 'big eye' phenotype [13], as found by RNAi knockdown of either clathrin heavy chain [44] or ARF1 [42], suggesting that endocytosis, but not exocytosis, is inhibited. Curiously, knockdown of NMT itself does not produce this phenotype, despite inhibiting endocytosis [41]. Nonetheless, the marked sensitivity of the *T. brucei* bloodstream parasite to NMT inhibition can be attributed at least partly to the high rate of endocytosis/exocytosis and the consequent high turnover of plasma membrane in the flagellar pocket [13].

Although DDD85646 is a potent inhibitor of the *T. cruzi* enzyme, there is a considerable drop off in potency against the intact parasite (epimastigote or amastigote), in marked contrast with *T. brucei* where DDD85646 is equipotent against both the enzyme and the parasite [13]. The reason for this is not clear, but could be due to differences in the rate of plasma membrane turnover, differences in other essential biological functions requiring N-myristoylation or due to differences in cellular pharmacokinetics of drug uptake or efflux. The kinetics of endocytosis has not been studied in *T. cruzi*. However, it is worth noting that endocytosis in *T. cruzi* epimastigotes occurs principally via another membrane invagination adjacent to the flagellar pocket (the cytostome) and not the flagellar pocket itself [45].

Our studies clearly demonstrate that NMT is an essential and druggable enzyme in *T. cruzi*, thus it is entirely plausible that parasite-specific N-myristoylated proteins may also be potential drug targets in their own right. To date, only two *T. cruzi* proteins (flagellar calcium-binding protein and phosphoinositide-specific phospholipase C) have been defin-

itively confirmed to be N-myristoylated [16,37], although two studies have predicted many proteins may undergo this modification [46,47]. Although our studies identify at least ten distinct bands, treatment of epimastigotes with DDD85646 was only able to specifically block the N-myristoylation of six *in vitro* under the experimental conditions used in the present study. Although it is possible to theoretically predict N-myristoylated proteins from any completed genome [46,48], these bioinformatics and predictive approaches have several drawbacks. Most notably, using known N-myristoylated motifs from various organisms to inform our identification of N-myristoylated proteins in *T. cruzi* may well lead to difficulties, since previous studies have shown a degree of variability in this motif across different organisms [49–51]. With this in mind, work is underway to identify directly the N-myristoylated proteins comprising the *T. cruzi* N-myristoylome using a click chemistry approach.

In conclusion, we have demonstrated that NMT from *T. cruzi* is both an essential and druggable target. However, discovery of more potent and selective inhibitors will be required to achieve a suitable therapeutic window for the treatment of Chagas' disease.

REFERENCES

1 Schmunis, G. A. (2007) Epidemiology of Chagas disease in non-endemic countries: the role of international migration. Mem. Inst. Oswaldo Cruz **102**, 75–85

2 Rassi, Jr., A., Rassi, A. and Marin-Neto, J. A. (2010) Chagas disease. Lancet **375**, 1388–1402

3 World Health Organization (2012) Chagas disease (American trypanosomiasis): fact sheet (revised in August 2012). Wkly Epidemiol. Rec. **87**, 519–522

4 WHO Expert Committee (2002) Control of Chagas disease. World Health Organ. Tech. Rep. Ser. **905**, 1–109

5 Cancado, J. R. (2002) Long term evaluation of etiological treatment of Chagas disease with benznidazole. Rev. Inst. Med. Trop. Sao Paulo **44**, 29–37

6 Jackson, Y., Alirol, E., Getaz, L., Wolff, H., Combescure, C. and Chappuis, F. (2010) Tolerance and safety of nifurtimox in patients with chronic Chagas disease. Clin. Infect. Dis. **51**, e69–e75

7 Hasslocher-Moreno, A. M., do Brasil, P. E., de Sousa, A. S., Xavier, S. S., Chambela, M. C. and Sperandio da Silva, G. M. (2012) Safety of benznidazole use in the treatment of chronic Chagas' disease. J. Antimicrob. Chemother. **67**, 1261–1266

8 Towler, D. A., Eubanks, S. R., Towery, D. S., Adams, S. P. and Glaser, L. (1987) Amino-terminal processing of proteins by *N*-myristoylation. Substrate specificity of *N*-myristoyl transferase. J. Biol. Chem. **262**, 1030–1036

9 Towler, D. A., Adams, S. P., Eubanks, S. R., Towery, D. S., Jackson-Machelski, E., Glaser, L. and Gordon, J. I. (1987) Purification and characterization of yeast myristoyl CoA:protein *N*-myristoyltransferase. Proc. Natl. Acad. Sci. U.S.A. **84**, 2708–2712

10 Lodge, J. K., Jackson-Machelski, E., Toffaletti, D. L., Perfect, J. R. and Gordon, J. I. (1994) Targeted gene replacement demonstrates that myristoyl-CoA:protein *N*-myristoyltransferase is essential for viability of *Cryptococcus neoformans*. Proc. Natl. Acad. Sci. U.S.A. **91**, 12008–12012

11 Knoll, L. J., Levy, M. A., Stahl, P. D. and Gordon, J. I. (1992) Analysis of the compartmentalization of myristoyl-CoA:protein *N*-myristoyltransferase in *Saccharomyces cerevisiae*. J. Biol. Chem. **267**, 5366–5373

12 Price, H. P., Menon, M. R., Panethymitaki, C., Goulding, D., McKean, P. G. and Smith, D. F. (2003) Myristoyl-CoA: protein *N*-myristoyltransferase, an essential enzyme and potential drug target in kinetoplastid parasites. J. Biol. Chem. **278**, 7206–7214

13 Frearson, J. A., Brand, S., McElroy, S. P., Cleghorn, L. A. T., Smid, O., Stojanovski, L., Price, H. P., Guther, M. L. S., Torrie, L. S., Robinson, D. A. et al. (2010) *N*-myristoyltransferase inhibitors as new leads to treat sleeping sickness. Nature **464**, 728–732

14 Bhatnagar, R. S., Futterer, K., Farazi, T. A., Korolev, S., Murray, C. L., Jackson-Machelski, E., Gokel, G. W., Gordon, J. I. and Waksman, G. (1998) Structure of N-myristoyltransferase with bound myristoylCoA and peptide substrate analogs. Nat. Struct. Biol. **5**, 1091–1097

15 Glover, C. J., Hartman, K. D. and Felsted, R. L. (1997) Human *N*-myristoyltransferase amino-terminal domain involved in targeting the enzyme to the ribosomal subcellular fraction. J. Biol. Chem. **272**, 28680–28689

16 Godsel, L. M. and Engman, D. M. (1999) Flagellar protein localization mediated by a calcium-myristoyl/palmitoyl switch mechanism. EMBO J. **18**, 2057–2065

17 Hunter, K. J., Le Quesne, S. A. and Fairlamb, A. H. (1994) Identification and biosynthesis of N^1,N^9-*bis*(glutathionyl)aminopropylcadaverine (homotrypanothione) in *Trypanosoma cruzi*. Eur. J. Biochem. **226**, 1019–1027

18 Silveira, F. T., Viana Dias, M. G., Pereira Pardal, P., Oliveira Lobâo, A. and Britto Melo, G. (1979) Nono caso-autóctone de doença de Chagas registrado no estado do Pará, Brasil (Nota prévia). Hiléia Médica **1**, 61–62

19 Ariyanayagam, M. R., Oza, S. L., Mehlert, A. and Fairlamb, A. H. (2003) Bis(glutathionyl)spermine and other novel trypanothione analogues in *Trypanosoma cruzi*. J. Biol. Chem. **278**, 27612–27619

20 Ammerman, N. C., Beier-Sexton, M. and Azad, A. F. (2008) Growth and maintenance of Vero cell lines. Curr. Protoc. Microbiol. **11**, A.4E.1–A.4E.7

21 Franzen, O., Ochaya, S., Sherwood, E., Lewis, M. D., Llewellyn, M. S., Miles, M. A. and Andersson, B. (2011) Shotgun sequencing analysis of *Trypanosoma cruzi* I Sylvio X10/1 and comparison with *T. cruzi* VI CL Brener. PLoS Negl. Trop. Dis. **5**, e984

22 Studier, F. W. (2005) Protein production by auto-induction in high-density shaking cultures. Protein Expr. Purif. **41**, 207–234

23 Martin, K. and Smith, T. K. (2005) The myo-inositol-1-phosphate synthase gene is essential in *Trypanosoma brucei*. Biochem. Soc. Trans. **33**, 983–985

24 Vazquez, M. P. and Levin, M. J. (1999) Functional analysis of the intergenic regions of TcP2 β gene *loci* allowed the construction of an improved *Trypanosoma cruzi* expression vector. Gene **239**, 217–225

25 Xu, D., Brandan, C. P., Basombrio, M. A. and Tarleton, R. L. (2009) Evaluation of high efficiency gene knockout strategies for *Trypanosoma cruzi*. BMC Microbiol. **9**, 90

25a Marques, A., Nakayasu, E. and Almeida, I. (2011) Purification of extracellular and intracellular amastigotes of *Trypanosoma cruzi* from mammalian host-infected cells. Protoc. Exch., doi:10.1038/protex.2011.265

26 Tovar, J. and Fairlamb, A. H. (1996) Extrachromosomal, homologous expression of trypanothione reductase and its complementary mRNA in *Trypanosoma cruzi*. Nucleic Acids Res. **24**, 2942–2949

27 Wyllie, S., Oza, S. L., Patterson, S., Spinks, D., Thompson, S. and Fairlamb, A. H. (2009) Dissecting the essentiality of the bifunctional trypanothione synthetase-amidase in *Trypanosoma brucei* using chemical and genetic methods. Mol. Microbiol. **74**, 529–540

28 Boisson, B. and Meinnel, T. (2003) A continuous assay of myristoyl-CoA:protein *N*-myristoyltransferase for proteomic analysis. Anal. Biochem. **322**, 116–123

29 Panethymitaki, C., Bowyer, P. W., Price, H. P., Leatherbarrow, R. J., Brown, K. A. and Smith, D. F. (2006) Characterization and selective inhibition of myristoyl-CoA: protein *N*-myristoyltransferase from *Trypanosoma brucei* and *Leishmania major*. Biochem. J. **396**, 277–285

30 Cruz, A. K., Titus, R. and Beverley, S. M. (1993) Plasticity in chromosome number and testing of essential genes in *Leishmania* by targeting. Proc. Natl. Acad. Sci. U.S.A. **90**, 1599–1603

31 Rohloff, P., Rodrigues, C. O. and Docampo, R. (2003) Regulatory volume decrease in *Trypanosoma cruzi* involves amino acid efflux and changes in intracellular calcium. Mol. Biochem. Parasitol. **126**, 219–230

32 Goncalves, V., Brannigan, J. A., Thinon, E., Olaleye, T. O., Serwa, R., Lanzarone, S., Wilkinson, A. J., Tate, E. W. and Leatherbarrow, R. J. (2012) A fluorescence-based assay for *N*-myristoyltransferase activity. Anal. Biochem. **421**, 342–344

33 Rampoldi, F., Sandhoff, R., Owen, R. W., Grone, H. J. and Porubsky, S. (2012) A new, robust, and nonradioactive approach for exploring *N*-myristoylation. J. Lipid Res. **53**, 2459–2468

34   Hertz-Fowler, C., Ersfeld, K. and Gull, K. (2001) CAP5.5, a life-cycle-regulated, cytoskeleton-associated protein is a member of a novel family of calpain-related proteins in *Trypanosoma brucei*. Mol. Biochem. Parasitol. **116**, 25–34

35   Weinburg, R. A., McWherter, C. A., Freeman, K. S., Wood, D. C., Gordon, J. I. and Lee, S. C. (1995) Genetic studies reveal that myristoylCoA-protein *N*-myristoyltransferase is an essential enzyme in *Candida albicans*. Mol. Microbiol. **16**, 241–250

36   Yang, S. H., Shrivastav, A., Kisinski, C., Sharma, R. K., Chen, M. H., Berthiaume, L. G., Peters, L. L., Chuang, P. T., Young, S. G. and Bergo, M. O. (2005) *N*-myristoyltransferase 1 is essential in early mouse development. J. Biol. Chem. **280**, 18990–18995

37   Martins, V. D., Okura, M., Maric, D., Engman, D. M., Vieira, M., Docampo, R. and Moreno, S. N. J. (2010) Acylation-dependent export of *Trypanosoma cruzi* phosphoinositide-specific phospholipase C to the outer surface of amastigotes. J. Biol. Chem. **285**, 30906–30917

38   Lodge, J. K., Jackson-Machelski, E., Devadas, B., Zupec, M. E., Getman, D. P., Kishore, N., Freeman, S. K., McWherter, C. A., Sikorski, J. A. and Gordon, J. I. (1997) *N*-myristoylation of Arf proteins in *Candida albicans*: an *in vivo* assay for evaluating antifungal inhibitors of myristoyl-CoA: protein *N*-myristoyltransferase. Microbiology **143**, 357–366

39   Bell, A. S., Mills, J. E., Williams, G. P., Brannigan, J. A., Wilkinson, A. J., Parkinson, T., Leatherbarrow, R. J., Tate, E. W., Holder, A. A. and Smith, D. F. (2012) Selective inhibitors of protozoan protein *N*-myristoyltransferases as starting points for tropical disease medicinal chemistry programs. PLoS Negl. Trop. Dis. **6**, e1625

40   Goncalves, V., Brannigan, J. A., Whalley, D., Ansell, K. H., Saxty, B., Holder, A. A., Wilkinson, A. J., Tate, E. W. and Leatherbarrow, R. J. (2012) Discovery of *Plasmodium vivax N*-myristoyltransferase inhibitors: screening, synthesis, and structural characterization of their binding mode. J. Med. Chem. **55**, 3578–3582

41   Price, H. P., Guther, M. L., Ferguson, M. A. and Smith, D. F. (2010) Myristoyl-CoA:protein *N*-myristoyltransferase depletion in trypanosomes causes avirulence and endocytic defects. Mol. Biochem. Parasitol. **169**, 55–58

42   Price, H. P., Stark, M. and Smith, D. F. (2007) *Trypanosoma brucei* ARF1 plays a central role in endocytosis and Golgi-lysosome trafficking. Mol. Biol. Cell **18**, 864–873

43   Engstler, M., Thilo, L., Weise, F., Grunfelder, C. G., Schwarz, H., Boshart, M. and Overath, P. (2004) Kinetics of endocytosis and recycling of the GPI-anchored variant surface glycoprotein in *Trypanosoma brucei*. J. Cell Sci. **117**, 1105–1115

44   Allen, C. L., Goulding, D. and Field, M. C. (2003) Clathrin-mediated endocytosis is essential in *Trypanosoma brucei*. EMBO J. **22**, 4991–5002

45   Porto-Carreiro, I., Attias, M., Miranda, K., de Souza, W. and Cunha-e-Silva, N. (2000) *Trypanosoma cruzi* epimastigote endocytic pathway: cargo enters the cytostome and passes through an early endosomal network before storage in reservosomes. Eur. J. Cell Biol. **79**, 858–869

46   Mills, E., Price, H. P., Johner, A., Emerson, J. E. and Smith, D. F. (2007) Kinetoplastid PPEF phosphatases: dual acylated proteins expressed in the endomembrane system of *Leishmania*. Mol. Biochem. Parasitol. **152**, 22–34

47   Cordero, E. M., Nakayasu, E. S., Gentil, L. G., Yoshida, N., Almeida, I. C. and da Silveira, J. F. (2009) Proteomic analysis of detergent-solubilized membrane proteins from insect-developmental forms of *Trypanosoma cruzi*. J. Proteome Res. **8**, 3642–3652

48   Maurer-Stroh, S., Eisenhaber, B. and Eisenhaber, F. (2002) N-terminal *N*-myristoylation of proteins: prediction of substrate proteins from amino acid sequence. J. Mol. Biol. **317**, 541–557

49   Traverso, J. A., Giglione, C. and Meinnel, T. (2013) High-throughput profiling of *N*-myristoylation substrate specificity across species including pathogens. Proteomics **13**, 25–36

50   Towler, D. A., Adams, S. P., Eubanks, S. R., Towery, D. S., Jackson-Machelski, E., Glaser, L. and Gordon, J. I. (1988) Myristoyl CoA:protein *N*-myristoyltransferase activities from rat liver and yeast possess overlapping yet distinct peptide substrate specificities. J. Biol. Chem. **263**, 1784–1790

51   Rocque, W. J., McWherter, C. A., Wood, D. C. and Gordon, J. I. (1993) A comparative analysis of the kinetic mechanism and peptide substrate specificity of human and *Saccharomyces cerevisiae* myristoyl-CoA:protein *N*-myristoyltransferase. J. Biol. Chem. **268**, 9964–9971